NASA Contractor Report 182249
RI/RD 89-179

LOX/Hydrocarbon Combustion Instability Investigation

R.J. Jensen, H.C. Dodson,
and S.E. Claflin

Rockwell International
Rocketdyne Division
Canoga Park, California

July 1989

Prepared for
Lewis Research Center
Under Contract NAS3-24612

National Aeronautics and
Space Administration

FOREWORD

The objective of this program was to evaluate if hydrocarbon fuels, such as methane, with liquid oxygen (LOX) produces combustion stability and performance behavior similar to the LOX/hydrogen propellant combination. Hot fire test data was acquired on the LOX/methane propellant combination performance analysis and combustion stability rating using stability bomb tests and stability temperature ramping techniques.

This report describes the results of the evaluation conducted under the scope of the program.

The program was performed at the Rocketdyne Division of Rockwell International under the sponsorship of the National Aeronautics and Space Administration - Lewis Research Center, Cleveland, Ohio, Contract Number NAS3-24612. Mr. H. C. Dodson of Rocketdyne was Program Manager. S. M. Pinkowski and K. W. Hunt were Project Engineers. The assistance of F. E. Dodd, J. J. Fang, M. D. Schuman, and J. R. Fenwick in modeling activities is gratefully acknowledged.

TABLE OF CONTENTS

EXECUTIVE SUMMARY

The LOX/Hydrocarbon Combustion Instability Investigation Program (NAS3-24612) was structured to determine if the use of light hydrocarbon fuels (such as methane) with liquid oxygen (LOX) produces combustion performance and stability behavior similar to the LOX/hydrogen propellant combination. In particular methane was investigated to determine if that fuel can be rated for combustion instability using the same techniques as previously used for LOX/hydrogen. These techniques included fuel temperature ramping and stability bomb tests.

The hot fire program probed the combustion behavior of methane from ambient to subambient (438 R at the manifold) temperatures. Very interesting results were obtained from this program that have potential importance to future LOX/methane development programs. This report contains a very thorough and carefully reasoned documentation of the experimental data obtained. The hot fire test logic and the associated tests that are discussed in this report are shown in Figure 1. Subscale performance and stability rating testing was accomplished using 40,000 lb. thrust class hardware. Stability rating tests used both "bombs" and fuel temperature ramping techniques. The 5.66 in diameter 82 coaxial element hardware incorporating no acoustic stability aids was operated over a mainstage mixture ratio range of 2.5 to 3.7 and mainstage durations of from 0.1 to 8 seconds in tests at a nominal chamber pressure of 2000 psig. Three tests were successfully driven unstable at low fuel temperature during fuel temperature ramping stability rating tests. Five tests experienced self induced 1T instabilities at higher fuel temperatures. Two of three bomb tests were dynamically unstable. Low mixture ratio performance and stability data was obtained at about 1500 psia during prestage for each mainstage test achieved. The test program was thus successful in generating data for the evaluation of the methane stability characteristics relative to hydrogen and to anchor stability models. Data correlations, performance analysis, stability analyses, and key stability margin enhancement parameters are discussed.

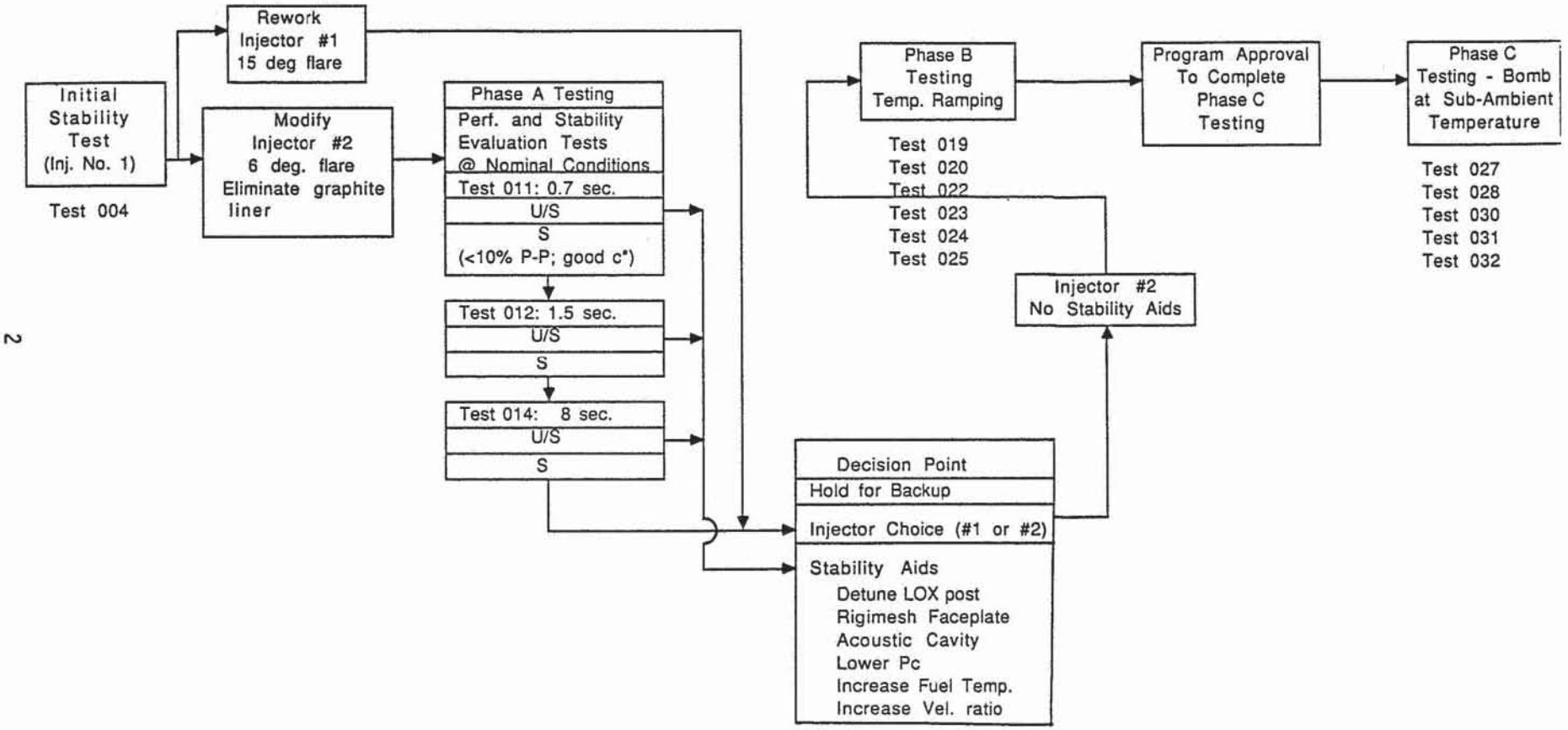

Figure 1 - Finalized Test Logic

INTRODUCTION

The use of a LOX/hydrocarbon fuel propellant combination in an advanced launch vehicle booster engine appears extremely attractive due to high propellant bulk density and the relatively high performance characteristics of these propellant combinations. The LOX/methane propellant combination has emerged as a leading candidate for the Space Transportation Booster Engine. Methane is a cryogenic fuel and would be injected in a fluid state similar to hydrogen.

The development histories of LOX/hydrogen engines have shown that, based on the characteristics of this propellant combination, it is possible to achieve high performance and stable operation in a more direct and cost effective manner than with LOX/RP-1. In view of the considerable resources expended to meet stability and performance criteria of previous high thrust LOX/hydrocarbon engines such as the F-1 ,it would be desirable to evaluate the general stability characteristics of methane and determine if these characteristics match those of hydrogen. In particular for methane testing, the applicability of stability rating techniques such as fuel temperature ramping which provided a measure of LOX/hydrogen injector stability margins on a test-by-test basis (Ref. 1-9) is of great interest. In this technique the fuel temperature is reduced from nominal operating conditions down toward the critical temperature while holding mixture ratio (oxidizer mass flow to fuel mass flow) and total mass flow constant. At some repeatable temperature, specific to the configuration and operating conditions, an acoustic instability would occur. Most often the instability would be a first tangential mode. Bomb testing at nominal and lower fuel temperatures was also used successfully to obtain the dynamic stability characteristics of engines like the J-2 and the RL-10.

The present program was structured to evaluate the characteristics of mild cryogenic hydrocarbon fuels relative to hydrogen, select a fuel most like hydrogen based on physical properties and the expected stability behavior, and conduct a hot fire test program to demonstrate the stability and performance of the selected fuel. The fuel selected was methane. The LOX/methane propellant combination was then rated for combustion stability using both fuel temperature ramping and bombing. Demonstration of an instability threshold as a function of fuel temperature and related parameters such that a comparison could be made with LOX/ hydrogen instability data was accomplished on this program. Overall, it was determined that coaxial injector element geometry and combustor operating conditions, such as velocity ratio, mixture ratio, and propellant temperatures are controlling factors on stability margin.

RESULTS AND DISCUSSION

Test Hardware Description

The overall design of the thrust chamber allowed the configuration flexibility necessary to achieve both types of stability rating tests. A thrust chamber assembly drawing is presented in Figure 2, with a photograph of the injector assembly details shown as Figure 3. The thrust chamber is of the 40 Klb thrust class with a 5.66-inch chamber diameter. The design closely approximates an 82 element injector and chamber developed for NASA Marshall Space Flight Center (Ref. 10) and utilized in LOX/methane performance testing at MSFC. In this report, that hardware is referred to as the NASA-MSFC design while the hardware on the current program is termed the NASA-LeRC design.

The LeRC injector is a breadboard configuration: that is, injector components are removable and interchangeable to maximize configuration flexibility. The details of the LeRC and MSFC coaxial element injector designs are listed in Table I. The nominal operating mixture ratio for these injectors is 3.5. The energy release efficiency of the thrust chamber at design conditions was predicted to equal or exceed 98% based on previous test experience with this type of injector.

The thrust chamber design provides for performance and stability test requirements through interchangeable spool sections. With water cooled chamber and throat sections the thrust chamber is capable of sustaining durations of ten seconds (facility limitation) for temperature ramp and performance tests. An uncooled spool section with high frequency pressure transducer and bomb ports was designed for two second bomb tests. A complete discussion of the detailed hardware design is provided in Reference 11 and Appendix A.

High frequency instrumentation varied with the configuration. Two different uncooled bomb spools equipped with three high frequency pressure transducers were utilized in the testing. Relative to the bomb location, these transducers are circumferentially located at 90, 210, and 300 degrees for the graghite lined spool used in test 004 and at 60, 150 and 270 degrees from the bomb for the copper lined bomb spool used in tests 027 through 032. The cooled hardware used in performance and ramping tests was not equipped with chamber high frequency pressure transducers due to the difficulty in providing sufficient cooling at the transducer aperture location in the side of the channel wall chamber. All configurations were equipped with LOX dome and inner and outer fuel manifold high frequency pressure transducers. Three axis accelerometers were mounted on the exterior of the fuel manifold.

Chamber pressure is measured two inches downstream of the injector face and at the start of nozzle convergence through slots in the seal joints. Fuel temperature was measured at the venturi and in the fuel manifold.

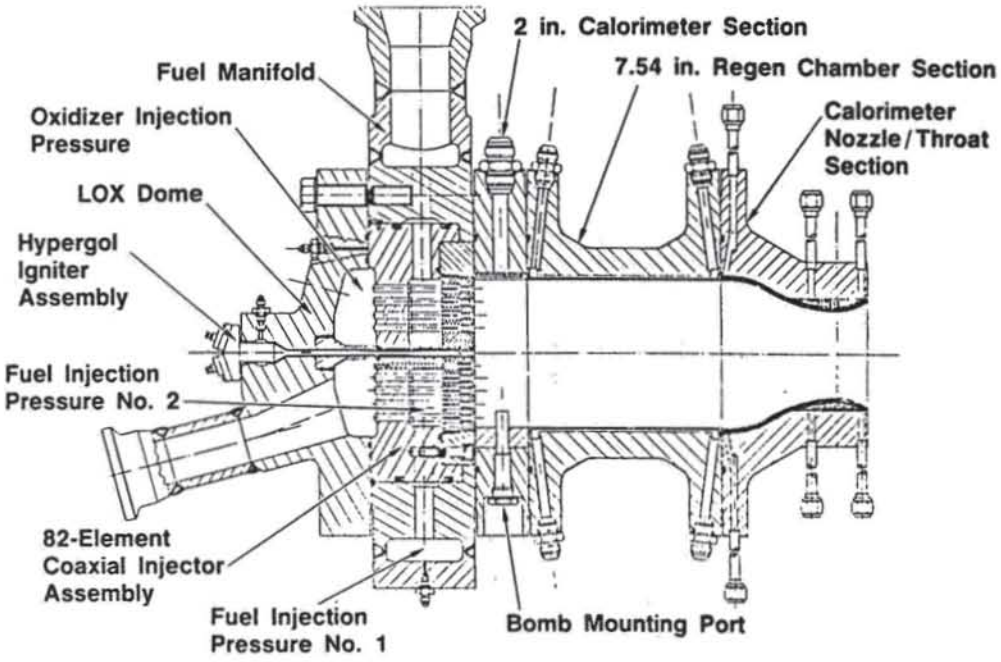

Figure 2 – 82–Element LOX/Methane Injector and Thrust Chamber

Figure 3 – Injector Assembly Details Including Injector Bodies and Faceplates

ORIGINAL PAGE
BLACK AND WHITE PHOTOGRAPH

TABLE I - LOX/Methane Coaxial Injector and Chamber Details

Feature	LeRC Design	MSFC Design
Faceplate	Solid NARloy (no bleed)	Rigimesh with facenuts (7.2% bleed)
Oxidizer post exit (deg half angle)	15° (Test 004) 6° (all other tests)	6°
Oxidizer post length (in.)	3.608	4.68
Fuel annulus gap (in.)	0.0105	0.0115
Oxidizer post recess (in.)	0.202	0.200
Acoustic absorber	none	Potential 1/4 wave gap (0.070 in. and 0.030 in wide by 1 in. deep)
Chamber interface	graphite liner (Test 004) OFHC liner (Phase C) cooled ring (all others)	cooled chamber
Methane purity (%)	99.9	95

NOTE: Chamber diameter = 5.66 in., length of cylindrical portion of chamber = 9.54 in., length of convergent section = 4.47 in., and nozzle contraction ratio = 2.92

A set of detailed drawings of the injector elements is presented in Appendix A

Test Facility Description

The high-pressure Peter Test Stand located in the Advanced Propulsion Test Facility at Rocketdyne's Santa Susanna Field Laboratory was the site of the testing (Fig. 4). A detailed description of the facility is presented in Appendix A. The high pressure facility was modified to conduct fuel temperature ramp testing and operation at constant sub-ambient fuel temperatures as well as ambient methane testing. The servo system on the fuel feed system can continuously ramp the methane temperature by mixing liquid and gaseous methane. See Figure A11. Fuel flow rate and mixture ratio can be controlled to within 3% of targeted values. The gaseous methane feed system was servo-controlled by a valve located upstream of the mixer with pressure feedback. Liquid methane flow was servo-controlled by a valve located upstream of the mixer with temperature feedback. A subsonic venturi downstream of the mixer was used for injector fuel flow measurement. Total fuel flow was controlled by a main fuel servo valve.

The gaseous methane was supplied from a 470 cubic foot blowdown run bottle. A 5000 psig, 100 gallon liquid methane run tank pressurized by servo-controlled gaseous helium supplied the liquid fuel. The servo system response feature maintained a constant liquid supply pressure throughout the test duration.

A 5000 psig, 180 gallon LOX run tank pressurized by servo-controlled gaseous nitrogen supplied oxidizer to the injector and igniter. See Figure A12. As in the liquid fuel case, the LOX servo system maintained a constant tank supply pressure during hot-fire test runs.

A two stage start sequence was required to minimize faceplate pressure differential and to insure smooth ignition. This two stage sequence required ramping the methane to half its total mainstage flow, igniting with CTF, and then ramping the LOX to half its mainstage flow. These operating parameters define the "prestage" condition. The methane was subsequently ramped to full flow and the LOX followed immediately to establish full power level operation. This sequence results in the stepwise increase in chamber pressure apparent in the data.

Hot Fire Test Results

The results of performance and fuel temperature ramp testing are summarized in Table II. In this table cup fuel thermodynamic properties were calculated on the basis of an assumed isentropic process which correctly predicted measured fuel manifold conditions. Of the seventeen tests in which significant data was obtained, six were checkout and performance tests, fuel temperature ramp stability rating was attempted on six tests,and dynamic stability (bomb) rating was attempted on the remaining five. A range of mixture ratios from 2.5 to 3.7 (at mainstage conditions) was also investigated. Nominal chamber pressure was 2000 psig. The injector was successfully driven unstable at a repeatable low fuel temperature on three of the temperature ramp

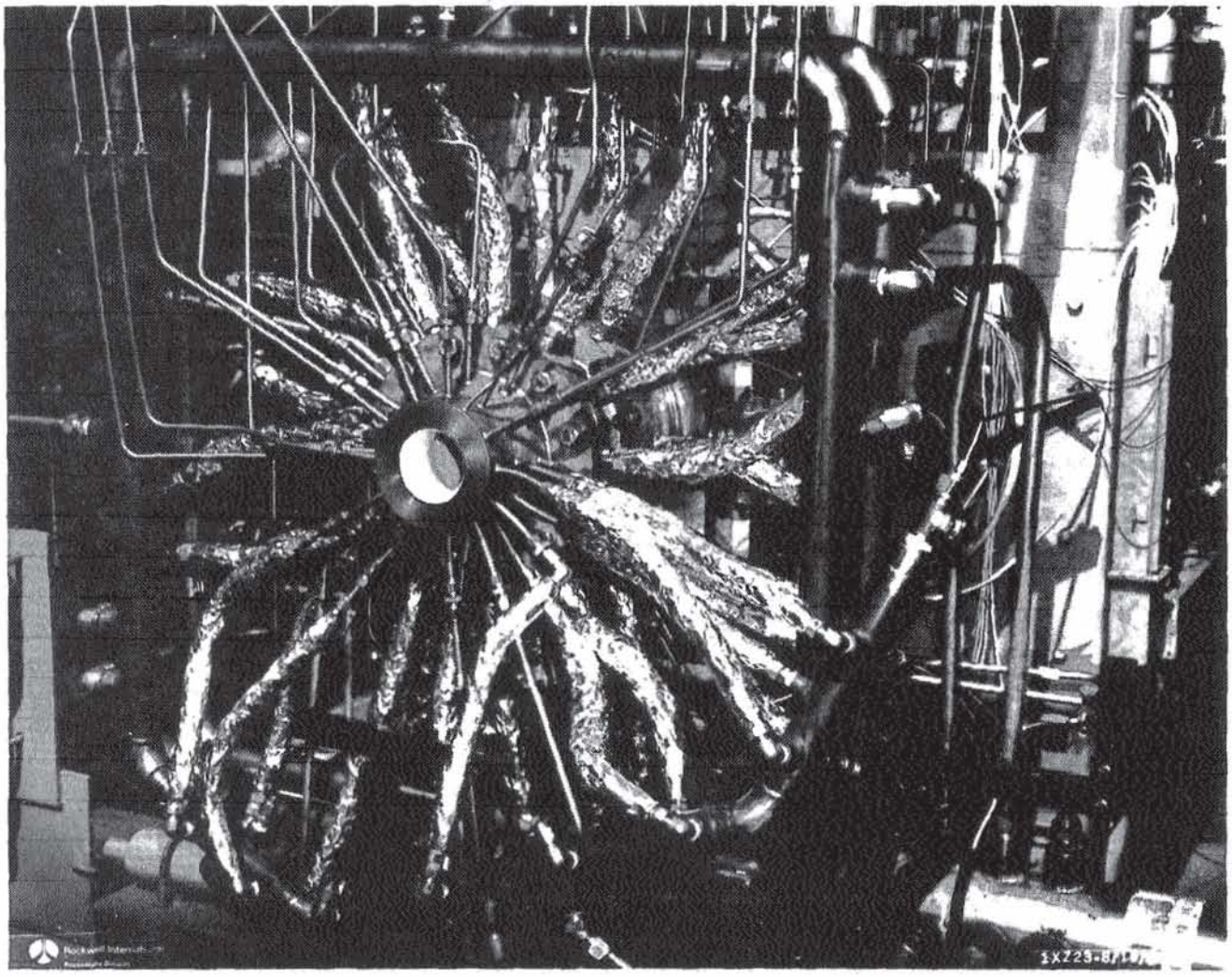

Figure 4 – LOX/Methane Hardware Installation in Peter Stand

Table IIa. - LOX/CH4 Instability Investigation Transition and Mainstage Data Summary

Test Number (014-)	004	011	012	014	018	019
Mainstage Duration (sec)	1.4 (1)	0.7	1.5	8	0.0 (8)	0.0 (5)
Pressure (psia)						
Chamber (nozzle stag.)	1930	1974	1980	2010	1866	1886
Fuel Injector	2640	2658	2688	2800	2741	2817
Oxid Injector	2450	2534	2529	2555	2298	2329
Temperature (F)						
Fuel Inj-2 (manifold)	36	43	46	64	40	46
Oxid Injector	-252	-252	-249	-259	-238	-244
Mass Flow, Main (lb/sec)						
LOX	68.13	68.78	68.96	69.51	63.11	61.74
Methane	21.82	19.54	19.8	20.27	23.66	24.23
Mass Flow, Ign (lb/sec)						
Gaseous Oxygen	.39	.37	.37	.37	.31	.31
Methane	.29	.29	.29	.29	.33	.33
Mixture Ratio						
Element	3.12	3.57	3.48	3.43	2.67	2.55
Main	3.12	3.57	3.48	3.43	2.67	2.55
Overall	3.1	3.54	3.45	3.4	2.64	2.53
c* efficiency (percent) (10)	92.1	96.4	96.8	97	-- (7)	--
Throat Heat Flux (BTU/sq.in-sec) (10)	64.1	69.7	63.2	58	30.8	24.9
Stability	U/S	S	S	S	S	U/S
Frequency	1-T					1-T
Estimated Data at the Cup (9)						
Temperature, Inj (F)						
LOX	-252	-252	-249	-259	-238	-244
Methane	15	24	27	43	14.5	20.7
Density, Inj (lb/cu.ft)						
LOX	66.3	66.2	65.8	67.5	63.6	64.7
Methane	8.5	8.5	8.4	7.9	10.7	8.1
Velocity, Inj (ft/sec)						
LOX	121	71	71	70	67	64
Methane	604	549	563	610	693	708
Velocity Ratio (F/O)	5	7.7	8	8.8	10.3	11
Momentum Ratio ($\dot{w}_f V_f / \dot{w}_o V_o$)	1.6	2.16	2.3	2.57	3.86	4.31
Mom. Flux Ratio [$(\rho v^2)_f / (\rho v^2)_o$]	3.2	7.6	8.17	9.06	13.51	15.15

NOTES: (1) Instability occurred at 0.7 sec into mainstage
(2) Instability encountered at the lowest fuel temperature
(3) Temperature at onset of instability
(4) Assumes LOX flow separates from post tip chamfer
(5) Self-induced instability while in transition to mainstage
(6) Successful bomb test
(7) Zirconia coating on hot gas wall (Tests 019 through 032)
(8) Test cut by facility or instrumentation redline
(9) Conditions calculated at the LOX post tip exit plane prior to jet expansion
(10) C* efficiency and heat flux values for test durations less than 1.5 seconds are questionable

S = stable U/S = unstable

020	021	022	023	024	025	027	028	030	031	032
6.26	0.0 (8)	2.1	6.2	6.5	6.4	0.3	0.0 (5)	0.3	0.0 (5)	0.5
2070	1990	2030	2037	2020	2015	1960	1526	1964	1885	2127
2838	2750	2819	2539	2529	2535	2690	2308	2632	2531	2686
2600	2470	2516	2534	2520	2502	2481	1820	2528	2420	2803
58	54	50	-16	-22	-23	67	19	22	33	2
-255	-253	-263	-259	-254	-261	-242	-236	-249	-235	-247
68.38	64.97	65.92	66.59	65.84	65.56	66.77	48.97	66.73	67.27	76.72
21.04	20.8	21.69	20.67	21.28	21.18	19.56	26.01	20.8	19.87	20.65
.37	.32	.34	.36	.36	.35	.34	.38	.34	.43	.48
.3	.29	.31	.34	.34	.35	.27	.35	.31	.28	.3
3.25	3.12	3.04	3.22	3.09	3.09	3.41	1.88	3.21	3.39	3.72
3.25	3.12	3.04	3.22	3.09	3.09	3.41	1.88	3.21	3.39	3.72
3.22	3.1	3.01	3.19	3.06	3.06	3.38	1.87	3.18	3.36	3.69
97.7	--	97.3	98.1	97.7	97.9	96.9	--	95.1	--	94.8
28.4	19.9	25.8	31.2	30	30.5	20.9	12.9	20	15	34.7
S	S	U/S 1-T	U/S (2) 14 KHz	U/S (2) 14 KHz	U/S (2) 14KHz	U/S (6) 1-T	U/S 1-T	U/S (6) 1-T	U/S 1-T	S (6)
-255	-253	-263	-259	-254	-261	-242	-236	-249	-235	-247
38	33.8	29	-27 (3)	-32 (3)	-33 (3)	47	-9	4	13.6	-10
66.9	66.4	68.1	67.5	66.6	67.8	64.6	63.1	65.8	63.3	65.8
8.3	8.1	8.5	11.9	12.2	12.4	7.5	7.5	9.4	8.5	11.1
69	66	65	67	67	65	70	53	68	72	79
604	610	609	414	414	408	620	821	528	559	444
8.8	9.2	9.3	6.2	6.2	6.2	8.8	15.5	7.7	7.8	5.6
2.71	2.95	3.06	1.94	2.01	2.01	2.58	8.24	2.4	2.3	1.51
9.16	10.32	10.8	6.78	7.04	7.03	9	28.56	8.47	8.17	5.29

Table IIb. - LOX/CH4 Instability Investigation Prestage Data Summary

Test Number (014-)	011	012	014	018	019 (1)
Pressure (psia)					
Chamber (nozzle stag.)	1472	1403	1483	1421	1429
Fuel Injector	2326	2113	2328	2519	2561
Oxid Injector	1770	1688	1760	1678	1681
Temperature (F)					
Fuel Inj-2 (manifold)	35	35	46	37	43
Oxid Injector	-219	-196	-232	-232	-235
Mass Flow, Main (lb/sec)					
LOX	47.79	48.34	47.15	45.76	45.7
Methane	20.88	18.66	20.11	24.25	24.33
Mass Flow, Ign (lb/sec)					
Gaseous Oxygen	.3	.28	.4	.36	.35
Methane	.3	.27	.29	.34	.34
Mixture Ratio					
Element	2.29	2.59	2.35	1.89	1.88
Main	2.29	2.59	2.35	1.89	1.88
Overall	2.27	2.57	2.33	1.88	1.87
c* efficiency (percent) (4)	93.6	90	95.6	90.4 (2)	90.8
Throat Heat Flux (BTU/sq.in-sec) (4)	34.8	22.2	36.4	26.8	25.7
Stability	S	S	S	S	S
Frequency					
Estimated Data at the Cup (3)					
Temperature, Inj (F)					
LOX	-219	-196	-232	-232	-235
Methane	3.3	3.6	15.2	-2.4	2.4
Density, Inj (lb/cu.ft)					
LOX	59	54	61.6	61.4	62
Methane	6.7	6	6.3	6.6	6.4
Velocity, Inj (ft/sec)					
LOX	55	60	52	50	50
Methane	742	736	757	877	900
Velocity Ratio (F/O)	13.6	12.2	14.6	17.4	18.1
Momentum Ratio ($\dot{w}_f V_f / \dot{w}_o V_o$)	5.94	4.71	6.21	7.72	9.63
Mom. Flux Ratio [$(\rho V^2)_f / (\rho V^2)_o$]	21	16.54	21.8	32.5	33.82

NOTES: (1) Self-induced instability while in transition to mainstage
(2) Zirconia coating on hot gas wall (Tests 019 through 032)
(3) Conditions calculated at the LOX post tip exit plane prior to jet expansion
(4) c* efficiency and heat flux values for test durations less than 1.5 seconds are questionable

S = stable

0	021	022	023	024	025	027	028 (1)	030	031 (1)	032
52	1500	1500	1529	1492	1480	1478	1495	1489	1585	1472
06	2415	2394	2461	2467	2434	2429	2337	2330	2384	2326
41	1766	1760	1793	1759	1741	1768	1777	1782	1930	1772
	47	41	53	50	51	60	35	34	31	29
231	-238	-237	-226	-221	-225	-232	-229	-225	-233	-229
3.36	46.88	45.9	46.37	45.7	45.1	47.41	47.55	48.18	53.41	48.91
9.03	21.32	21.44	21.03	22.11	21.42	21.01	24.2	20.8	20.39	21.04
41	.37	.37	.39	.36	.38	.38	.4	.39	.45	.51
28	.3	.31	.3	.3	.3	.29	.3	.29	.27	.3
.54	2.2	2.14	2.21	2.07	2.11	2.26	1.96	2.32	2.62	2.32
.54	2.2	2.14	2.21	2.07	2.11	2.26	1.96	2.32	2.62	2.32
.53	2.18	2.13	2.19	2.05	2.09	2.24	1.96	2.3	2.61	2.32
6.8	94.2	95.9	96.7	95.3	96	93.3	91.4	93	91.1	90.7
.5	16	17.2	15.4	15	15	22.3	12.8	15.6	14.9	15.2
	S	S	S	S	S	S	S	S	S	S
-231	-238	-237	-226	-221	-225	-232	-229	-225	-233	-229
16.7	14.2	8.7	20.6	15.4	16.6	26.5	3.5	3.4	2.7	-2.1
51.6	62.8	62.6	60.5	59.4	60.2	61.6	61.1	60.3	62.1	61
5.6	9.3	6.6	6.3	6.3	6.3	6	6.8	6.8	7.3	6.9
53	50	50	52	52	51	52	53	54	58	54
685	789	768	790	829	813	840	847	731	663	721
12.9	15.7	15.5	15.3	16	16.1	16.2	16.1	13.5	11.4	13.3
5.08	7.13	7.24	6.92	7.73	7.63	7.17	8.21	5.82	4.35	5.73
17.83	36.5	25.33	24.38	27.15	27.13	25.56	28.84	20.55	15.27	20

tests. Spontaneous instabilities were encountered on five tests at nominal and subambient fuel temperature. Four of the five occurred at relatively low mixture ratio.

Performance Tests

Characteristic Velocity Efficiency

A total of 17 hot-fire tests were conducted on this program. The tests are summarized in Table II. Although c* efficiency is given for every mainstage test, the credibility of the c* efficiency value for tests with short mainstage durations is questionable. Tests 014-011, 012, 014, 020, and 022 were reviewed and analyzed for performance correlations due to the duration of mainstage conditions during the tests. Also, data from the temperature ramp tests (014-023 through 025) yield valuable information on efficiency variation with varying injection conditions. Each data point during a temperature ramp was considered psuedo-steady state because of the relatively slow nature of the transient.

Prior to transitioning to mainstage conditions for each test, a 500 millisecond prestage condition was established at full fuel flow and reduced oxidizer flow. Even though performance data from prestage shows considerable scatter, the off-nominal conditions present during prestage provide valuable data for performance correlations. Prestage conditions are presented in Table IIb for all tests which achieved mainstage except test 004. The start-up sequence used on test 004 did not allow a definite prestage condition to be established.

Figure 5 shows the variation of c* efficiency with time for a long duration performance test. Variations in c* efficiency of +/- 0.5% exist throughout the test. The mean c* efficiency shown in Figure 5 also appears to be higher during the early portions of mainstage than later in mainstage. This is most likely due to temperature measurement lag causing calculation of artificially low propellant flow rates early in mainstage. This data motivated the selection of only longer duration tests for further performance correlations.

The value of characteristic velocity used in the c* efficiency calculations was established from the chamber pressure measured at the start of the nozzle convergence and 2 inches downstream of the faceplate. A correction for Rayleigh losses and a conversion from static to total pressure were made to chamber pressure before calculating the characteristic velocity. Of course, the pressure measured at the start of nozzle convergence did not include the Rayleigh correction. C* efficiency also was corrected for heat loss to the chamber coolant between the injector and the throat although this effect was small (< 0.7%). For Phase C testing (test 027 though 032) chamber pressure was not measured at the position at the start of nozzle convergence to eliminate a potential problem encountered early in the test program in which hot gas pumping occured within the downstream pressure port.

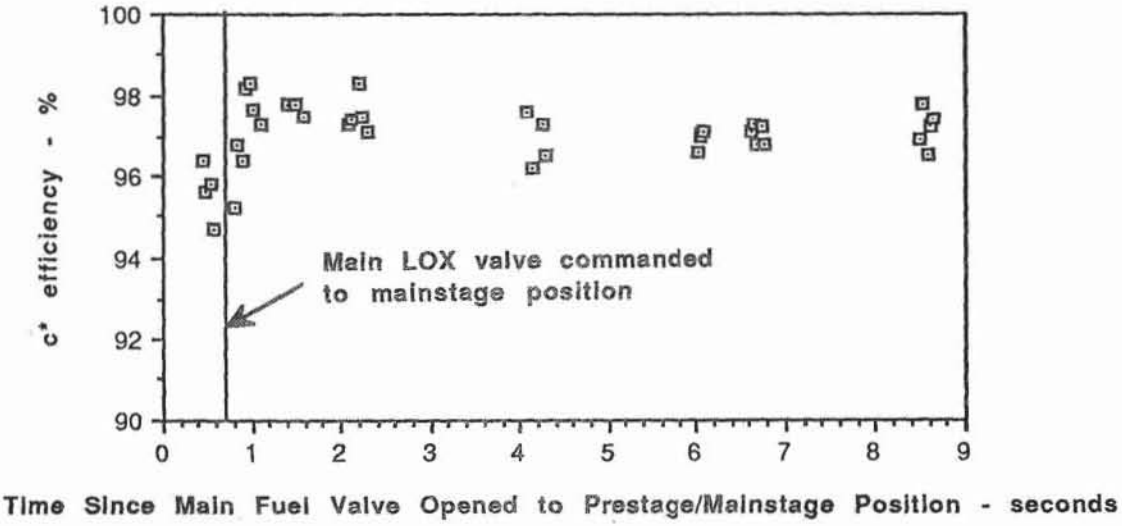

Figure 5 - C* Efficiency Variation with Time (Test 014-014)

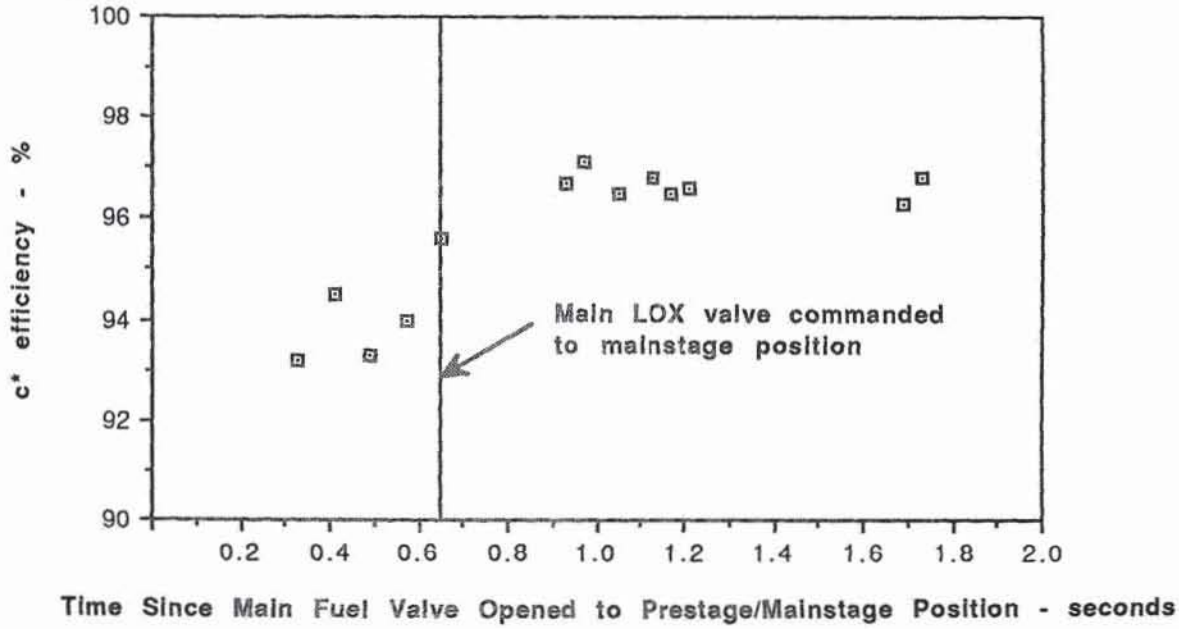

Figure 6 - C* Efficiency Variation with Time (Test 014-012)

The mainstage mixture ratio range for the overall test series was from 3.0 to 3.69. However, the maximum mixture ratio during a performance test was 3.45 on test 014-012. The plot of c* efficiency versus time for test 014-012 is shown in Figure 6. Both Figure 5 and Figure 6 illustrate that the c* efficiency during prestage was considerably lower than mainstage efficiency. Potential reasons for the low prestage efficiency will be discussed in later paragraphs. Mixture ratio during prestage typically fell between 1.85 and 2.70 while prestage chamber pressure was approximately 1480 psia.

Since the coaxial injector tested is dependent on shear between the fuel and oxidizer streams to acheive atomization and mixing, parameters which affect propellant stream shear have been plotted against c* efficiency in an attempt to determine if any meaningful correlations between these parameters and c* efficiency exist. It should be recognized that there is an interdependence between many of the parameters of interest and therefore it is difficult to arrive at strong, consistent, simple correlations. For instance, decreasing fuel temperature increases fuel injection density which decreases fuel injection velocity which has a corresponding effect on injection velocity ratio and momentum ratio ($\dot{w}_f V_f / \dot{w}_o V_o$). Over the range of conditions tested, no well-defined correlation was found between c* efficiency and mixture ratio or injection velocity differential. This agrees with the results from previous LOX/methane coaxial element testing at NASA-MSFC (Ref. 10) which involved similar hardware except that a rigimesh faceplate was utilized instead of the solid copper faceplate used on this program. Figure 7 shows the affect of propellant momentum ratio on c* efficiency. It appears from the figure that efficiency drops off if the momentum ratio is greater than 2.9. Unfortunately, no additional mainstage test data is available for momentum ratios greater than 2.9. Figure 8 shows data from test 014-022 which further supports the momentum ratio correlation, however, both chamber pressure and mixture ratio are changing along with momentum ratio. Figure 9 illustrates the change in mixture ratio that occurred in transition from prestage to mainstage. Plots similar to Figure 7 and 8 are obtained if efficiency is plotted against injection velocity ratio.

For all of the tests performed for this program, the calculated c* efficiency in prestage was typically 4% lower than the mainstage efficiency. It is interesting to note that NASA-MSFC testing included long duration tests at prestage conditions (Pc from 1200 to 1530 psia, MR from 2.48 to 3.2) and recorded c* efficiencies as high as 99.7% for these tests.

Testing of a 61 element swirl coaxial injector at NASA-MSFC indicated a potential correlation between c* efficiency and LOX flow per element (Figure 10) where increasing LOX flow per element decreases efficiency. Figure 11 shows an opposite trend exists for LeRC solid faceplate injector if prestage performance data is considered. If only mainstage data is considered, no significant trend is apparent in Figure 11. Data from testing the 82 element shear coaxial element injector at MSFC also indicates that LOX flow per element has no significant effect on c* efficiency

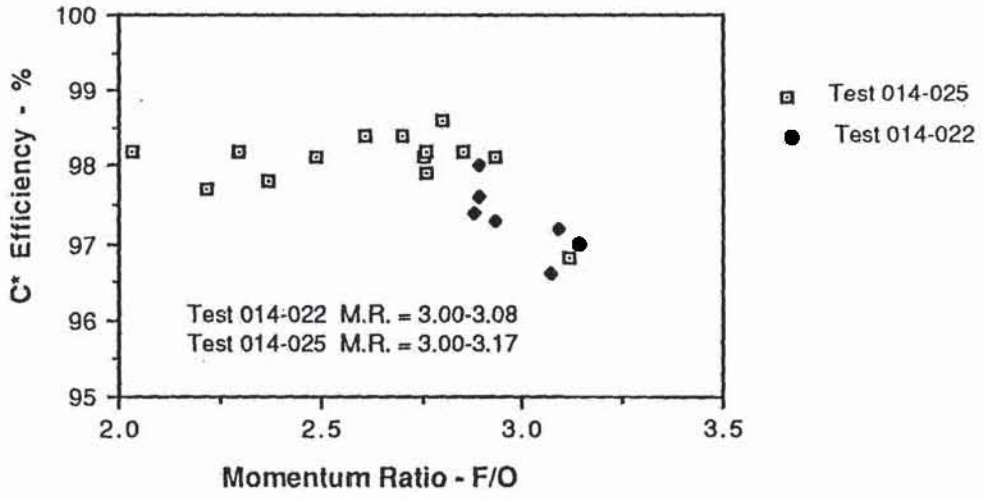

Figure 7 - C* Efficiency Variation with Injection Momentum Ratio

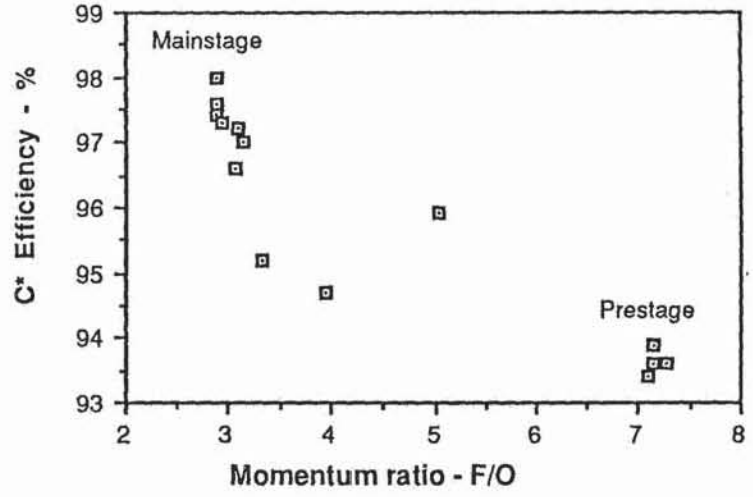

Figure 8 - C* Efficiency Variation with Injection Momentum Ratio (Test 014-022)

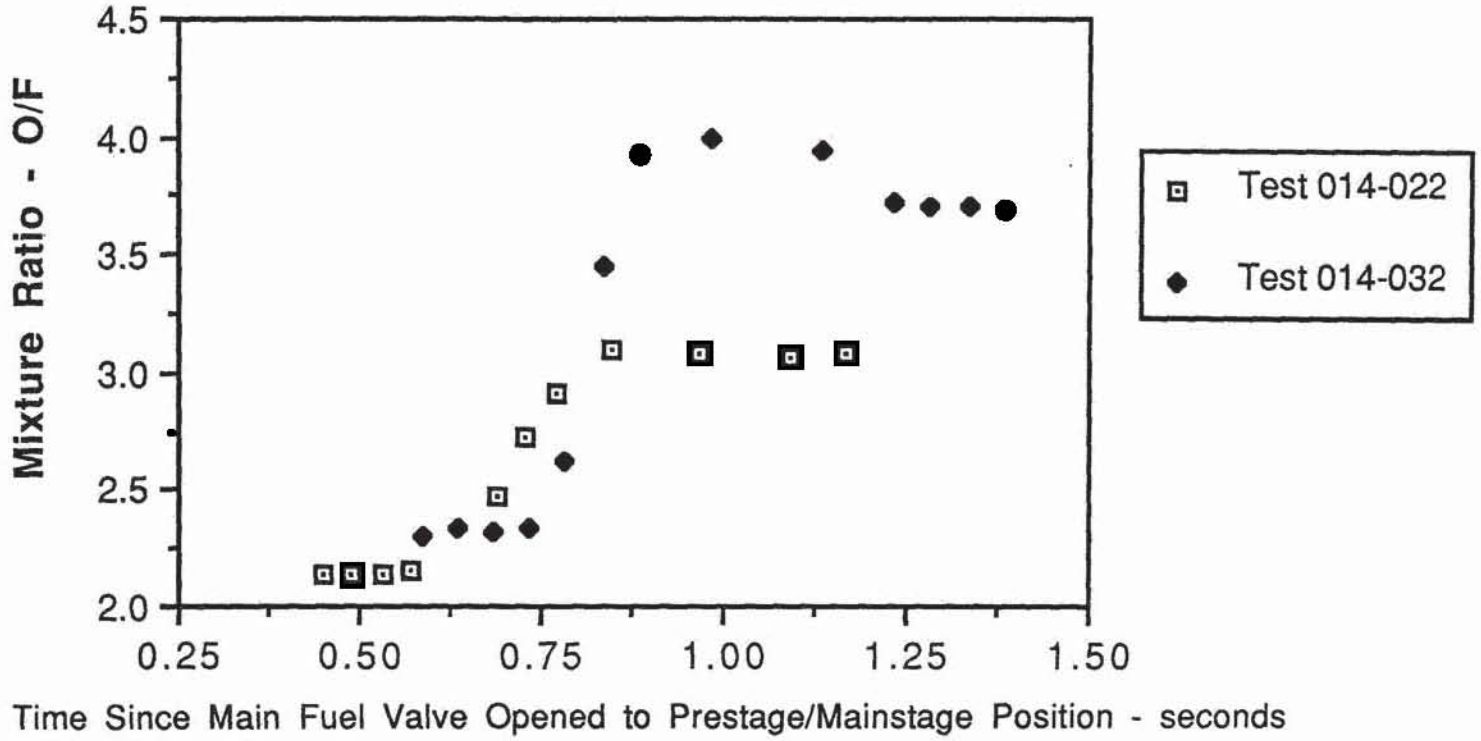

Figure 9 - Mixture Ratio Variation with Time

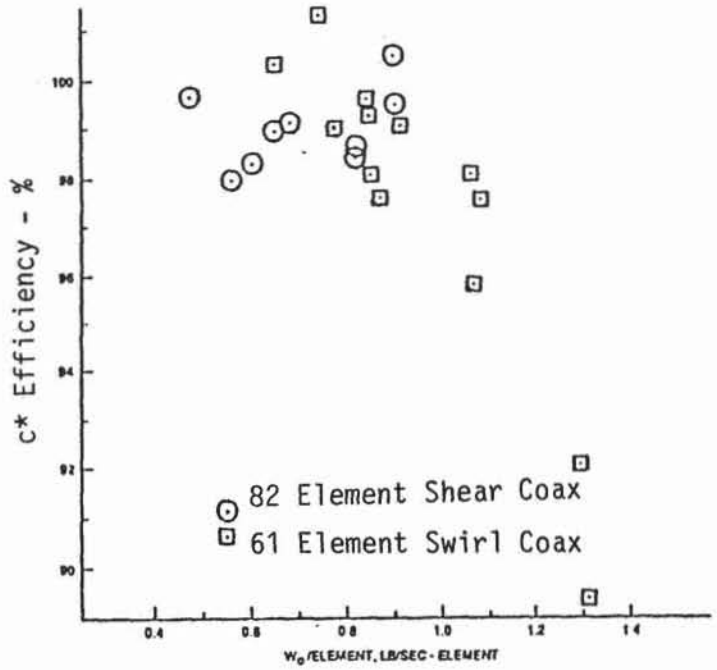

Figure 10 - Performance Variation with LOX Flowrate per Element for NASA-MSFC injectors (Reproduced from Ref. 10)

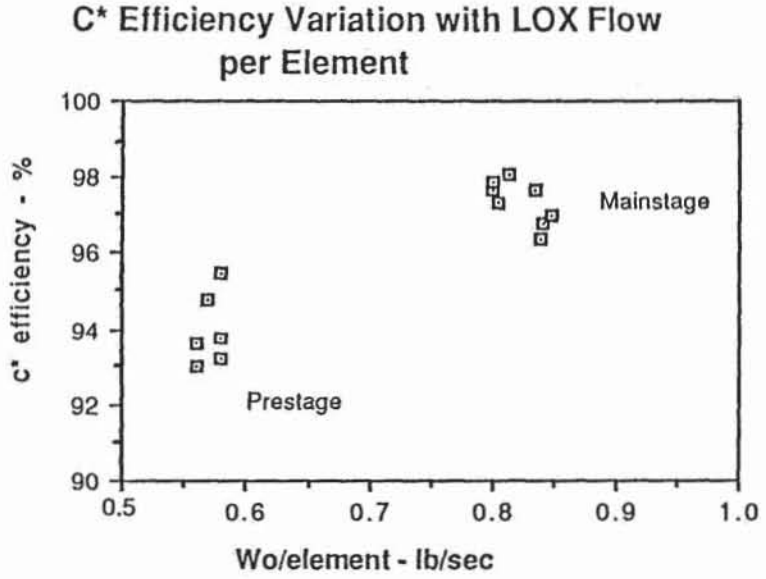

Figure 11 - C* Efficiency Variation with LOX Flowrate for the NASA LeRC Injector

(Figure 10). The reasoning behind correlating c* efficiency with LOX flow per element is based on the premise that an increase in LOX flow will disproportionally increase LOX velocity relative to the methane velocity (due to the compressibility of methane) if mixture ratio is held constant. More importantly, the fuel will also have insufficient available energy to adaquately atomize and mix with the LOX stream.

Performance Model Analysis

Past coaxial injector experience has indicated that coaxial injectors should theoretically behave in the manner shown in Figures 12 and 13. Figure 12 shows a plot of vaporization c* efficiency versus relative momentum flux $[\rho_f(V_f - V_o)^2]$. The vaporization efficiency increases with increasing relative momentum flux due to increasing atomization rate and decreasing droplet size. The decrease in droplet size (and therefore an increase in the vaporization rate) is due to increased shear between the coaxial streams. Shown in Figure 13 is the mixing c* efficiency versus the momentum flux ratio $(\rho_f V_f^2/\rho_o V_o^2)$. The minimum in the curve is due to reduced turbulent mixing when the momentum flux ratio is close to one. On the left side of the minimum, mixing is being driven by the liquid jet momentum. On the right side of the minimum, mixing is being driven by the gas momentum. At large momentum flux ratios, stream integrity limitations cause an eventual decrease in efficiency. It has been shown experimentally in cold-flow tests that the gas can have sufficient energy (high momentum flux) to atomize the liquid stream in a manner which forces the liquid droplets outside of the gas stream, which causes a reduction in the mixing efficiency. The overall engine c* efficiency is the product of the vaporization and mixing efficiencies. For a particular coaxial engine, the overall c* efficiency can increase with increasing momentum ratio due to improved vaporization and/or mixing or can decrease with increasing momentum ratio due to a reduction in mixing. Figure 14 shows the solid faceplate test data momentum flux ratio correlation. The trend would indicate that mixing losses due to LOX stream break-up and/or turbulent mixing are causing the lower prestage performance.

The data generated by the Coaxial Injection Combustion Model (CICM) code also gives insight into potential mechanisms causing the lower c* efficiency at high momentum flux conditions. Table III lists the CICM predicted c* efficiency and nozzle stagnation chamber pressure for several tests. The code estimates the vaporization limited performance of a single coaxial element. The code was anchored to the temperature ramp tests because it was suspected that the performance on those runs was more limited by vaporization losses than the ambient methane tests were. To anchor CICM to the temperature ramp tests, it was necessary to limit the maximum droplet size to 305 microns. Additionally, for test 004, a case was run in which the LOX flow was assumed to be separated from the LOX post chamfer. On tests other than test 004, the LOX post chamfer was reduced to six degrees (from fifteen degrees) and thus LOX flow separation from the post chamfer was

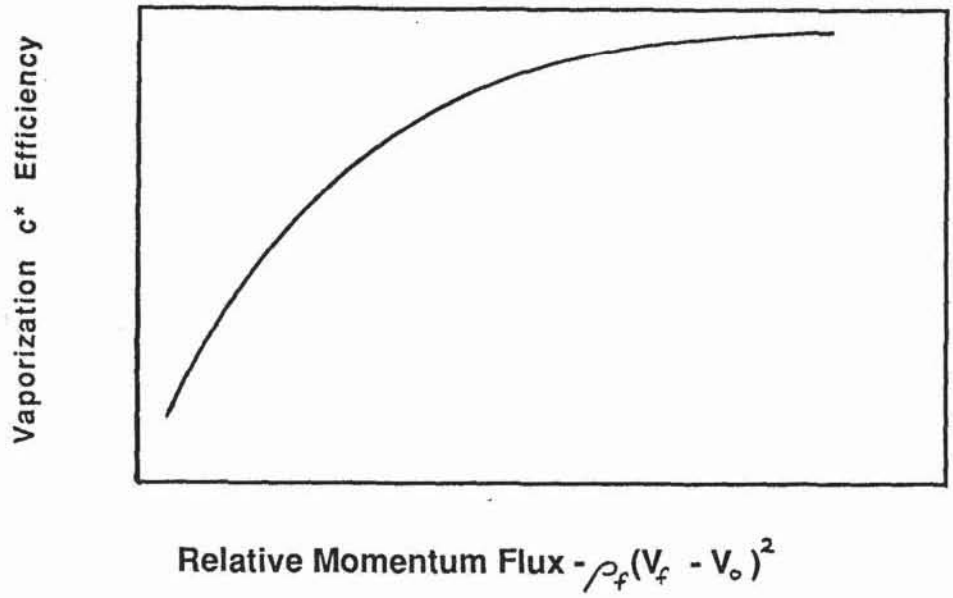

Figure 12 - Coaxial Characteristic Vaporization Performance

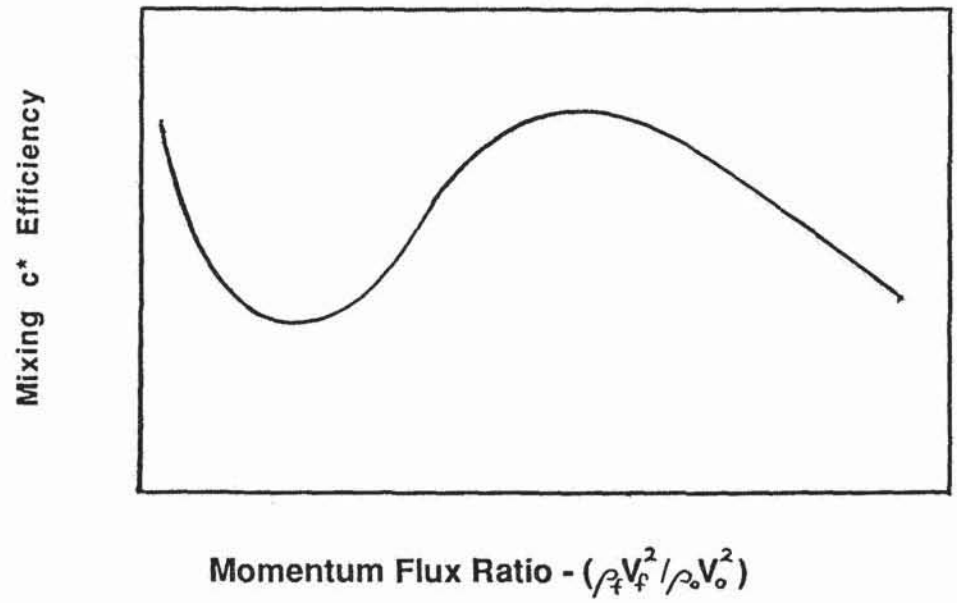

Figure 13 - Coaxial Characteristic Mixing Performance

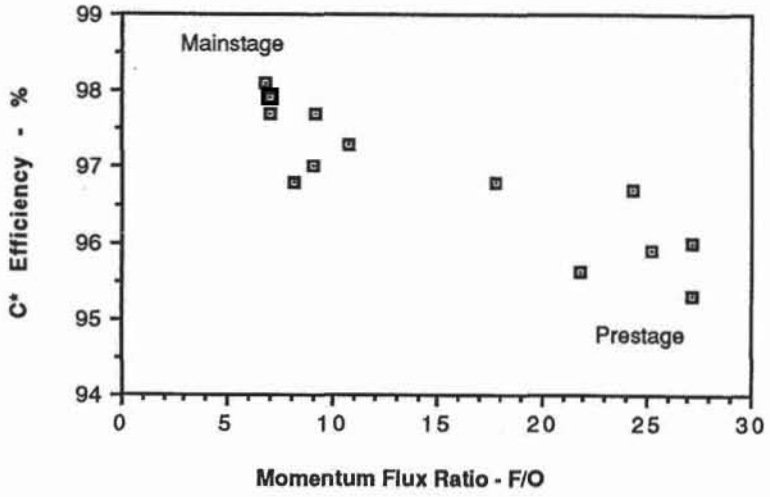

Figure 14 - C* Efficiency Variation with Momentum Flux Ratio

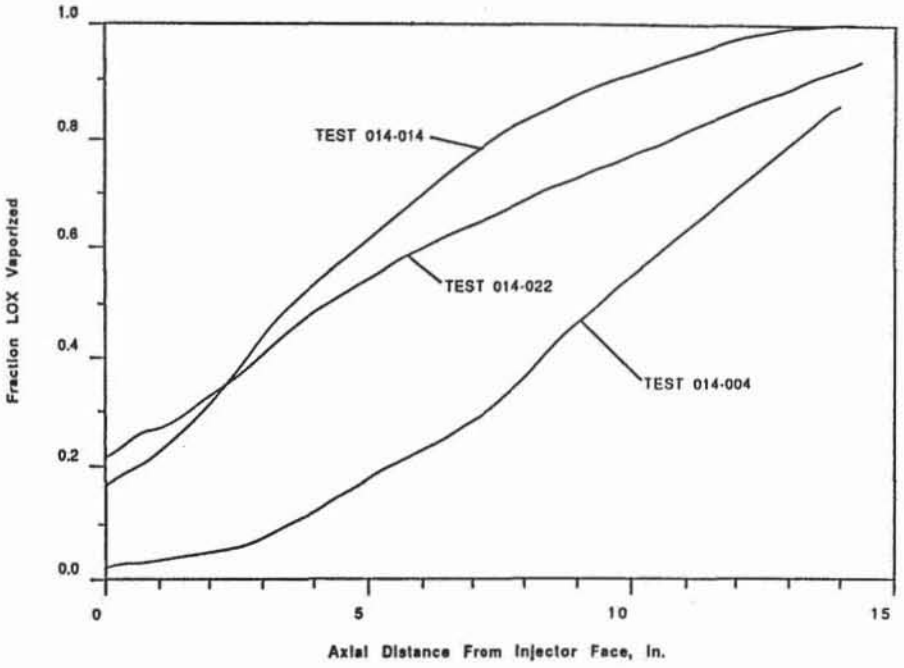

Figure 15 - CICM Code Predictions of Axial Vaporization Distributions for Various Tests

not assumed. Figure 15 shows the results of the CICM analysis. As Figure 15 and Table III indicate, CICM over-predicted LOX vaporization (thus c* efficiency) and under-predicted nozzle stagnation pressure for all of the runs which were not temperature ramped and where LOX flow separation from the post chamfer was not assumed. It should be noted that mixing losses which may be substantial on tests with high momentum flux ratios (ie. test 014-019 which went unstable before mainstage) are not accounted for in the CICM code. The code indicates that the c* efficiency during ambient temperature methane tests is not atomization or vaporization limited and thus suggests that mixing losses predominantly control efficiency since no other losses or sources of error would explain the lower performance.

Performance Summary

For the testing conducted on this contract, at a mixture ratio range from 3.01 to 3.45, ambient fuel temperature, and a chamber pressure of 2000 psia, the average c* efficiency was 97.2% with a variation between tests of +/- 0.5%. Temperature ramping tests yielded average c* efficiencies between 97.7 and 98.1% at mixture ratios from 3.06 to 3.19, at a chamber pressure of 2000 psia, and fuel injection temperatures from 437 to 444 degrees R. The apparent slight increase in c* efficiency is probably caused by lower momentum flux ratio which decreased mixing losses. A correlation between c* efficiency and momentum flux ratio which utilized both mainstage and prestage data indicates that mixing losses cause performance degradation (~4%) at low chamber pressure and low mixture ratio (prestage) conditions.

Heat Flux

Chamber heat flux profiles for three of the mainstage performance tests are shown in Figures 16 through 18. To increase chamber durability, a zirconium oxide (zirconia) coating was applied to the hot-gas wall of the combustor and nozzle for all tests after test 014-014. The heat flux profile of the zirconia coated chamber is presented in Figure 19. Although the heat flux in the cylindrical combustor section was not significantly affected by the coating, the peak heat flux in the throat was reduced by over 60%. Heat flux comparisons between tests which used the coated chamber are not possible because of the degradation of the zirconia coating as hot-fire time accumulated.

The peak heat flux for tests 014-011 and 012 is greater than 95% of the theoretical value for LOX/H2. Test 014-014 had a peak heat flux of 58 BTU/sq.in-sec (approximately 89% of the theoretical LOX/H2 value) and, due to the duration of the test, is considered the most accurate value. Due to the magnitude and duration of the transients in the water coolant system, mainstage tests less than 2 seconds long (ie. tests 011 and 012) yield artificially high heat flux values. It must be pointed out that the peak heat flux value for test 014-014 is significantly higher than the peak heat flux values for the NASA-MSFC 82 element coaxial injector. Testing of the MSFC injector yielded peak heat fluxes (29.4 to

TABLE III - CICM Performance Predictions

Test		CICM Predicted C* Efficiency (%)	CICM Predicted $Pc_{n.s}$ (psia)	Test Data C* Efficiency (%)	Test Data Pc_{ns} (psia)	CICM Conditions
-004	(1)	100	1883	92.1	1930	305 micron maximum droplet diameter
-014		100	1927	97.0	2010	
-022		99.14	1976	97.3	2030	
-023		97.40	1980	98.1	2037	
-004	(2)	91.55	1798	92.1	1930	

(1) LOX flow attached to LOX post chamfer
(2) LOX flow separated from LOX post chamfer

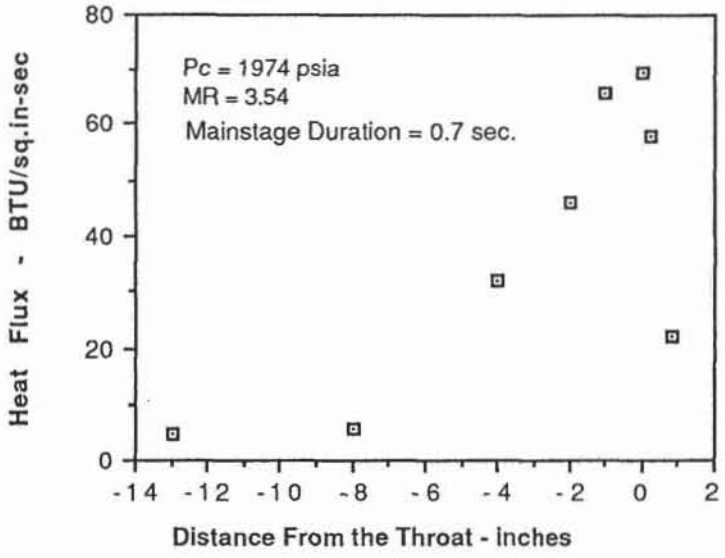

Figure 16 - Test 014-011 Heat Flux Profile

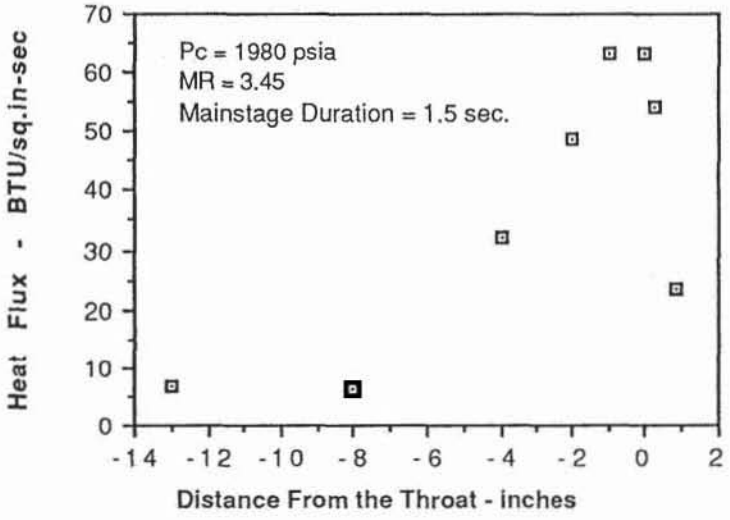

Figure 17 - Test 014-012 Heat Flux Profile

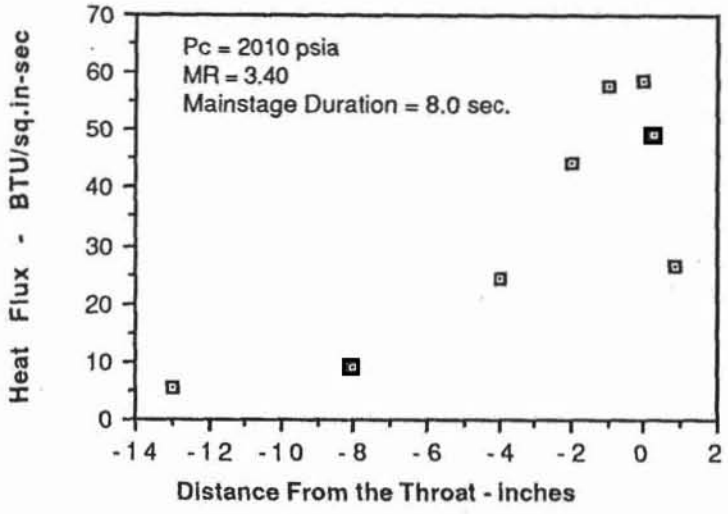

Figure 18 - Test 014-014 Heat Flux Profile

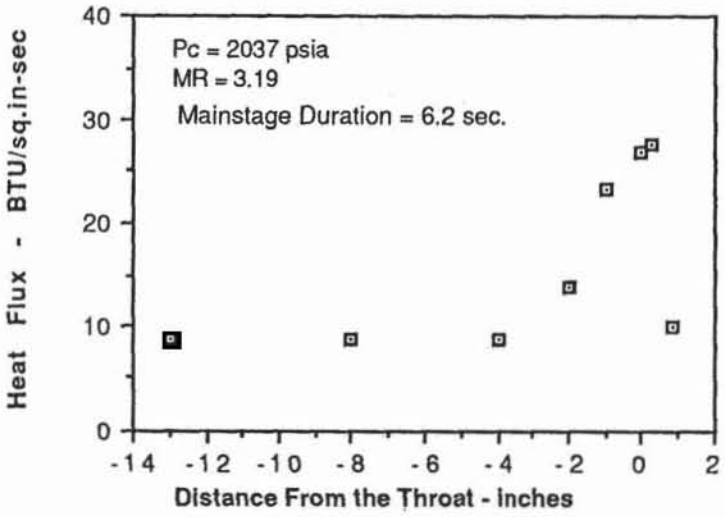

Figure 19 - Test 014-023 Heat Flux Profile (Zirconia Coated)

46.2 BTU/sq.in-sec) which were 60 to 74% of the theoretical value for LOX/H2. Further testing and analysis are necessary to resolve this discrepancy.

Fuel Temperature Ramp Stability Testing

One of the most significant test efforts in this program was the temperature ramping stability rating demonstration achieved on tests 014-023, 024, and 025 in which the injector was driven unstable during fuel temperature ramp. Test 014-020 was also temperature ramped but was cut early due to fuel valve oscillations, and did not exhibit any instabilities. The general characteristics of these tests are shown in Figure 20. The test duration was from 6.2 to 6.5 seconds. After about 2 seconds, the fuel temperature was reduced in a continuous fashion at approximately 20 degree R per second. The measured manifold fuel temperature variation during a ramp test is shown relative to the overall test sequence in Figure 21.

Figure 22 shows that the mixture ratio was held relatively constant by the servo-controlled fuel feed system during the temperature ramp. See Figure 10 in reference 1 for a similar plot of hydrogen temperature vs mixture ratio during typical LOX/hydrogen temperature ramp tests at NASA LeRC.

As shown in Table II, all three tests went unstable at 14 kHz. However, 14 kHz does not correspond to any expected acoustic combustor modes. The hydrogen temperature ramp test data primarily exhibited 1T mode instabilities. For comparison the first tangential mode is at about 5.2 kHz. The nearest combustor modes are the 3T-4L, 1R-5L and 8L at 13.7, 13.9 and 14.2 kHz, respectively. These modes correspond to a chamber acoustic velocity corresponding to well-mixed equilibrium combustion at the injected mixture ratio. However a pure transverse mode at a reduced chamber acoustic velocity seems a more likely candidate for the 14 kHz oscillation based on past coaxial injector instability test experience.

Prior to the onset of high amplitude 14 kHz oscillations, the high frequency records indicated low level 14 kHz and 8.6 kHz peaks on the oxidizer manifold and accelerometers as well as additional accelerometer activity that shifted in frequency from approximately 12 kHz to 14 kHz during the temperature ramp. Figures 23 and 24 which are isoplots (frequency content vs time) for the oxidizer manifold pressure transducer and axial accelerometer show these phenomena.

Figure 25 shows the accelerometer and manifold high frequency pressure transducer brush chart records before and during the high amplitude 14 kHz activity. The indicated amplitudes on the accelerometers were from 200 to 900 g's. However, the accelerometers utilized have an advertised range of up to 10 kHz. Hence, the actual acceleration levels were likely somewhat different. Fuel and oxidizer manifold pressure oscillations were about 100 and 500 psi peak-to-peak, respectively, during high

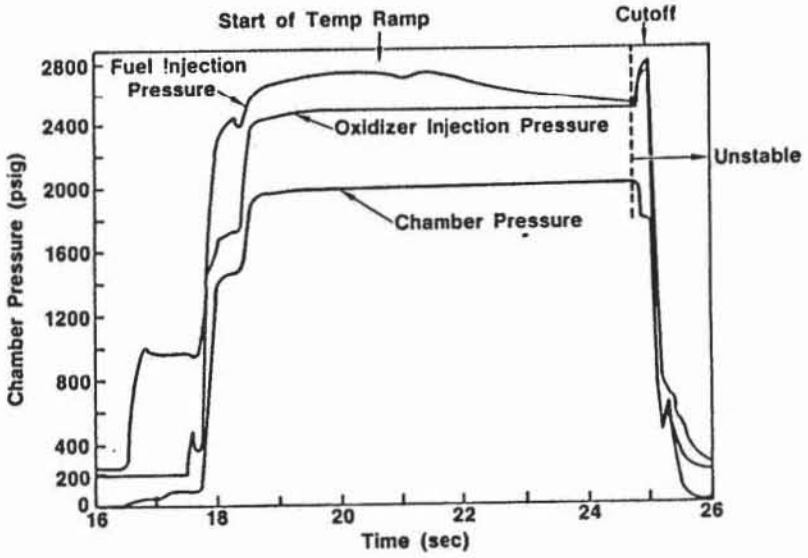

Figure 20 - Manifold and Chamber Pressures During Test 014-025 (A Typical LOX/Methane Fuel Temperature Ramp Test)

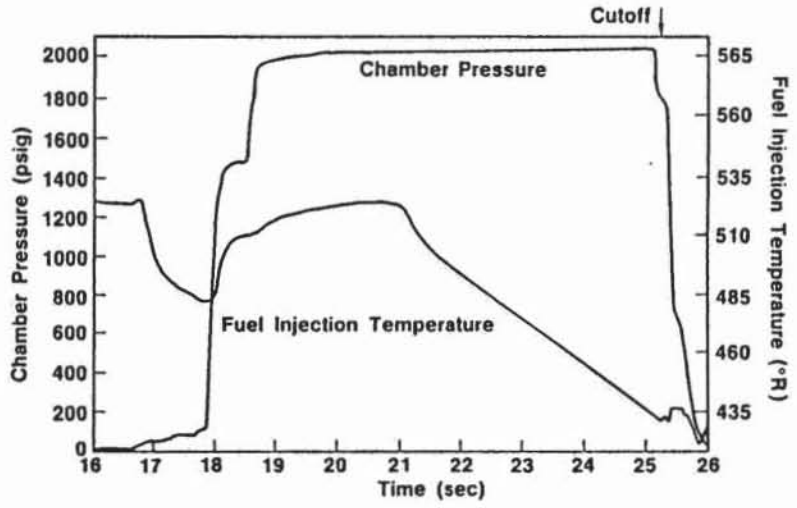

Figure 21 - Manifold Fuel Temperature Variation (A Typical Fuel Temperature Ramp Test Using the LeRC Hardware)

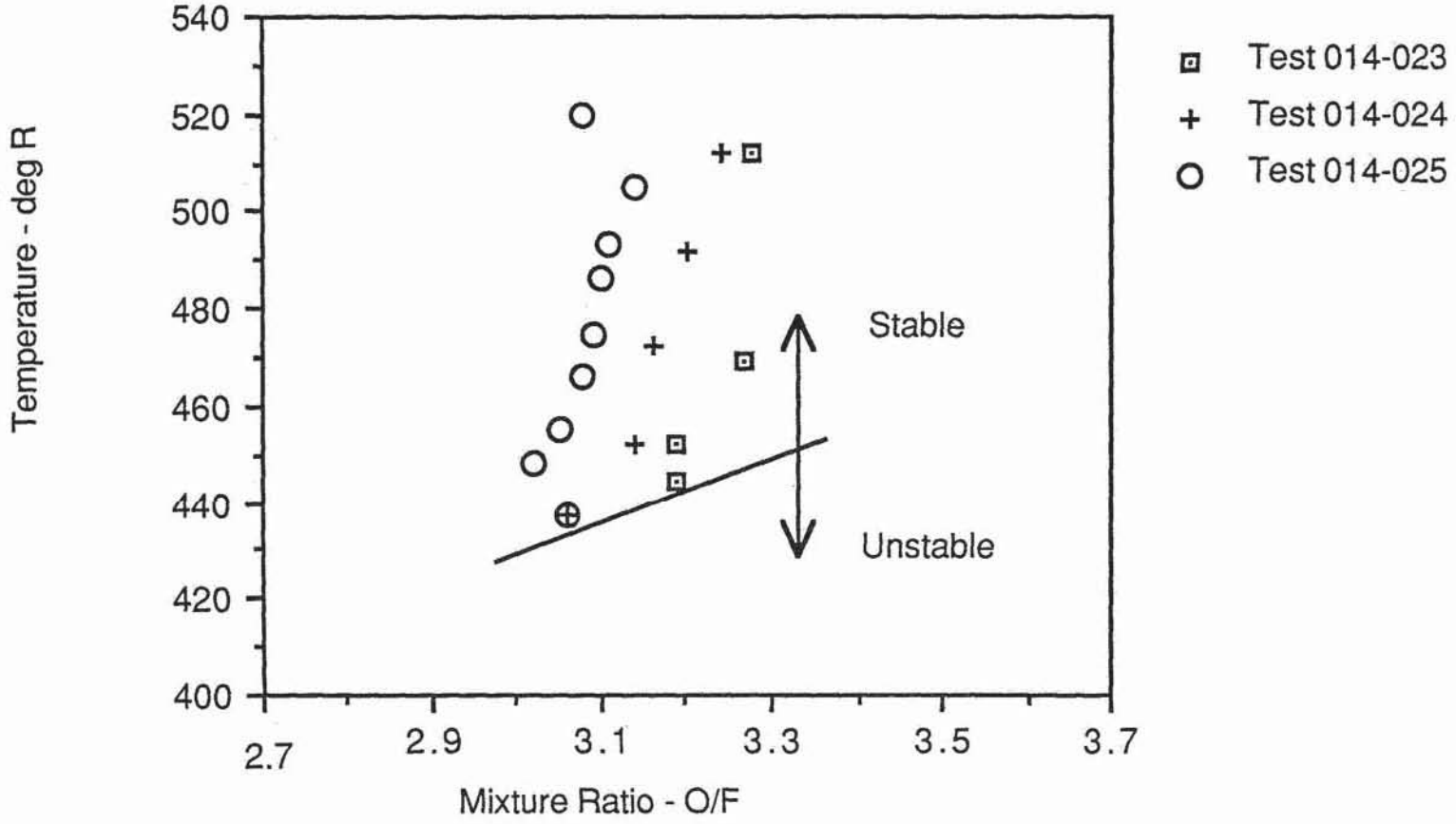

Figure 22 - Temperature versus Mixture Ratio during LOX/Methane Temperature Ramp Tests.

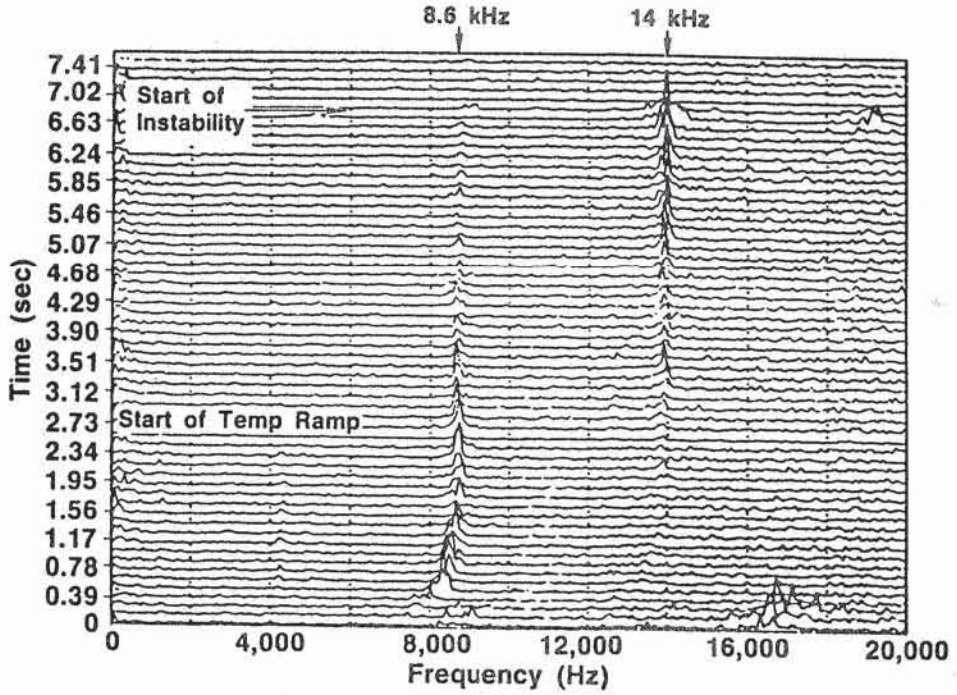

Figure 23 - Oxidizer Manifold High Frequency Pressure Transducer Isoplot for Test 014-025

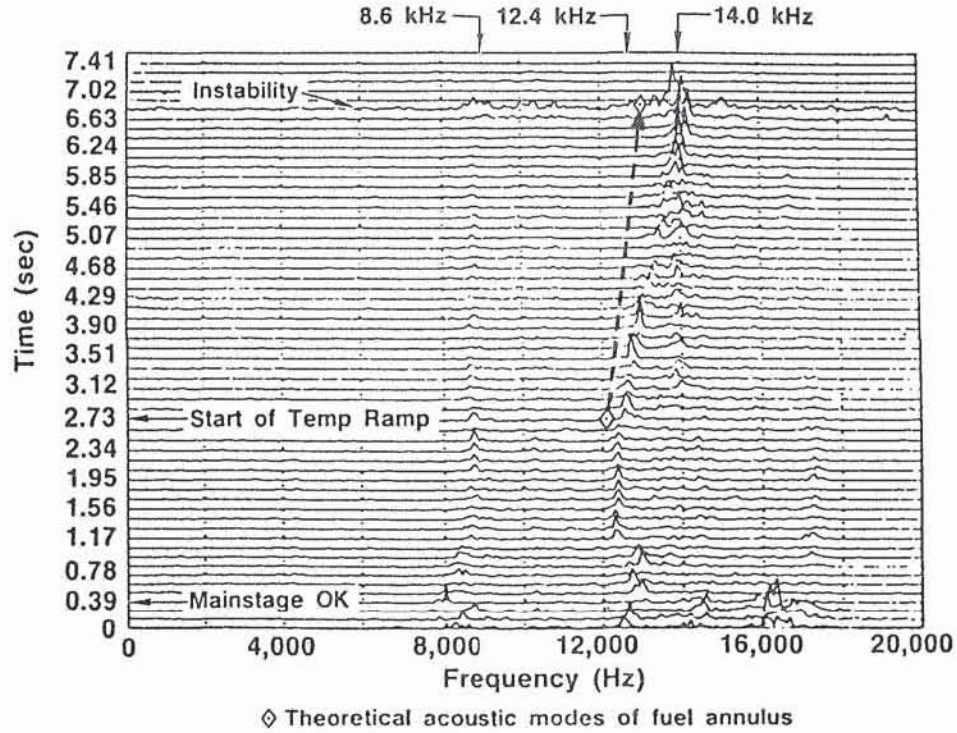

Figure 24 - Axial Accelerometer Isoplot for Test 014-025 - Theoretical Fuel Annulus Tuned Frequency Variation Shown

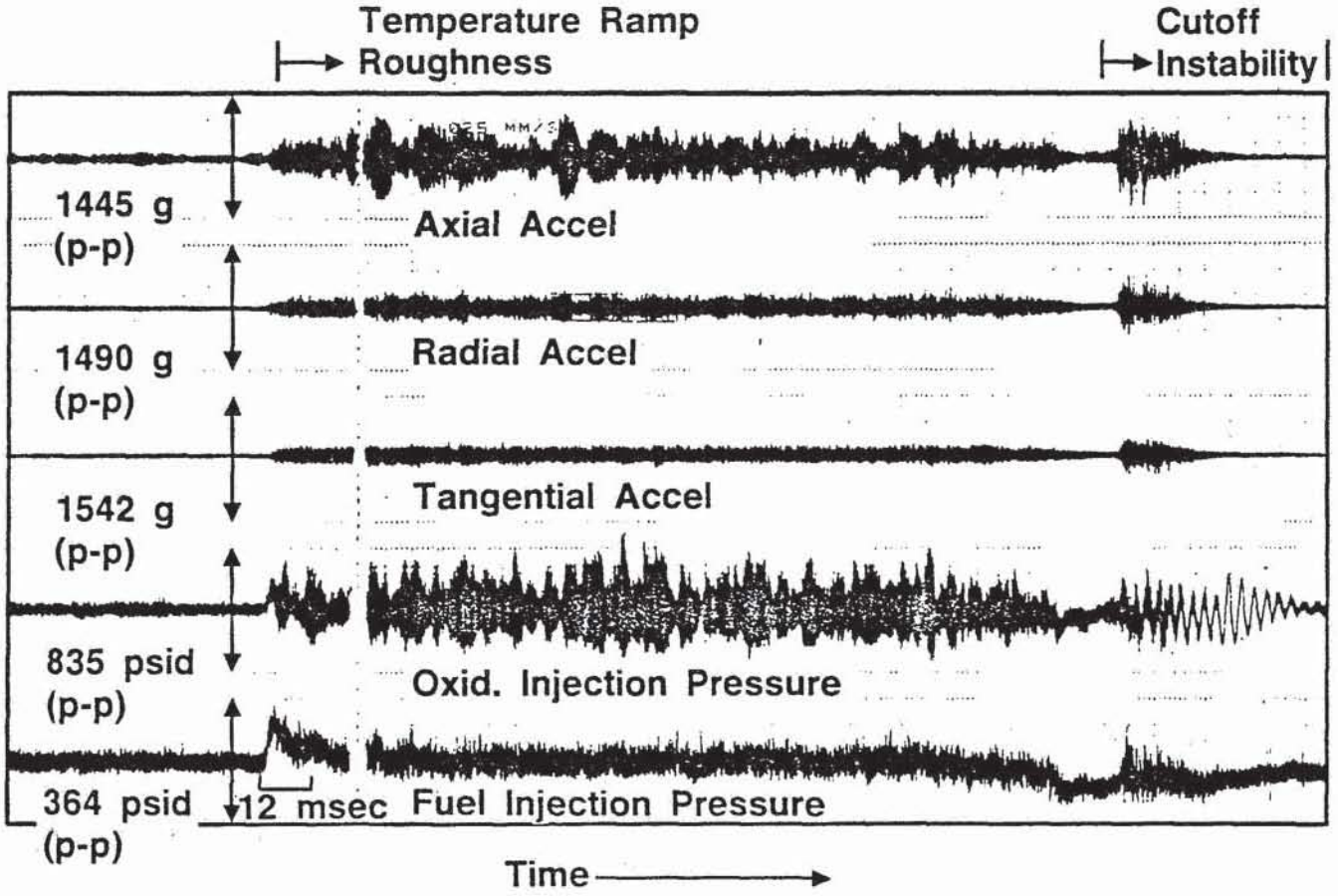

Figure 25 – Brush Chart of High Frequency Transducers for Test 014-025

amplitude activity. As indicated in Figure 20, the fuel manifold pressure typically decreased (as the flow resistance decreased due to higher fuel density) until the fuel and oxidizer manifold pressures are equal. The instability occurs at that point and both manifold pressures rise the same amount (approximately 300 psi). Simultaneously, the chamber pressure dropped approximately 250 psi. These step changes in pressure are similar to behavior seen on LOX/hydrogen temperature ramping tests.

Analysis of the Temperature Ramp Testing

With regard to the fuel temperature ramping tests, the observed frequencies may be related to potential axial resonance or "organ pipe" modes of both the fuel annulus and oxidizer post coupled with chamber acoustics. A LOX post mode was found to be the cause of a 4400 Hz oscillation on the J2-S (Ref. 12), while fuel annulus dynamics at low fuel temperature were investigated in support of temperature ramp testing (Ref. 13). To better understand the stability characteristics of this injector, a model was selected in which the axial dynamic characteristics of the LOX feed system is modeled based on one dimensional wave (water hammer) equations. Similar equations were used to model the propellant manifold, propellant passages in the element and longitudinal thrust chamber modes. Both lumped resistances at the ends of the acoustic elements and distributed resistances were considered. Open loop gain (ratio of injector flow variation to combustor pressure variation) and phase angle were obtained. Theoretical modes for the LOX post were computed. For a LOX temperature of 195 degrees R at 2200 psia, the LeRC post exhibits open loop gain peaks at approximately 4.0, 8.6, and 13.6 kHz as shown on Figure 26. Also shown on that figure are the MSFC hardware LOX post modes. It should be noted that the calculated absolute magnitude of the gain has not been anchored although the agreement with the observed modes is excellent. For example, Figure 23, which shows an isoplot of oxidizer manifold pressures from test 014-025, indicates a decreasing amplitude 8.6 kHz mode and an increasing amplitude 14 kHz mode which appear to correspond to the two highest theoretically calculated frequencies to within 5%.

The characteristic modes of the fuel annulus depend on the fuel acoustic velocity which for supercritical methane is a function of both temperature and pressure. A simple analysis of the fuel annulus acting as a quarter-wave tube predicts modes that closely match the observed data. At the start of fuel temperature ramping, the fundamental mode of the fuel annulus was approximately 11.9 kHz, based on an annulus fuel temperature of 500 degrees R and a pressure of 2348 psia. That fuel temperature is calculated for the annulus based on an assumed isentropic process while the pressure represents an average of the manifold and chamber pressures. The frequency calculated is reasonably close to the 12.4 kHz frequency seen on the accelerometers before the start of the temperature ramp. In making such comparisons some allowance should be made for the potential that structural modes may influence the measured frequencies. At the conclusion of fuel temperature ramping, the predicted annulus conditions of

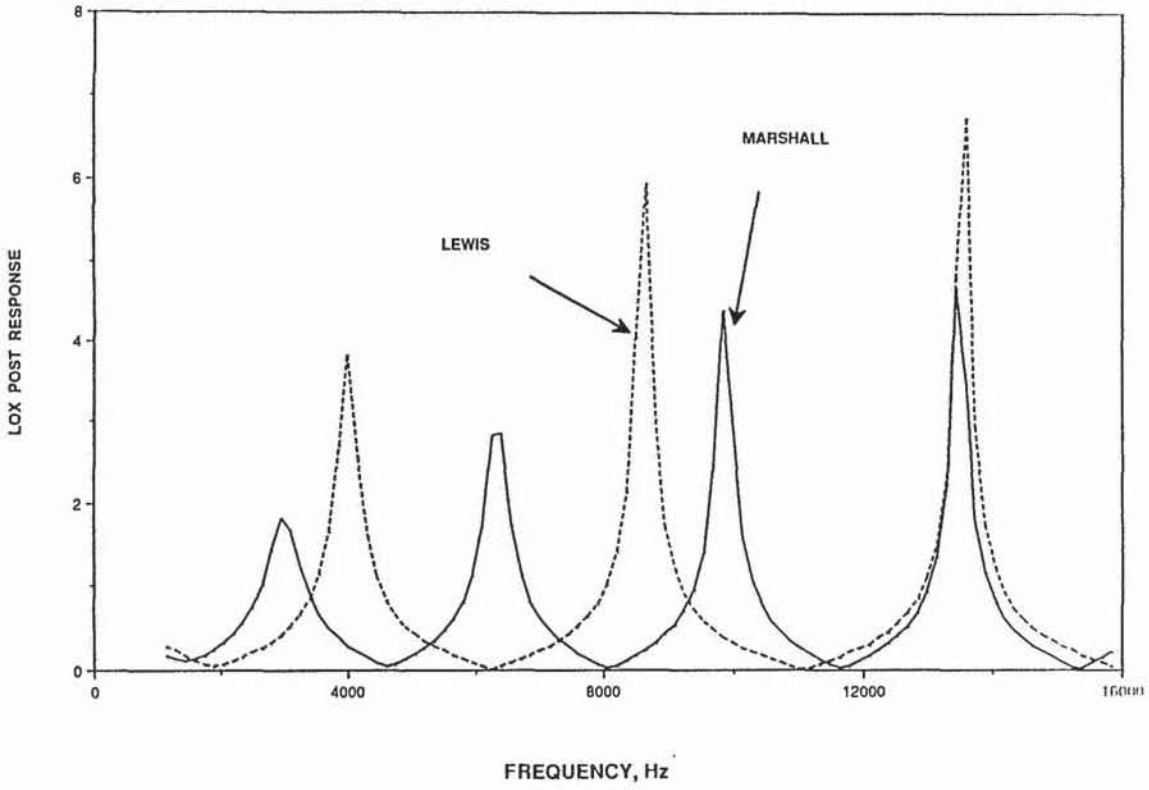

Figure 26 - LOX Post Perturbation Flow Response for NASA-LeRC and NASA-MSFC LOX/Methane Injectors

2266 psia and 426 degrees R yield a frequency of 12.8 kHz. A review of methane properties indicates that a monotonic increase in methane acoustic velocity and fuel annulus resonant frequency can be expected during temperature ramping. This is illustrated in Figure 24. The dashed line is a linear interpolation between the starting and final conditions and shows the general trend is in agreement with the data. The fact that the data indicates activity at slightly higher frequencies than the analysis may be related to coupling with the 13.6 kHz LOX post mode. This issue is also considered with the 1-D wave model in the Stability Modeling section.

Comparisons of Spectral Energy Distributions

It is useful to evaluate the energy spectra (power spectral densities or PSD's) for various phases of the testing to evaluate the effects of changing hardware and instrumentation. Nominal operational levels can be established to some degree on the basis of these PSD's to assist in identifying combustor stability characteristics. Transfer functions relating the relative phase and amplitude of accelerometers which were present for all the tests to that of the high frequency pressure transducers which were only available for short duration testing have also been evaluated. These functions provide a limited means of estimating the pressure oscillation levels for tests in which no high frequency pressure transducers were available.

Shown in Figures 27-31 are accelerometer and chamber high frequency pressure transducer data from tests 004, 011, and 030 for stable operation. Peaks in the accelerometer PSD's are typically at 8 to 8.5 kHz, 10 kHz and 12 to 13 kHz with an occasional peak in the 4 kHz range as on test 004. Strong test to test variations in relative amplitudes exist, making the determination of an envelope curve difficult. However, as shown in the figures, the 8 to 8.5 kHz activity appears frequently although as on test 004 it may simply be a harmonic of the 4 kHz mode. For the chamber pressure transducers, the peaks primarily occur at 4 and 8 kHz and also show strong test to test variation. The composite rms amplitudes for the accelerometers are in the range of 20 to 60 g's rms when a 25 kHz low pass filter is used. On tests such as 011 and 030 in which a 20 kHz low pass filter was employed, the rms range drops to 6 to 20 g's with the 0-10 kHz range accelorometers and 10 to 30 g's for the 0-20kHz transducers used in the last five tests. The substantial change in level gives a relative estimate of the amounts of activity above and below 20 kHz, much of which may be noise considering the instrument ranges. Considering all of the tests in which high frequency chamber pressure transducers were installed, the stable rms pressure amplitudes ranged from 10 to 40 psi, independent of the transducer installation and the low pass filter range.

After the instability has been initiated on a given test and for a given mode, the relative maxima in the energy spectra occurred at the same frequencies. Figures 32-36 show power spectra for the unstable portions of tests 004, 025 and 030. Primary frequencies and harmonics are evident. In the case of the accelerometers, the

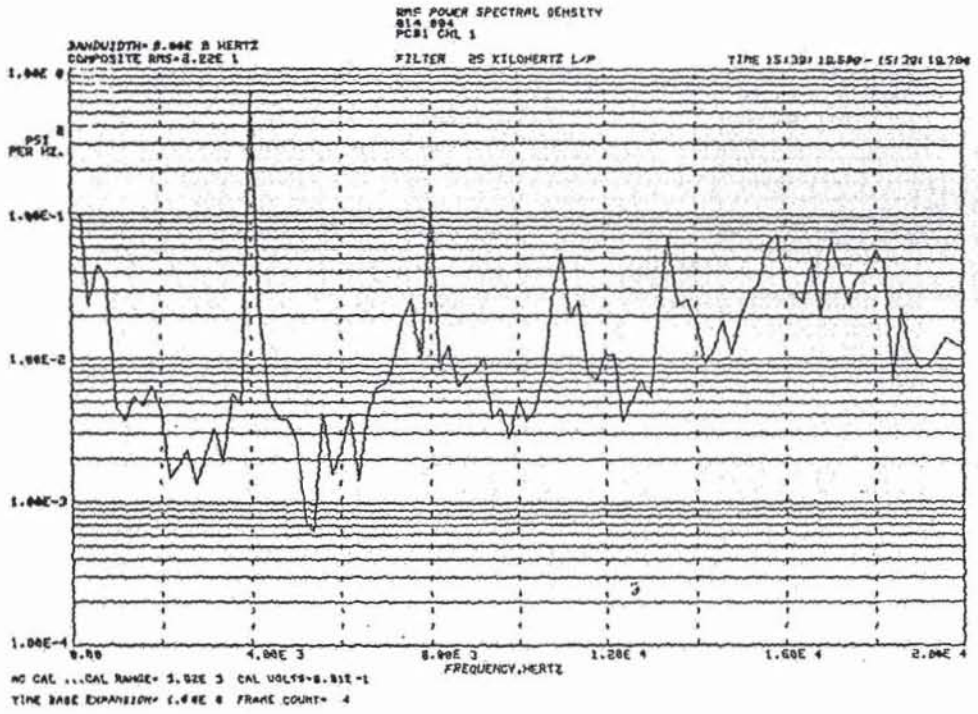

Figure 27 - Chamber High Frequency Pressure Transducer Power Spectral Density for Test 014-004 During Stable Mainstage Operation

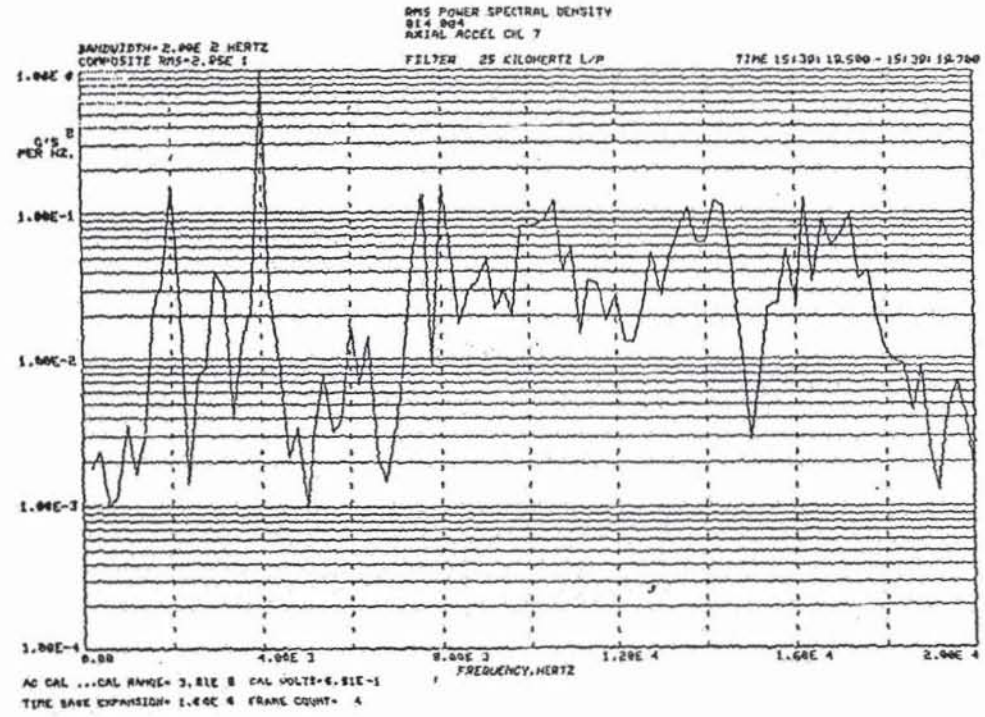

Figure 28 - Axial Accelerometer Power Spectral Density for Test 014-004 During Stable Mainstage Operation

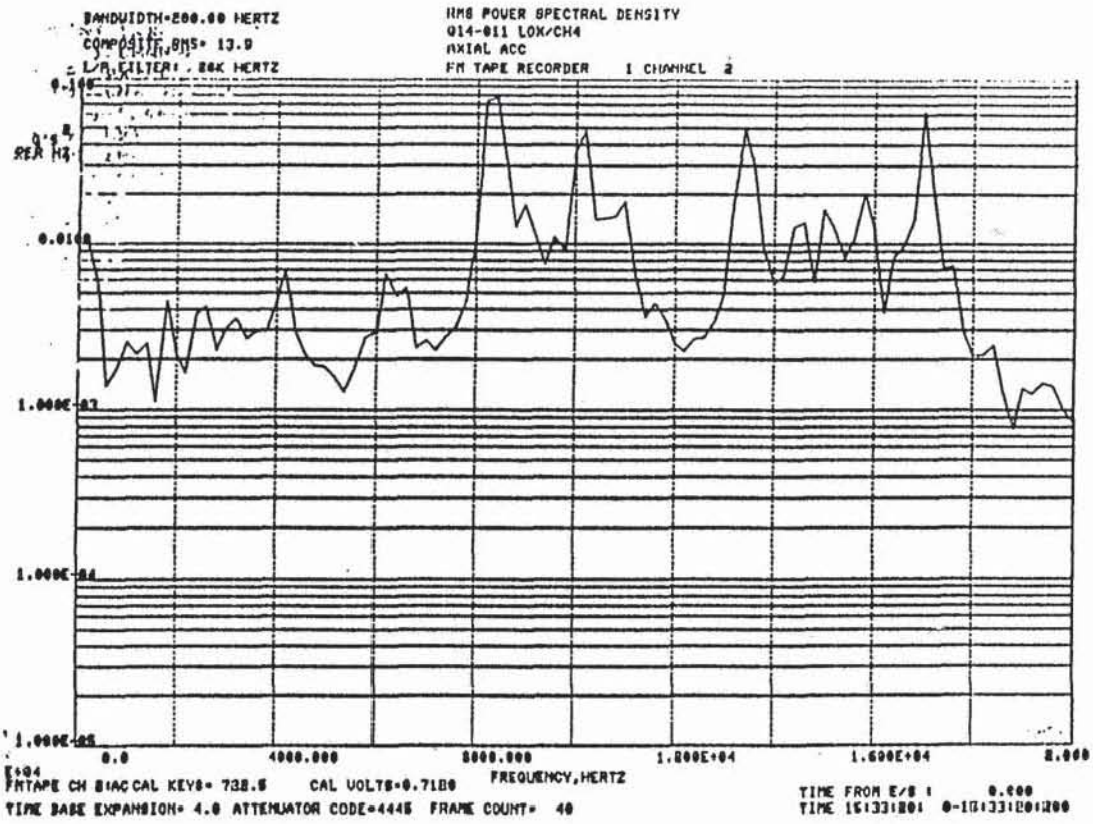

Figure 29 - Axial Accelerometer Data for Test 014-011 During Stable Mainstage Operation

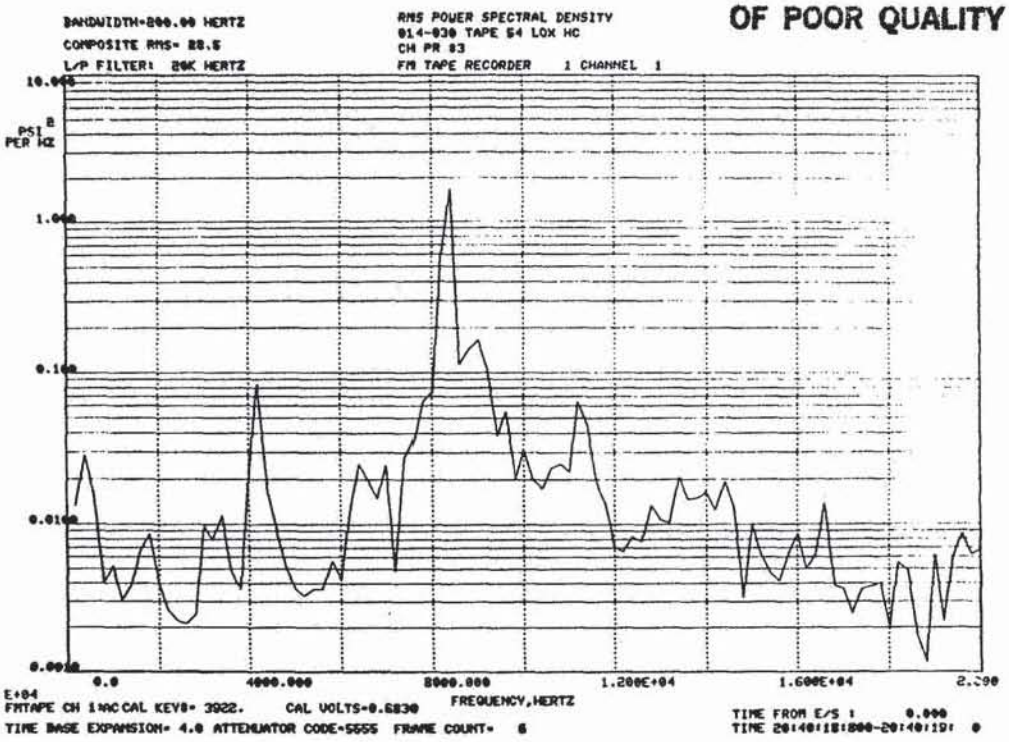

Figure 30 - Chamber High Frequency Pressure Transducer Power Spectral Density for Test 014-030 During Stable Mainstage Operation (Prior to the Bomb)

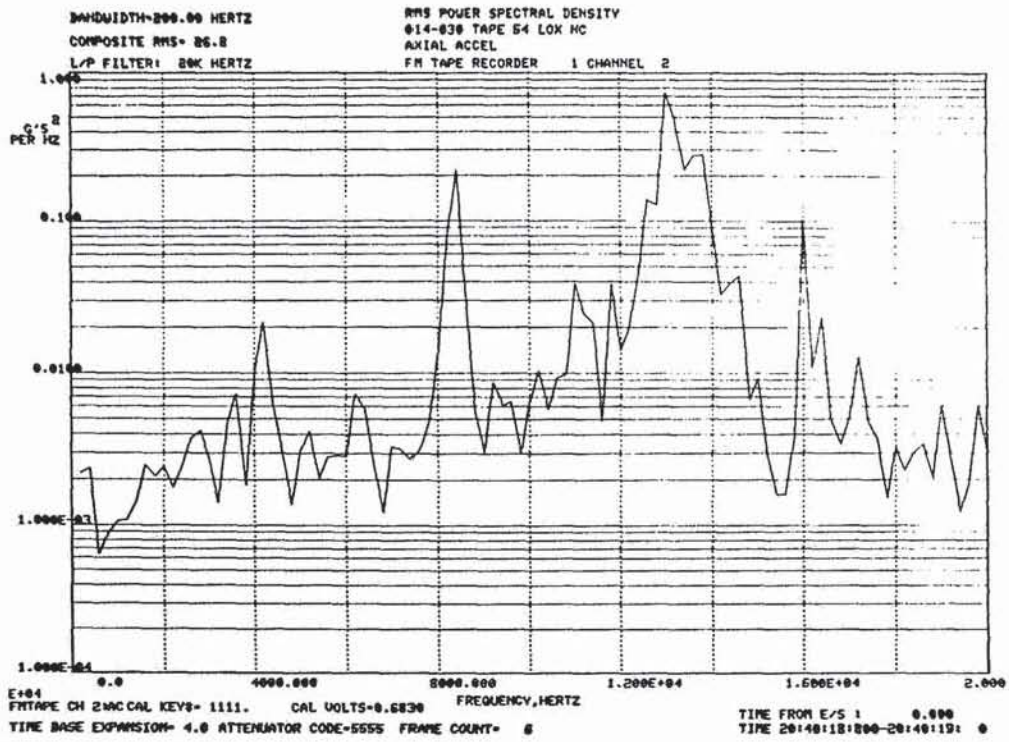

Figure 31 - Axial Accelerometer Power Spectral Density for Test 014-030 During Stable Mainstage Operation (Prior to the Bomb)

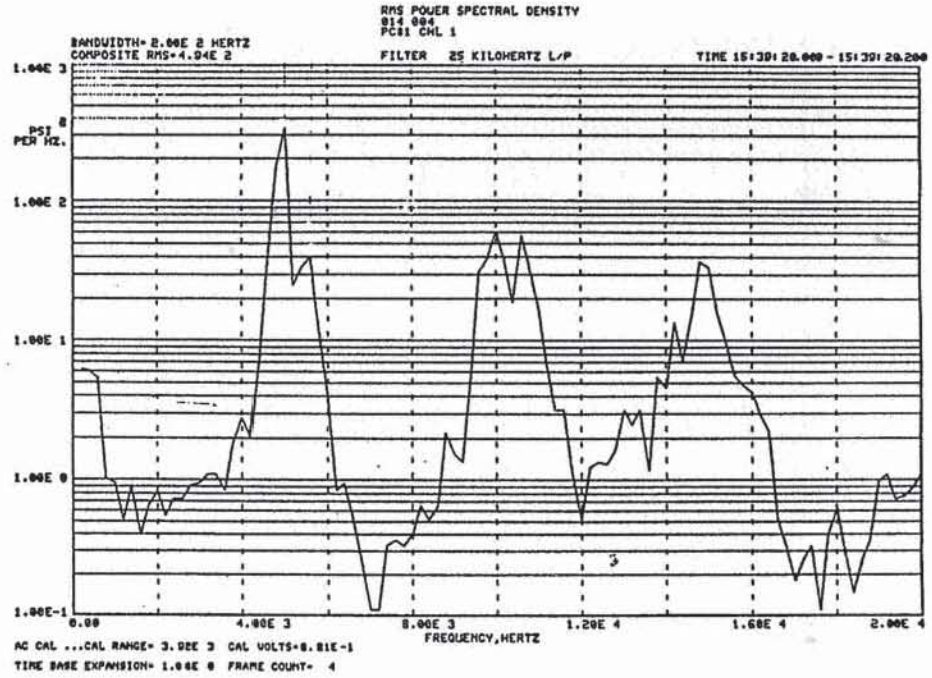

Figure 32 - Chamber High Frequency Pressure Transducer Power Spectral Density for 1T Instability on Test 014-004

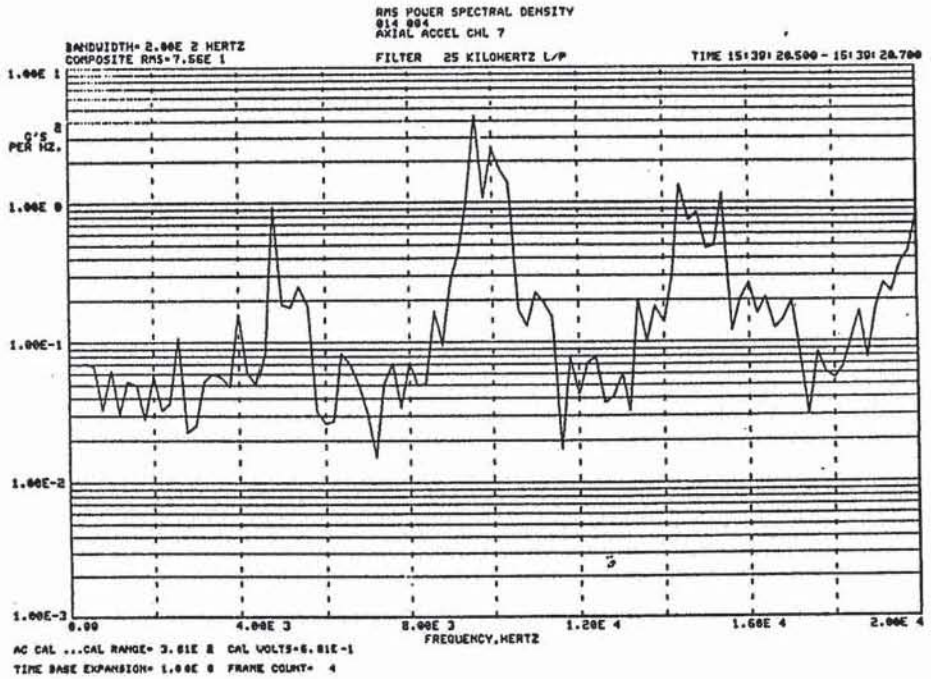

Figure 33 - Axial Accelerometer Power Spectral Density for 1T Instability on Test 014-004

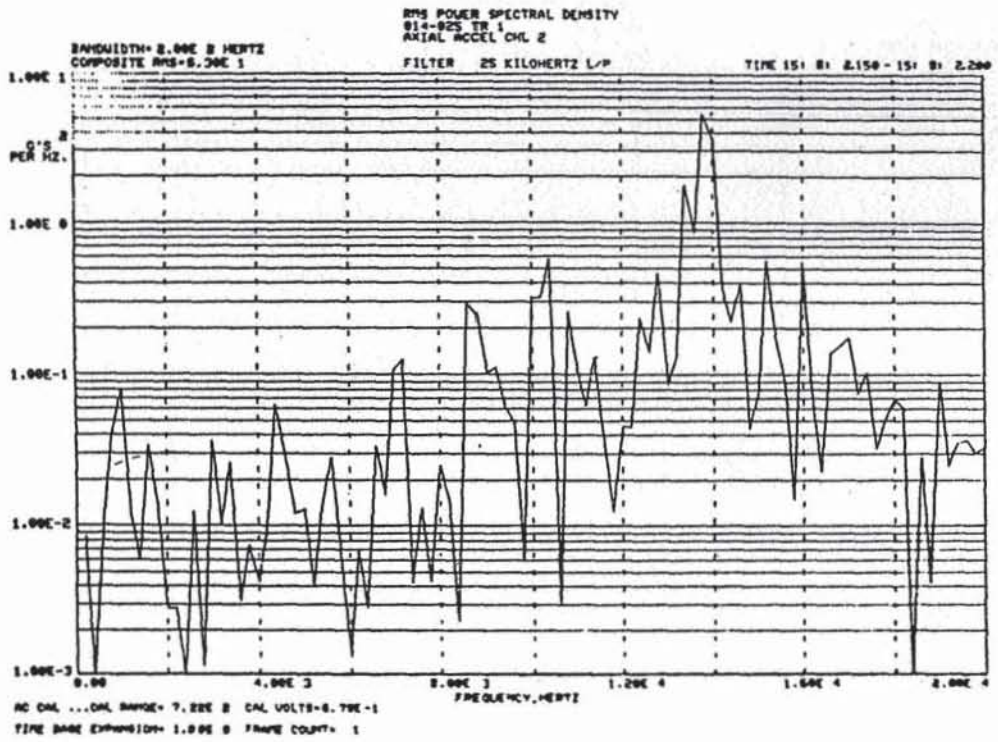

Figure 34 - Axial Accelerometer Power Spectral Density for 14 kHz Instability on Test 014-025

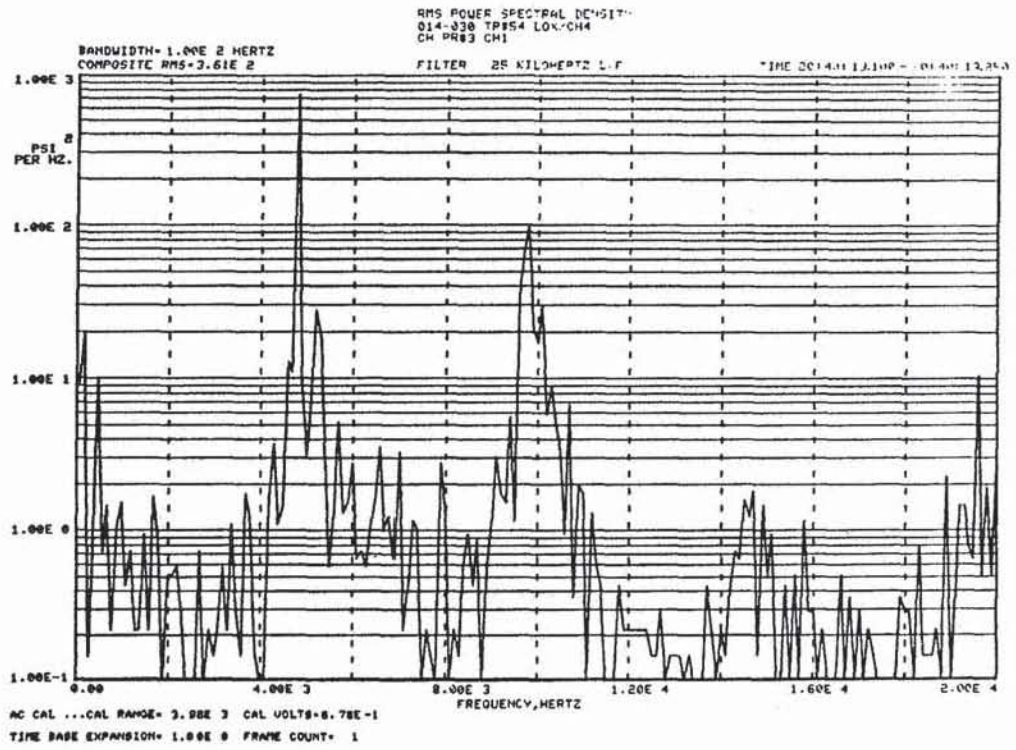

Figure 35 - Chamber High Frequency Pressure Transducer Power Spectral Density for 1T Instability on test 014-030

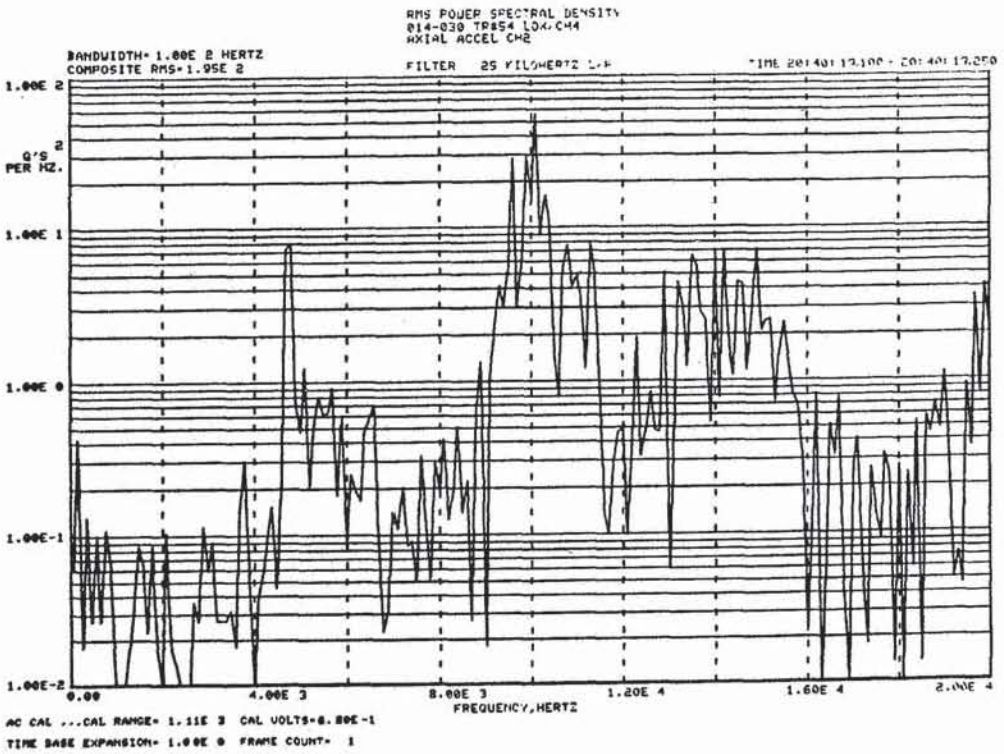

Figure 36 - Axial Accelerometer Power Spectral Density for 1T Instability on Test 014-030

first harmonic of the 1T instability appears to be more amplified although other data not presented show better agreement between the high frequency pressure transducers and the accelerometers. Typical 1T instability rms pressure fluctuation magnitudes for unstable operation are 200 to 400 psid. The Electra ES-6011 10 kHz accelerometers used on tests 004 through 025 registered 60 to 80 g's rms during 1T instabilities. The Endevco 2225 20 kHz accelerometers used on the last five tests indicated 200 g's during first tangential instabilities and reflected higher levels even within the 0 to 10 kHz range which was common to both transducer types. By way of comparison, the estimated resonant frequencies for the chamber high frequency PCB pressure transducers as installed are about 9 kHz for test 004 and about 16 kHz for tests 027 through 032.

The 14 kHz instability accelerometer levels must be interpreted with care since the primary frequency was outside of the range of the Electra 10 kHz transducers. Rms amplitudes were primarily associated with the variable 12 to 14 kHz peak that was a function of fuel temperature. Typical instability levels ranged up to 60 g's with the 10 kHz transducers.

Shown in Figures 37-39 are relative gain plots which form part of the transfer function between the 0 to 20 kHz accelerometers and high frequency pressure transducer 3 for test 028. This gain relationship can be used to relate the magnitudes of the accelerometers and pressure transducers on a proportional basis as a function of frequency. Perhaps the most interesting features are that the axial accelerometer shows relatively greater response at 4 kHz and 12 to 15 kHz which corresponded to frequency ranges of observed activity. The other two accelerometers showed relatively less gain over the 0 to 20 kHz band. Hence the peak levels in the axial accelerometer spectra need to be evaluated carefully to avoid interpreting a peak as necessarily an indication of chamber pressure fluctuations.

Hypothesized Causes of Sudden Changes in Delta-P

Both the 1T and 14kHz instabilities exhibited characteristic shifts in injection pressures and chamber pressure as discussed. The causes of this behavior are not clear although two leading candidate mechanisms can be identified. They are so-called injector cup burning and the effective added nonlinear resistance of the injector during unstable operation.

The term "cup burning" is applied to a condition in which a substantial fraction of the combustion occurs within the cup of a coaxial injector. Estimates of the pressure drop across the cup based on CICM model predictions for tests 022 and 023 which are spontaneous 1T and temperature ramp 14 kHz tests, respectively, were calculated. A cup pressure drop of from 247 to 286 psid is predicted with 9 to 11% of the LOX mass flow reacted within the cup. The reduced gas density that results from the burning causes a significant gas acceleration in the cup which accounts for the increased pressure drop. This calculated pressure drop is

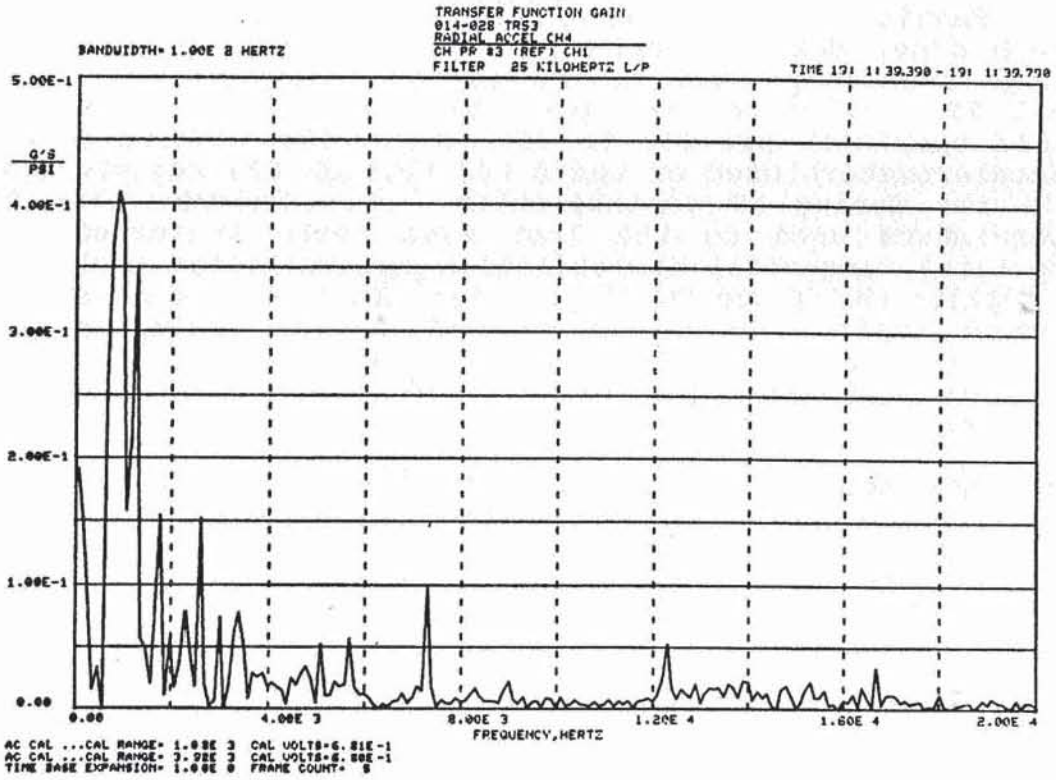

Figure 37 - Transfer Function Magnitude for Radial Accelerometer Referenced to Chamber Pressure 3 on Test 014-028

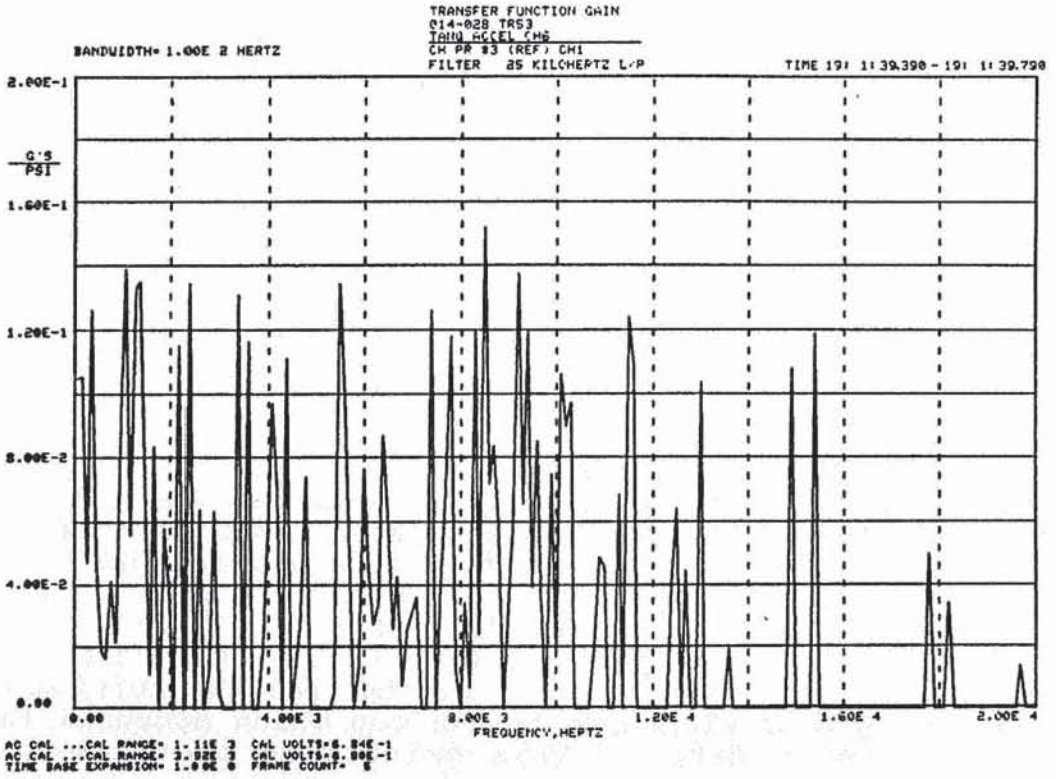

Figure 38 - Transfer Function for Tangential Accelerometer on Test 014-028

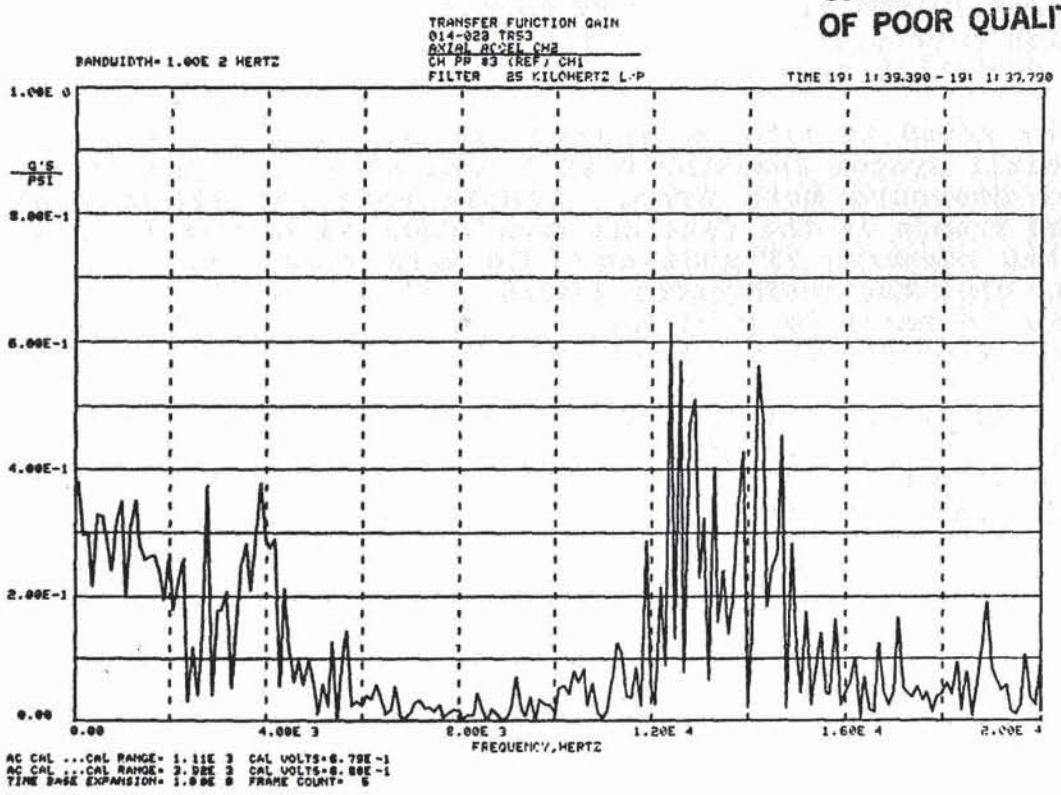

Figure 39 - Transfer Function for Axial Accelerometer on Test 014-028

approximately the right order of magnitude for the net increase in injection pressure difference for the 1T instabilities observed in the current test program.

With the added resistance between the manifold and the chamber, the overall system resistance is increased and the mass flow and chamber pressure both drop. Simple analysis shows that the observed trends in the data are consistant with this explanation. Using the measured 1T mode unstable mass flow for test 027 and assuming that the resistances upstream of the cup do not vary, an increase in manifold pressure of 112 psid is calculated which compares favorably with a measured increase of 80 psid. Using the reduced mass flow to evaluate the (linear) decrease in stagnation pressure, a value of 1881 psia is calculated which can be compared to a measured chamber pressure of 1835 psia. Finally the cup pressure drop based on the mass flow is 190 psid which is somwhat low compared to the CICM calculations. To perform this analysis, the mass flows are calculated on the basis of limited data during the transitory conditions of the instability and the LOX flow must be evaluated on the basis of feed system resistance downstream of the venturi since the increased resistance "uncavitates" the venturi. Furthermore the shift in mass flow between the fuel and oxidizer is not equal and hence a slight change in mixture ratio (from about 3.4 to 3.6 for test 027) and c^* efficiency also occurs during an instability. Hence the error margin on these calculations is likely to be greater than for stable operation and cup burning is a reasonable explanation for the sudden changes in manifold and chamber pressures during 1T type instabilities.

However, the overall increase in injection pressure drop during the temperature ramp tests at the onset of instability was observed to be of the order of 550 psid which is much larger than estimated on the basis of cup burning alone. Accordingly, the potential for effectively increased injector resistance based on nonlinear effects under conditions of large injected mass flow fluctuations was examined. Customary engineering practice relates the pressure drop across an orifice to the square of the flow rate. For small mass flow fluctations the average pressure drop is unchanged and a linear analysis is appropriate. However for larger mass flow fluctuations as might occur when an unstable combustion chamber and its injection element flow passages are in resonance, a nonlinear increase in the average pressure drop of the form

$$\text{delta-}P_{nl}/\text{delta-}P_o = 0.5(w^*/w_o)^2$$

can be expected. Here delta-P and w are the pressure drop across the injector and the mass flow respectively, the subscript o refers to stable conditions, delta-P_{nl} is the increase due to nonlinear effects, and w^* is the fluctuating mass flow. As much as a 50% increase in the pressure drop can be supported without reverse flow in the element. This potentially may occur in the case of temperature ramping tests where the 14 kHz instability in the combustion chamber occurs near a resonance of the LOX post as indicated above. In contrast, the 5kHz 1T type instability is not in resonance with the 4 kHz LOX post mode even though low

amplitude post and chamber coupling at 4 kHz appears likely before the onset of the high amplitude 1T instability.

Some further support for this hypothesized nonlinear flow loss mechanism can be seen in the NASA LeRC LOX/hydrogen temperature ramp data of TN D-3373 where as much as a 10% decrease in chamber pressure was noted at the onset of the instabilities for coaxial elements that typically had no cup recess and hence no potential for cup burning. In this case the only apparent candidate mechanism that could cause the added flow loss and reduce the injected mass flow and chamber pressure is this nonlinear flow loss due to large injected mass flow fluctuations during the observed instabilities.

Although the LOX/hydrogen data are too limited to verify the magnitude of the nonlinear effects without the cup, an analysis of the current LOX/methane temperature ramp data does suggest the importance of nonlinear losses. For the case of test 025, assuming that the unstable fluctuating injected mass flow is 100 % of the steady value and the increase in LOX manifold to chamber pressure drop due to cup burning is 340 psid the measured unstable LOX mass flow rate (which is 87 % of the stable value) can be matched. Furthermore during the instability, the calculated LOX manifold and chamber pressures of 2690 and 1760 psia compare favorably with the measured values of 2740 and 1790 psia. To obtain such large fluctuations in mass flow required to observe nonlinear effects, it is likely that the injector element hydraulic oscillation modes would have to be in resonance with some permitted chamber mode. For the 14 kHz instabilities this would appear to be possible since (as discussed above) both the LOX and fuel side exhibited near 14 kHz modes at the conditions at which the temperature ramp instabilities occurred. As indicated earlier, numerous chamber modes exist in this frequency range. The magnitude of the injection response required also seems to be reasonable if the results of the linear post resonance analysis are extended to this case. In particular for a LOX post flow response of 0.001 lbm/psid which is typical of the current LOX post at 14 kHz, a 1600 psid peak to peak pressure oscillation is required to obtain a 100 % mass flow fluctuation amplitude. Although no high frequency pressure measurements were obtained in the LOX/methane temperature ramp tests, a comparison of rms accelerometer levels on tests 004 and 025 for example suggest that the maximum peak to peak pressure oscillations could be as large as 2500 psid on test 025. Hence flow oscillations in the LOX injector passages of up to 100 % appear possible for the methane temperature ramp tests. It is likely that the fuel annulus also exhibits a 14 kHz resonance at the low temperature and supercritical presure ranges tested and thus exhibits similar flow oscillations and increased pressure drop (from nonlinear effects) over what might be expected from cup burning alone. Although LOX flow oscillations are also possible for the 1T instabilities, the LOX post flow response appears to be a half an order of magnitude lower at 5 kHz than at 14 kHz based on the hydraulic wave equation model. It is thus likely that nonlinear losses do not play as large a role in 1T instability pressure shifts as in the case of the 14 kHz tests.

In conclusion, although the assumed cup burning pressure drop in the example for the methane temperature ramp test is about 90 psid higher than calculated (on the basis of a CICM analysis) for the conditions of a temperature ramp test, the overall agreement of the magnitudes of the shifts in pressure is encouraging and reinforces the hypothesis that both cup burning and nonlinear effects due to large injected mass flow fluctuations each play a role in determining these shifts in the temperature ramp testing. Further refinement of the cup burning pressure drop estimate requires better anchored atomization and drop size models for the burning cup.

Bomb Testing and Spontaneous Instabilities

In this section both dynamic stability rating test results and spontaneous instability tests are reported together to allow comparison of the stability characteristics. As indicated earlier in Table II, two out of three successful bomb tests developed first tangential mode instabilities as a result of the bomb disturbance. The other successful bomb test damped. Data from the three successful bomb tests are summarized in Table IV. Spontaneous first tangential mode instabilities were encountered on five other tests including two planned bomb tests. Four of the five spontaneous instabilities and the two bomb induced instabilities occurred at mixture ratios less than or equal to 3.38. All of the 1T instabilities occurred at mainstage conditions (greater than 1800 psia) except for one (test 028) which happened during prestage at a mixture ratio of 1.9. The test condition which showed dynamic stability was at a mixture ratio of 3.69. Hence the instabilities tended to occur mainly at low mixture ratio and at mainstage conditions.

Bomb Tests

The bomb tests were of considerably shorter duration than the fuel temperature ramping tests to preserve the bomb until the desired firing time. A typical plot of chamber and propellant pressures during a dynamic stability rating test is shown in Figure 40. The approximately 100 to 150 psi rise in fuel and oxidizer injection pressures and the 100 to 150 psi drop in chamber pressure are characteristic of the bomb induced and spontaneous instabilities. Some further discussion of these phenomena are presented in the Data Analysis section which follows the discussion of the individual tests.

Table V presents the test conditions and bomb overpressure characteristics for the three successful bomb tests. Here p'_i indicates the initial overpressure as measured at PCB 3, p'_p refers to the peak overpressure during the bomb disturbance, delta-P_o refers to the stable LOX side injector pressure drop (manifold pressure minus nozzle stagnation pressure) and P_c is the nozzle stagnation chamber pressure. With reference to Table V and Figures 41, 42, and 43 which show expanded chart presentations of pressure fluctuations versus time, for the three bomb tests the 2 grain RDX bombs used for all of the dynamic stability rating tests

TABLE IV - Bomb Test Performace Results

Test Number	027	030	032
Mainstage Duration (sec)	0.3	0.3	0.5
Pressure (psia)			
Chamber-1	1967	1970	2134
Chamber-2	1969	1974	2137
Fuel Injection	2690	2632	2686
Oxid Injection	2481	2528	2803
Temperature (Deg F)			
Oxid Injection	-242	-249	-247
Fuel Injection	67	22	2
Mass Flow, Main (lb/sec)			
LOX	66.77	66.73	76.72
Methane	19.56	20.80	20.64
Mass Flow, Ign (lb/sec)			
Gaseous oxygen	0.34	0.34	0.48
Methane	0.27	0.31	0.30
Mixture Ratio			
Main	3.41	3.21	3.72
Overall	3.38	3.18	3.68
c* (percent)	96.9	95.1	94.8
Stability	U/S	U/S	S
Frequency	1T	1T	

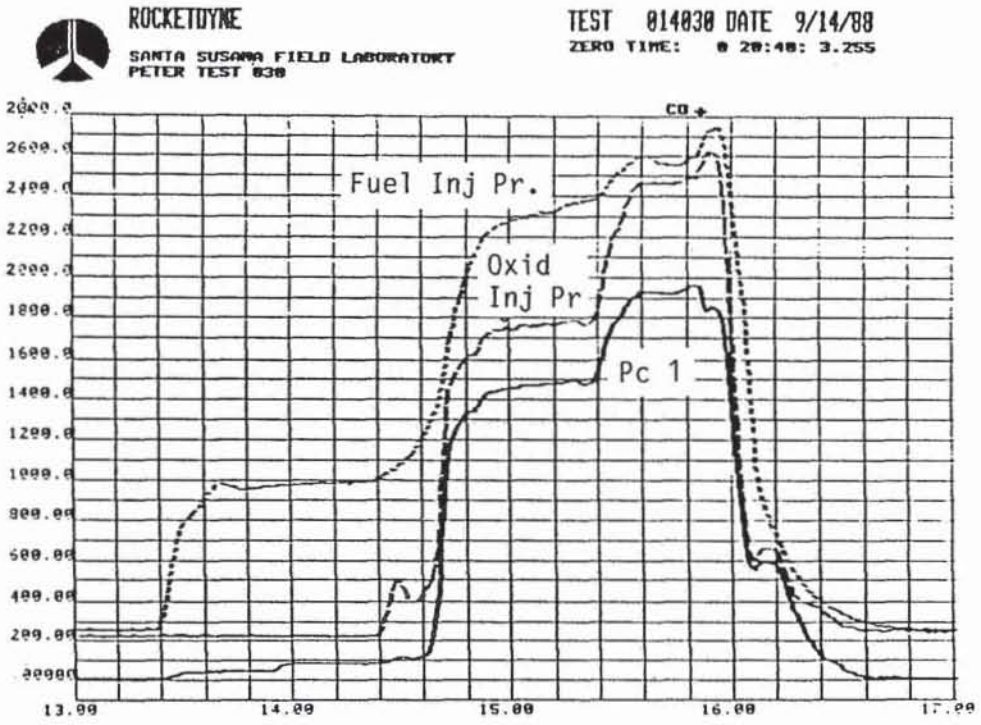

Figure 40 - Typical Propellant and Chamber Pressure Histories During Test 014-030 Which was Bombed Unstable

TABLE V - Dynamic Stability Rating Test Characteristics

Test	Pc (psia)	MR	p'_i (psid)	$\frac{p'_i}{Pc}$	p'_p (psid)	$\frac{p'_p}{Pc}$	$\frac{\text{delta-P}_o}{Pc}$	Comments
027	1960	3.38	630	.32	1060-1330	.54-.68	.266	Unstable, 4 msec after bomb disturbance
030	1964	3.18	550	.28	1390-1720	.71-.88	.290	Unstable, 13 msec after bomb disturbance
032	2127	3.69	720	.34	1450-2430	.68-1.14	.318	Stable, recovered in 13 msec.

produced a 490 to 720 psi initial overpressure as measured on high frequency pressure transducer 3 at 60 degrees from the bomb. Of the three high frequency transducers in the chamber, this one is located closest to the bomb and likely shows the least combustion enhancement or attenuation of the bomb pulse. This perturbation level ranged from approximately 24 to 36% of the chamber pressure. Since the first test demonstrated the effectiveness of this grain size to induce a dynamic instability no larger bomb sizes were investigated. By comparison, initial overpressures measured at transducer 4 which is 150 degrees from the bomb ranged from 19 to 100% of the chamber pressure and shows the effects of attenuation as well as combustion enhancement. The results for transducer 4 also satisfy the 10 to 100% criteria for the peak initial overpressure as indicated in CPIA 247.

Typical maximum overpressures seen within 1 to 2 milliseconds as a result of the bomb disturbance ranged from about 1100 to 2400 psid (peak). The maximum overpressure is defined here to be the maximum realized within the first few milliseconds after the bomb disturbance and before the high amplitude instability is fully developed. This resulted in peak disturbances of 35 to 114% of chamber pressure. However from Table V it appears that the stability of this combustor is not strongly a function of peak disturbance level. Instead if anything the stability charcteristics appeared related to the ratio of the stable LOX pressure drop to the chamber pressure. This ratio gives a measure of the stiffness of the LOX feed system and is hence an indicator of the tendency to resist the development of LOX flow oscillations. In fact, Fang (ref. 24) has indicated that the normalized injection fuel and oxidizer pressure drops determine the stability of LOX/hydrogen combustors in fuel temperature ramping tests. Both 027 which required about 4 msec to develop (Figure 41) into a large amplitude 1T instability and 030 (Figure 42) which grew to full amplitude in about 13 msec exhibited delta-P_o/P_c values less than test 032 which damped in about 13 msec (Figure 43). It is interesting to note that test 030 (Figure 42), which takes longer to develop into a high amplitude instability (about 13 milliseconds) than test 027, has a higher normalized injection pressure drop ratio than test 027 does. Test 032 which exhibited a slightly higher normalized LOX side injection pressure drop required about 13 milliseconds to damp (Figure 22). This suggests that as the normalized LOX side injection pressure drop is decreased, the injector may exhibit a greater tendancy to develop an instability.

By way of comparison NASA LeRC LOX/H_2 pulse gun stability rating testing (ref. 18) and J2 dynamic stability rating tests did show a sensitivity to the peak bomb disturbance overpressure. For the data of reference 18, values of p'_p/P_c of roughly 0.26 to 0.5 were sufficient to cause instabilities although no upper limit was found. This range of overpressures was below that explored in the methane testing. It should be noted that the reference 18 data indicated that a stronger correlation was found between charge size and stability. The range of normalized overpressures that was most efficient in causing instabilities during J2 dynamic stability rating tests (0.3 to 0.7) was similar to that of

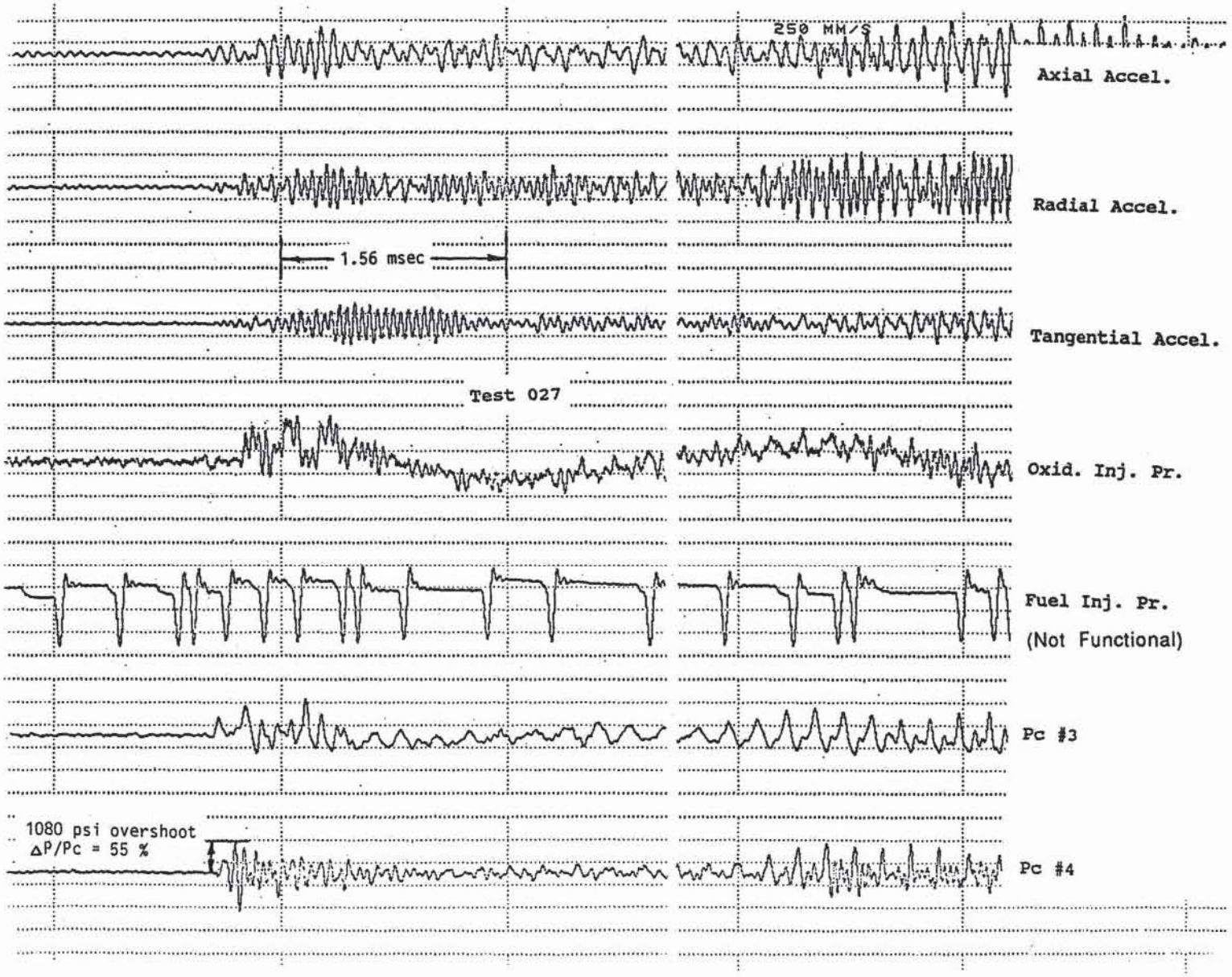

Figure 41 - Test 014-027 Expanded Brush Data

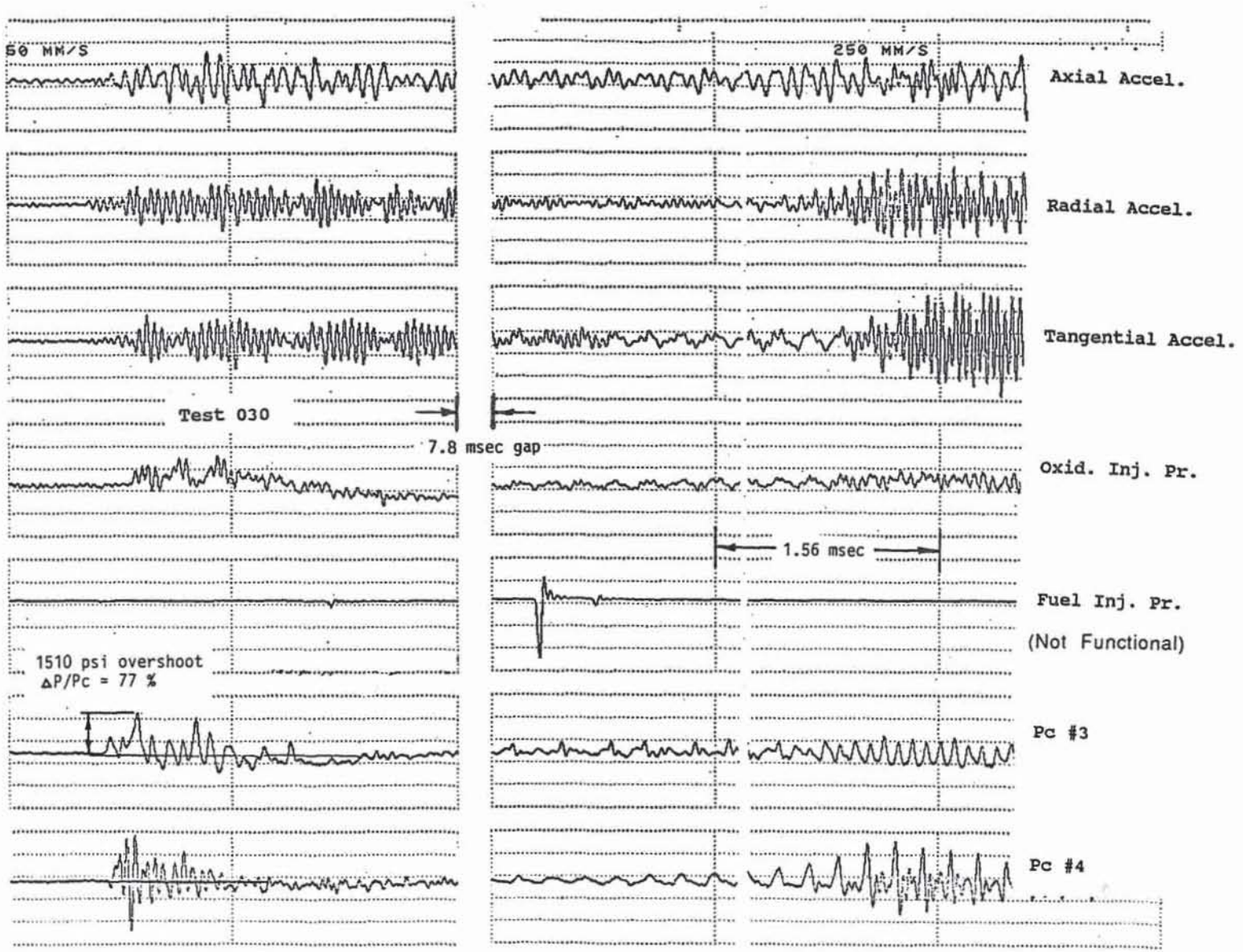

Figure 42 - Test 014-030 Expanded Brush Data

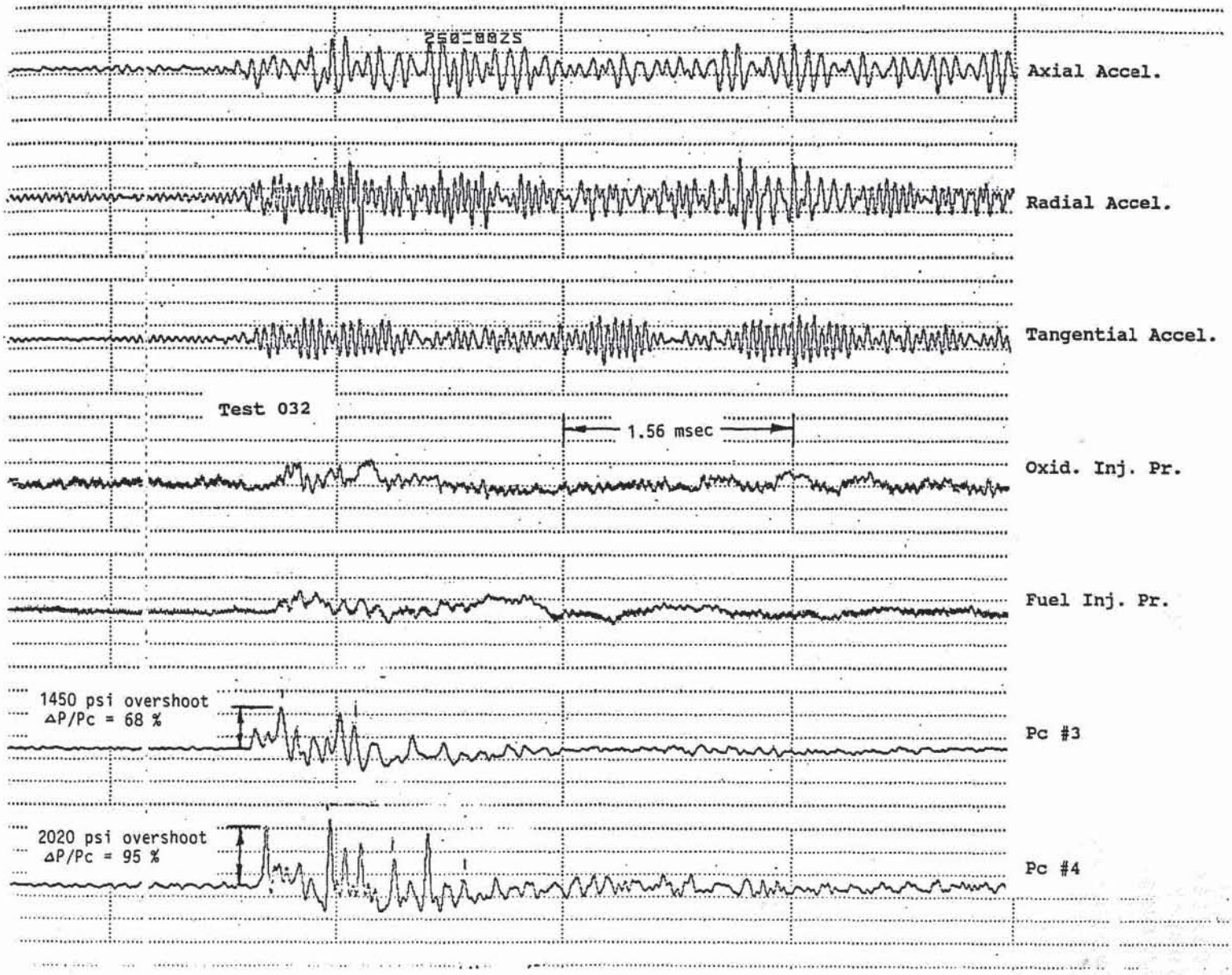

Figure 43 - Test 014-032 Expanded Brush Data

reference 18. Larger overpressures did not excite instabilities in the case of the J2. Although the test (032) that exhibited the highest normalized overpressure level of the three tests was (similar to the J2 behavior) the only test that recovered from the bomb disturbance, more data is necessary to establish on a statistically rigorous basis whether the current LOX/methane injector is more sensitive to a particular range of peak overpressures.

Unfortunately the injection pressure drop was not documented in the LeRC LOX/H_2 data set to permit comparisons with the pressure drop parameter discussed above. However some inferences can be made from the LeRC hydrogen data. The peak overpressure response to the machine gun pulses in the LeRC LOX/hydrogen testing increased with decreasing fuel temperature. Since the pressure drop and hence "stiffness" of the fuel side decreased as the fuel temperature was ramped downward, the increase in the peak response may indicate a reduced stability margin. It is suspected that the LOX/hydrogen stability characteristics (taking into account the greater sensitivity to fuel side coupling in those tests) are analagous to the LOX/methane results for which the LOX side response is larger. A dynamic instability temperature threshold was not demonstrated in reference 18. However, the decrease in peak overpressure as the fuel temperature increased and the tendency for dynamic instabilities to occur at the largest peak overpressures suggest that for a given charge size a dynamic instability threshold temperature exists for the LOX/hydrogen injector. That is, for a given charge size at low enough values of the fuel temperature and hence for small fuel side pressure drops, the LOX/hydrogen dynamic stability margin may be reduced or eliminated in a manner similar to the two methane bomb tests with the low LOX-side pressure drops. Thus (for a fixed charge size) the LOX/H_2 injector is likely dynamically unstable below a certain fuel side pressure drop value in a manner similar to the methane injector operating at LOX-side pressure drops less than that of test 032. In the case of the methane injector, based on some evidence of 4kHz oscillations before the 1T instability is established it is suspected that the critical pressure drop for instability in the case of the methane is also a function of the LOX post tuning with respect to chamber modes.

For the two bomb tests that produced instabilities, the fully developed 1T instability appeared after the initial bomb perturbation had begun to decay. For example, the high amplitude 1600 to 2800 psi (peak to peak) instability on test 027 was fully developed within 4 msec from a lower amplitude oscillation that followed the peak overpressure (Figure 41). On test 030 a similar amplitude instability was fully developed in about 13 ms and after the initial disturbance had almost fully damped (Figure 42). Accelerometer measurements indicated typical maximum peak to peak levels of 1200 to 2700 g's. For both tests that were driven unstable, the chamber oscillation frequency rose from about 4 kHz to the 1T frequency while growing in amplitude. An isoplot of test 027 is shown in Figure 44. The 1T instability exhibited a 5.0 kHz mode with a secondary peak at 5.3 kHz. The second harmonics of those two modes appear at 10 and 10.6 kHz. This

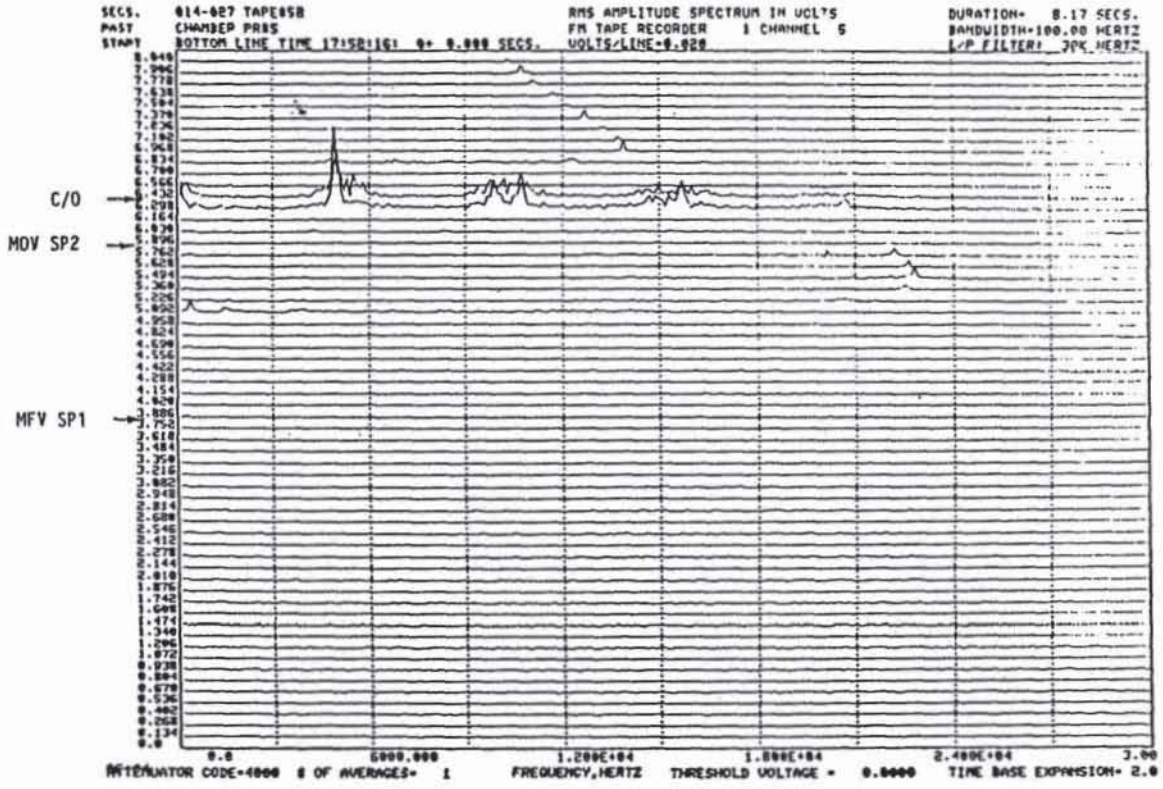

Figure 44 - RMS Amplitude Spectrum versus Time (Isoplot) of High Frequency Chamber Pressure During Test 014-027

double peak characteristic is typical of the 1T instabilities and gives rise to a variable perturbation amplitude at the beat frequency in the high frequency data. For test -030 these peaks were at 5 and 5.6 kHz. In test -032, activity at 4.5 and 5.2 kHz damped in about 13 msec (Figure 43) while intermittent, self damping 13.5 kHz activity (which appeared to be a standing 1T/1R mode from the relative amplitudes of the three transducers and a spinning mode from the relative phases) persisted into cutoff at amplitudes up to 10% of chamber pressure. Typical oscillations in the inner fuel manifold and oxidizer dome ranged from about 100 psi to 400 psi (peak to peak). For these tests prior to the bomb, the chamber exhibited a 150 to 300 psi (peak to peak) oscillation at 8 to 8.6 kHz which could be either a 2T or 1R mode depending on the effective acoustic velocity at the injector prior to the instability. The effective acoustic velocity is discussed further in the next section.

Spontaneous Instabilities

As indicated previously, the instability characteristics of the 1T spontaneous instabilities are similar to the dynamically unstable tests. An isoplot of high frequency chamber pressure of a spontaneous instability is shown for test 014-004 in Fig. 45. As in the bomb tests a dual peaked mode between 5 and 6 kHz is evident in this and the other 1T instabilities as well as harmonics of the basic mode. Figure 46 shows a brush chart of high frequency pressure transducers on that same test. Chamber pressure oscillations of nearly 3000 psi peak-to-peak or 150% mean chamber pressure were measured. LOX dome and inner fuel manifold pressure fluctuations are on the order of 600 and 300 psi peak-to-peak similar to the levels experienced in fuel temperature ramping. For comparison accelerometer levels of approximately 1000 g's were noted for the fully developed instability. Although oscillations at a well defined frequency of 4 kHz are detected before the onset of the high amplitude 1-T instability, they are of a much lower amplitude and hence are not apparent in Figures 45 and 46.

Test 022 was the only other test to exhibit a spontanous 1T instability well after mainstage conditions had been established. Two tests 019 and 031 went unstable near the end of the transition from prestage to mainstage conditions. Notably a nearly 500 psid "pop" in test 031 occurring about 5 msec before onset appeared to cause the instability in a manner similar to a bomb. Test 028 was the only test to develop a spontaneous instability at prestage (approximately 1500 psia and low mixture ratio) conditions. In fact on a statistical basis the low chamber pressure-low mixture ratio conditions of the prestage phase yielded the best stability characteristics for the hardware tested.

All first tangential instabilities were characterized by 4 kHz and sometimes 8 kHz activity before the onset of high amplitude activity. Most tests tend to show relatively less 4 kHz than test 014-004 but are similar in that the growing instability shifts in frequency from 4 to 5 kHz and becomes a cusp-shaped, steep fronted

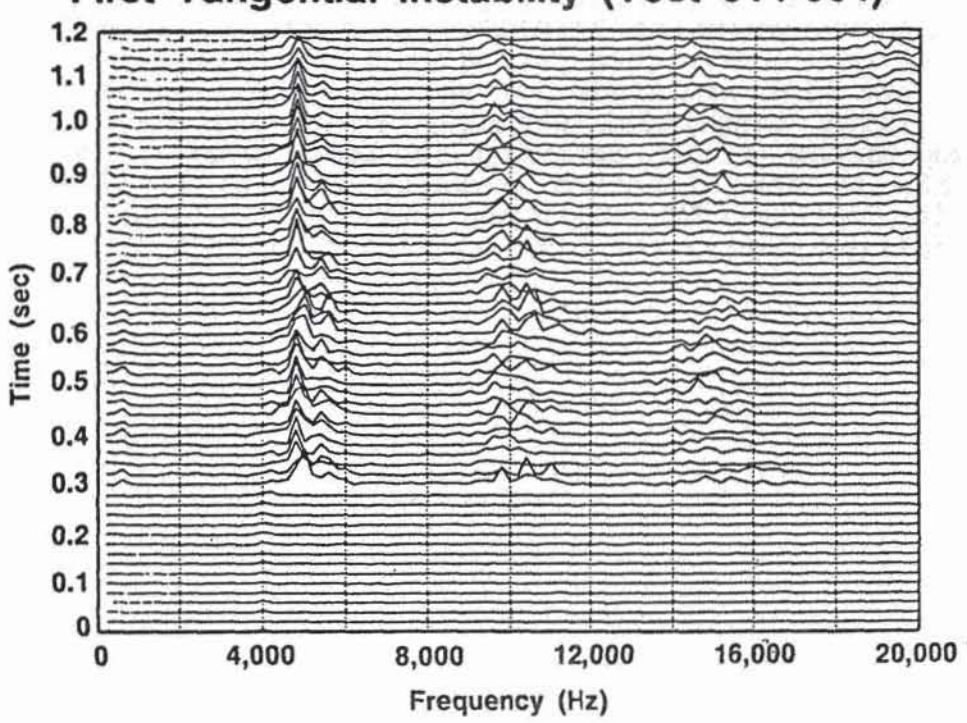

Figure 45 - High Frequency Chamber Pressure Isoplot for a First Tangential Instability (Test 014-004)

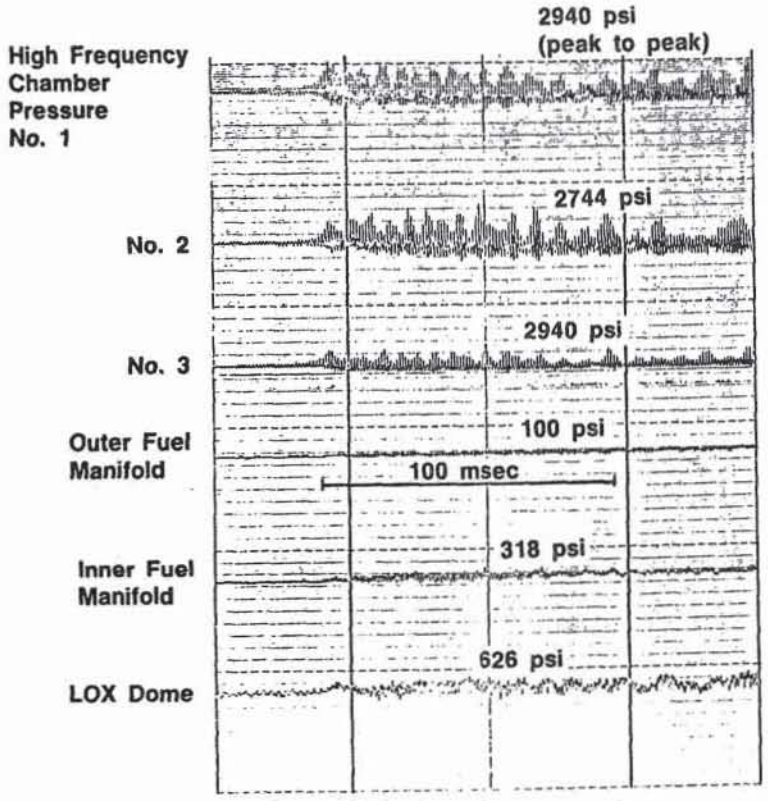

Figure 46 - Brush Chart of High Frequency Pressure Transducer Data for a First Tangential Unstability (Test 014-004). Peak to Peak Oscillation Levels are Indicated

waveform. Usually this process takes on the order of 5 to 10 ms or less once the 4 kHz has achieved sufficient amplitude. Based on an examination of the relative phase and amplitudes of the chamber high frequency pressure transducers on tests 004, 027, 028, and 030 for which a protracted period of 4 kHz activity was seen prior to the 5 kHz high amplitude instability, the 4 kHz appears to be a type of first tangential standing mode. The mode on tests 032 which exhibited 4 kHz activity is less clear. This would be reasonable if the effective acoustic velocity near the injector face prior to the high amplitude instability is about 80% of the value realized during the high amplitude instability. Similar and even greater reductions in the near face acoustic velocity have been observed in 2-D combustor tests with coaxial LOX/H_2 injectors based on bomb induced disturbance wave speeds (Ref. 27). If the chamber 1T frequency is near 4 kHz, coupling may be promoted between the LOX post 4 kHz mode and the chamber, facilitating the onset of an instability. The acoustic velocity during the high amplitude instability correspond to the equilibrium chemistry result for a well-mixed combustor operating at the injected mixture ratio. Hence the conditions prior to the high amplitude instability must correspond to a partially vaporized and/or mixed flowfield near the injector face.

Some support can be found for this hypothesis in the results of the CICM code for test 022 which exhibited a spontaneous instability and which was preceeded by 4.4 and 8.7 kHz low amplitude activity. The calculated axial distribution of the acoustic velocity is shown in Figure 47 for tests 022 and 014. The acoustic velocity for 022 is seen to be lower that that for 014 for the first eight inches of the combustor. Over the first few inches of the combustor the acoustic velocity for both conditions is in the range of 70 to 90% of the value achieved at the nozzle inlet plane of the combustor. Hence it would appear that a 4 kHz 1T mode could be supported near the injector faceplate. This matter will be examined further in the Stability Modeling discussion.

It can be anticipated that the high amplitude 1T wave motion will cause rapid mixing and combustion such that regions of low acoustic velocity may not exist anywhere in the chamber. To precisely model this acoustically variable and combustion-process-dominated phenomena (including the effects of turbulent mixing which is not modeled by the CICM code) and accomplish a true a priori stability assessment would require a comprehensive CFD combustion modeling analysis of the stable combustor conditions. However it is felt that the trends indicated by these simple analyses are correct.

Comparisons with LOX/H2 Data

Amplitude and frequency characterics of the 1T mode instabilities can be compared with LOX/hydrogen data. Recall that Figures 32 and 35 show power spectral densities for chamber high frequency pressure transducers for tests 004 and 030 during high amplitude 1T mode instabilities. The dual peaked instability mode at nominally the 1T instability frequency is seen. Taking into

Figure 47 - LOX/CH4 CICM PREDICTIONS OF SOUND SPEED VERSUS AXIAL POSITION

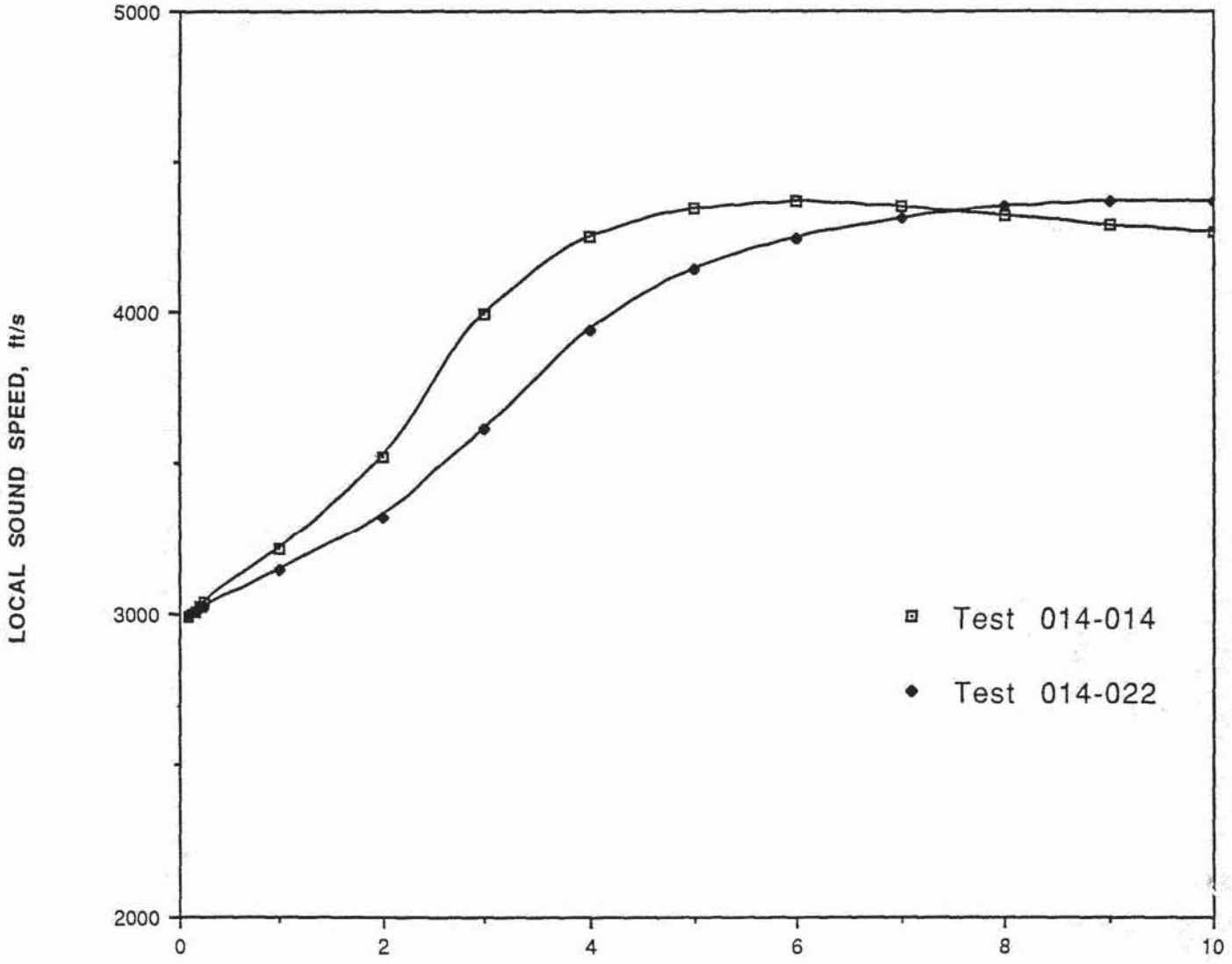

account the different bandwidths of the spectra, an estimate of the equivalent peak to peak amplitudes of the highest peaks in similar PSD's for tests 004, 027, and 030 yields an average maximum peak to peak amplitude of 0.4 P_c. Although the agreement is not perfect, the relative amplitudes of the peaks for each of the transducer locations support the existence of a standing 1T mode. Similar estimates of the peak to peak amplitude can be formed for typical LeRC LOX/hydrogen stability ramping test data from reference 23. Amplitude spectra taken on LeRc 421 element injector reveal a dual peaked instability mode with the primary frequency at the 1T mode similar to the methane results. In fact most of the LeRC LOX/hydrogen temperature ramping data exhibited a 1T type mode. Typical 1T mode amplitudes are 0.5 and 0.18 P_c for the LeRC 421 and 100 element injectors. The methane result is thus within the spread of the reference 23 data. The secondary peaks in the current data exhibit an average maximum of 0.11 P_c. The frequency of this smaller peak is about 12% higher than the primary mode and shows circumferential variability in amplitude proportional to the primary peak. Hence it would appear that the secondary peaks in the methane data also represents standing 1T mode activity. In comparison the LeRC 421 element LOX/hydrogen data indicate a secondary peak of 0.22 to 0.3 P_c peak to peak amplitude for a mode identified as a second longitudinal. The 100 element data did not exhibit a secondary mode. On the basis of this comparison it would appear that the methane data tends to be unique in that two closely spaced 1T modes seem to be supported while the multiple modes when present in the hydrogen data appear to be independent.

Comparisons of growth rate between the methane and the hydrogen data base are limited since no growth rate data is provided in the LOX/hydrogen temperature ramping literature. From the much reduced plots provided in the LeRC reports, the time required to grow to full amplitude appeared to be much less than 50 ms. The LOX post coupled mode on the J2-S typically would grow to full amplitude in a complex fashion. A pre-LOX post resonance period of variable length on the order of 10 to 100 seconds (based on onset time and limited chart data) after which the 4400 Hz oscillation organized and exhibited linear growth. This was followed by a period of exponential growth. As shown in Figure 48, typical exponential growth constants were 1/sec to 10/sec. This period of exponential growth lasted typically about 1 second.

In contrast, prior to a 1T spontanous instability the LOX/methane injector would typically exhibit some constant low amplitude modes which corresponded to LOX post resonances from the beginning of mainstage. Exponential growth would occur over a period of from 5 to 10 ms typically with growth rates in the range of 500/sec which is much larger than the J2-S. In all cases the oscillation would take multiple cycles to grow in amplitude and shift in frequency from near 4 kHz to 5kHz. See Figure 49. Near the pressure nodes of the 1T mode higher frequency activity in a range of from 8 to 10 kHz and possibly representing 1R activity is also seen to grow in amplitude.

The growth rates associated with the LOX/methane bomb testing are

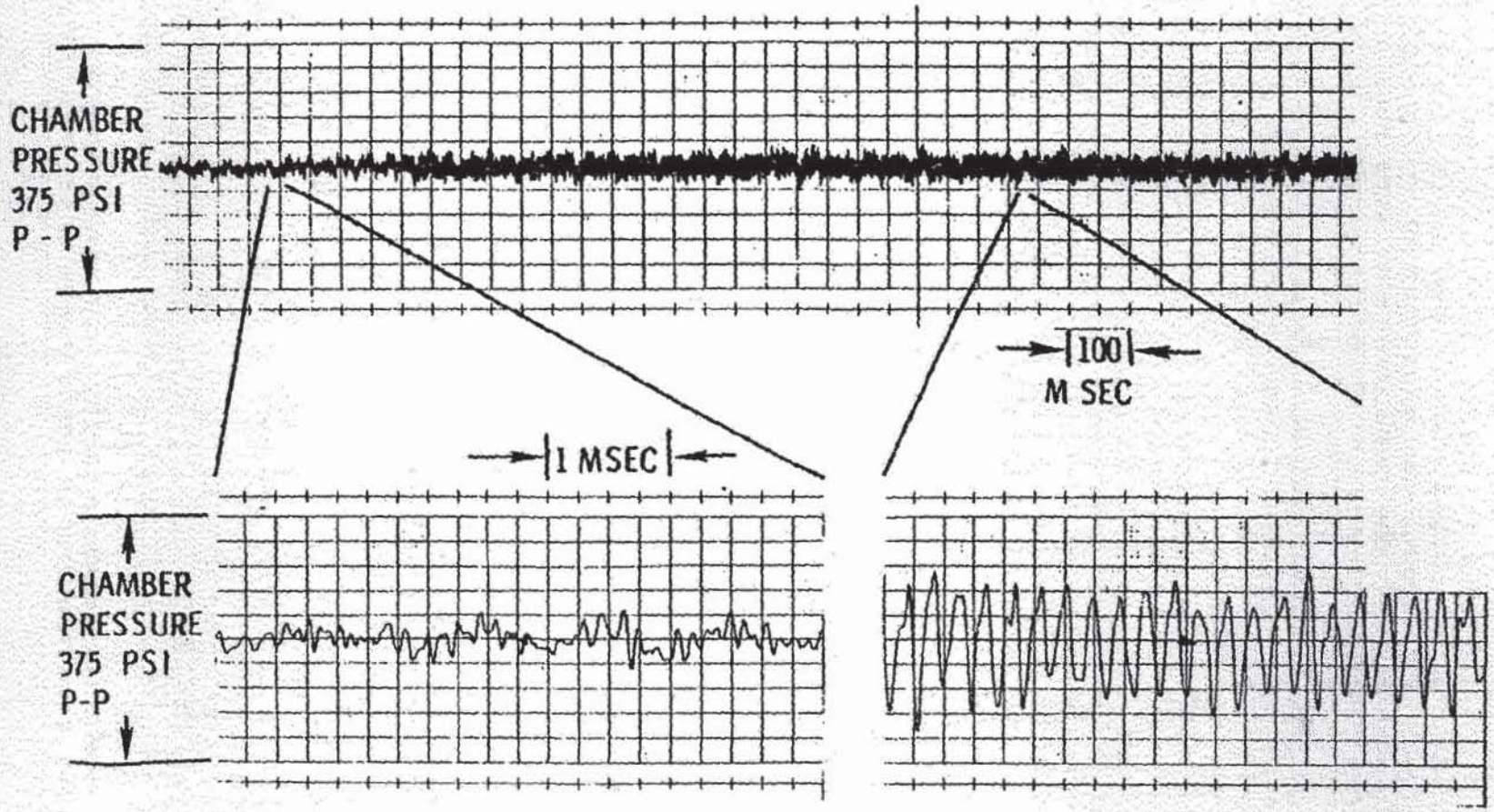

Figure 48 - J-2S High Frequency Feed System Coupling

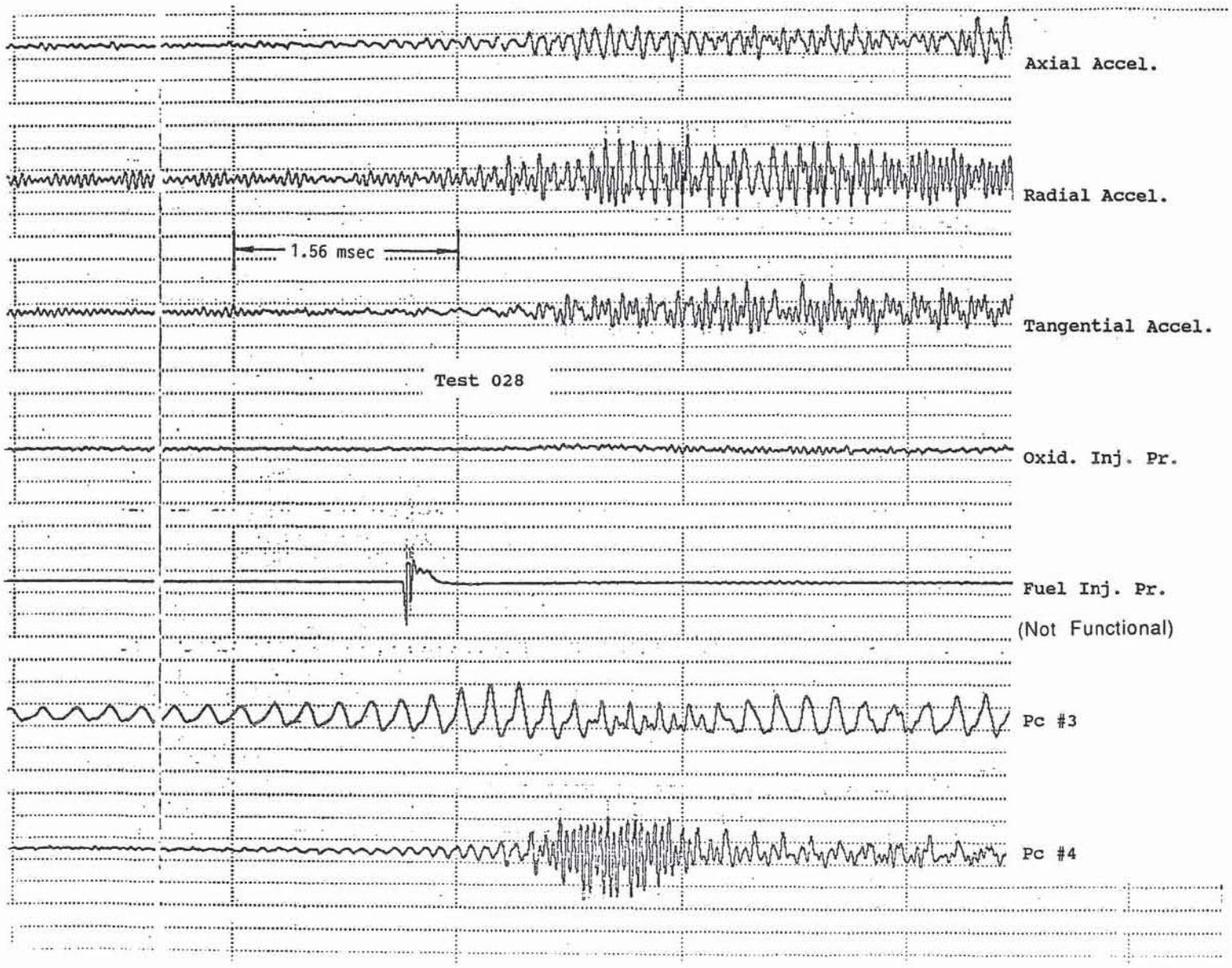

Figure 49 - Test 014-028 Expanded Brush Data (Spontaneous Instability)

similar to the spontaneous instability growth rates. Typical values based on the two successful bomb tests on this program are in the neighborhood of 500/sec. See Figures 41 and 42. The instability tends to grow out of 4 to 4.5 kHz low level activity that is excited by the bomb event and which persists after the initial disturbance has decayed. As in the case of the spontaneous instabilities the frequency and amplitude of the activity increases until a 5 kHz instability develops.

The growth rates in the case of the temperature ramp data are less well defined since no high frequency chamber pressure data was recorded. Based on accelerometer levels at the time of instability onset, growth rates in the range of 300-700/sec were typical. Since there is no means of directly comparing these rates with the LeRC LOX/hydrogen data, it is not clear if methane behaves like hydrogen in this regard.

Stability Analyses

Data Correlations

The motivations for the effort to correlate the data included facilitation of the stability modeling effort as well as a need to understand the overall stability trends of this injector and their relationship to stability trends of LOX/Hydrogen injectors for which a considerable data base exists. The modeling would benefit from either identification or improved understanding of the controlling physical parameters which need to be modeled to correctly predict stability characteristics. It was hoped that the comparison of the hydrogen and methane data would help answer the fundamental questions of whether methane has similar stability characteristics to hydrogen and whether methane can be rated for stability like hydrogen. This effort to correlate the data (which was initiated before the propellant selection was made in the program) tentatively identified both mixture ratio and a weighted velocity ratio (that is $V_f/(V_o*N_{el})$ where N_{el} is the number of injector elements) as important factors in determining the stability margin of LOX/hydrogen coaxial injectors. Due to the strong variation of hudrogen density with temperature, LOX/H_2 engine velocity ratio stability margins could be evaluated by varying the fuel injection temperature while holding the fuel mass flow constant. Based on that correlation, methane was selected as the hydrocarbon fuel most likely to emulate the stability characteristics of hydrogen (See Task I report). This selection was influenced both by the fact that the methane density varies a significant amount (a factor of 2.6 at 2000 psia) as a function of temperature from ambient conditions down to its critical temperature. As a result, methane injector stability could be examined over a range of velocity ratios by varying fuel temperature similar to hydrogen.

At the conclusion of testing the methane data was examined for evidence of an instability threshold as a function of various parameters, including those used for the LOX/hydrogen stability data correlation effort. Figure 50 shows both stable and unstable data as functions of the ratio of the fuel side pressure drop to

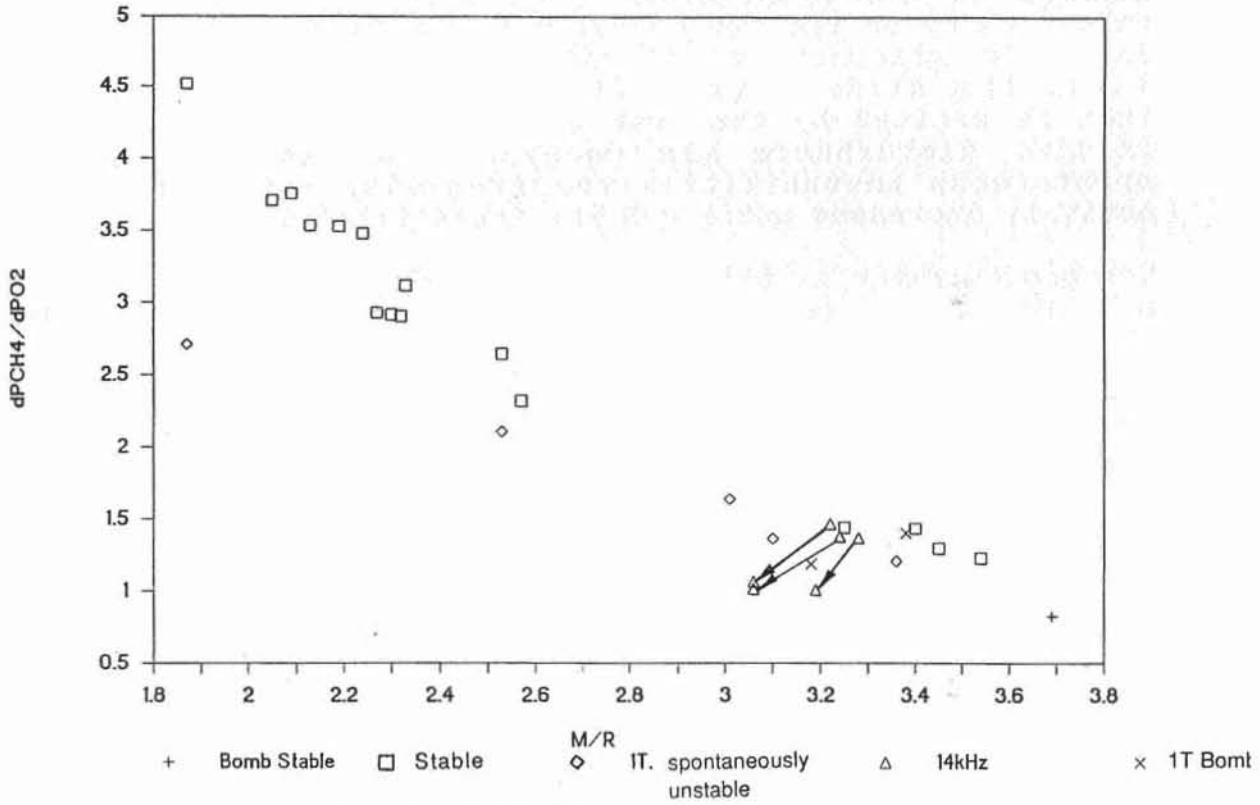

Figure 50 - Propellant Pressure Drop Ratio versus Mixture Ratio (NASA-LeRC LOX/Methane Data Only)

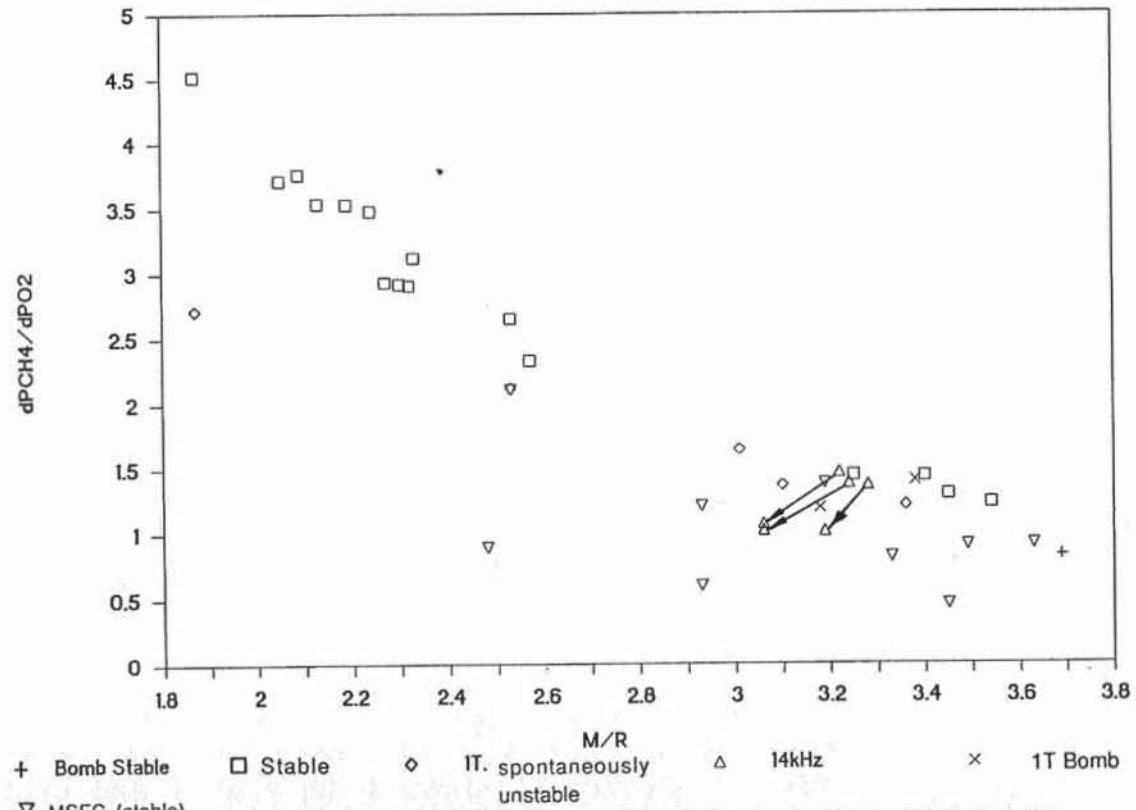

Figure 51 - Propellant Pressure Drop Ratio versus Mixture Ratio Including Both LeRC and MSFC LOX/Methane Data

the LOX side pressure drop and mixture ratio. Both prestage (approximately 1500 to 1600 psia) and mainstage data are included. This pressure drop ratio was selected based on limited success in correlating the stability modeling results in reference 21. Stable, spontaneously unstable, bomb-induced instabilities and fuel temperature ramp instabilities are included. In the case of the fuel temperature ramp instabilities, both the initial condition at the start of the ramp and the final condition at the onset of the 14 kHz instability are shown for this and the remaining data presentations. The line drawn connecting the initial and final temperature ramp conditions is mainly done to aid the eye and indicates only the approximate range of conditions covered in the ramp. Although the stable data for this injector tend to exhibit a higher delta-pressure ratio at a given mixture ratio than the unstable data, Figure 51 which includes the NASA MSFC 82 element injector data (Ref. 10) shows that this is not a universal correlation. It should be noted that as a result of injector (LOX post) response modeling, the stability margin of the MSFC injector with the 1.072 inch longer LOX posts was expected to be different than the LeRC injector. Correlating the data in this fashion mainly indicates common regions of stability for the MSFC and LeRC injectors. The instability threshold for the MSFC and other less similar injectors cannot be implied from this presentation alone.

Better agreement between the two sets of methane data is seen when the velocity ratio (V_f/V_o) is plotted against the mixture ratio (Figure 52). Although some stable MSFC test conditions are at velocity ratios equal to or less than that of unstable LeRC data, the overall trend indicates the potential for a (hardware specific) LOX/methane instability threshold based on the velocity ratio as a function of mixture ratio. A tentative spontaneous instability threshold for the LeRC injector is indicated in Figure 52 by the region labeled "marginal" in that figure which indicates a region of increased spontaneous instability occurrence.

One potential explanation for the correlation is the hypothesis that a high velocity fuel stream tends to shroud the LOX stream from transverse wave perterbations. Thus for conditions of high velocity ratio the LOX atomization is more dominated by the coaxial gas flow than velocity fluctuations caused by transverse wave motion in the chamber. At high enough values of the velocity ratio, the correlation seems to indicate that even the LeRC injector with a LOX post tuned to close to the 1T frequency of the 5.66 inch diameter chamber can operate in a stable manner. At lower values of the velocity ratio, increases in the atomization and vaporization time lags likely induce a reduction in stability margin.

Additionally these parameters tend to indicate that range of operating conditions likely to result in chamber acoustic velocities that permit frequency matching between the LOX posts and the chamber transverse acoustic modes. In this regard mixture ratio may influence the stability margin for a given velocity ratio by reducing the acoustic velocity to a value such that the transverse modes of the chamber can couple efficiently with the

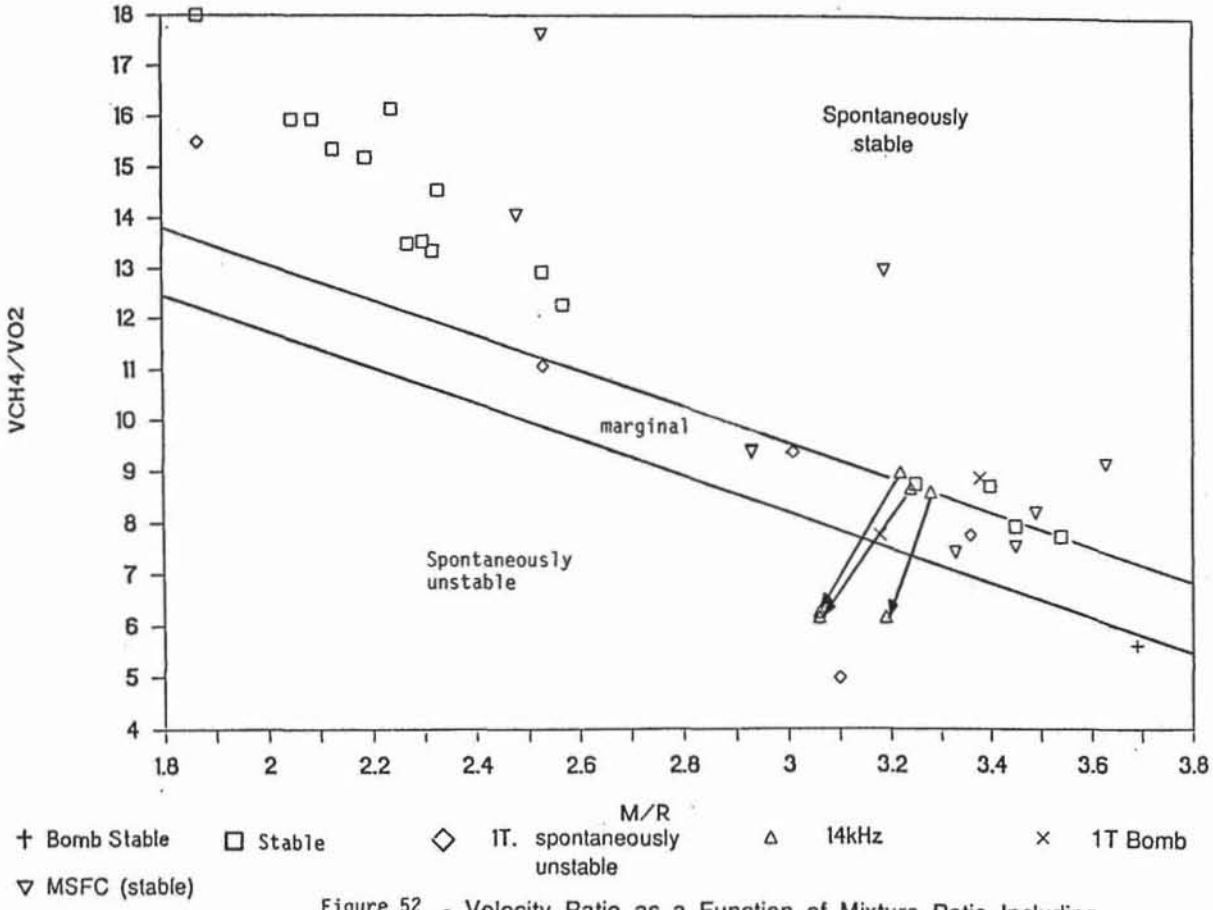

Figure 52 - Velocity Ratio as a Function of Mixture Ratio Including Both LeRC and MSFC LOX/Methane Data

LOX post modes of the LeRC injector. Here again the velocity ratio may also influence the combustion distribution and the acoustic velocity for a given mixture ratio. This matter will be discussed further in the section on stability modeling.

Correlating the data in this fashion mainly indicates common regions of stability for the MSFC and LeRC injectors. The instability threshold for the MSFC and other less similar injectors cannot be implied from this presentation alone.

It is however useful to compare the instability trends of the LeRC methane and published LOX/hydrogen combustors to assess the relative similarity of the two fuels. Recalling the results of fuel temperature ramp testing in the case of LOX/hydrogen combustors (ref.1-9) the effect of ramping the fuel temperature until a self-induced instability occurred. Hence like the methane injector, the LOX/hydrogen combustors exibited improved stability margin at high velocity ratios. Although the instability mode differed in the case of the LOX/methane injector temperature ramping tests, the same tendency toward reduced stability margin as the fuel side resistance and velocity are reduced is seen in both the methane and hydrogen data.

With regard to comparing the dynamic stability behavior of the methane and hydrogen coaxial injectors, the trends with methane are less clear due to the lack of data. Based on the results of reference 18, a pulse gun rated LOX/hydrogen injector could be driven unstable at fuel temperatures and hence fuel velocities above the respective instability threshold values as determined during temperature ramping tests. If the methane injector were to behave in an identical manner, the dynamic stability threshold would be at some range of fuel velocities above its spontaneous instability threshold. However, as discussed in the section entitled Bomb Testing and Spontaneous Instabilities, the greater sensitivity of the LOX/hydrogen injector at low fuel temperatures is suggested to be analagous to the reduced stability margin of the LOX/methane injector at low values of the LOX injection pressure drop. Figure 52 in which LOX side pressure drop is a complex function of the correlating parameters is thus not the best presentation to illustrate this hypothesis.

Stability Modeling

While stability correlations are useful to provide insight into overall trends as functions of operating parameters, such correlations are often hardware specific if (as in the case of LOX/methane data) the data base is limited. To provide a more objective basis for comparison between different injectors as well as to calculate both injector and chamber admittance characteristics and to evaluate the stability margin of the LeRC thrust chamber assembly as a whole, a Rocketdyne version of the Distributed Oscillatory Rocket Combustion (NDORC) code which is a sensitive time lag combustor analysis and POST9A which models the injection response (LOX post and fuel annulus acoustic modes) were used to model the results of several tests on the program.

The NDORC sensitive time lag model developed by Mitchell (Ref. 14 and 22) includes distributed combustion effects and has the capacity to analyze cavities, liners and nozzles. This code calculates the chamber admittance under conditions of neutral stability or growth or decay. The POST9A code solves the "waterhammer" equations for the injection response of a one dimensional flow with both concentrated and distributed resistances (ref. 19) as would occur within an injector element. This selection was motivated by the observed significance of the LOX post resonances in the data and the likelihood of fuel side coupling in the case of the fuel temperature ramp testing.

Three earlier efforts to analyze this data involved the Module code,a predecessor of NDORC (ref.21); a proprietary sensitive time lag analysis with somewhat different capabilities (ref. 15) and a combined injection, combustion and combustor admittance analysis by Priem and Breisacher (ref. 20). While the sum of these efforts has provided insights into the significance of various features of the injector element design with regard to the observed stability behavior, the modeling under discussion was initiated to attempt to explain low amplitude activity at lower than expected acoustic frequencies that preceeded the instabilities.

Analysis of Spontaneous First Tangential Instabilities

The 1-T mode instabilities on the LeRC tests at constant ambient fuel temperature were unexpected when compared to stable results obtained by NASA-MSFC using similar 82-element 5.66-inch diameter hardware. Unlike the LeRC methane tests, the MSFC injector showed stable operation for both prestage and nominal (1860 to 2380 psia) conditions for overall mixture ratios of from 2.48 to 3.63.

The two injectors differ in some specific details. Most notable is the difference in LOX post lengths as shown in Table I. The NASA-MSFC post has an overall length of 4.68 in. vs 3.608 in. on the LeRC hardware. As a result of the longer length, the MSFC post exhibits theoretical resonant frequencies of approximately 3, 6 and 10 kHz based on the POST9A analysis discussed earlier. Another significant difference between the LeRC and MSFC injectors is the Rigimesh faceplate on the MSFC injector. Based on the Rigimesh porosity, fuel side pressure drop, and the net porous face area, 7.2% of the total fuel flow was assumed to pass through the Rigimesh. The element based mixture ratios for the MSFC injector are hence somewhat higher than the overall mixture ratios. Additionally the NASA-MSFC injector had an annular gap at the perimeter which may have acted as an acoustic cavity. The gap was 0.031 in. wide and 1 in. deep.

Since the LOX post resonances for the LeRC injector were significantly different (4.0, 8.6, and 13.6 kHz for the first three post modes) and since unexpected activity in the neighborhood of 4 kHz was almost always observed immediately prior to spontaneous and bomb induced high amplitude 1T instabilities (at the expected 5 kHz frequency), it was reasoned that a combined analysis involving both the LOX post modes and

the chamber responses for carefully evaluated operating conditions would help explain both the different stability characteristics of the LeRC and MSFC injectors as well as the 4 kHz precursor activity.

Description of the Analysis Method

As discussed above, the analysis is based upon two separate open loop acoustic response techniques: a Rocketdyne modification of the NDORC code and POST9A which analyzes the acoustic response of the propellants in the injection elements. The NDORC code uses the equations of linear perturbation acoustics to calculate the complex chamber response required for a neutrally stable chamber oscillation (ie. with no decay or growth). The complex response can be translated into a phase and gain (magnitude) of the form

$$C_{res} = M(\cos\phi + i \sin\phi)$$

where C_{res} is the complex chamber response, M is the response magnitude and ϕ is the phase angle in radians. The chamber response magnitude is in the form of a normalized admittance

$$M = w' P_c / W p'$$

where w' and p' are the fluctuating mass flow rate and pressure in the chamber and W and P_c are the mean flow rate and chamber pressure.

The version of the NDORC used for the analyses presented here requires the axial distribution in the combustion product mass release as an input. Hence a separate prediction of the fraction of propellants reacted vs axial distance is needed to initiate the stability analysis. Coaxial Injection Combustion Model (CICM) code (Ref. 16) calculations of the vaporization limited performance were used to provide the needed combustion distribution. As discussed in the section on Performance Tests this code was anchored to measured combustion efficiencies on specific tests and hence was felt to be reasonably accurate.

In addition to providing the combustion mass release profiles for the NDORC code, the CICM runs were used to determine an effective chamber acoustic velocity near the face of the injector. An average acoustic velocity was calculated on the basis of the axial distribution of the acoustic velocity over the first three inches of the combustor. Two such distributions are shown in Figure 47 and indicate that the relative variation in the computed acoustic velocity can be large near the injector face. The region near the injector face is of significance to the stability of the combustor since this zone can be expected to couple effectively with the LOX posts and also represents a region of substantial available chemical energy to support a high amplitude combustion instability. Furthermore this is also the region of maximum burning rate which controls the axial distribution of all gas properties including the acoustic velocity. The analyses based on this average acoustic velocity was found to anchor well with the overall stability characteristics of the LeRC and MSFC combustors.

The POST9A code used to analyze the LOX post uses linear perturbation acoustic theory to predict injected propellant flowrate fluctuations due to downstream (chamber) pressure fluctuations. The code models both distributed (viscous) and concentrated (area change) resistances to calculate response magnitudes. The output of this code (see Figure 26, for example) is converted to a nondimensional admittance of the same form as the chamber response.

The two results are then plotted on a response magnitude vs frequency plot (or Bode plot as it is known in control theory). If the magnitude of the injector response is greater than the chamber response at neutral stability for a given frequency, the possibility for an instability exists if the overall time lag or phase of the combustion matches that of the chamber. The fuel and burning responses were not included in the modeling. For the 1T instability analyses it is felt that the fuel response is a secondary effect. The atomization and vaporization that are part of the burning response modify the injection response and provide a true overall combustion response. The burning response is required for calculation of the overall time lag or phase angle of the combustion process. Hence the present results should be regarded as providing a relative margin rather than an absolute stability prediction.

For the case of the 14 kHz activity, a fuel side admittance analysis was conducted. Further model development to better address that condition is in progress.

Results for the First Tangential Mode

The relative margins of stability of two tests, one stable and one spontaneously unstable, at well defined operating conditions in mainstage were analyzed. Test 014 which exhibited 8 seconds of stable operation and test 022 which produced a 1T instability after 2.1 seconds of operation at mainstage were selected. The operating conditions of other tests such as 019 which exhibited an instability in transition could not be defined with as much confidence. Dynamic stability margins cannot be directly evaluated by the linear models used so the bomb tests were not considered.

Shown in Figure 53 are the injector and chamber response curves for test 022. Note that the injector response exceeds the chamber response at neutral stability over a region or band near 4 kHz. For comparison in Figure 54 are shown the injector and chamber responses for test 014. The lack of a region of overlap in that figure indicates that the available damping in the chamber exceeds the injection gain.

The key difference between 014 and 022 is seen to be the tuning of the chamber response relative to the LOX injection response as a function of the combustion profile near the face and the operating conditions. While the conditions of test 014 result in a minimum chamber response at roughly 4.3 kHz the conditions of test 022

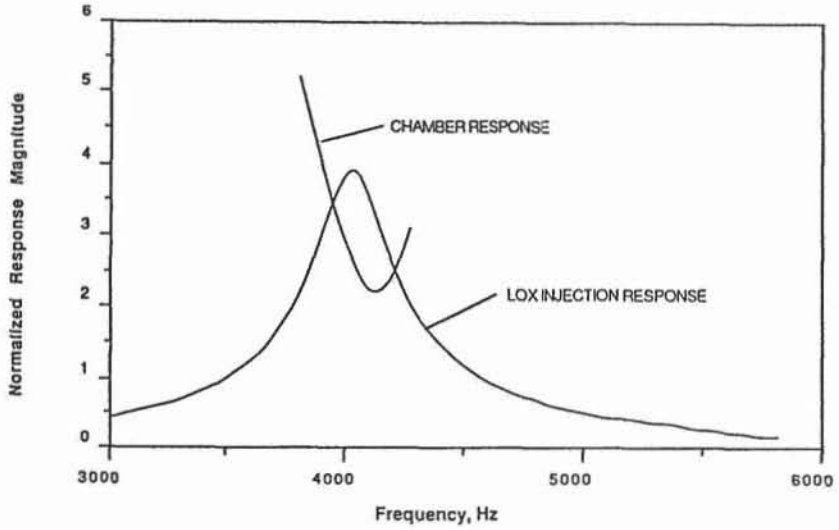

Figure 53 - Chamber and LOX Post Injection Response for Test 014-022 which Exhibited a Spontaneous 1T Instability

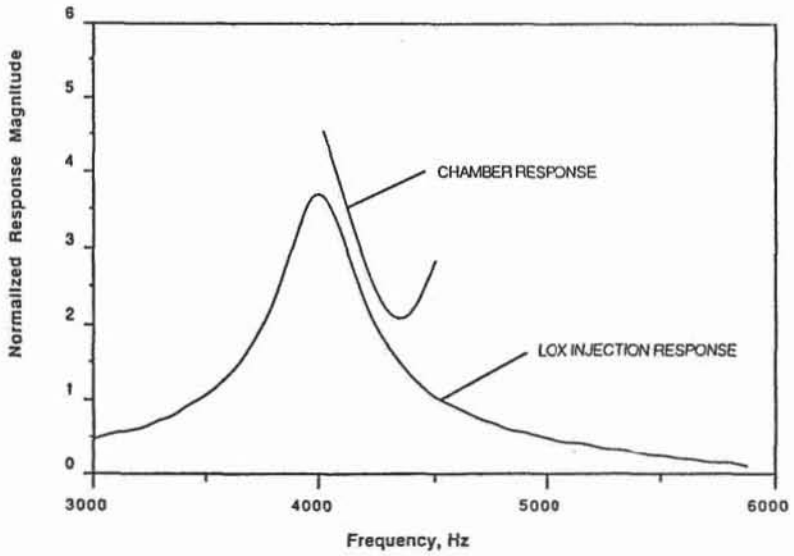

Figure 54 - Chamber and LOX Post Injection Response for Test 014-014 (Stable)

lead to a minimum at 4.1 kHz. The key difference between the two tests which led to this shift are that 022 was at a slightly lower mixture ratio (3.01 vs 3.4) relative to test 014. Additionally, the results of the analysis indicate that a low amplitude 1T mode at approximately 4 kHz could be supported in the chamber for the conditions of test 022. As the amplitude of the activity increased, wave induced mixing and perhaps changes in the element cup combustion processes could be expected to increase the percent completeness of the burning and hence increase the acoustic velocity and 1T mode frequency to a value expected for a well-mixed, equilibrium combustor (ie. 5 kHz).

These predictions are corroborated by the fact that the accelerometers on test 022 indicated 4.4 kHz activity prior to the onset of the high level instability at 5 kHz. Other tests in which high frequency pressure transducers were available indicate the presence of a 1T standing mode at about 4 kHz prior to the high amplitude instability, based on relative phase and amplitudes. Hence a reduction in acoustic velocity near the injector face would seem to both explain the reduced stability on test 022 and the chamber acoustic activity at a frequency below that expected for a 1T mode.

An additional observation that supports the analytical results is that the combustor typically exhibited a burst of 1T activity at the start of cutoff (including test 014). Since the cutoff involves a sequenced reduction of the LOX flow before the fuel (fuel override condition), the LOX injection pressure drop decreases early in cutoff and results in a temporary increase in the LOX injection response. Simultaneously the instantaneous mixture ratio is decreasing rapidly due to the lag in the fuel shutdown sequence which is done to preserve the hardware. The reduced mixture ratio may result in a reduction of the chamber acoustic velocity and 1T frequency band as on test 022. Referring to Figure 54, it is apparent that the indicated stability margin is low and any increase in the LOX injection response could trigger an instability, as indeed occurred. Hence this limited model appears to indicate the stability trends of the LeRC injector fairly well.

The stabilizing influence of the longer MSFC LOX posts is seen in Figure 55. The peak injector response is shifted to 3 kHz approximately, well separated from the chamber response. Hence the MSFC injector is predicted to show a better stability margin at operating conditions (such as low mixture ratio) which lead to reduced acoustic velocities as in test 022.

The influence of the near face acoustics on the stability margin is interesting. The fact that a 1T instability would only be predicted for the LeRC hardware on the basis of an acoustic velocity lower than that exhibited during the high amplitude instability indicates a sensitivity to the pre-instability combustion conditions that is not often accounted for in stability analyses. Similar CICM analyses of the acoustic velocity of test 023 during the temperature ramp just before the 14 kHz activity indicate a low-valued acoustic velocity distribution. The cold

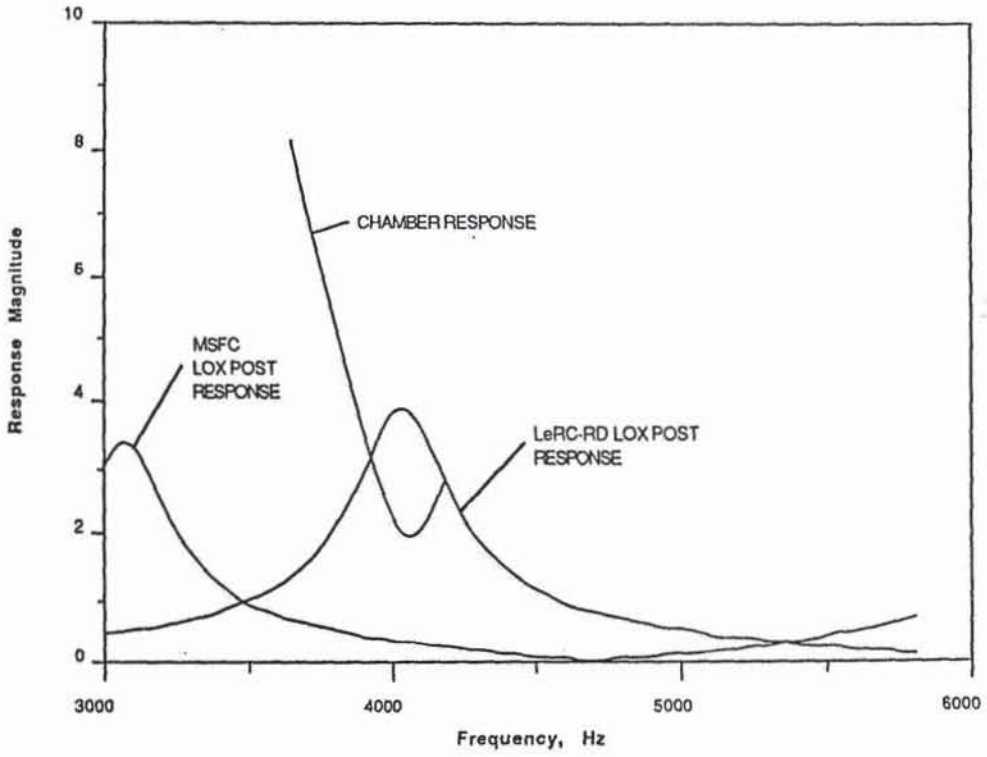

Figure 55 - Comparison of LeRC and MSFC LOX Post Response versus Typical Chamber Response Curve

methane conditions result in a low fuel velocity (low velocity ratio) and lower burning rates over the first few inches of the combustor. Based on these analyses it may be that the correlation of Figure 52 indicates reduced stability margin for the LeRC injector for conditions of lower average acoustic velocity near the injector face, either as a result of low mixture ratio or low velocity ratio. While the correlation is likely not general since it does not account for the effects of LOX post and fuel annulus tuning, for the LeRC injector the correlation and modeling interpreted in this manner appear consistent.

Results for the 14 kHz Mode

A limited analytical effort was conducted to asses the effects of the fuel temperature ramp on the peak fuel side injection admittance. Although the LOX side was determined to have a resonant mode near 14 kHz, the instability was in each instance caused as a result of the reduction in fuel temperature to about 430 degrees Rankine (at the point of injection). As discussed earlier a simple closed-open mode model of the fuel annulus at the operating conditions at the start and conclusion of the ramp model the increasing frequency activity (from 12 kHz to 14kHz) observed in the accelerometer isoplots (see Figure 24).

The POST9A code was used to substantiate these results for the entire fuel passage geometry from the manifold to the tip of the LOX post. The results are shown in Figure 56. Both the frequency and response magnitude increase as the fuel temperature is reduced. Coupled to the LOX response at the proper phase, the variable fuel response potentially can exceed the chamber response (at neutral stability) near 14 Khz for modes such as the 5T, assuming an average acoustic velocity based on the CICM predictions for the acoustic velocity distribution for the first few inches of the combustor at the conditions of 14 kHz onset.

In summary, the modeling effort apears to substantiate the significance of LOX post resonant modes with respect to the 1T stability margin and the fuel annulus mode frequency variation with respect to the 14 kHz activity in fuel temperature ramping tests.

Figure 56 - PREDICTIONS OF THE FUEL RESPONSE AT THE START AND END OF THE TEMPERATURE RAMP FOR THE LOX/METHANE TEST NUMBER 23

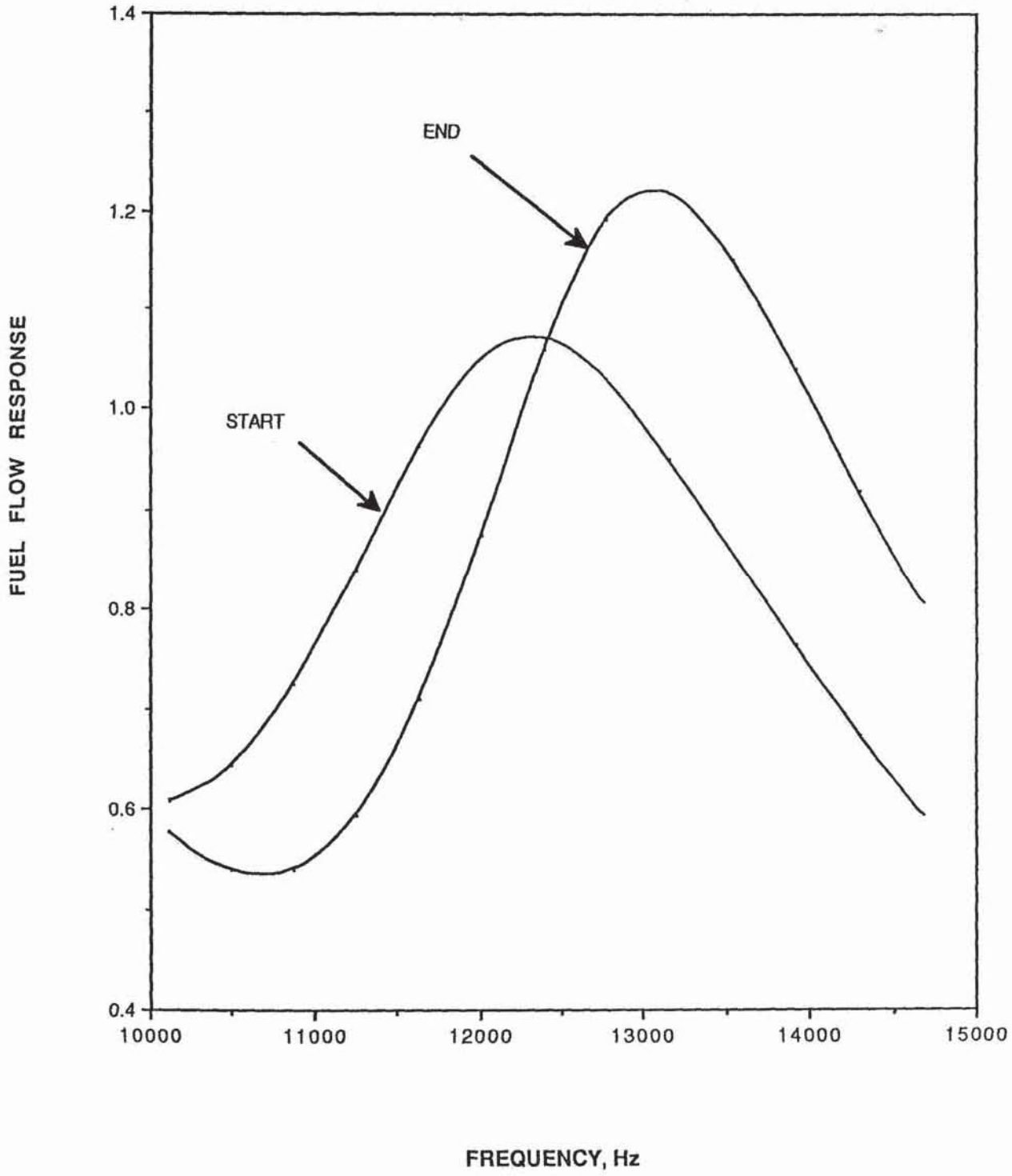

CONCLUSIONS

The LOX/Hydrocarbon Combustion Instability Investigation Program was structured to determine if the use of light hydrocarbon fuels (such as methane) with liquid oxygen (LOX) produces combustion performance and stability behavior similar to the LOX/hydrogen propellant combination. In particular, methane was investigated to determine if it can be rated for combustion instability using the same techniques as previously used for LOX/hydrogen. These techniques included fuel temperature ramping and stability bomb tests.

The hot fire test program, using a 40,000 lb. thrust class of experimental hardware, probed the combusiton behavior of the LOX/methane propellant combination from ambient to subambient (438 degrees R in the manifold) fuel temperatures. Significant results were obtained from this program that have potential importance to future LOX/methane development programs. Even though this program was directed toward the combustion stability mechanisms of LOX/methane, injector performance and chamber heat flux data were also obtained.

The 40,000 lb. thrust experimental hardware used for this program incorporated 82 coaxial injector elements in a 5.66 inch diameter thrust chamber calorimeter configuration. It is very important to note that no acoustic stability aids were incorporated in the thrust chamber assembly. The program was oriented toward defining a stability margin, and in order to do that, combustion instabilities had to occur in order to define the stability threshold for this combustor. Therefore, the goal of the test program, to demonstrate an instability threshold as a function of fuel temperature and related parameters such that a comparison could be made with LOX/hydrogen instability, was achieved.

The experimental test program operated the LOX/methane combustor over a mainstage mixture ratio range of 2.5 to 3.7 and mainstage durations fo from 0.1 to 8 seconds. in tests at a nominal chamber pressure of 2000 psia. Three tests were successfully driven unstable at low fuel temperature during fuel temperature ramping stability rating tests. Five tests experienced self induced 1T instabilities at higher fuel temperatures. Two of three bomb tests were dynamically unstable. Low mixture ratio performance and stability data was obtained at about 1500 psia (prestage conditions) for each mainstage test. The test program generated data for the evaluation of the methane stability characteristics relative to hydrogen and for anchoring stability and performance models.

The primary results and conclusions obtained as a result of the LOX/Hydrocarbon Combustion Instability Investigation Program are summarized below.

Performance

For the testing conducted on this contract, at a mixture ratio range from 3.01 to 3.45, ambient fuel temperature, and a chamber

pressure of 2000 psia, the average c* efficiency was 97.2% with a variation between tests of +/- 0.5%. Temperature ramping tests yielded average c* efficiencies between 97.7 and 98.1% at mixture ratios from 3.06 to 3.19, at a chamber pressure of 2000 psia, and fuel injection temperatures from 437 to 444 degrees R. The apparent slight increase in c* efficiency is probably caused by lower momentum flux ratio which decreased mixing losses. A correlation between c* efficiency and momentum flux ratio which utilized both mainstage and prestage data indicates that mixing losses cause performance degradation (~4%) at low chamber pressure and low mixture ratio (prestage) conditions.

Chamber Heat Flux

Peak throat heat fluxes were obtained and evaluated during the experimental test portion of this program. the results indicated that, for this combustor, 89 to 95% of the theoretical peak heat flux value for LOX/hydrogen were realized. It should be pointed out that the peak heat flux values achieved on this program are significantly higher than the peak heat flux values for the NASA-MSFC 82 element coaxial injector. Testing of the MSFC injector yielded peak heat fluxes (29.2 to 46.2 BTU/sq.in-sec) which were 60 to 74% of the theoretical value for LOX/hydrogen. Further testing and analysis is necessary to resolve this discrepancy.

Stability

1.) The temperature ramp stability rating technique appears to be a valid stability rating approach for LOX/methane engines. It was applied successfully, resulting in reproducable instabilities in a narrow range of injected fuel temperatures. However, the temperature ramp technique excited a 14 kHz instability mode rather than the first tangential acoustic instability mode as in LOX/hydrogen testing.

2.) First tangential instabilities occurred spontaneously and as a result of bomb disturbances and appear to be related to a similar mechanism in that most were preceeded by 4 kHz activity. As a result, for this configuration temperature ramping alone did not fully characterize the combustion stability of the injector.

3.) Stability bombing was capable of exciting 5 kHz instabilities in an operating region similar to the region where spontaneous 5 kHz instabilities occurred. Stability bombing tests at lower fuel temperatures did not lead to the 14 kHz mode.

4.) Based on a correlation of the data, the NASA LeRC combustor appears less sensitive to spontaneous instability at higher mixture ratios. Also for a given mixture ratio, the stability margin improves at higher velocity ratios.

5.) When compared to the results of combustion stability analyses, the high frequency instability data showed strong evidences of injection coupling - in which the injector propellant (LOX post and/or fuel annulus) dynamics couple with chamber pressure oscillations - on virtually every unstable test.

6.) The LOX/methane system demonstrated characteristics similar to LOX/hydrogen systems. Overall similarities are seen between hydrogen and methane with regard to the sensitivity to injection coupling with chamber pressure oscillations and the applicability of bombing for stability rating purposes.

7.) Based on the data correlation, stability modeling and comparisons with the data of a similar (MSFC) combustor (with an injector having dissimilar injection coupling characteristics), injector element internal geometry and combustor operating conditions (such as propellant velocity ratio, mixture ratio, and fuel temperature) appear to be effective factors to enhance the stability margin of coaxial LOX/methane injectors.

The results from this program will provide significant guidance in the development of stable, high performance coaxial element injectors for future booster engine applications.

REFERENCES

1. Wanhainen, J. P., et al, "Effect of Propellant Injection Velocity on Screen in 20000-pound Hydrogen-Oxygen Rocket Engine," NASA TN D-3373, 1966.

2. Salmi, R. J., et al, "Effect of Thrust Per Element on Combustion Stability Characteristics of Hydrogen-Oxygen Rocket Engines, "NASA TN D-4851, 1968.

3. Bloomer, H. E., et al, "Chamber Shape Effect on Combustion Instability," NASA TM X-52361, 1967.

4. Wanhainen, J. P., et al, "Effect of Chamber Pressure, Flow Per Element, and Contraction Ratio on Acoustic-Mode Instability in Hydrogen-Oxygen Rockets, "NASA TN D-4733, 1968.

5. Conrad, E. W., et al, "Interim Summary of Liquid Rocket Acoustic-Mode-Instability Studies at a Nominal Thrust of 20,000 Pounds," NASA TN D-4968, 1968.

6. Wanhainen, J. P., and Morgan, C. J., "Effect of Injection Element Radial Distribution and Chamber Geometry on Acoustic-Mode Instability in a Hydrogen Oxygen Rocket, "NASA TN D-5375, 1969.

7. Hannum, N. P., et al, "Some Injector Element Detail Effects on Screech in Hydrogen-Oxygen Rockets, "NASA TM X-2982, 1974.

8. Hannum, N. P., et al, "Stabilizing Effects of Several Injector Face Baffle Configurations on Screech in a 20000-Pound-Thrust Hydrogen-Oxygen Rocket, "NASA TN D-4515, 1968.

9. Barsotti, R. J., et al, "Development of Liquid Oxygen/Liquid Hydrogen Thrust Chamber for the M-1 Engine," NASA CR-54813, NASA Contract NAS3-2555, 1968.

10. Bailey, C. R., "Test Evaluation of Oxygen-Methane Main Injectors," 1987 JANNAF Propulsion Conference.

11. , "Detailed Task III and IV Report : Detailed Hardware Design and Fabrication," Contract NAS3-24612, Rocketdyne document 87RC02157, Feb. 1987.

12. , 4400-Hz Vibration Investigation Final Report, Rocketdyne Report R-8742, Contract NAS8-25156, June 1971.

13. Feiler, C. E., and Heidmann, M. F., "Dynamic Response of Gaseous - Hydrogen Flow System and Its Application to High-Frequency Combustion Instability", NASA TN D-4040, 1967.

14. Mitchell, C. E.,"Improvement of an Integral Stability Model," 22nd JANNAF Combustion Meeting, October 1985.

15. Philippart, K. D., Stability Characteristics and Analysis of Liquid Oxygen/Methane Injectors, 24th JANNAF Combustion Meeting, October, 1987.

16. Sutton, R. D., et al. Operating Manual for Coaxial Injector Combustion Model, Final Report, Contract NAS8-29664, April 1974.

17. Smith, A. J. Jr., et al. The Sensitive Time Lag Theory and Its Application to Liquid Rocket Combustion Instability Problems, Vol I, AFRPL-TR-67-314, March, 1968.

18. Sokolowski, D. E., et al. Characterization of Pressure Perturbations Induced in a Rocket Combustor by a Machine Gun, TN D-5214, May,1969.

19. Fenwick,J., private comm.

20. Priem, R. and Breisacher, K. J.,"Combustion Instability Coupling with Feed System Acoustics," 1988 Earth to Orbit Conference, MSFC, May 1988.

21. Jensen, R. J., et al.,"Oxygen/Methane Combustion Stability Investigation," 1988 Earth to Orbit Conference, MSFC, May 1988.

22. Mitchell, C. E., et al,"Acoustic Cavity Model Development," 23rd JANNAF Combustion Meeting, October 1986.

23. Wanhainen, J. P., et al., "Evaluation of Screech Suppression Concepts in a 20000-Pound Thrust-Hydrogen-Oxygen Rocket," NASA TM X-1435, April 1967.

24. Fang, J. J., "Comparison of Analytical Modeling Results with O_2/H_2 Combustion Stability Data," 21st JANNAF Combustion Meeting, Oct. 1984.

APPENDIX A - HARDWARE AND FACILITY DESCRIPTION

A1. Hardware Description

A conceptual design was developed in Task I for a thrust chamber configuration that would be capable of determining the combustion stability characteristics of the liquid oxygen and methane propellant combination. Results of Task I are summarized in the contract report entitled "Detailed Task I Report: Analysis of O2/H2 Stability Rating Techniques" released in June 1986 under Rocketdyne document number 86RC10202. In Task III, Detailed Test Hardware Design, the conceptual design was finalized and detailed. The results of Task III are presented in the contract report entitled "Detailed Task III and Task IV Reports: Detailed Design and Fabrication" released in February 1987. Much of this appendix is taken from the Task III report.

The thrust class and chamber size of the test hardware were selected based on stability criteria and past test experience. Originally a chamber diameter of 3.5 inches was proposed based upon fabrication and test costs. However, testing at NASA-MSFC of a 5.66 inch diameter chamber had produced no instabilities at ambient methane temperature. By increasing the diameter of an unbaffled chamber, the potential for producing an instability increases. Furthermore, data correlations indicate that increasing the number of injector elements also leads to lower stability margins. Testing an inherently more stable 3.5 inch diameter chamber perhaps would not demonstrate the stability rating techniques for proven high performance LOX/methane injector designs. Therefore, the 40K pound thrust class, larger chamber diameter combustor was selected for stability testing.

The thrust chamber design was similar to the configurations previously hot fire tested which have demonstrated stable operation and high performance (98-99% c* efficiency). The chamber was designed to be tested at a nominal mixture ratio of 3.5 and varied 20% greater and 20% less than nominal. This ensured that as the stability margins were probed, the instabilities encountered were relevant to the correlation parameters being investigated and not attributed to a new, unproven configuration which may be inherently unstable. The thrust chamber accommodates the installation of a bomb rating device, and provides for performance and stability measurement instrumentation. Depending on the hardware configuration, the thrust chamber is capable of sustaining durations of ten seconds for temperature ramp tests and two seconds for bomb tests. The thrust chamber assembly is shown in Figure A1.

Injector Assembly

The baseline injector incorporates 82 coaxial injection elements with recessed LOX posts in five concentric rows and a centrally located igniter. The faceplate is designed to be removable and interchangeable with other faceplate configurations. The injector is pictured in Figure A2.

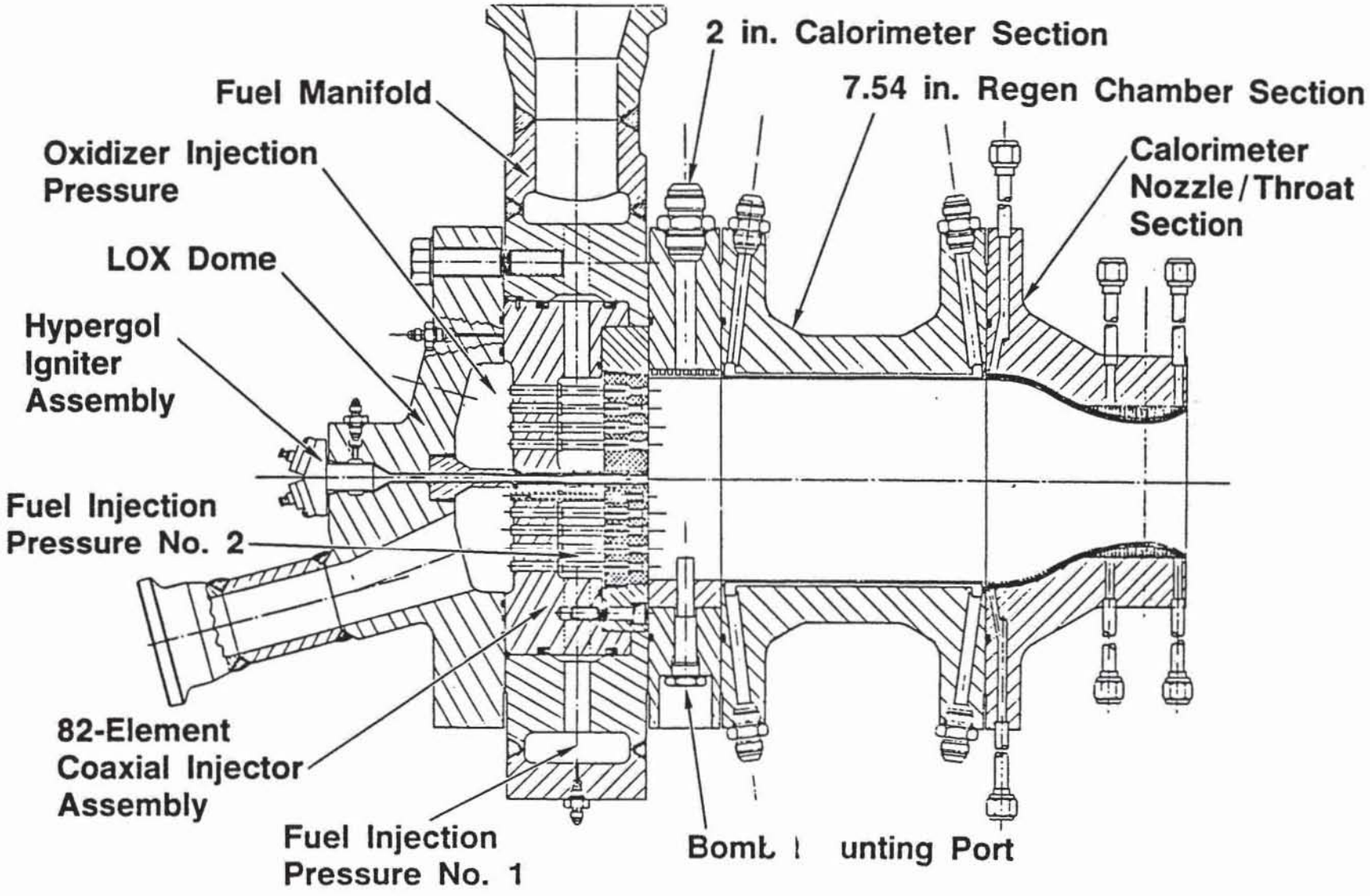

Figure A1 - 82-Element LOX/Methane Injector and Thrust Chamber

Hot fire testing required that the fuel injection velocity be varied to determine influences on combustion performance and stability characteristics. Fuel injection velocity was to be varied by changing the coaxial element fuel injection area in addition to fuel flowrate control (mixture ratio) and fuel injection temperature. The fuel injection area is controlled by the gap established between the LOX post outer diameter and the faceplate hole inner diameter. Three interchangeable faceplates with associated hole diameters and configurations were designed and fabricated to vary both the fuel injection area and pressure differential between the fuel manifold and combustion chamber. The nominal fuel injection area faceplate establishes an 0.011 inch fuel annulus gap in the element. This configuration has been demonstrated in hot fire testing (NASA-MSFC) of a Rocketdyne designed thrust chamber providing spontaneous stable operation and high performance (98% c* efficiency) at chamber pressures to 2300 psia in a 5.6 inch chamber diameter. The second faceplate has .007 inch gap which greatly increases the fuel velocity to be utilized if the nominal gap faceplate demonstrates instability. The third faceplate configuration has a 0.021 inch gap which significantly reduces the fuel flow velocity yet incorporates a restrictor step at the element fuel entrance to provide the same resistance of pressure differential as the nominal configuration. Maintaining the same resistance lessens the potential for feed system instabilities. This faceplate was to be used if the nominal gap demonstrated stable operation.

Initial design of the faceplate used rigimesh material to provide porosity to enhance face cooling. After fabricating a 1.25 inch thick faceplate, however, flow calibration indicated that the necessary porosity was not provided. For a redesign, high conductivity NARloy-Z was substituted for the faceplate material. Heat distress to the injector face was not expected for the solid NARloy-Z design since the high conductivity and close element spacing should provide adequate heat transfer.

The LOX posts have integrally machined centering devices which position the posts in holes drilled through the removable faceplate. LOX flow is metered through the 0.086 inch diameter LOX post orifice located at the post entrance. The posts also incorporate a 6 degree inner diameter taper at the exit to control velocity, pressure differential, and flow direction. For the first four tests only (tests 014-001 through 014-004), a 15 degree inner diameter taper was employed. The LOX posts are brazed into the component which comprises the interpropellant plate and inner fuel manifold.

Two injector inserts were designed to provide the capability to test with recessed LOX posts (creating an element cup) or with LOX posts which are flush with the faceplate. All testing was performed with the recessed LOX posts.

Provisions were made to temporarily deactivate the outer row LOX post directly upstream of the bomb device which protrudes into

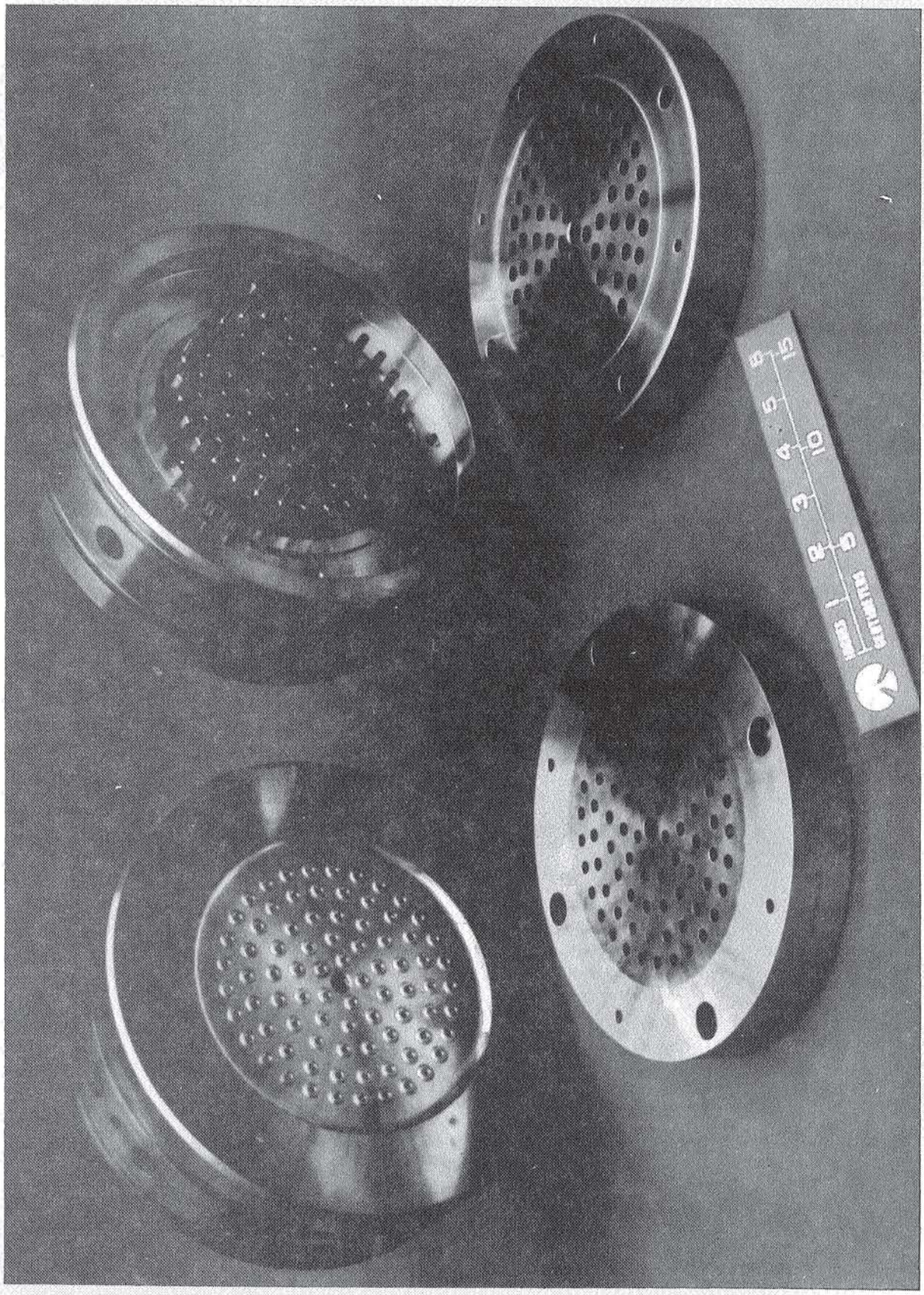

Figure A2 – 82–Element Injector

the combustion chamber when installed. The post was deactivated during the bomb tests so the bomb would not be prematurely detonated and the LOX stream would not be inadvertently deflected toward the chamber wall.

The LOX enters the dome housing through an offset inlet (1.689 in. I.D.) to provide clearance for the centrally located igniter. The inlet is flared upstream of the LOX manifold to diffuse the velocity. The LOX dome has ports for high frequency and steady state pressure measurements, temperature measurement, and to provide access to deactivate the LOX post upstream of the bomb during testing. The fuel passage manifold has a side mounted fuel inlet (2.30 in. I.D.) which feeds sixteen 0.687 inlet holes which are offset from the injector insert fuel passages. The fuel passage manifold has ports for high frequency and steady state pressure and temperature instrumentation as well as taps for mounting accelerometers on three axes.

Detailed drawings of the injector components are presented in Figures A3 through A6. Additionally, a summary of the injector details is presented in Table A.I along with a comparison to the NASA-MSFC injector.

CTF Igniter

Ignition of the injector propellant was accomplished with the hypergolic reaction of methane and chlorine-triflouride (CTF). The ignition system employed a coaxial igniter element centrally located in the injector which consisted of a removeable inner post housed in an outer tube welded into the LOX dome housing. The igniter CTF post was positioned within the outer tube with four centering devices located in the aft end.

CTF was injected through the center tube and igniter methane is injected through the coaxial annulus. The CTF and methane mix at the injector face plane and ignite. During start CTF was injected from a run tank through a metering orifice until mainstage OK timer check was achieved. Expulsion of the CTF was accomplished by purging with GOX for mainstage operation. This was to ensure that CTF was exhausted from the combustion chamber so that during bomb firing residual hypergol would not affect stability.

Combustion Chamber Assembly

The combustion chamber was designed for a nominal 2000 psia operating pressure. Dimensions of the assembled chamber were 5.66 inches in diameter, 15.1 inches in overall length (14 inches from the injector face to the throat plane), 3.252 inch throat diameter and a resultant 3.03 contraction ratio. The combustion chamber assembly is illustrated in Figure A1.

The combustion chamber was an assembly of three major components: a 2 inch instrumentation/bomb ring, a 7.5 inch regen section, and

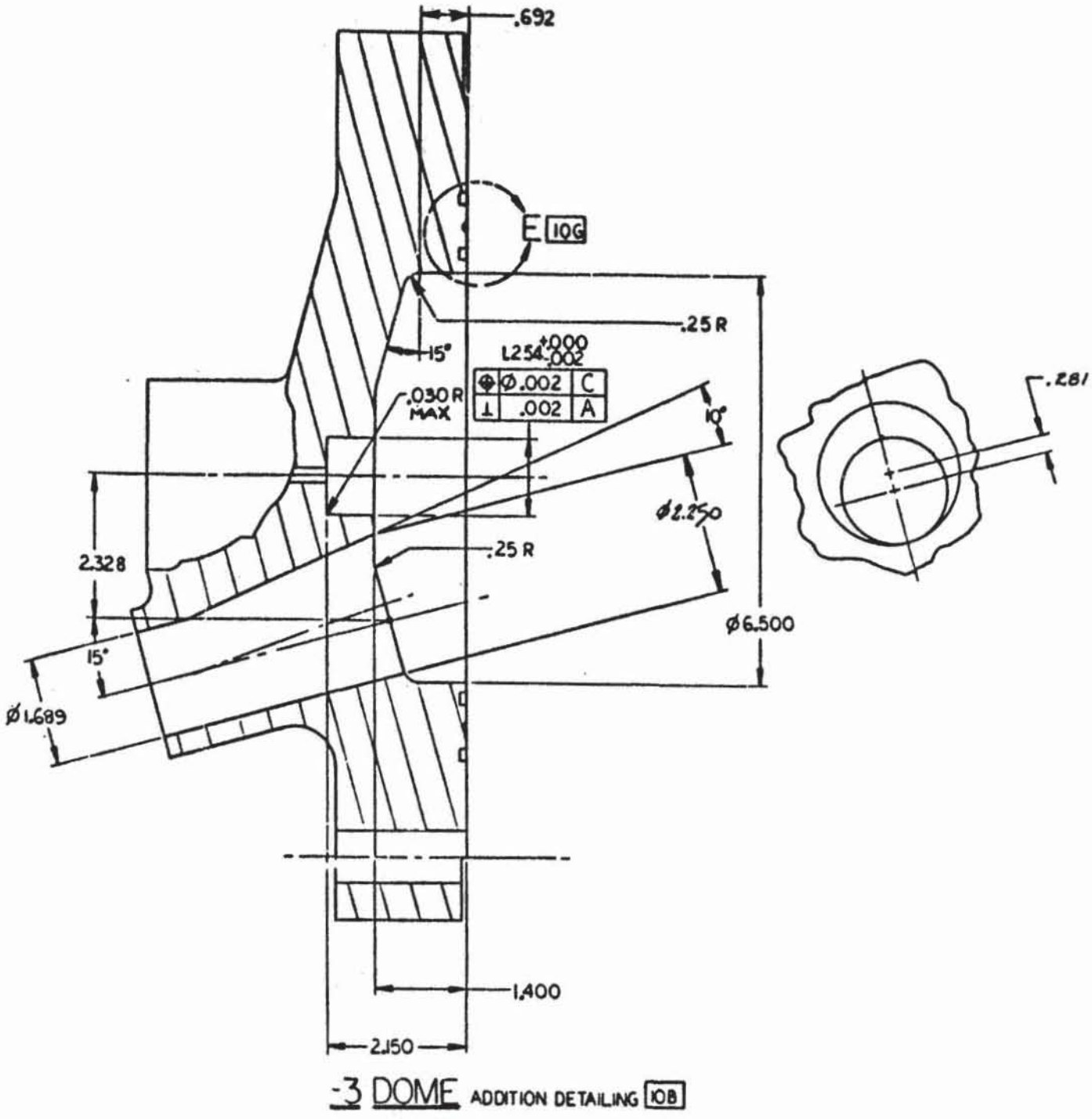

Figure A3 - LOX Dome Geometry

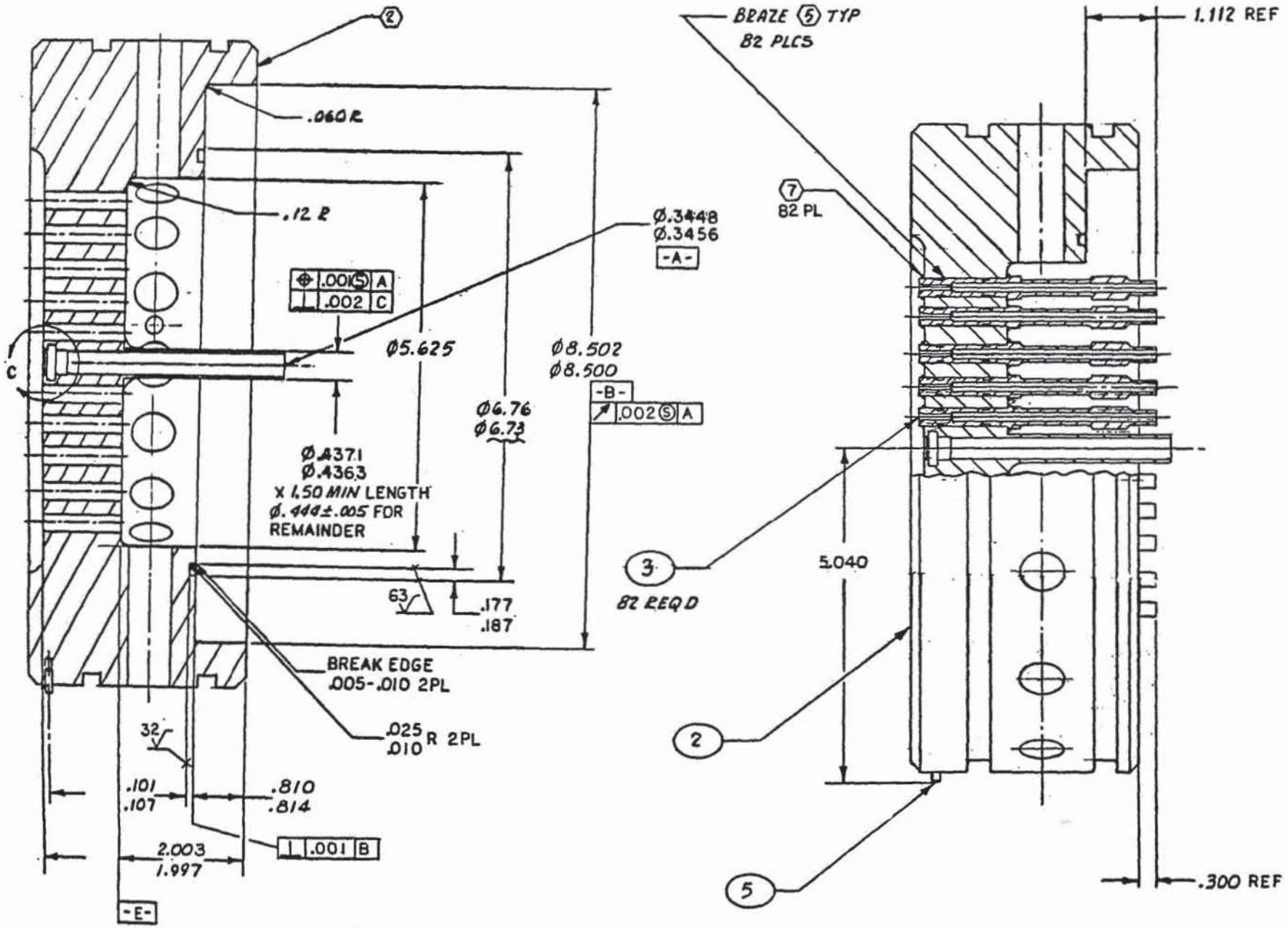

Figure A4 - Fuel Manifold Geometry

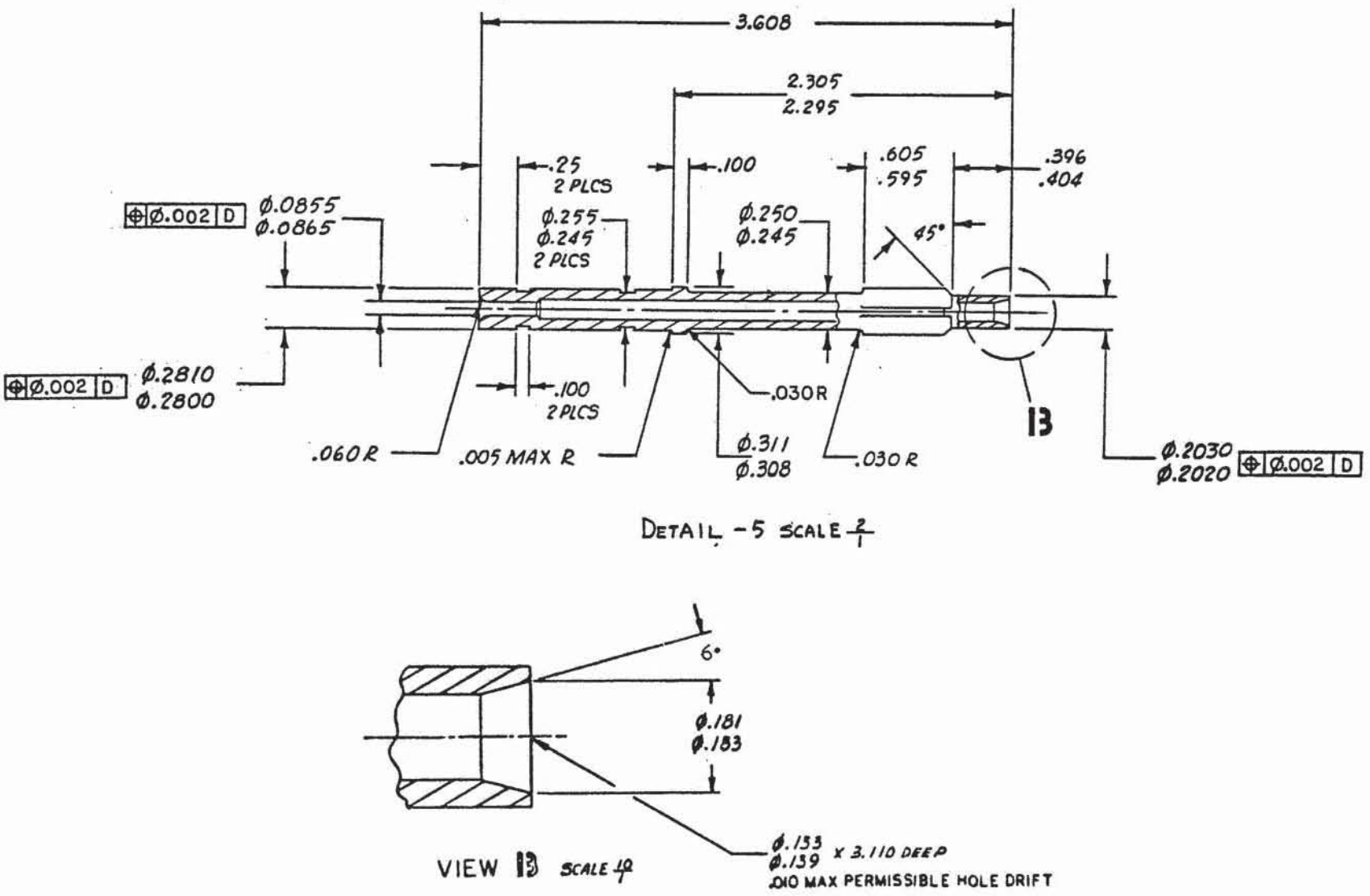

Figure A5 - LOX Post Geometry

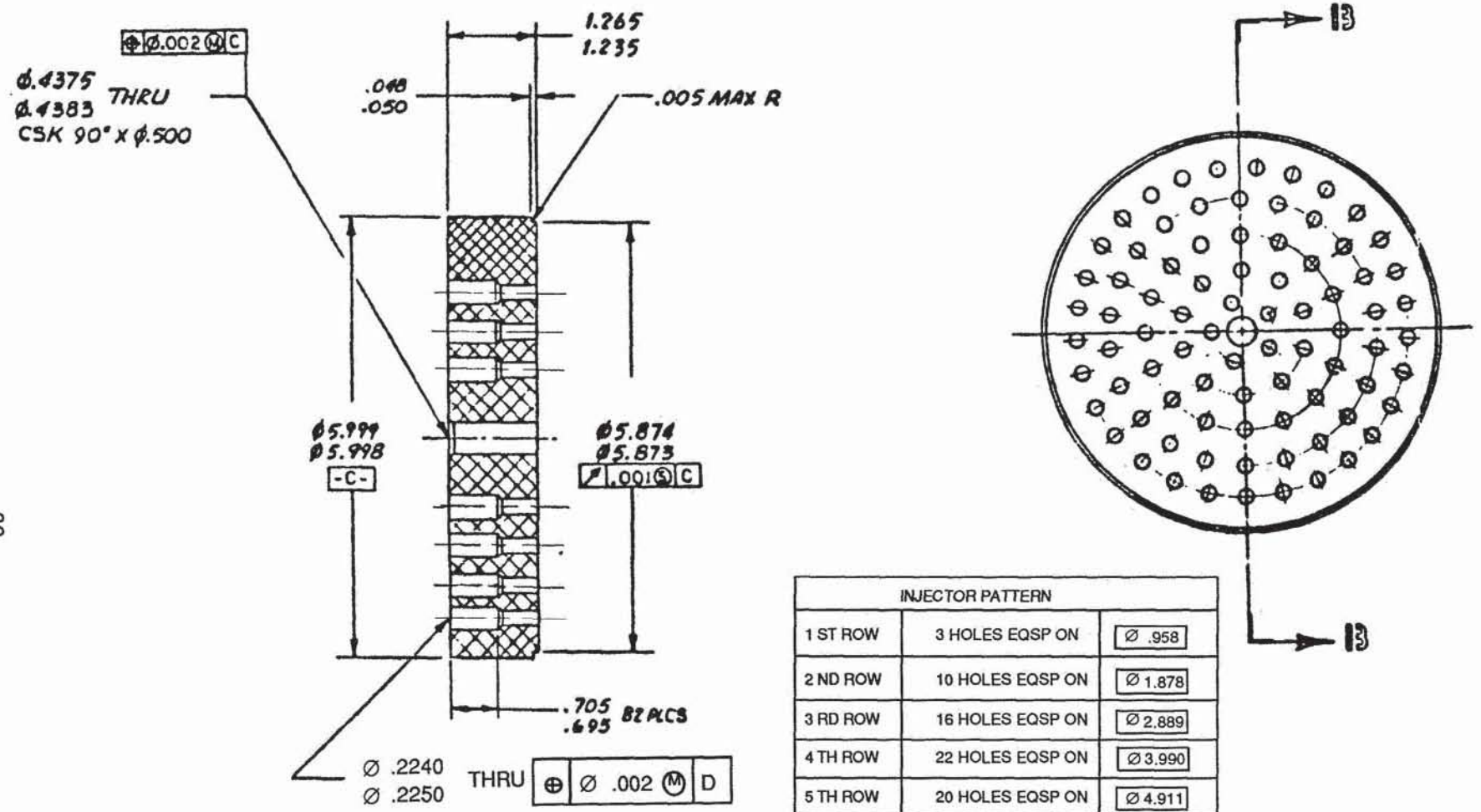

INJECTOR PATTERN		
1 ST ROW	3 HOLES EQSP ON	Ø .958
2 ND ROW	10 HOLES EQSP ON	Ø 1.878
3 RD ROW	16 HOLES EQSP ON	Ø 2.889
4 TH ROW	22 HOLES EQSP ON	Ø 3.990
5 TH ROW	20 HOLES EQSP ON	Ø 4.911
TOTAL 82 HOLES		

Figure A6 - Solid Faceplate Geometry

TABLE A.I - LOX/Methane Coaxial Injector and Chamber Details

Feature	LeRC Design	MSFC Design
Faceplate	Solid NARloy (no bleed)	Rigimesh with facenuts (7.2% bleed)
Oxidizer post exit (deg half angle)	15 (Test 004) 6 (all other tests)	6
Oxidizer post length (in.)	3.608	4.68
Fuel annulus gap (in.)	0.0105	0.0115
Oxidizer post recess (in.)	0.202	0.200
Acoustic absorber	none	Potential 1/4 wave gap (0.070 in. and 0.030 in wide by 1 in. deep)
Chamber interface	graphite liner (Test 004) OFHC liner (Phase C) cooled ring (all others)	cooled chamber
Methane purity (%)	99.9	95

NOTE: Chamber diameter = 5.66 in., length of cylindrical portion of chamber = 9.54 in., length of convergent section = 4.47 in., and nozzle contraction ratio = 2.92

a nozzle-throat section. A 2 inch chamber section was installed adjacent to the injector faceplate. This section differs for the bomb and temperature ramping tests. For the initial bomb tests, this 2 inch section was an uncooled stainless steel strongback with a replaceable graphite insert which accommodates the bomb device. The graphite insert was extensively damaged on test 014-004 and on subsequent bomb tests (Phase C) the graphite was replaced by a zirconia-coated OFHC section which was brazed to the steel strongback. For the temperature ramping tests a 2 inch water cooled calorimeter spool was installed. Both of the 2 inch sections had accomodations for three high frequency pressure transducers and two static pressure transducers. The high frequency pressure transducers were placed at locations 90, 120, and 300 degrees from the top (12 o'clock) position. Figure A7 illustrates the high frequency transducer location in the instrumentation/bomb ring. The static pressure transducers were located 180 and 90 degrees from the 12 o'clock position and measurements were made at the interface of the 2 inch section and the regen section (2 inches from the faceplate).

The regen section was a 7.5 inch long cylindrical section which is installed between the 2 inch chamber and the nozzle-throat section. The chamber was water cooled through 120 regerative-type longitudinal passages. These channels were machined in a NARloy-Z liner and had a .100 inch wall thickness. This chamber section had 12 feeder and 12 discharge tubes connected to a common inlet and outlet manifold.

The nozzle-throat section was a water cooled calorimeter configuration which measures 5.64 inches in total length. The aerodynamic contour of the nozzle is indicated in Figure A8. There were 50 circumferential coolant channels in this component which were grouped into 17 coolant circuits. Wall thickness of the coolant channel liner walls was .040 inches. Coolant flow entered the circuit and was discharged 180 degrees around. Each of the first sixteen coolant circuits fed and discharged 3 channels while the last coolant circuit fed and discharged the aft two channels.

Bomb Device

The purpose of the stability rating bomb device is to artificially induce an overpressure in the combustion chamber. The bomb was a cylindrical, wall mounted electrically initiated device which delivered a nondirectional output in the chamber. The output charge assembly was made of lead-azide plus RDX. The bomb was designed to be nondamaging to the injector by using a minimum charge assembly case, low density ceramic/quartz thermal shield, and low density ablative plug. For the Phase C testing, modifications were made to enhance the survivability of the bomb. These include wrapping the bomb in aluminum tape and coating the bomb tip with epoxy. These modifications are illustrated in Figure A9.

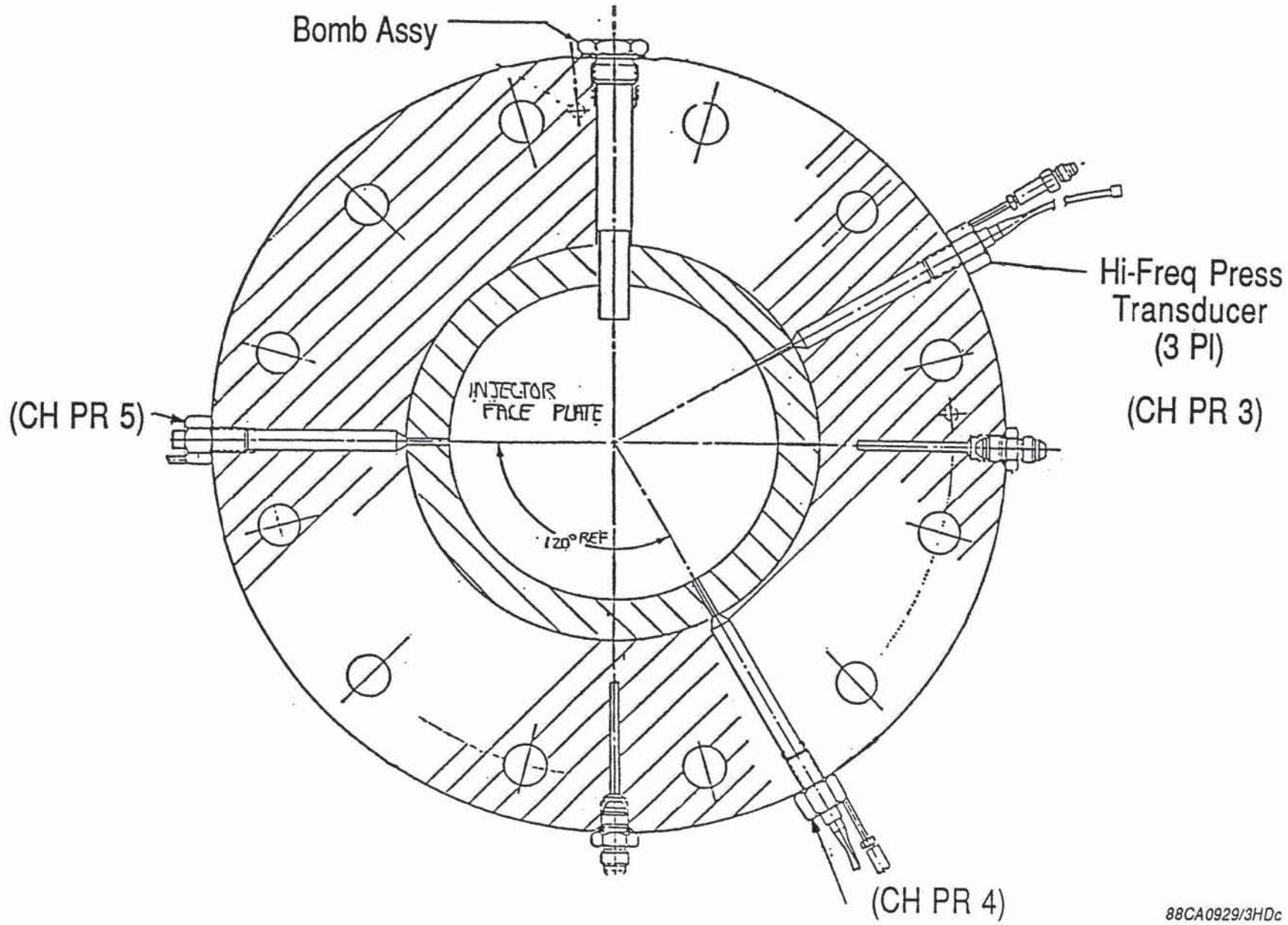

Figure A7 - Bomb Spool (Looking through the throat at the injector)

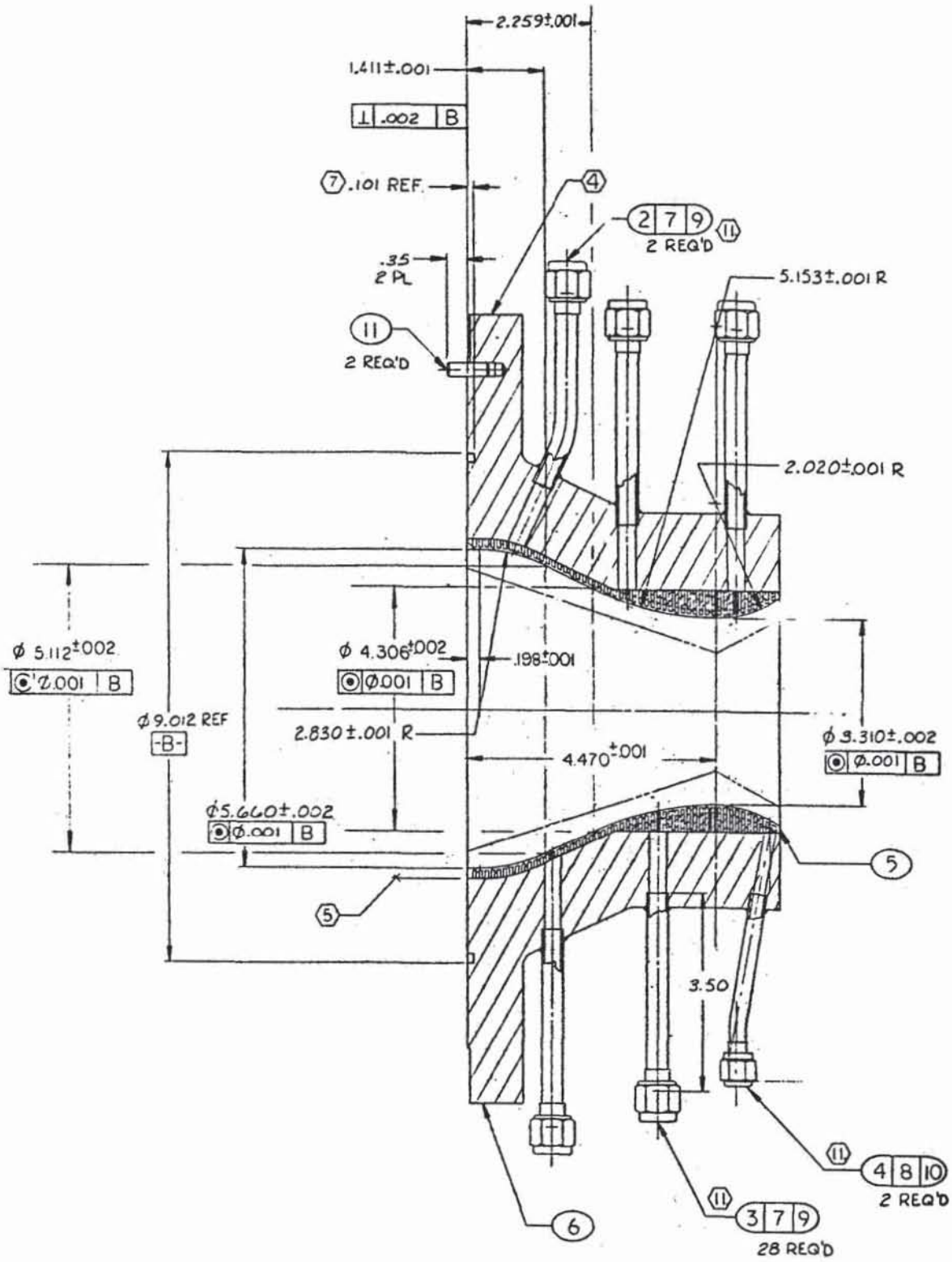

Figure A8 - Nozzle Geometry

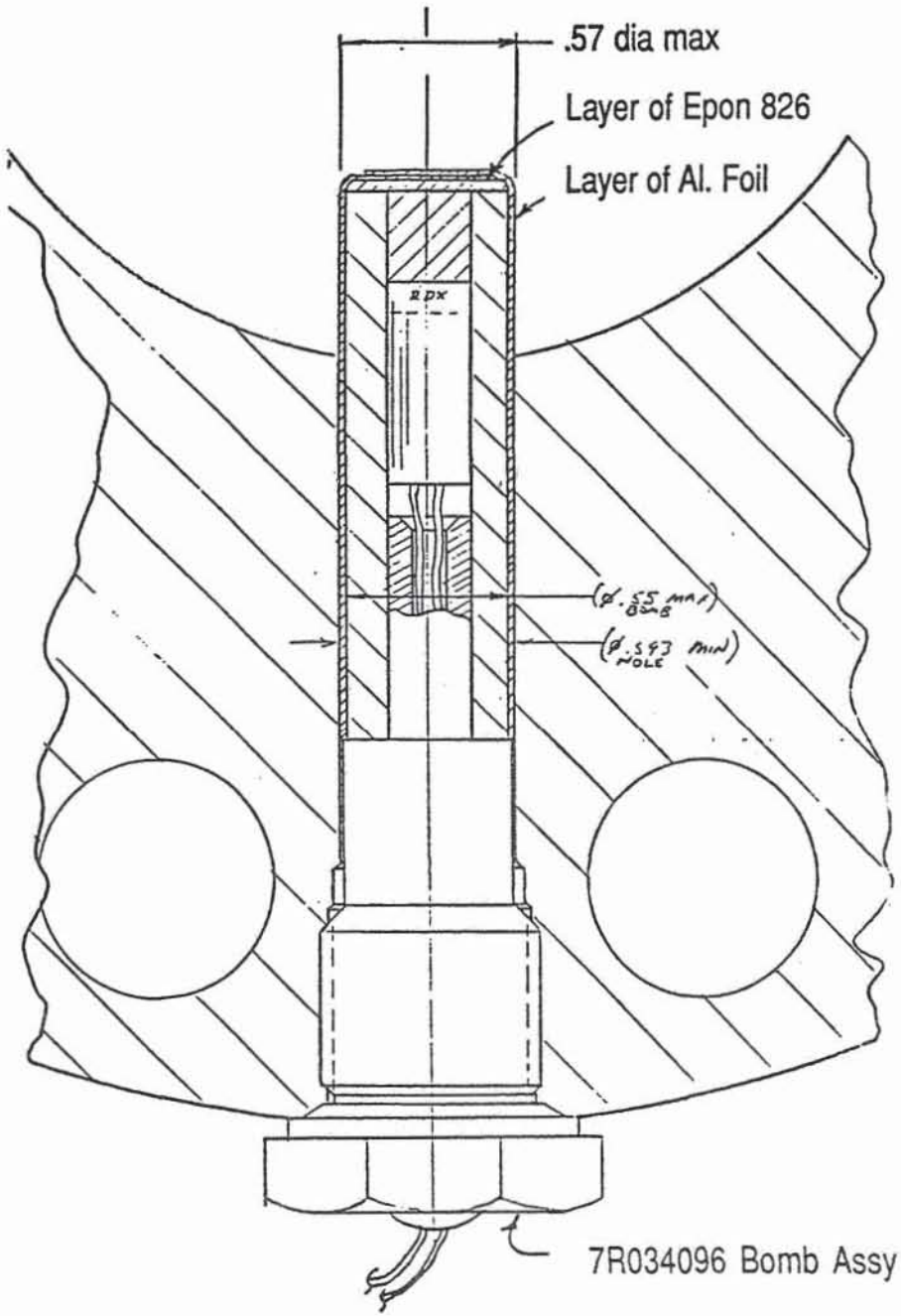

88CA0929/3HDe

Figure A9 - Modification to the Bomb Assembly

A2. Facility Description

The high-pressure Peter Test Stand located in the Advanced Propulsion Test Facility at Rocketdyne's Santa Susanna Field Laboratory was used to perform the hot-fire testing. An overall pictorial view of the test stand is shown in Figure A10. The testing described in this report was structured into three phases to accomodate facility preparation and an accelerated hot-fire test schedule. The staged approach achieved more expeditious testing by conducting Phase A testing without delaying for the more extensive facility preparations required in Phase B (fuel temperature ramping) testing. Phase C (stability bomb) testing proceeded with very little additional facility modifications. The hot fire test phases are outlined below:

Phase A. Ambient fuel temperature tests: constant, ambient (gaseous) methane injection temperature. Test variations in mixture ratio.

Phase B. Fuel temperature ramping tests: decreasing methane injection temperature from ambient to critical. Test variations in mixture ratio.

Phase C. Stability bomb testing: constant methane injection temperature. Test dynamic stability at various methane injection temperatures and mixture ratios.

A list of valve and venturi/orifice requirements is presented in Table A.II and Table A.III, respectively. Details of the methane system, LOX system, and water cooling system are presented in the following paragraphs.

Methane System

The methane fuel propellant was fed from both gaseous and liquid propellant tanks as determined by the fuel injection temperature. The methane system is shown schematically in Figure A11. The desired fuel temperature was achieved by metering the proper amounts of gaseous and liquid methane in a facility mixer prior to injection. The gaseous methane was supplied from a 470 cubic foot blowdown run bottle. A 5000 psig, 100 gallon liquid methane run tank pressurized by servo-controlled gaseous helium supplied the liquid fuel. The servo system response feature maintained a constant liquid supply pressure through the test duration.

The injector fuel control system which was employed was dependent on the type of testing being conducted. During Phase A testing, the main fuel servo valve was used to control the ambient gaseous methane flowrate to the injector in a closed loop control mode with a subsonic venturi. In Phase B testing, a three servo valve system was utilized to provide a fuel temperature ramping capability from ambient to critical temperatures while

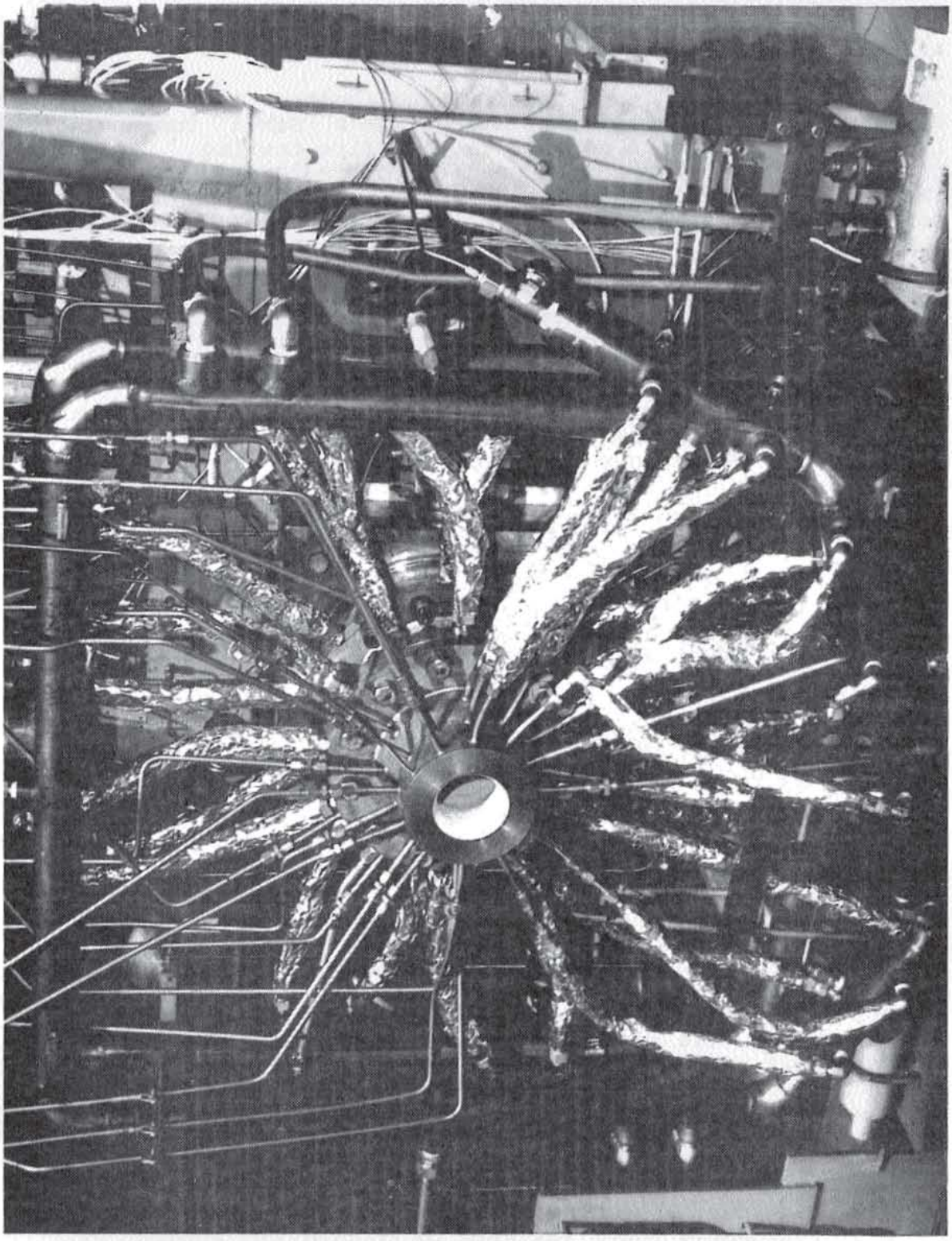

Figure A10 – LOX/Methane Hardware Installation in Peter Stand

C-2

ORIGINAL PAGE
BLACK AND WHITE PHOTOGRAPH

TABLE A.II - Facility Valve Requirements

Valve Name	Function
Phase A:	
Igniter CTF	Supply CTF to the igniter
Igniter GOX	Supply GOX to the igniter
Main Fuel Serve Valve (MFV)	Servo control fuel venturi flowrate
Main Oxidizer Serve Valve (MOV)	Servo control LOX valve position
Main Water Valve (MWV)	Servo control chamber water coolant supply pressure
Phase B and C: (additional requirements/changes from Phase A)	
Mixer Liquid Fuel Servo Valve (MLFV)	Servo control mixer fuel temperature
Mixer Gas Fuel Servo Valve (MGFV)	Servo control mixer fuel pressure

TABLE A.III - Facility Venturi and Orifice Requirements

Item	Type
Igniter Oxidizer Orifice	Drilled Orifice
Igniter Fuel Orifice	Drilled Orifice
Main Fuel Venturi	Subsonic Venturi with throat tap
Main Oxidizer Venturi	Cavitating Venturi without throat tap

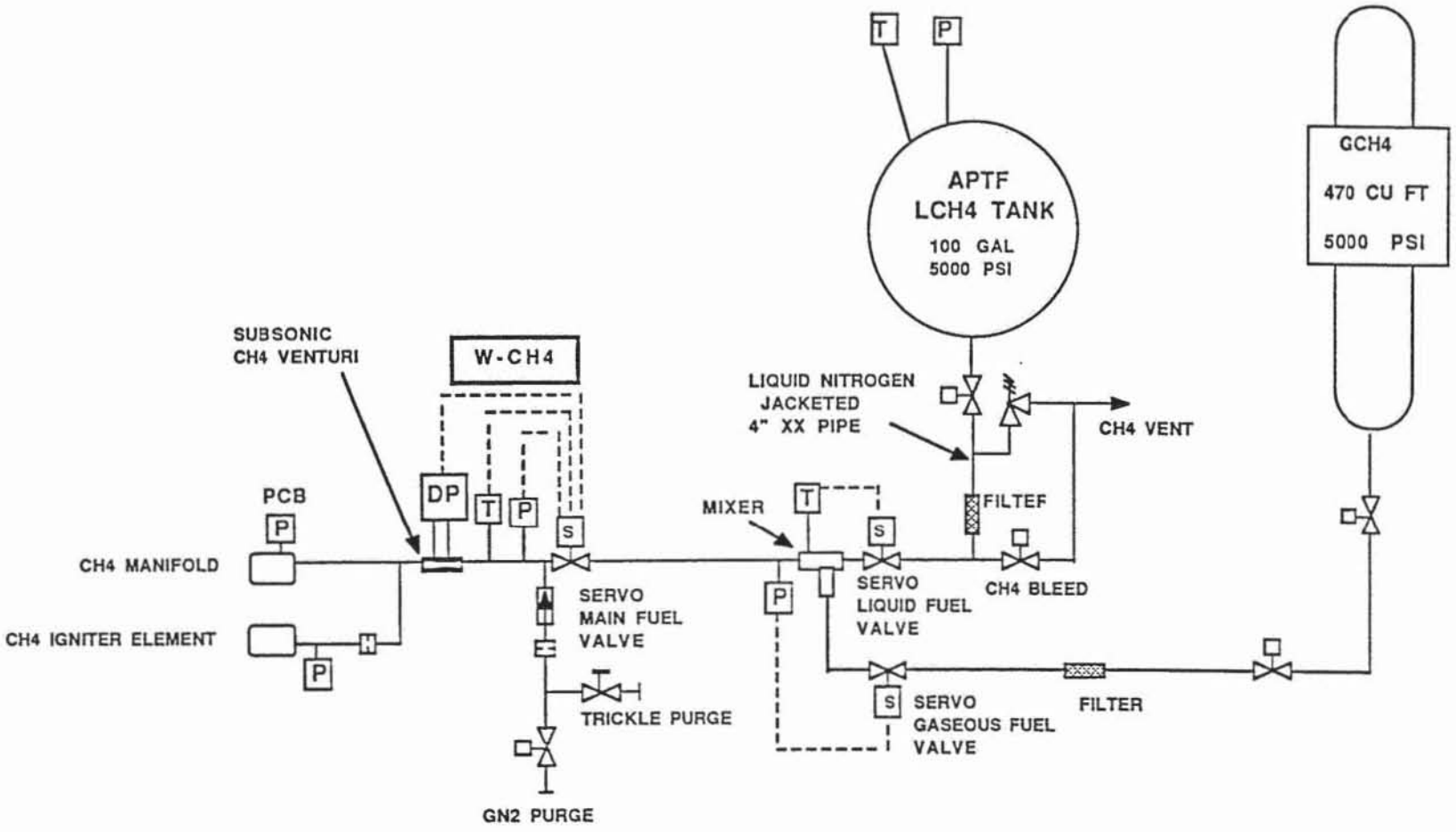

Figure A11 - Methane System Schematic, Peter Stand

maintaining a constant flowrate to the injector. A feed system dynamic model was used to simulate the methane feed system for controlling and mixing the liquid and gaseous methane. A mixer gaseous methane servo valve, a mixer liquid methane servo valve, and a main fuel servo valve comprised the fuel control system. The gaseous and liquid methane systems interfaced at a facility mixer. The gaseous methane feed system was servo-controlled by a valve located upstream of the mixer and was closed-loop controlled by feedback of pressure upstream of the main fuel valve. Liquid methane flow was servo-controlled by a valve located upstream of the mixer and was closed-loop controlled by mixer outlet temperature feedback. Total fuel flow was servo-controlled by the main fuel valve which was closed-loop controlled by feedback from a fuel flow calculator. The fuel flow calculator utilized data from the subsonic venturi located downstream of the main fuel valve. Phase C testing used only one closed-loop system; the mixer gas fuel valve controlling pressure upstream of the main fuel valve. Utilizing data from Phase B testing to achieve the target conditions, the main fuel valve position (fuel flow) and mixer liquid fuel valve position (fuel injection temperature) were fixed during mainstage for Phase C testing.

The igniter fuel supply was tapped downstram of the main fuel valve. Flow control of the igniter fuel was accomplished by a calibrated drilled orifice.

LOX System

The LOX system is illustrated schematically in Figure A12. A 5000 psig, 180 gallon LOX run tank pressurized by servo-controlled gaseous nitrogen supplied oxidizer to the injector and igniter. As in the liquid fuel case, the LOX servo system maintained a constant tank supply pressure during hot-fire test runs. LOX flow was controlled by a combination of tank pressure and main LOX valve position. Obviously, flow control with the main LOX valve was only effective when the LOX venturi was not cavitating.

Igniter GOX was supplied by tapping the LOX system upstream of the LOX venturi and running the LOX through 150 feet of coiled tubing which served as a heat exchanger. Flow control was implemented with a calibrated drilled orifice.

Water System

A 3500 gallon (700 gallon useable), 5000 psig tank supplied cooling water to the 5.66 inch diameter thrust chamber assembly. The water system is shown schematically in Figure A13. Water pressure in the inlet manifold was closed-loop coupled to the main water servo valve. Flow control to each element of the chamber assembly was achieved with drilled orifices.

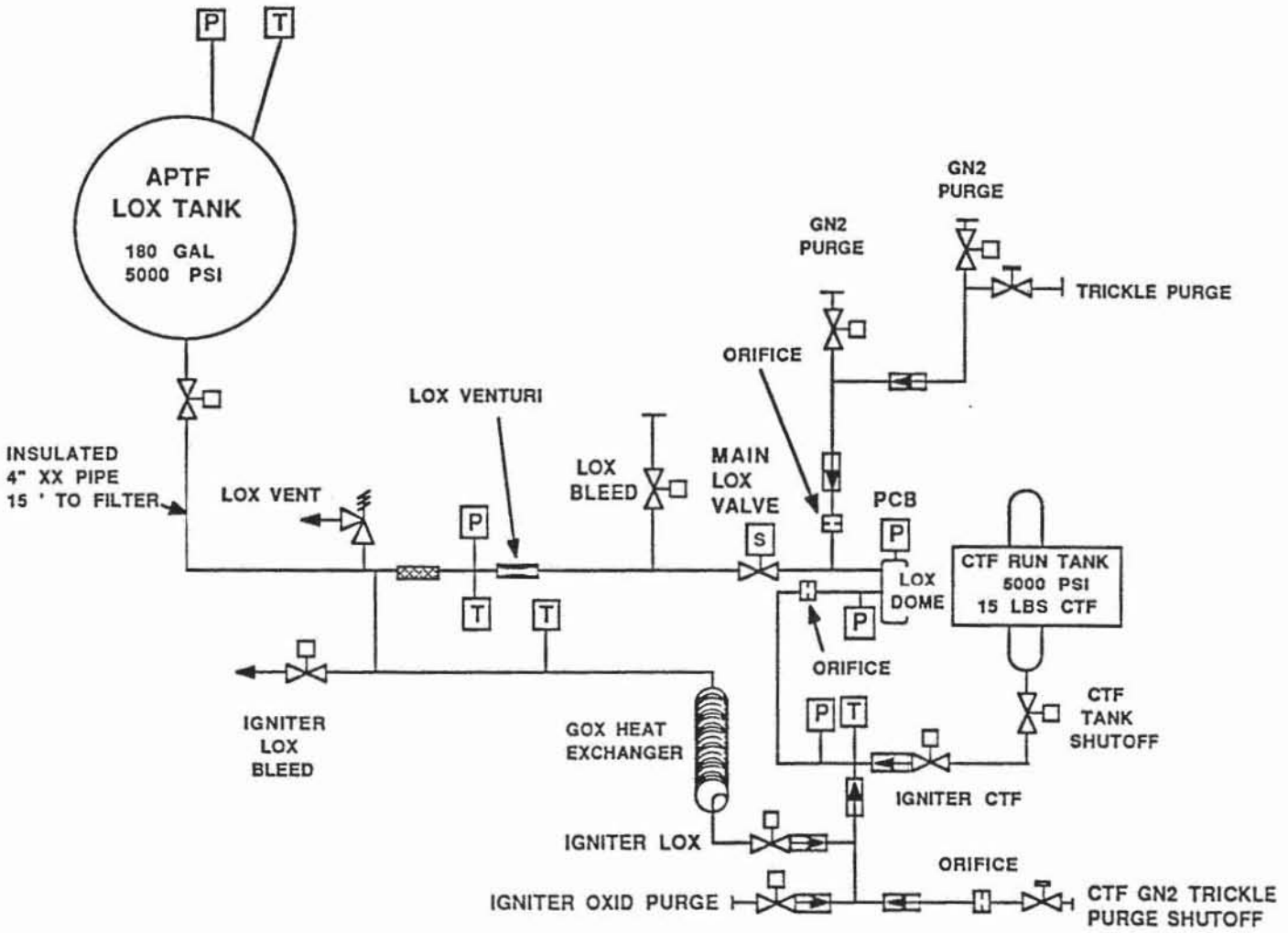

Figure A12 - LOX and CTF System Schematic, Peter Stand

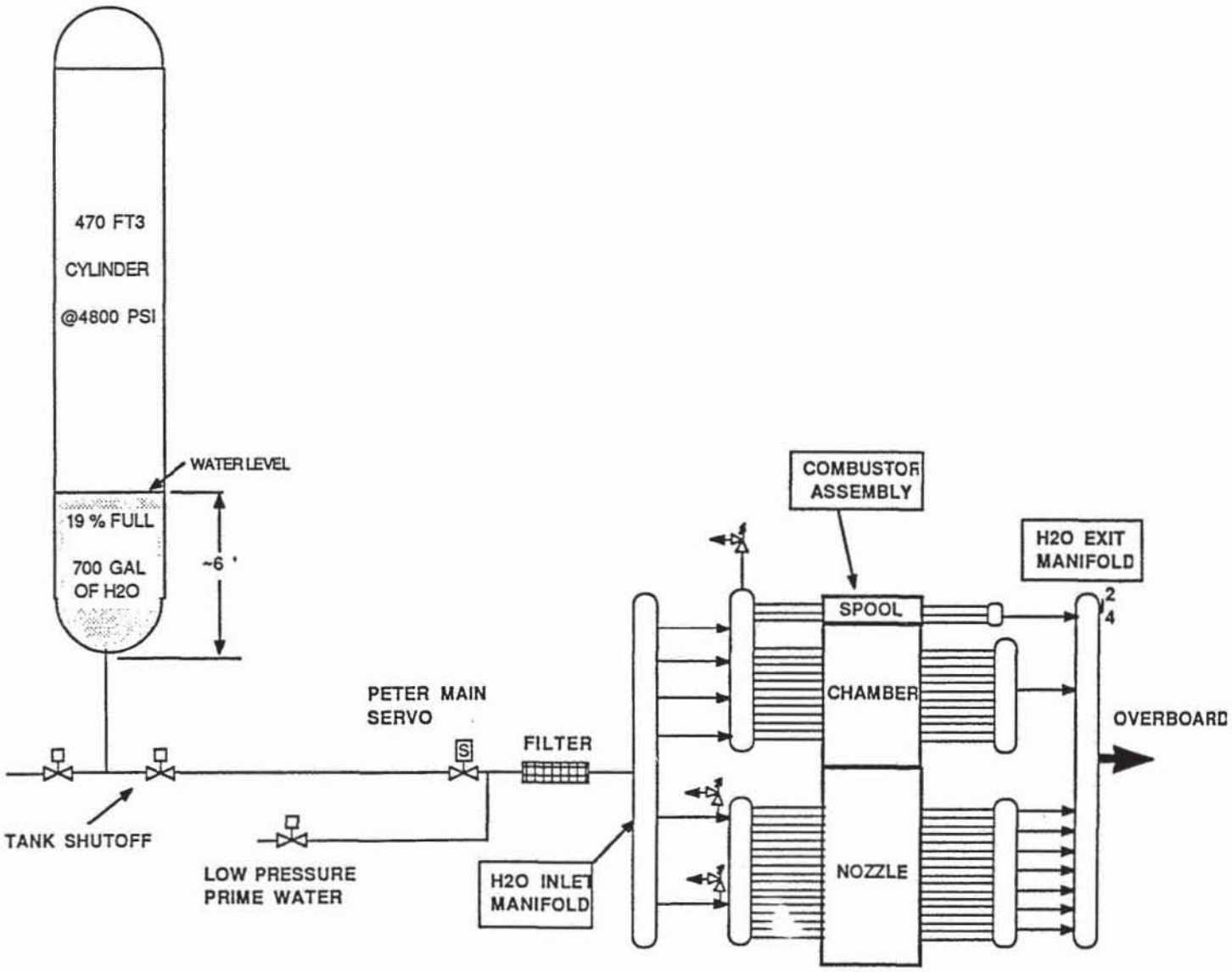

Figure A13 - Water Calorimeter Coolant System Schematic, Peter Stand

Appendix B - Phase A Chronology

B.1 Phase A Testing Through Test 014-004

Initially, two ignition tests were performed to demonstrate methane ignition with CTF and to further characterize the gains of the main fuel valve and mixer gas fuel valve. During the first hot fire test (014-001), satisfactory ignition was demonstrated, however, the mixer gas fuel valve opened to the 15% open position instead of the requested 23% open position. A servo valve control adjustment was made and a subsequent ignition test was conducted (014-002). During this test the valves operated as prescribed.

The first attempt at a mainstage hot fire test (014-003) was preempted due to exceeding the maximum redline value for LOX venturi inlet pressure prior to achieving sequence start. This pressure was oscillating over the redline value prior to start in reaction to oscillating tank pressure. The oscillation ceased when the MOV was opened. Activation of the redline was subsequently delayed until after the MOV was opened.

During the first successful mainstage hot fire test (014-004), a high amplitude acoustic combustion instability occurred. The high frequency accelerometer and pressure transducer records showed a complex development in oscillation amplitude and frequency. An initial period of 600 msec at 1915 psig (700 msec total mainstage operation), in which the dominant frequency was approximately 4 KHz and peak-to-peak chamber pressure amplitudes are less than or equal to 10 % was followed by transition to high amplitude first tangential (1-T) mode instability. The 1-T instability, which was characterized by two frequencies (approximately 4800 and 5400 Hz) separated by 600 Hz, persisted for 800 msec and on into cutoff. These periods are shown relative to chamber pressure in Figure B1. In the following discussion, characteristic oscillation modes of the hardware, the sequence of events for the test, and hypothesized causes for the oscillations are presented.

The chamber and feed system characteristic frequencies are given in Table B.I. The first four LOX post frequencies (hydraulic "organ pipe modes") are shown. A range of LOX post structural modes can be obtained, depending on assumed boundary conditions relating to the manner in which the post is supported.

An overview of the instability is provided by the statos sample and the isoplot (root-mean-square pressure fluctuation versus time and frequency) in Figures B2 and B3, respectively. The dual peak nature of the high amplitude instability in the neighborhood of 5 to 6 Khz is quite apparent. Although oscillations at a well defined frequency (4 KHz) do occur before the onset of the high amplitude 1-T instability, they are of a much lower amplitude and hence are not apparent in Figures B2 and B3. Figure B4 shows

TABLE B.I - Computed Chamber and Feed System Frequencies

Combustion Chamber

1L	1875 Hz
2L	3751 Hz
3L	5625 Hz
1T	5105 Hz
2T	8462 Hz
1R	10626 Hz

Hydraulic

LOX Post	4.0 KHz, 8.6 KHz, 13.6 KHz, ...

Structural

LOX Post	1.5 - 5 KHz

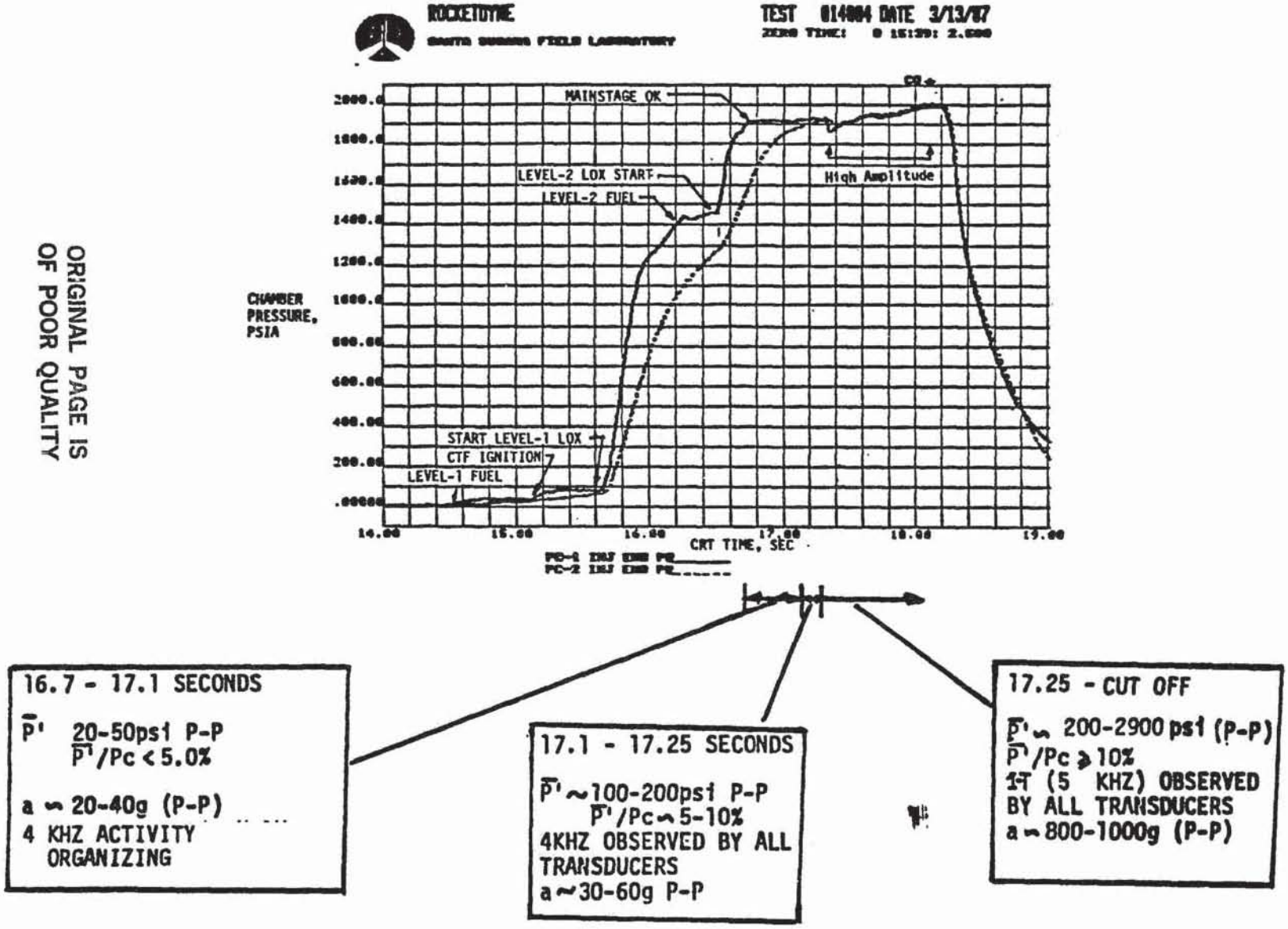

Figure B1 - Test 014-004 Instability History

Figure B2 - States at onset of High Amplitude Instability

ORIGINAL PAGE IS
OF POOR QUALITY

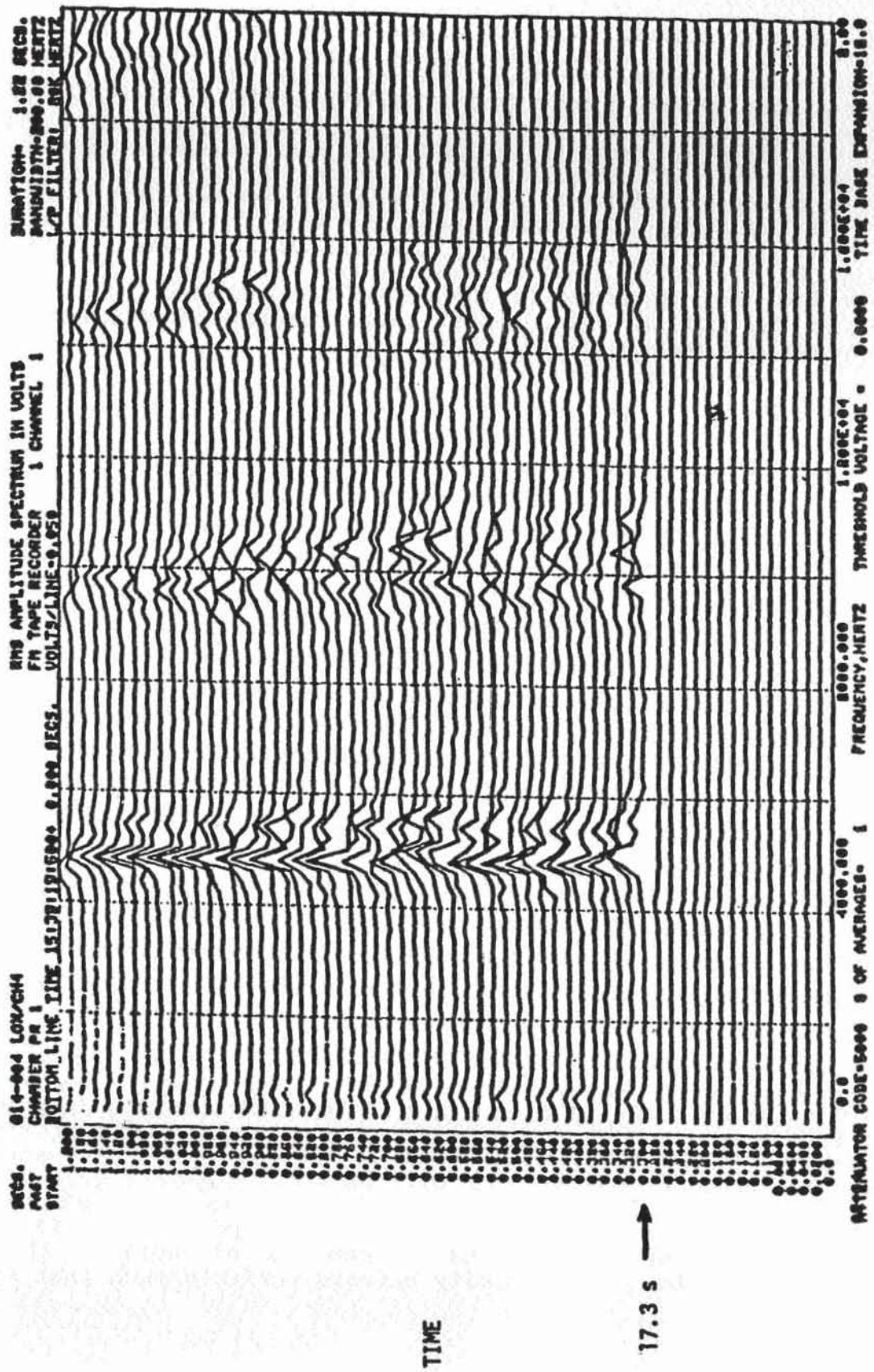

Figure B3 - Test 004 Isoplot of High Frequency Chamber Pressure

isoplots of chamber and LOX dome high frequency pressure measurements during a 260 msec period prior to the onset of high amplitude instability. These plots, which were made with a higher amplification, clearly show the existence of activity both in the dome and in the chamber in the neighborhood of 4 KHz. Lower frequency activity in the LOX dome characteristic of a dome hydraulic mode is also apparent. Other transducers in the chamber and fuel manifold as well as accelerometer data confirm the 4 KHz activity. The development of the 4 KHz oscillation and the first tangential high amplitude instabilty can be traced through six distinct time periods in the test run. These six time slices are discussed in the following sections. It should be noted that the CRT time in this test numerically equals IRIG B time minus 2.5 seconds.

Test 014-004 Sequence of Events (CRT Time)

Time Slice 1: 15.8 to 16.2 sec (Level 1 Transient)

Figure B5 shows the duration and relationship of this time slice to overall test events. Figures B6a through B6d show PSD plots for chamber and LOX dome PCB transducers. Slight peaks at 3.9 KHz are seen in PCB chamber pressures 1 and 2 and in the high frequency oxidizer dome transducer. Some activity is also seen at 6.8 KHz on all three transducers as well. Additionally, the LOX dome exhibits a strong peak at 2.8 KHz which appears to be the dome mode.

Time Slice 2: 16.5 to 16.7 sec (Level 2 Transient)

This time slice is shown in Figure B7. PCB chamber transducers 1 and 3 show activity in the neighborhood of 4 KHz, as seen from the PSD plots in Figure B8. Expanded statos plots of PCB chamber pressure transducer 3 show sporatic appearance of 4 KHz oscillations, damping within 10 to 20 cycles. The average magnitude at 4 KHz is below 5% of the steady state chamber pressure. LOX dome activity (Figure B8d) is mainly centered at 2 KHz.

Time Slice 3: 16.7 to 17.0 sec (Level 2 - First 300 msec After Mainstage OK)

Figure B9 shows the time slice corresponding to this period. 4 KHz peaks appear in the PSD plots of all high frequency transducers, as shown in Figure B10. The 4 KHz peak is dominant in all chamber pressure transducer power spectra. Peaks in the neighborhook of 7 to 8 KHz appear in the PSD plots of chamber pressure transducers 1 and 2 as well as the LOX dome transducer. The 8 KHz activity may reflect harmonics of the 4 KHz activity and the next higher frequency mode of the LOX post. Some 18 KHZ activity is seen in the statos records as well. Phase correlation of the 4 KHz activity appears variable such that the

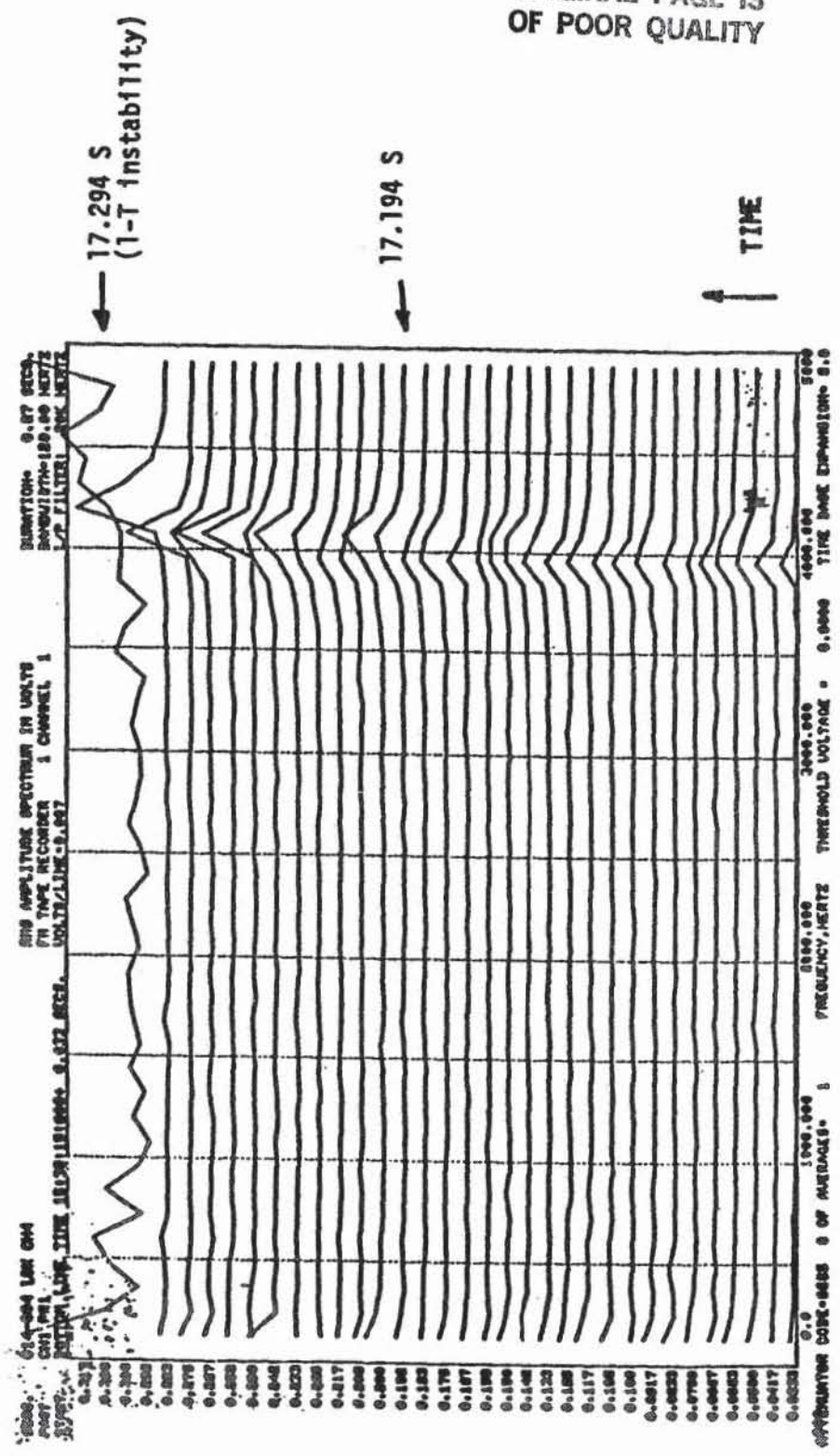

Figure B4 -a) - Chamber PCB Transducer Isoplot

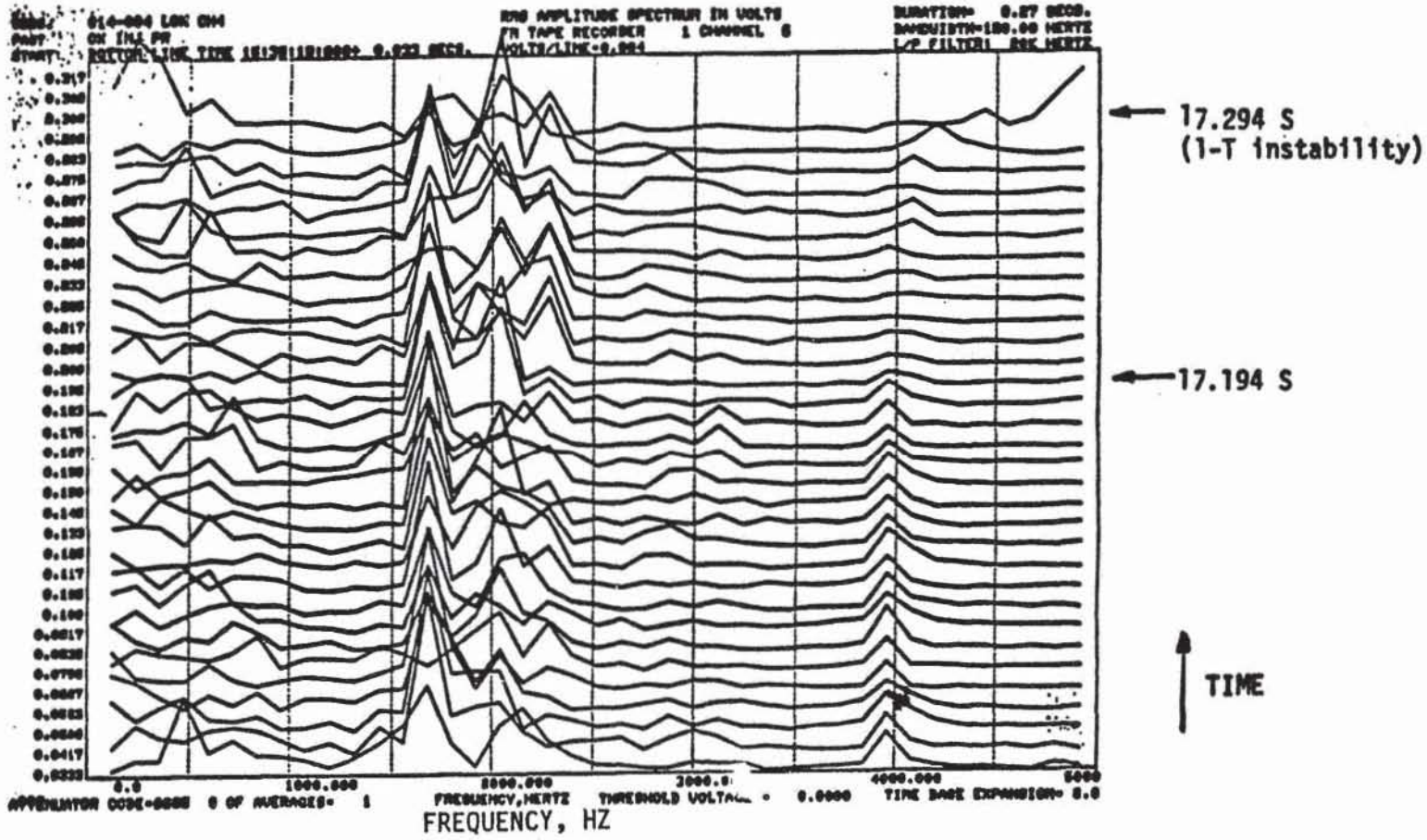

Figure B4 b) - LOX Dome PCB Transducer Isoplot

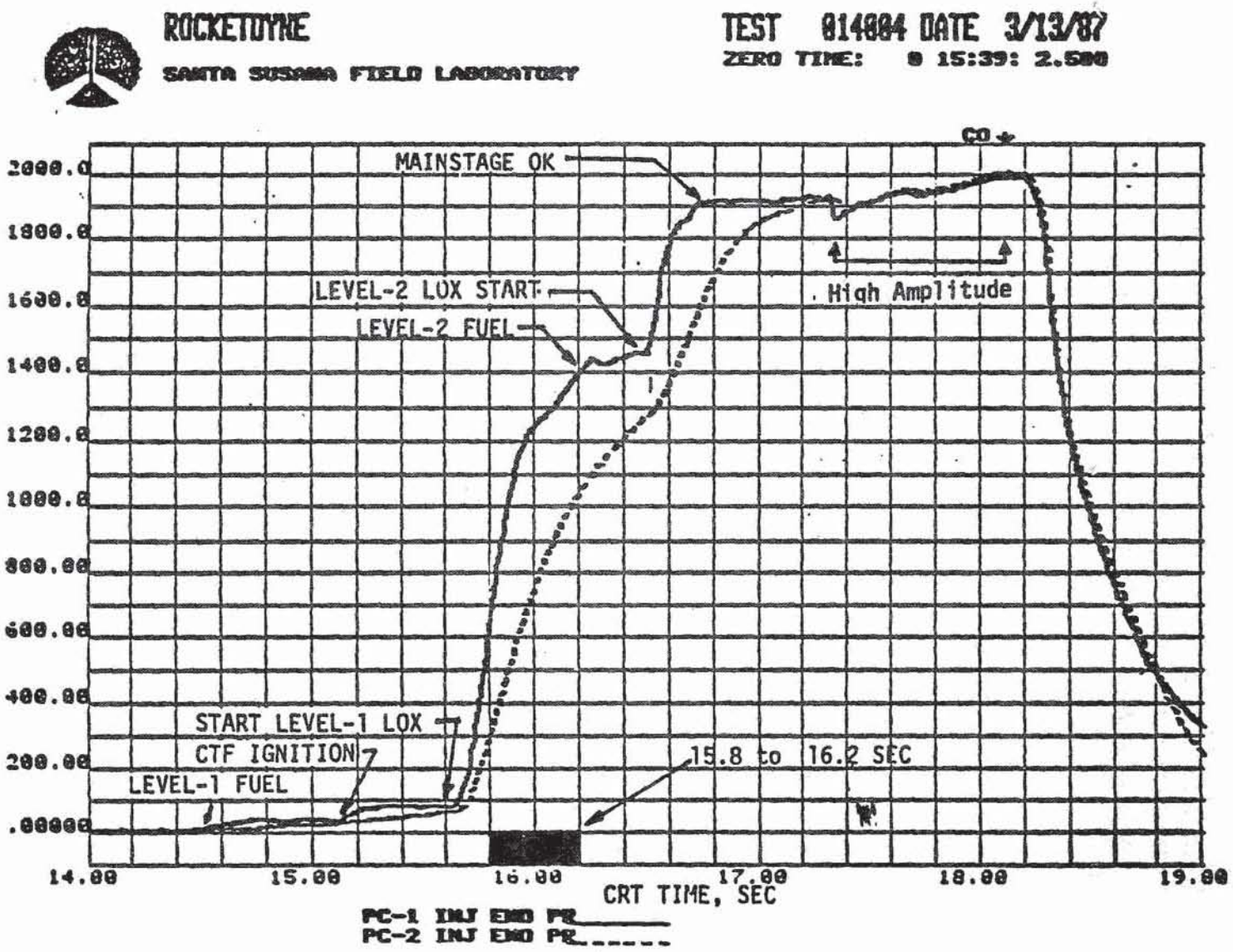

Figure B5 Time Slice for PSD of Level 1 Transient

Figure B6 PSD of High Frequency Pressure Measurements (Level 1 Transition)

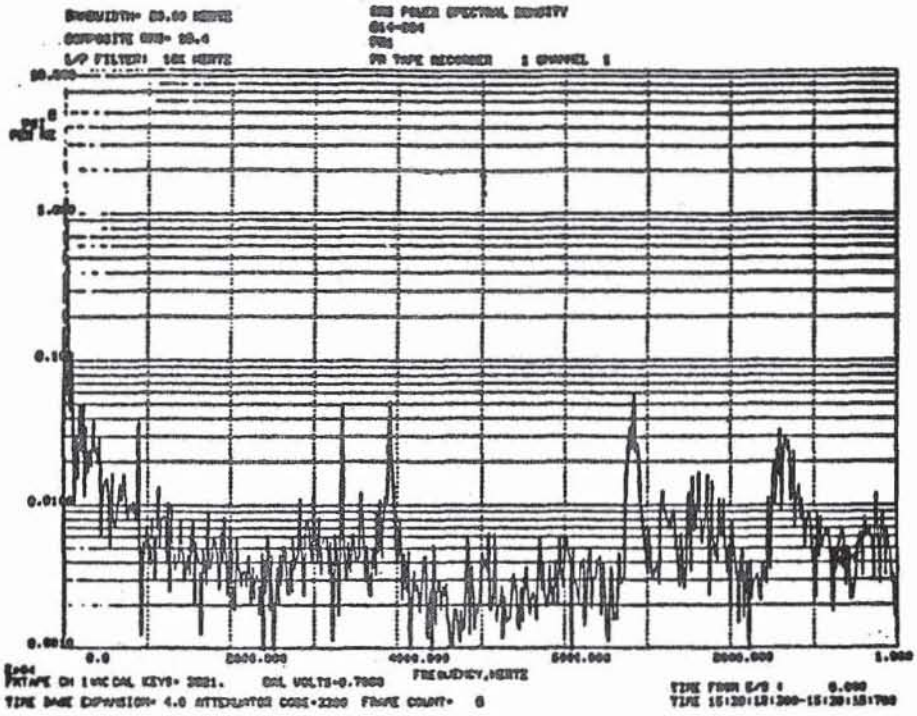

(a) Chamber PCB Transducer

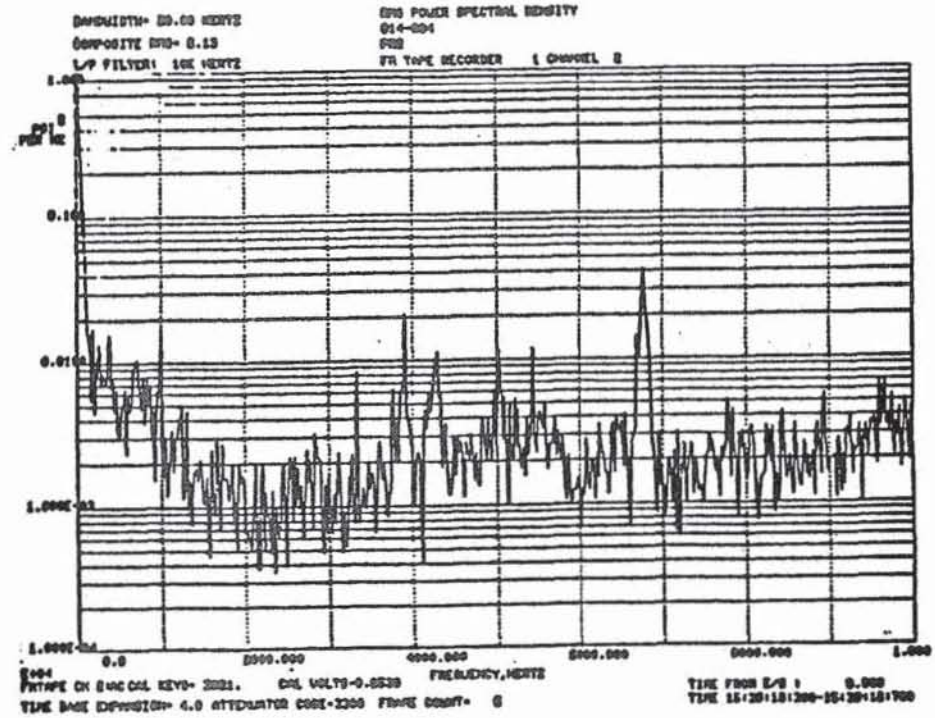

(b) Chamber PCB Transducer

Figure B6 (continued)

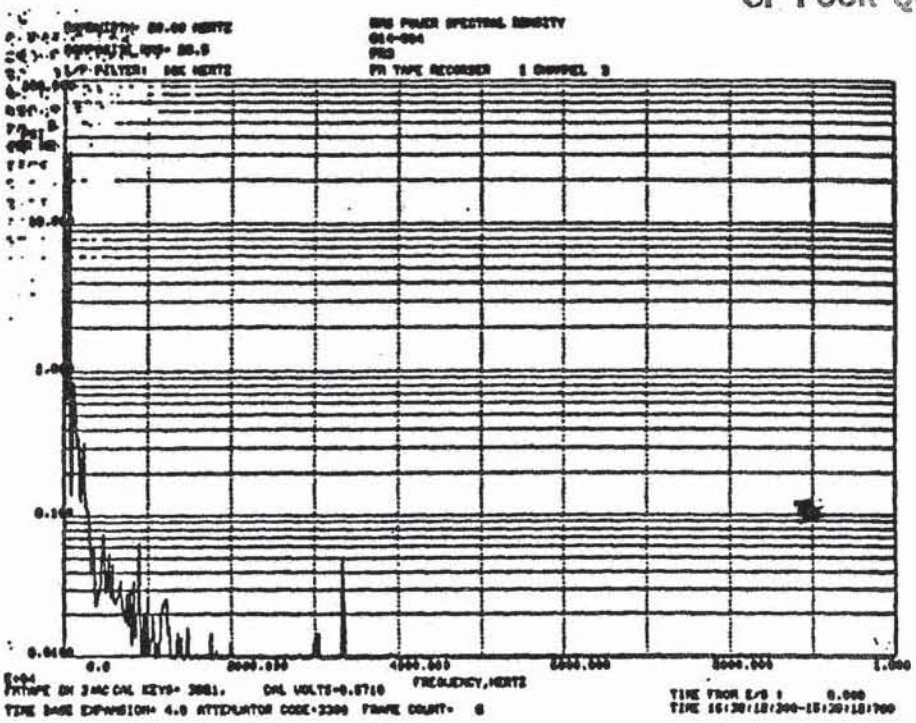

(c) Chamber PCB transducer

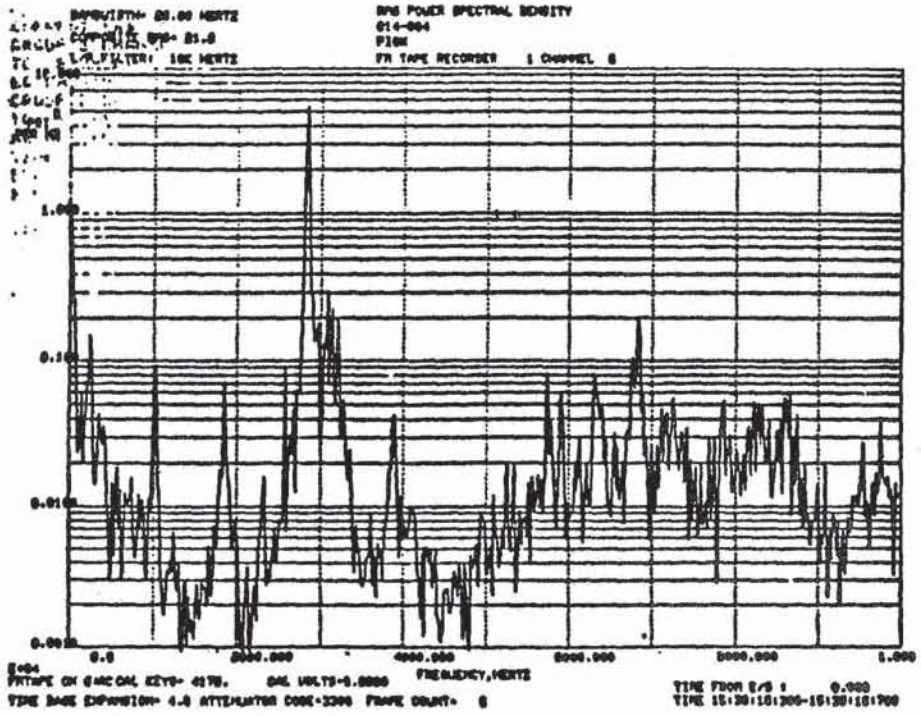

(d) LOX Dome PCB Transducer

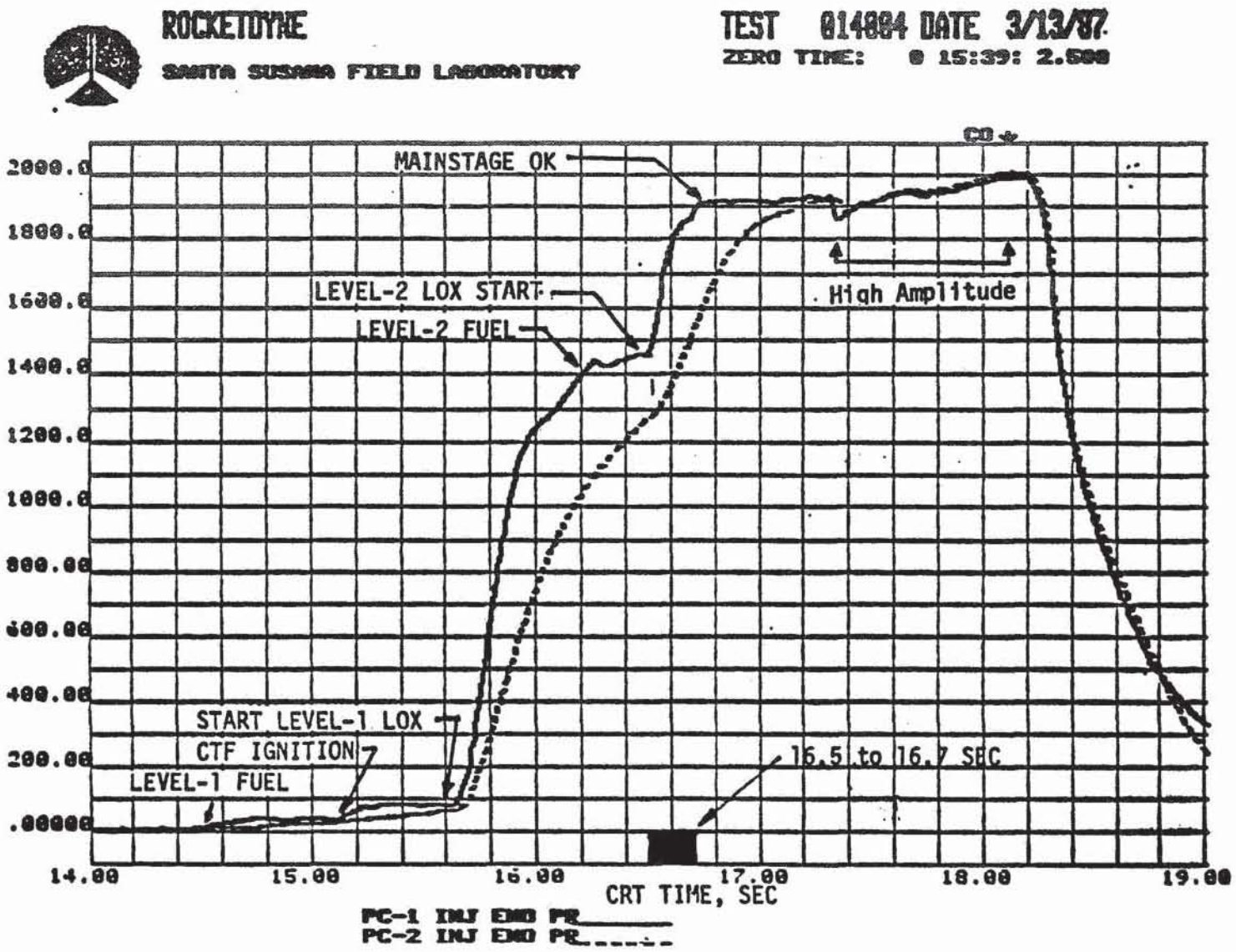

Figure B7 Time Slice for PSD of Level 2 Transient

Figure B8 PSD OF HIGH FREQUENCY PRESSURE MEASUREMENTS. LEVEL 2 TRANSITION

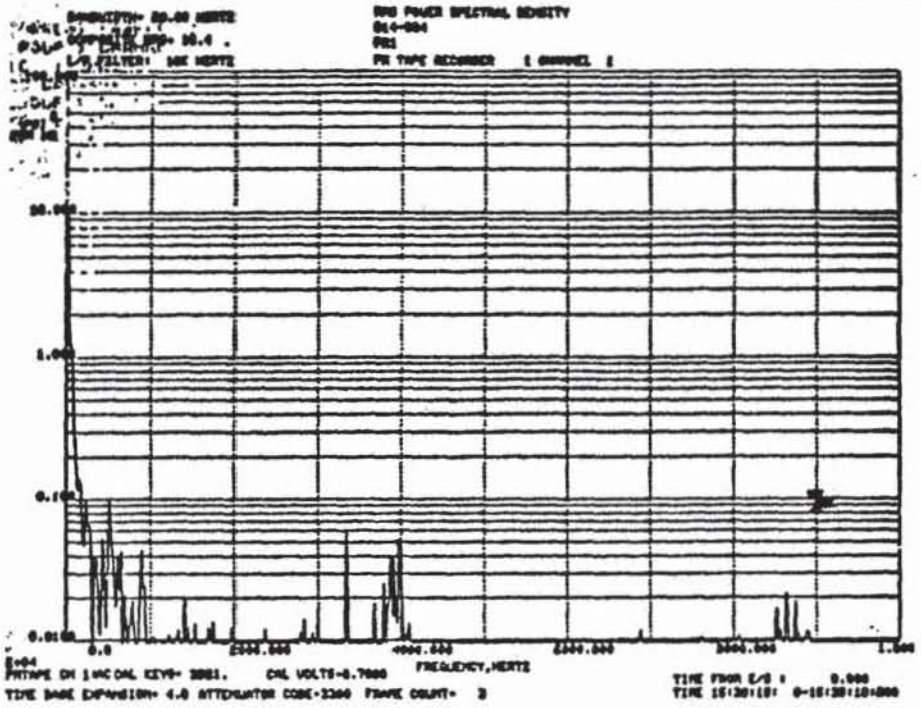

(a) Chamber PCB transducer 1

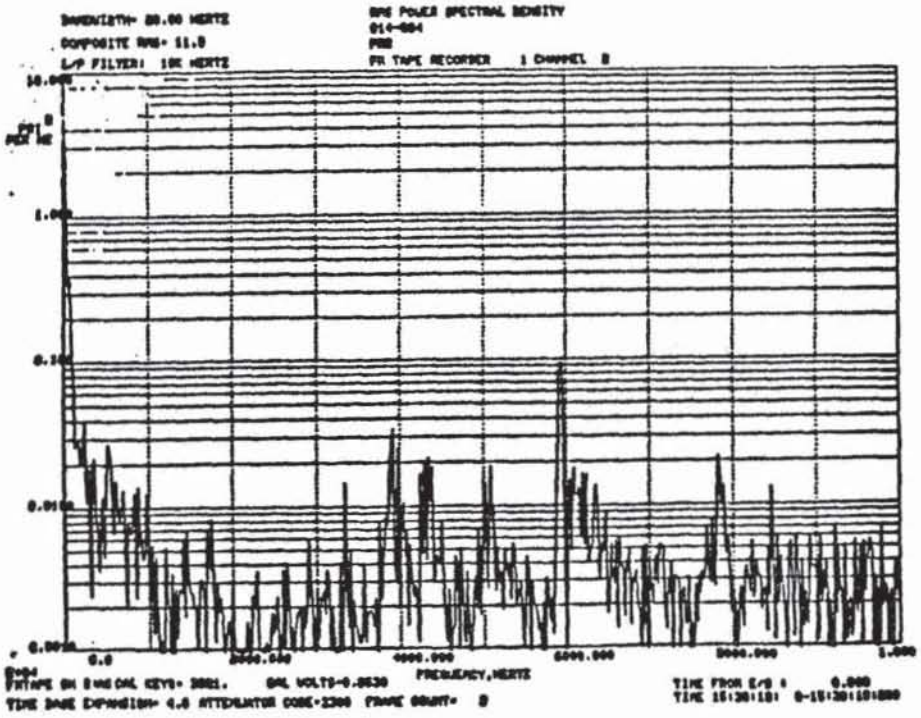

(b) Chamber PCB Transducer 2

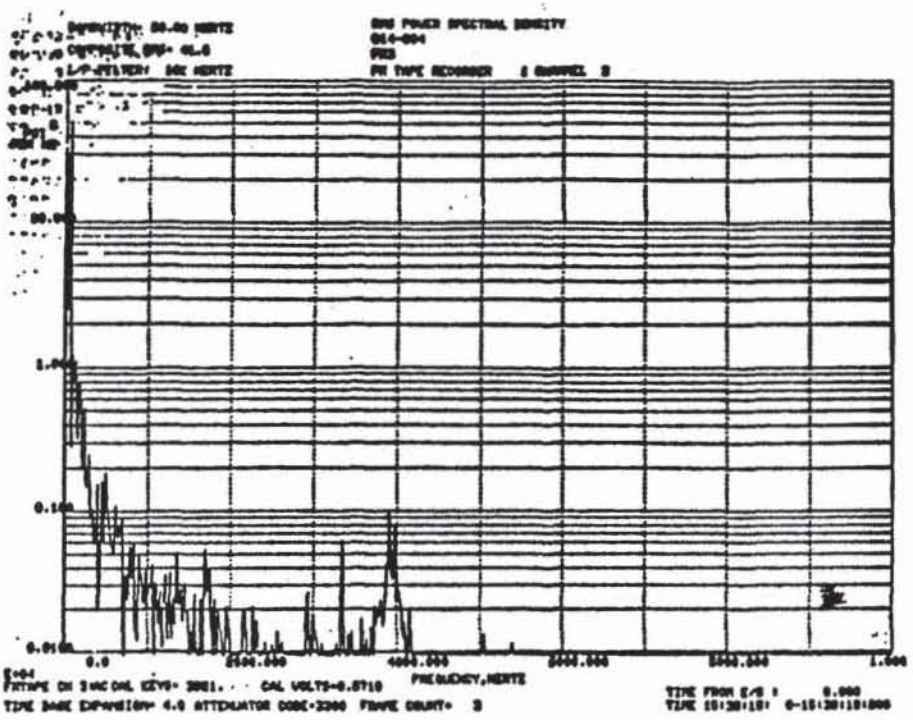

(c) Chamber PCB Transducer 3

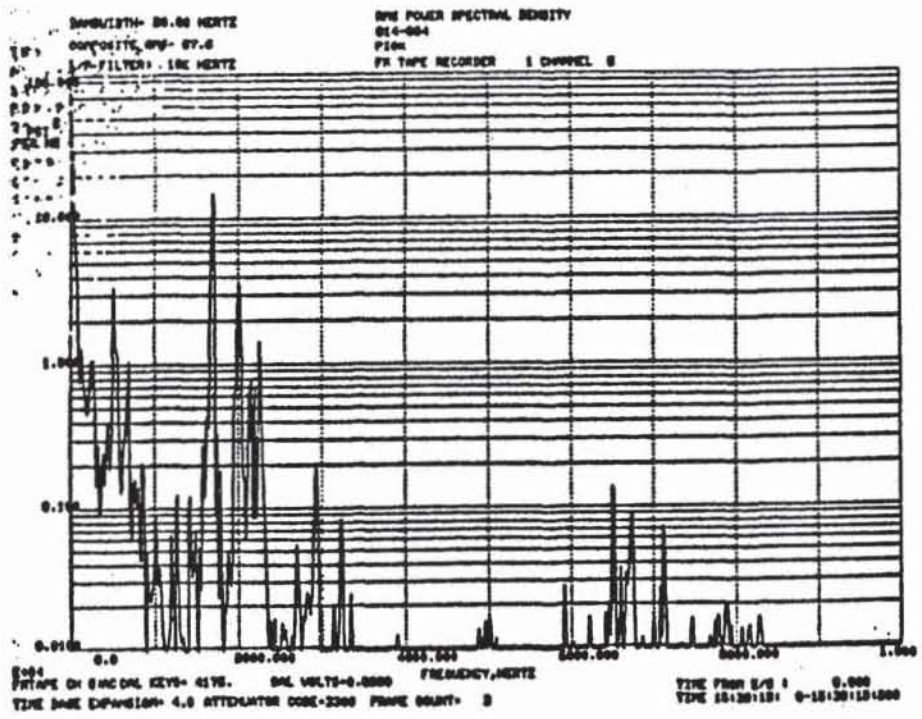

(d) LOX Dome PCB

Figure B8 (continued)

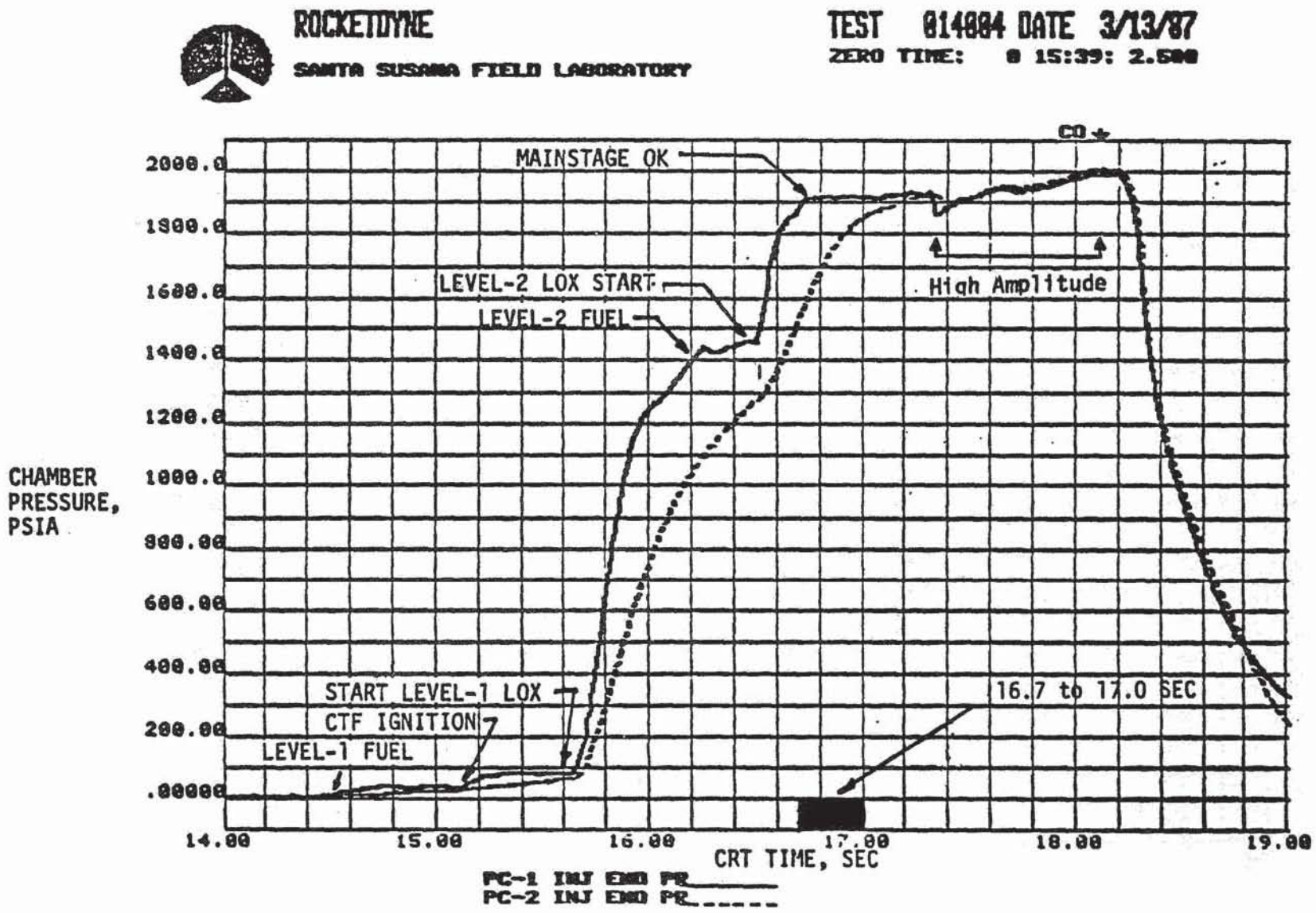

Figure B9 Time Slice for PSD Plots of First Mainstage Period

Figure B10 LEVEL 2 - FIRST 300 MS AFTER MAINSTAGE OK (16.7 to 17.0S)

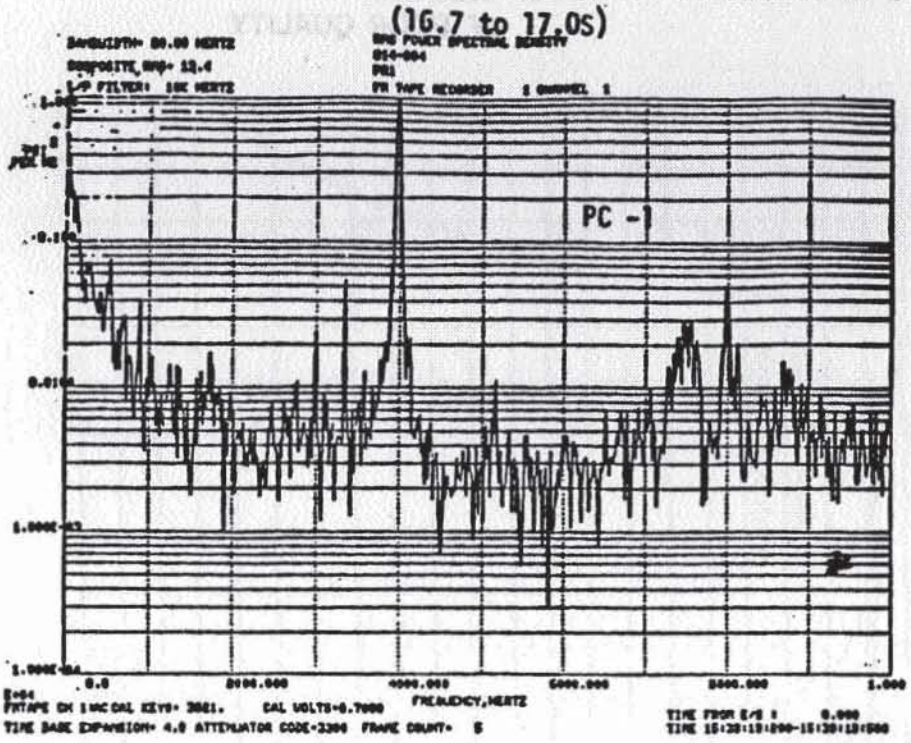

(a) Chamber Pressure Transducer 1

FIRST PERIOD AFTER MAINSTAGE OK

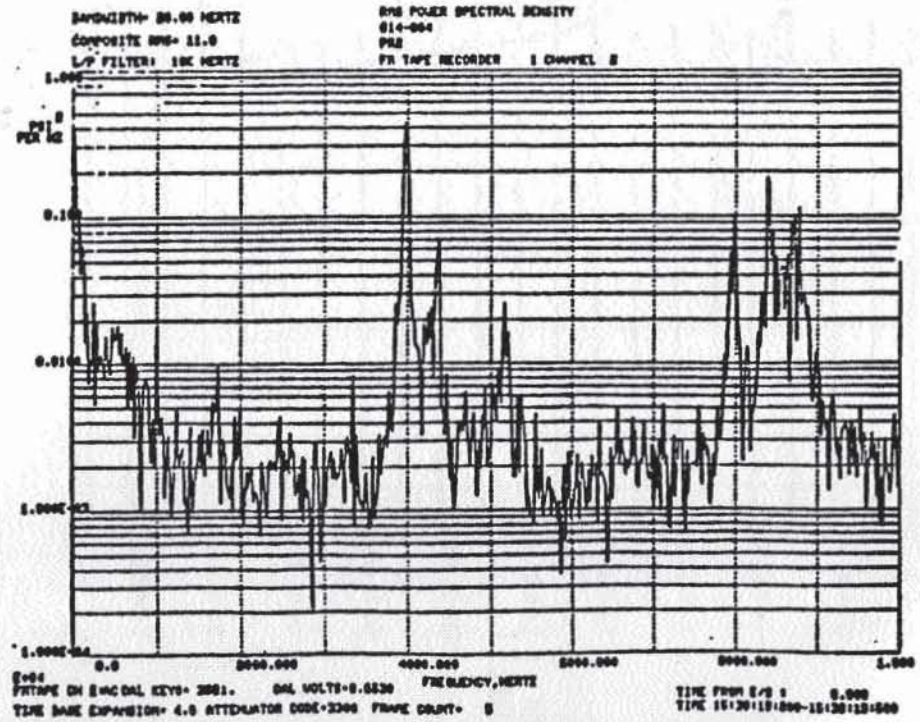

(b) Chamber Pressure Transducer 2

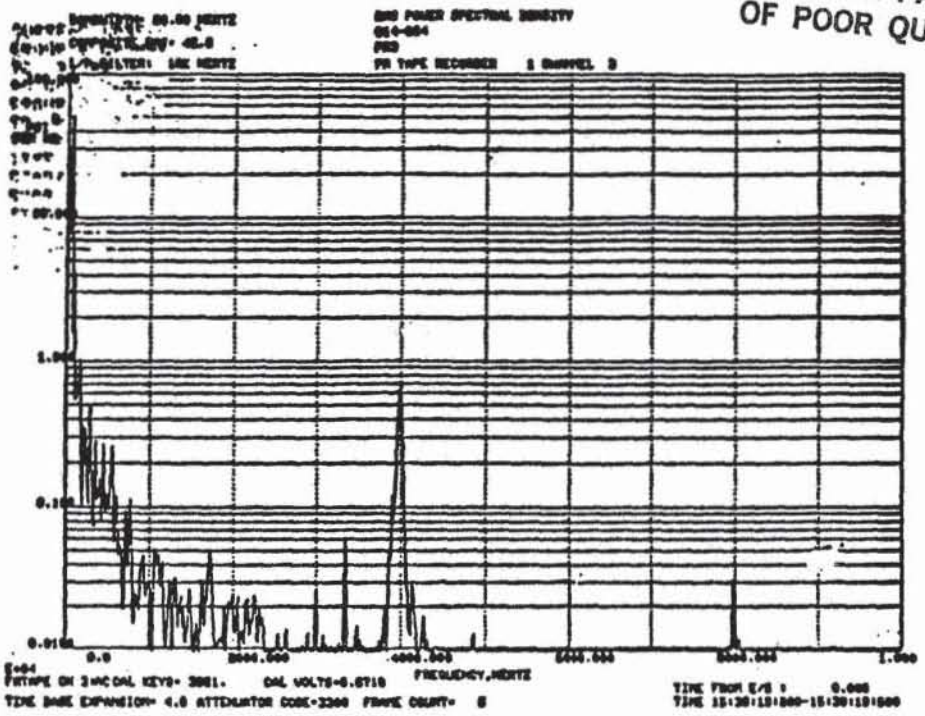

(c) Chamber Pressure Transducer 3

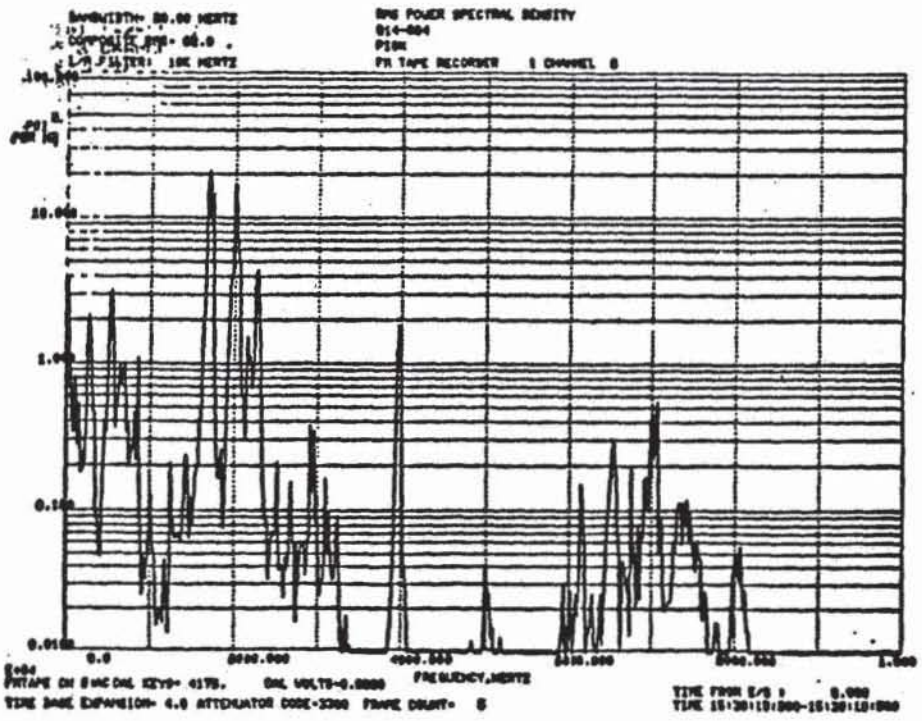

(d) LOX Dome Pressure Transducer

Figure B10 (continued)

oscillation does not yet appear coupled to a fixed chamber mode. At this point, peak-to-peak chamber pressure oscillations are less than 10%. LOX dome oscillations are approximately 10 to 20% of the chamber pressure and represent activity mainly in the neighborhood of 2 KHz. The maximum throat heat flux is approximatley 47 BTU/sq.in-sec during this time period.

Time Slice 4: 17.0 to 17.25 sec (Mainstage - 300 to 50 msec Prior to Onset of High Amplitude Instability)

The time slice for the PSD's from this period is shown in Figure B11. Figures B12 through B17 show power spectra for chamber and manifold PCB pressure transducers and the radial accelerometer for the time period 17.0 to 17.2 seconds. A narrow band 4 KHz oscillation is seen on all transducer records. The dome also continues to exhibit a dominant 1.8 to 2 KHz oscillation. However, the dominant peaks in the accelerometer spectrum are at 8 KHz and 11 KHz. Broadband peak-to-peak oscillation levels at 4 KHz attain 10% of Pc, while dome pressure oscillations exceed 20% of Pc. Chamber pressure transducers 1 and 3 indicate a constant relative phase of 180 degrees, especially after 17.1 seconds. This appears to suggest the existence of a standing tangential wave at 4 KHz. As seen from the isoplot of dome pressure fluctuations in Figure B16, the 4 KHz activity which shows a constant amplitude up until 17.2 seconds suddenly decays at that time. Closer inspection of both the dome and chamber PCB transducer 1 isoplots indicates that the actual oscillation frequency is 3.9 KHz up until 17.2 seconds. Near that point, the chamber oscillation shifts to 4.1 KHz on the average. During this period (17.0 to 17.25 seconds), the 4 KHz oscillation in the chamber grows and decays over 5 to 10 msec periods. The LOX dome 4 KHz oscillations prior to 17.2 seconds are larger in amplitude than fuel manifold fluctuations at that frequency.

Time Slice 5: 17.25 to 17.294 sec (Mainstage - 50 msec Prior to Onset of High Amplitude Instability)

The 4 KHz activity in the chamber grows and shifts in frequency during transition to the high amplitude instability, as is seen in Figure B4a. Peak-to-peak 4 KHz chamber amplitudes range from 10 to 20% of Pc, which exceeds th CPIA 247 combustion instability criterion. Just prior to the onset of the 1-T high amplitude instability, the LOX dome PCB transducer, the fuel injection PCB transducer #2, and the radial and axial accelerometers reflect the growth and shift in frequency observed in the chamber. As seen in Figure B4a, the initial 4 KHz oscillation grows in amplitude on the high frequency side, closest to the 1-T mode frequency. A growth rate approximately 100 /second is observed at approximately 10 msec prior to the time which the high amplitude instability reaches full development. In the last msec before full development, the growth rate reaches 100 /sec. In the video record at approximately 30 msec before the onset of the 1-T high amplitude instability, a bright flash was observed in

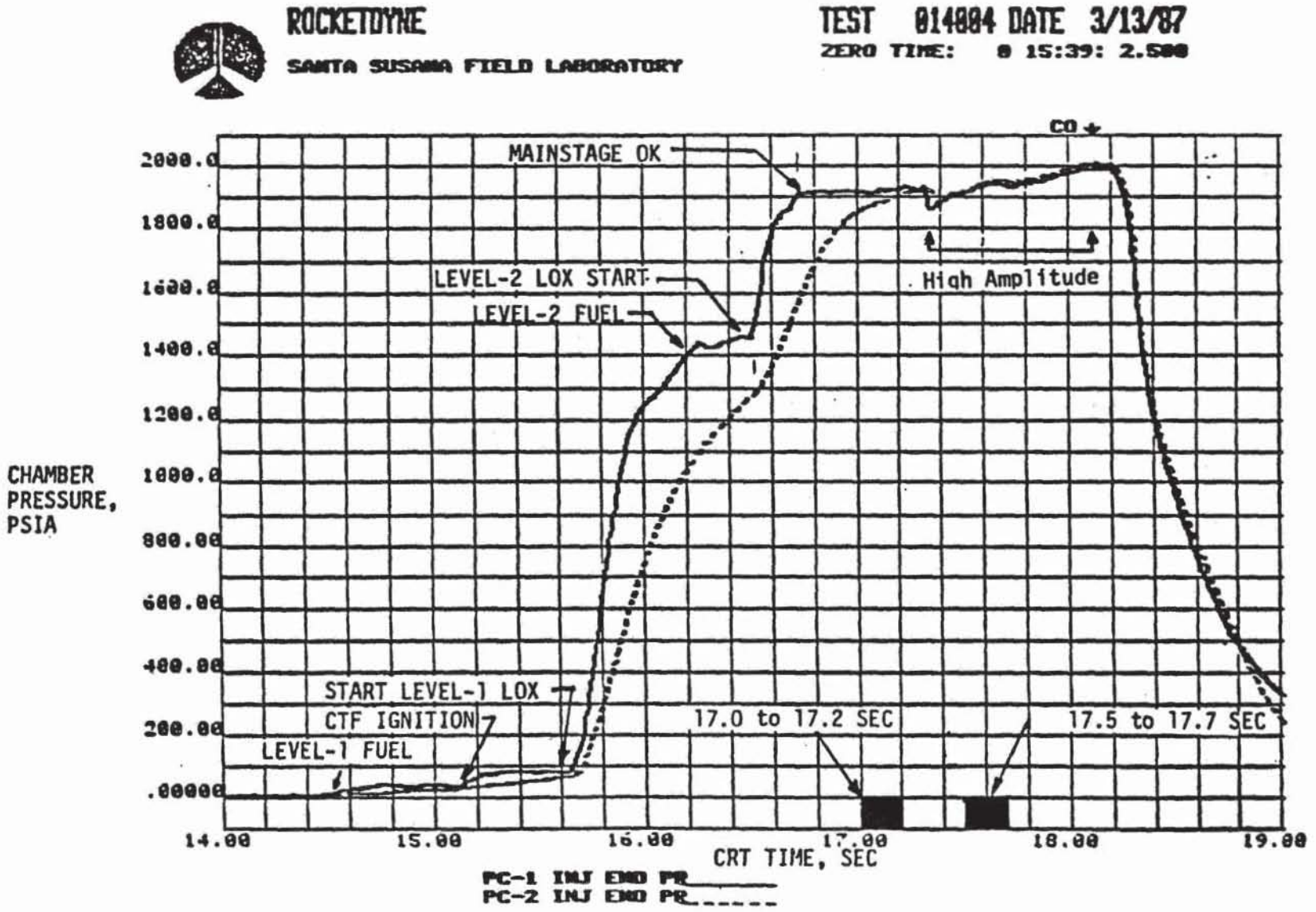

Figure B11 TIME SLICES FOR PSD PLOTS IN MAINSTAGE BEFORE AND AFTER THE ONSET OF HIGH AMPLITUDE FIRST TANGENTIAL MODE INSTABILITY.

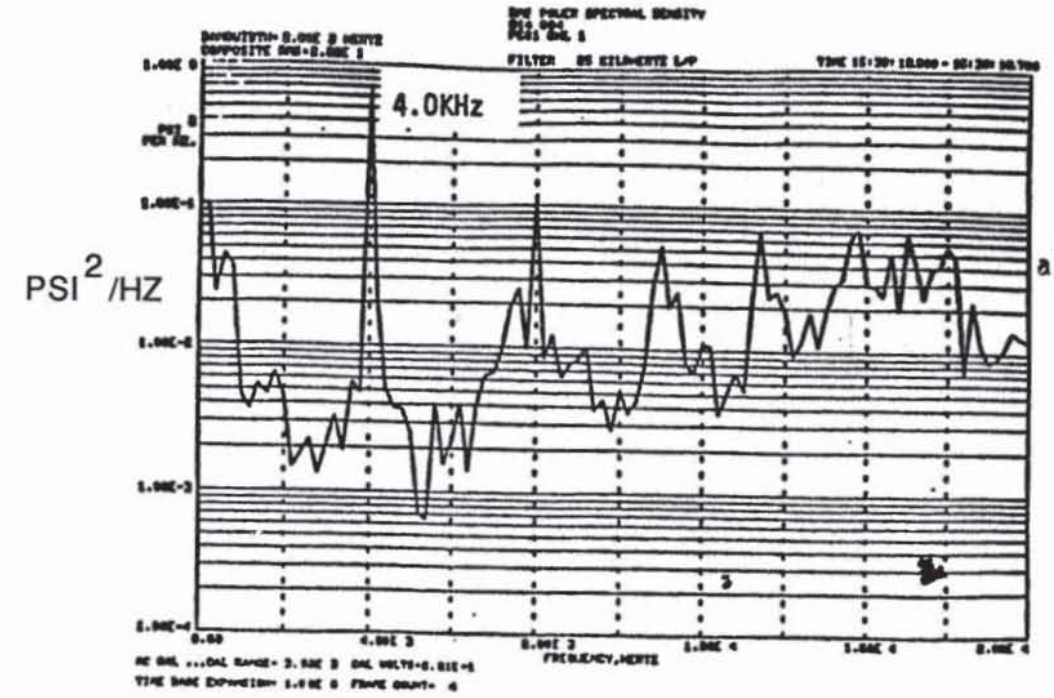

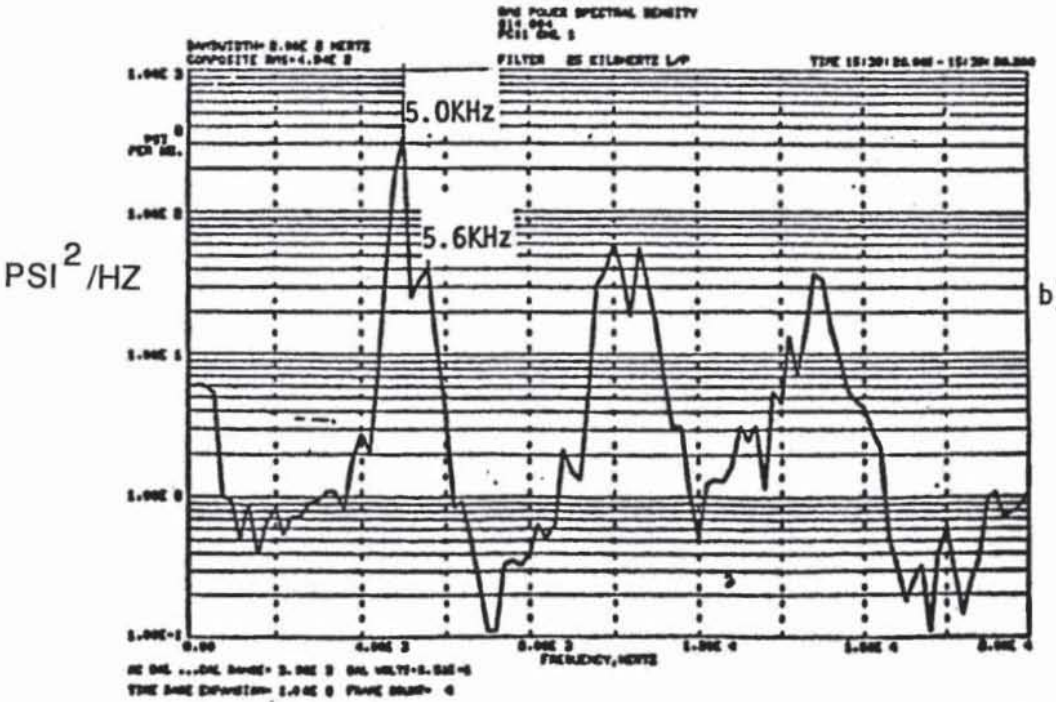

Figure B12 PSD OF HIGH FREQUENCY CHAMBER PRESSURE #1 BEFORE AND AFTER ONSET OF HIGH AMPLITUDE INSTABILITY

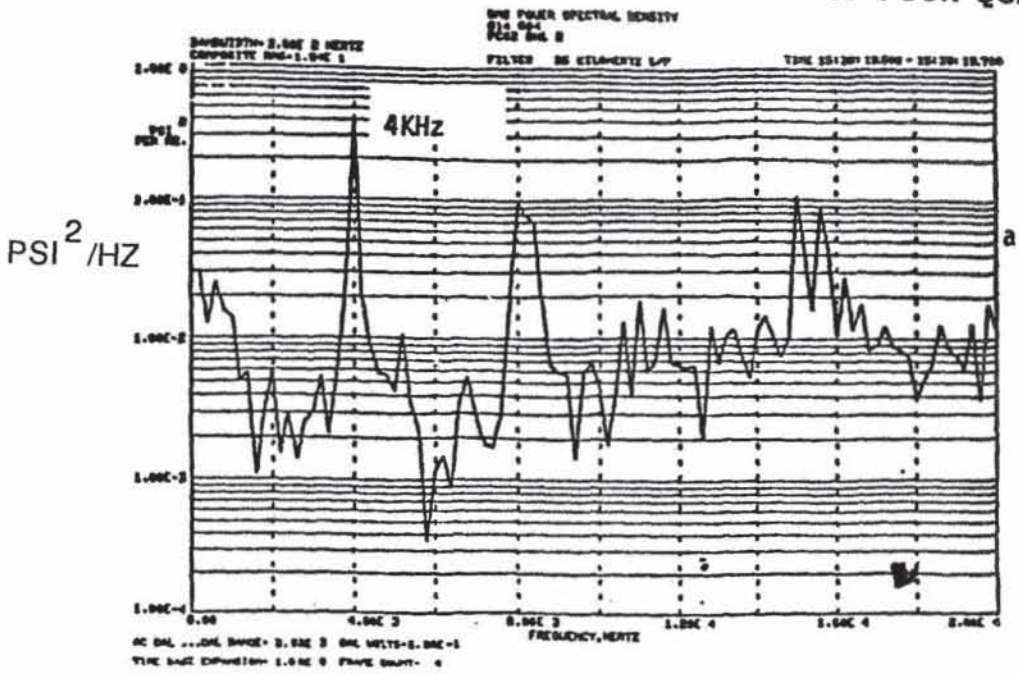

a) 17.0-17.2 s (before)

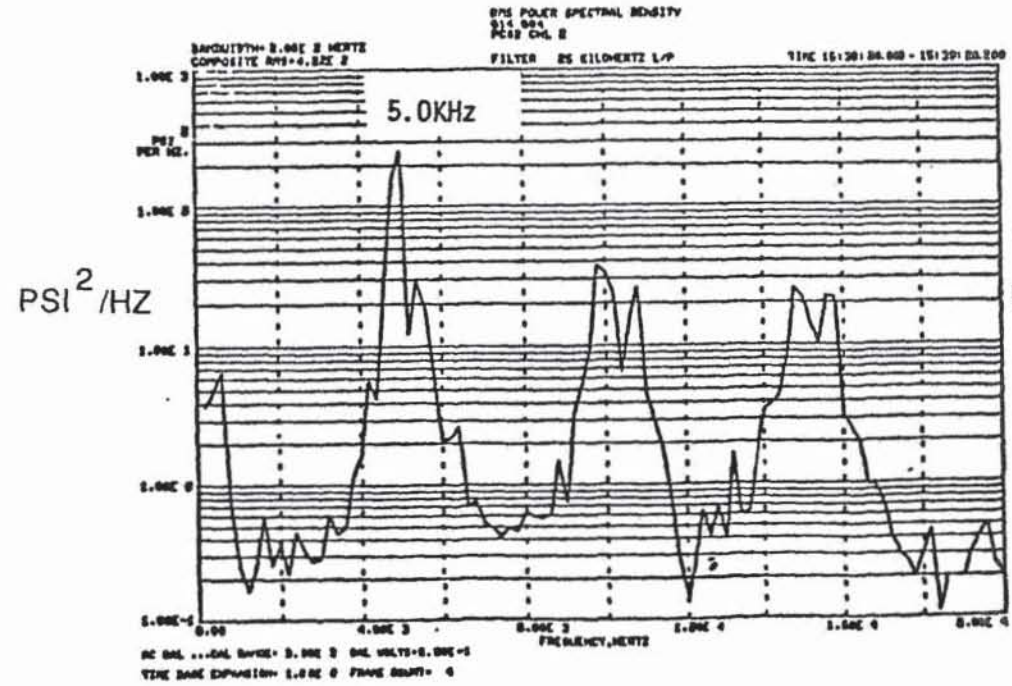

b) 17.5-17.7 s (after)

Figure B13 PSD OF HIGH FREQUENCY CHAMBER PRESSURE 2 BEFORE AND AFTER ONSET OF HIGH AMPLITUDE INSTABILITY

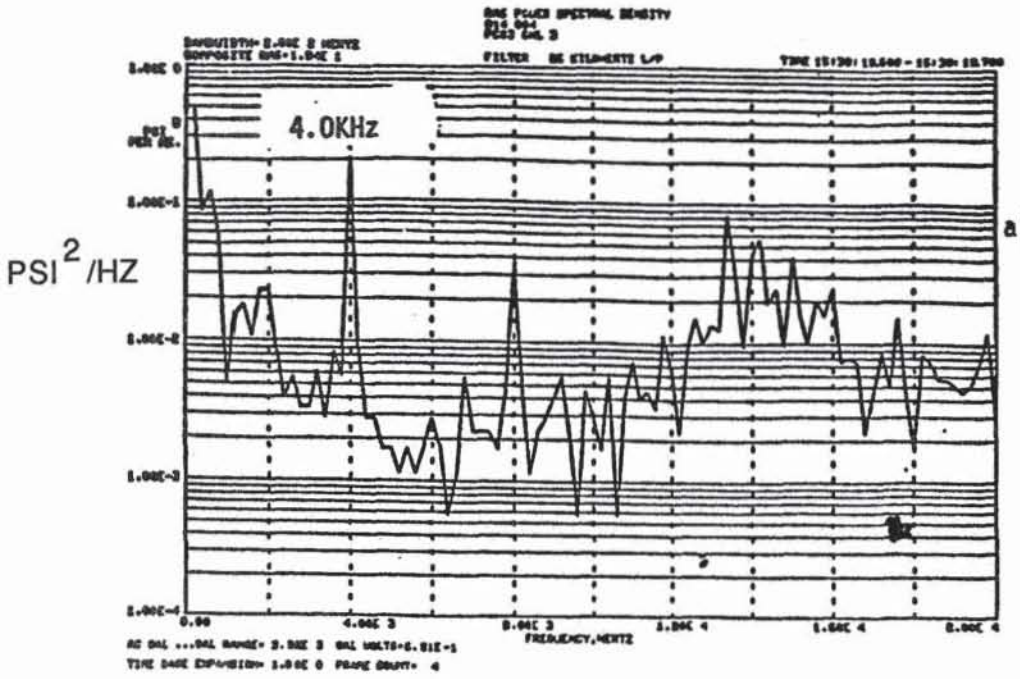

a) 17.0-17.2 s (before)

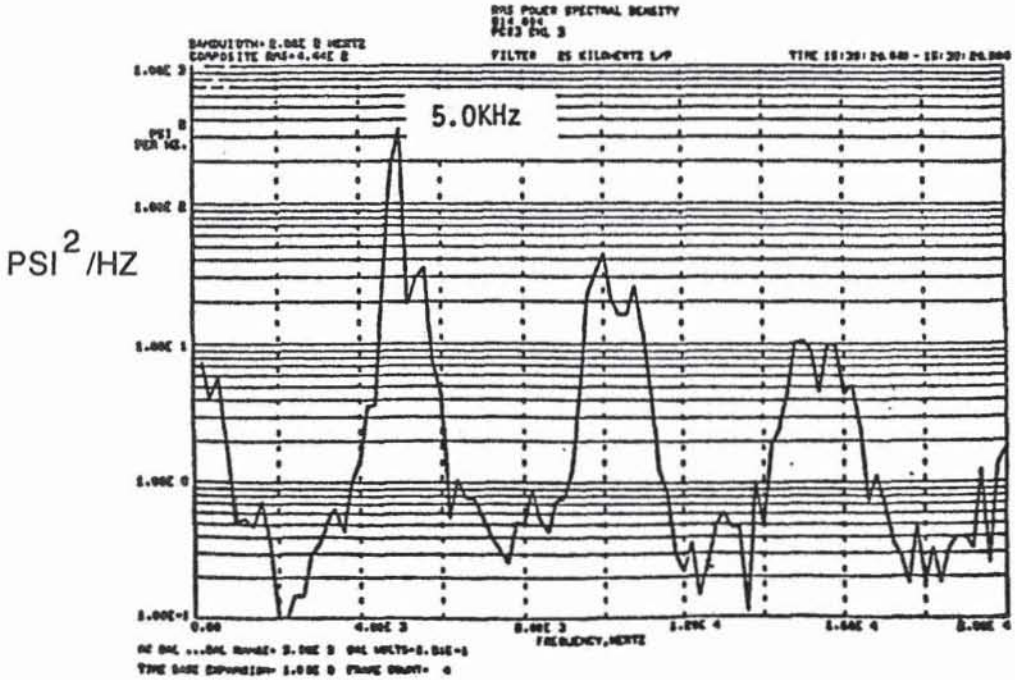

b) 17.5-17.7 s (after)

Figure B14 PSD OF HIGH FREQUENCY CHAMBER PRESSURE 3 BEFORE AND AFTER ONSET OF HIGH AMPLITUDE INSTABILITY

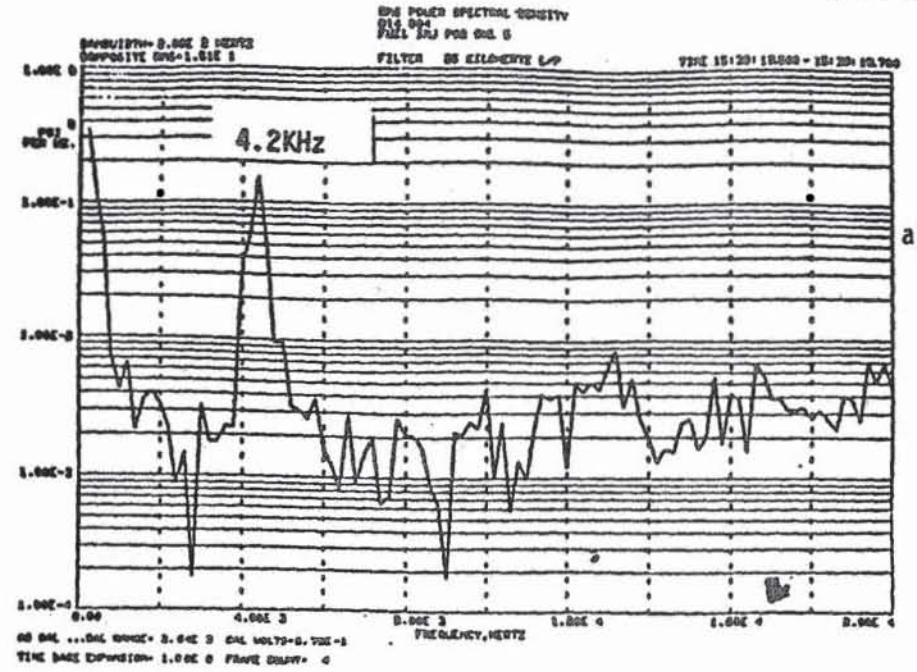

a) 17.0-17.2 s (before)

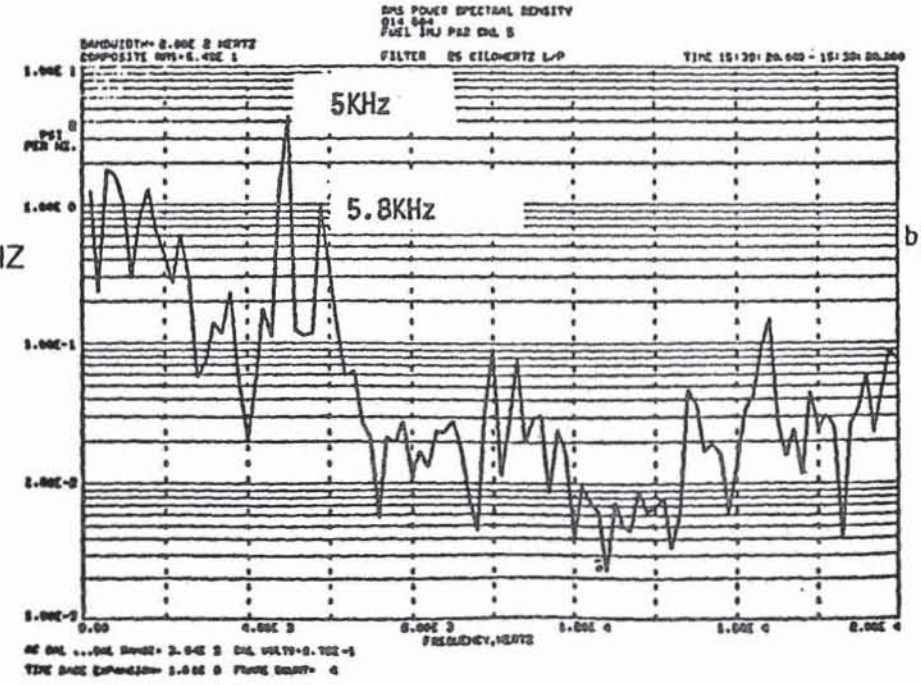

b) 17.5-17.7 s (after)

Figure B15 FUEL INJECTION PRESSURE #2 BEFORE AND AFTER ONSET OF HIGH AMPLITUDE INSTABILITY

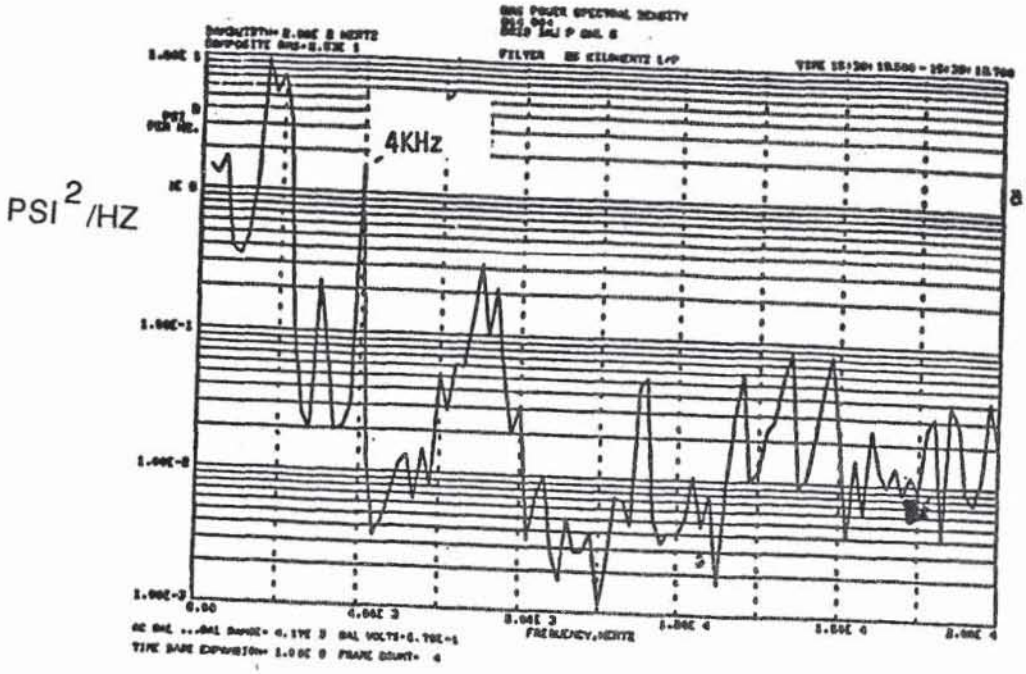

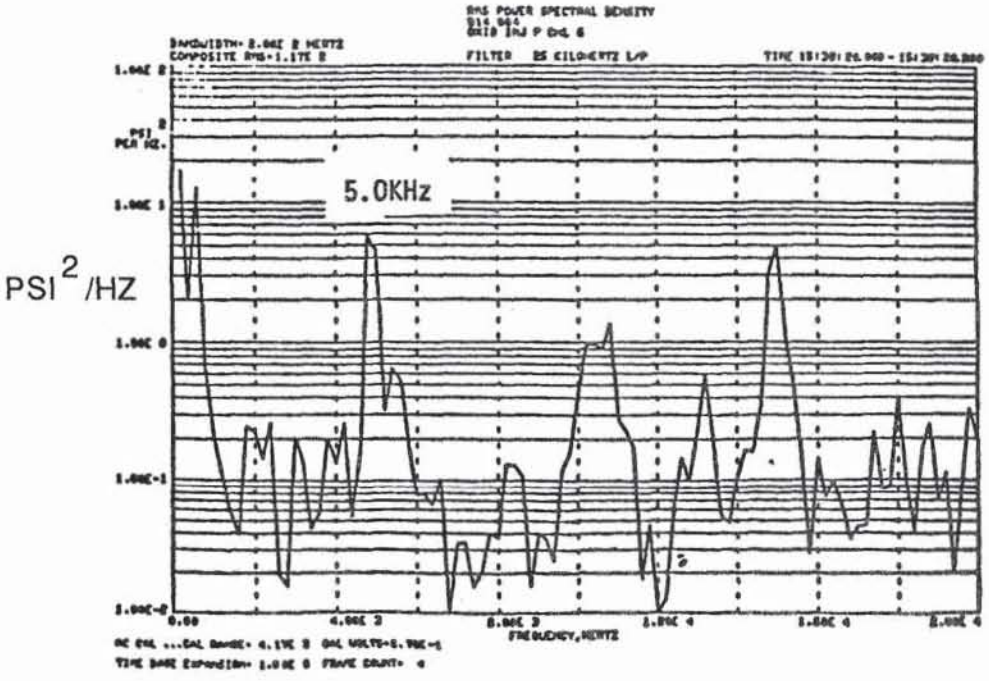

Figure B16 PSD OF HIGH FREQUENCY OXIDIZER DOME PRESSURE BEFORE AND AFTER ONSET OF HIGH AMPLITUDE INSTABILITY

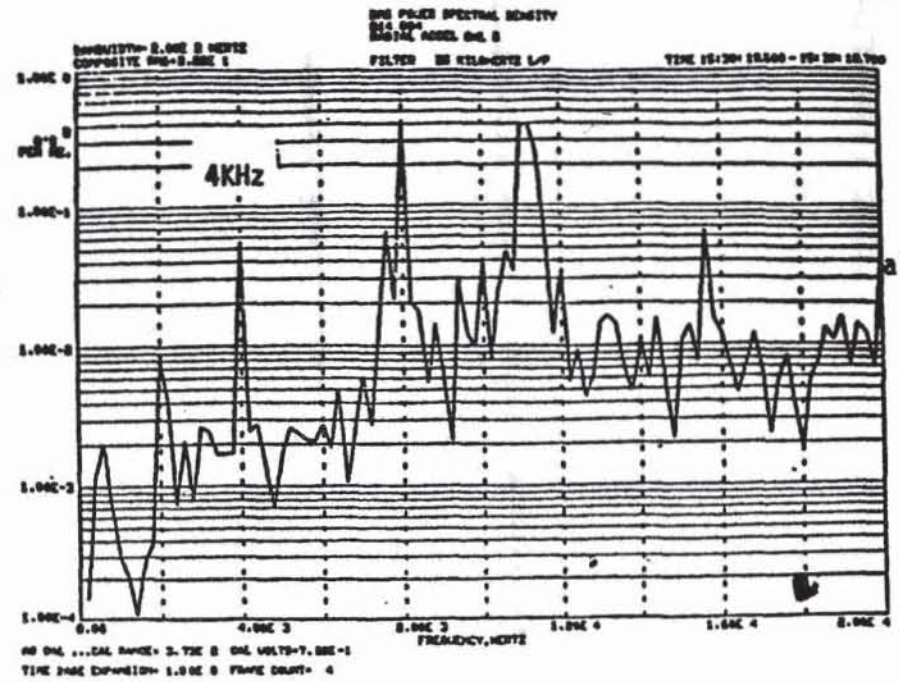

a) 17.0-17.2 s (before)

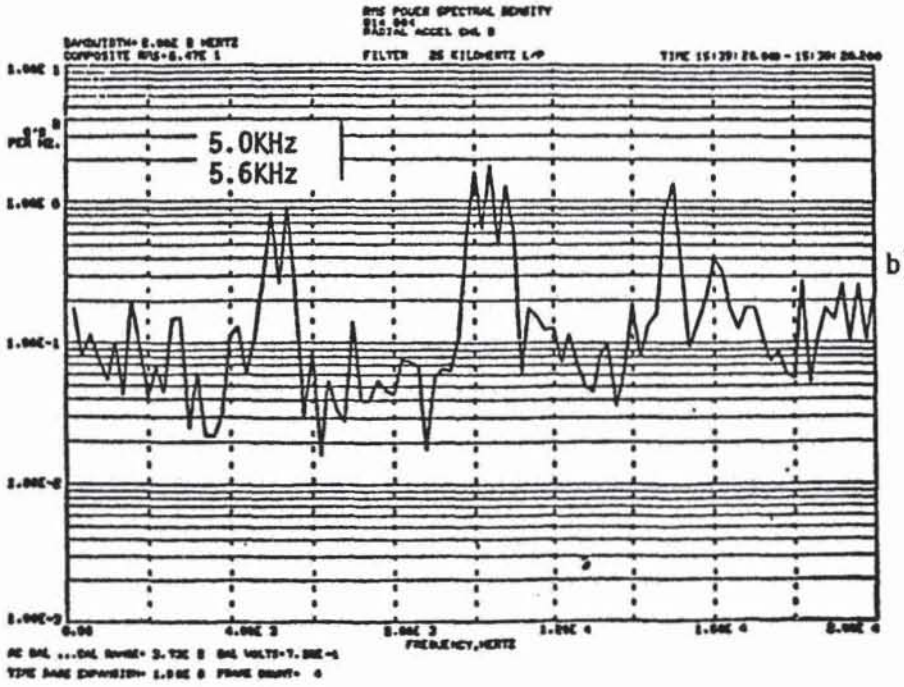

b) 17.5-17.7 s (after)

Figure B17 PSD OF RADIAL ACCELEROMETER BEFORE AND AFTER ONSET OF HIGH AMPLITUDE INSTABILITY

the lower half of the plume.

Time Slice 6: 17.294 sec to Cut-off (High Amplitude 1-T Mode Instability)

The time slice for PSD's during this period is also shown in Figure B11. Figures B12b through B17b show power spectra for PCB pressure transducers and the radial accelerometer after the onset of the high amplitude instabilty. The statos records suggest a mode in which two waves of similar amplitude and slightly different frequency coexist in the chamber. All spectra show either one or two peaks. These peaks shift in frequency during the high amplitude instability. From 17.5 to 17.7 seconds these peaks occur at 5 KHz and 5.6 KHz. During a later time slice which includes cut-off (18 to 18.2 seconds), the dominant frequencies are 4.8 and 5.4 KHz. The isoplot of PCB transducer 1 in Figure B3 suggest that these latter values are characteristic of most of the high amplitude instability. The 600 Hz beat frequency which is caused by these two frequencies can be seen in the PCB transducer 2 statos record shown in Figure B2. Indicated peak-to-peak amplitudes in the chamber reach 2900 psia, or 145% of chamber pressure. A relative phase of approximately 150 degrees is seen between the chamber PCB transducers 1 and 3. The 150 degree angular separation of these two transducers suggests that a spinning mode wave exists. Dome pressure fluctuations are in excess of 600 psia peak-to-peak (30% of Pc). Accelerometer g levels reach 1000 g's peak-to-peak. The maximum throat heat flux during the instability is typically 54 BTU/sq.in-sec.

B.2 Phase A Testing Through Test 014-014

An attempt at the first mainstage hot-fire test in the revised test plan (014-006) was terminated during the start transient prior to achieving the first stage power level due to excessive accelerometer vibrational levels seen by the TASCOS cutoff unit. The redline levels were set at 450 g's peak-to-peak. Comparison of start transient data between this test and the stable portion of the previous hot-fire mainstage test (014-004) showed similarly low operation acceleration levels. Review of the high frequency data aquisition system revealed erroneously high acceleration levels as seen by the TASCOS unit above a frequency of 10 KHz. To avoid a recurrent erroneous TASCOS cutoff, a 10 KHz filter was installed in the TASCOS unit.

Test 014-007 was prematurely cut due to a redline indicating low ignition pressure. Review of the data showed that chamber pressure rise time was slower than previous hot-fire tests, and the digital events recorder timeline indicated that the CTF igniter valve responded approximately 100 msec slower than previously. The activation of the CTF valve was moved up 200 msec to allow for the chamber pressure rise to pass the ignition detect minimum pressure level redline.

Test 014-008 was cut prematurely due to a minimum required chamber pressure redline at the first stage power level. The manifold injection pressures were nominal, however, the chamber pressures were lower than expected, prompting the redline cut. The line sizes for the chamber pressure pick-ups were decreased from .25 inch diameter to .125 inch diameter to enhance response time. In addition, the first stage power level was extended to allow a longer dwell time, and the redline activation time was delayed before checking for the minimum chamber pressure level.

Test 014-009 was cut by the fuel venturi inlet pressure redline. Data review indicated that the pressure was right at the required minimum value. Activation of this redline was delayed 200 msec to allow more time for the fuel venturi pressure to adequately rise through this redline.

Test 014-010 was cut by the main fuel valve minimum position redline (55% open) due to a dip in the position to 50% when the valve was commanded into mass flow control. This redline was lowered to 45% open to pass this redline and to provide for minimum hardware protection.

Test 014-011 was successfully conducted for a 0.7 second mainstage duration. Analysis of the high frequency data showed no activity which would indicate any instability mode. Performance of the thrust chamber during this test showed a significant increase in performance to nearly 97%, as compared to test 014-004. However, chamber heat flux remained high. Inspection of the hardware showed a minor area of erosion to the nozzle throat section at the nine o'clock position in the entrance to the convergence zone, which was refinished by polishing. To enhance cooling to this zone, two orifices were enlarged in the nozzle coolant system discharge circuits 1 and 2. Review of the high speed films showed green streaking at the nine o'clock position exiting the nozzle, indicating the erosion in the throat section.

Test 014-012 was also successfully conducted for a programmed duration of 1.5 seconds. Hardware and data inspection revealed no anomalies. Data review indicated that additional coolant could be added to the first nozzle coolant circuit, since the discharge pressure was 400 psi higher than the chamber pressure. The orifice in this circuit was enlarged to provide additional coolant margin. A spike occurred in the MFV position during transition from manual set point to the mass flow control mode. In addition, the mass flow control system required approximately the entire test duration to adjust from 18.5 lb/sec to the required value of 20.0 lb/sec. The integral and proportional gains of the MFV were increased to enhance valve response.

Test 014-013 was prematurely cut at 600 msec into mainstage due to a redline violation for maximum main fuel valve position, set

at 65%. This redline was increased to 75% open to compensate for a higher fuel injection temperature, which was up 15 degrees Rankine from test 014-012, resulting in a greater MFV position for the same flowrate.

Test 014-014 was successfully conducted for a programmed 8 second mainstage duration. Data review indicated nominal operation with no anomalies. Post-test hardware inspection revealed damage to the nozzle-throat section in the convergence zone in several locations, indicative of overheating. One location at the discharge to the coolant tube outlet 9 showed a small channel rupture. Inspection of the areas of damage by engineering personnel verified that continued use of the nozzle section was possible after polishing and increasing the coolant pressure and flowrate. Inspection of the 2 inch calorimter section, the 6 inch regen section, and the injector revealed no anomalies. Completion of test 014-014 concluded Phase A testing with ambient temperature methane.

APPENDIX C - Phase B Test Chronology

C.1 Phase B Testing Through Test 014-019

A low mixture ratio operating condition of 2.8 was selected for the initial Phase B temperature ramping test. This lower mixture ratio was selected to limit the heat loads on the nozzle, which had small coolant channel leaks as a result of damage sustained on test 014-014. The first attempt at a Phase B fuel injection temperature ramping hot-fire test (014-015) was aborted prior to ignition due to exceeding the maximum allowable water coolant inlet manifold pressure. The redline value was set at 3850 psig and the pressure reached 4100 psig at cut. The rapid pressure rise was due to a slow prime rate during the clamp stage (7.5% MWV open position until reaching 2200 psig inlet pressure), resulting in an excessive error signal to the pressure controlled closed loop water main servo valve on the clamp was removed to achieve the desired 3700 psig operating pressure. The error signal was reduced by increasing the clamp pressure to 3100 psig.

Test 014-016 was aborted in the water flow only stage due to a minimum water coolant inlet manifold pressure redline. This attempt was aborted because the 3100 psig clamp never released, and therefore, the minimum 3600 psig redline value was not achieved. The clamp value was reduced to 2800 psig to allow the clamp to release at the desired 3700 psig operating pressure.

Test 014-017 was also prematurely cut during the water flow only stage by a facility redline which indicated that the MWV close microswitch was actuated. Inspection of the MWV revealed a loose micro trip lever, which had erroneously indicated that the MWV had closed. This lever was fixed for the subsequent test.

Test 014-018 was prematurely terminated by the required minimum chamber pressure redline, due to a lower than anticipated chamber pressure rise rate when ramping to full power level. This condition was attributed to differences in thrust chamber starting characteristics at the low mixture ratio condition. The redline criterion for the time to achieve the targeted 2000 psia chamber pressure was extended prior to the next test.

Test 014-019 was cutoff by vibration levels which exceeded TASCOS accelerometer vibration limits during the transition to mainstage (approximately 1900 psia chamber pressure) at a mixture ratio of 2.8. Data analysis indicated the high accelerometer activity was caused by a first tangential acoustic instability characterized by two frequencies: the strongest activity was at 5 KHz (1-T) and was accompanied by a secondary peak between 5.5 and 6 KHz. The instability frequency and amplitude characteristics were similar to test 014-004. Prior to the instability on each of these tests, similar low level organized activity was observed on the

accelerometers and pressure transducers. In particular, a 4 KHz oscillation was noted prior to the onset of the high amplitude instability in each test. Figure C1 shows chamber pressure and propellant injection pressures as a funtion of time, and indicates the onset of the instability at 33.327 seconds (file time).

Table C.I presents a comparison of digital data 90 msec after mainstage OK for tests 014-014 (MR = 3.66), 014-018, and 014-019. The time slice for test 014-019 corresponded to a stable portion that test. Based on the stagnation pressure, it is suspected that both tests 014-018 and -019 exhibited a considerably lower c* efficiency than test 014-014, possibly due to the low mixture ratio condition. By comparison, NASA-MSFC testing of a similar injector at 2000 psia and a mixture ratio of 2.9 exhibited a c* efficiency of 98.7%. Hence the performance characteristics of the NASA-LeRC injector being tested at Rocketdyne may differ considerably from that of the MSFC injector. Although test 014-014 was conducted at a higher fuel temperature (512 degrees R) than tests 014-018, and 014-019 (501 and 506 degrees R, respectively) it must be observed that tests 014-011 and 014-012 were stable for fuel injection temperatures of 503 and 506 degrees R, respectively. Hence, the low fuel temperature on tests 014-018 and 014-019 is not considered significant.

Figure C2 shows enlarged brush chart records of the chamber and propellant injection pressures for test 014-019. As in test 014-004, simultaneous increases in the propellant injection pressures and a decrease in chamber pressure occur at the onset of the instability. These phenomena (which are also observed in LOX/hydrogen temperature ramp testing at NASA-LeRC during the 1960's and 1970's) are possibly related to an increase in injector element cup resistance. The cause is not clear, although a change in combustion within the cup known as "cup burning" has been suspected.

Expanded brush chart records indicate low level 4 KHz ocillations on many of the channels before the onset of the instability. Based on the brush chart records, the 4 KHz activity dominates the inner fuel manifold PCB transducer data first. At that time, the oxidizer injection pressure exhibits both 4 KHz and higher frequency oscillations. Later, the 4KHz dominates the oxidizer PCB data. Within the last few milliseconds before the high amplitude instability, there is a growth in amplitude and a shift in frequency toward 5 KHz. It should be noted that anomalous peaks at 6 KHz on the PSD's and isoplots for the fuel manifold PCB transducer are unexplained. Isoplots of the tangential and axial accelerometer just prior to the instability are shown in Figure C3 Both 4 and 8 KHz activity are seen. The 8 KHz may be either a higher order harmonic of the basic 4 KHz oscillation and/or the next higher organ pipe mode of the LOX post.

ORIGINAL PAGE IS
OF POOR QUALITY

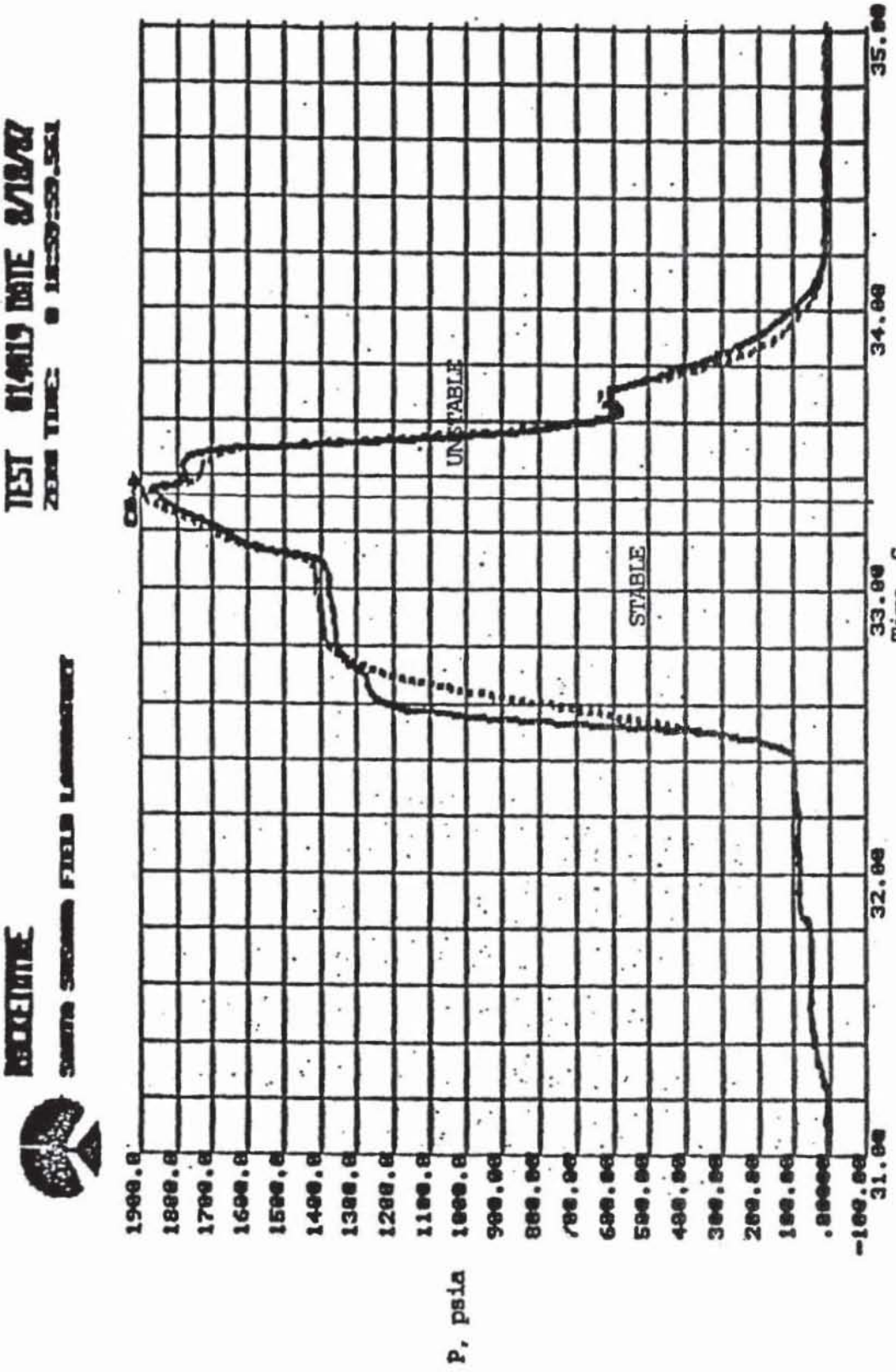

Figure C1 Test 014-019 Chamber Pressure

TABLE C.I **TEST PARAMETRIC COMPARISON FOR 3 TESTS STABLE OPERATION**

ITEM	(UNITS)	014-014	014-018	014-019
Pc-2 (inj end)	(PSIA)	1943.5	1870	1877
P_{io}	(PSIA)	2474.8	2327.4	2314.6
P_{if}	(PSIA)	2625.	2767.3	2803.1
T_{io}	(F)	-241.6	-239.8	-243.8
T_{if}	(F)	52.17	40.87	46.01
W_{LOX} (inj ele)	(lb/s)	70.28	65.78	65.92
W_{fuel} (inj ele)	(lb/s)	19.07	22.85	23.45
Mixture Ratio		3.66	2.86	2.79

*Data taken from time slice 90 ms after mainstage ok.

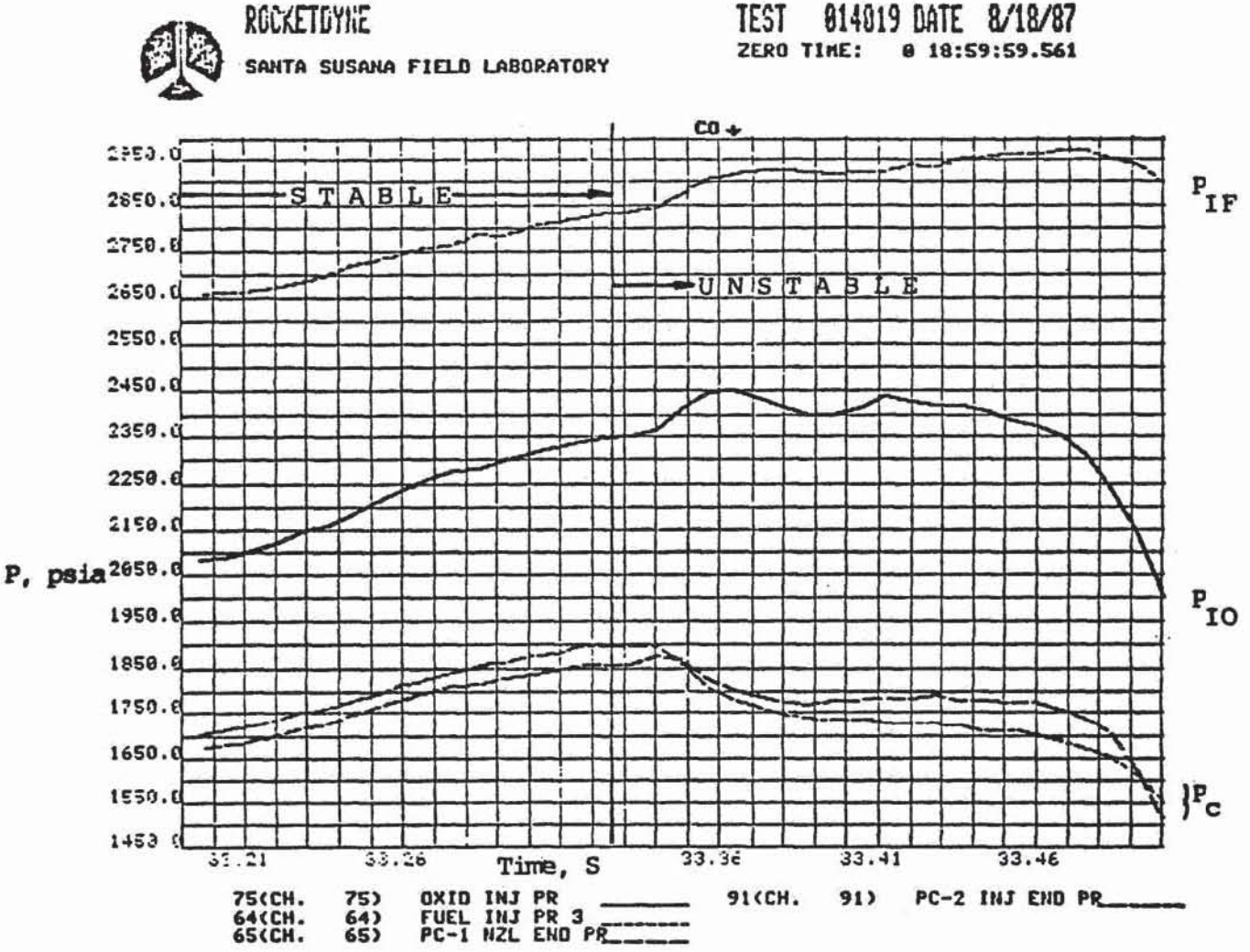

Figure C2 -Test 019 Propellant injection pressures and chamber pressure at the time of the instability

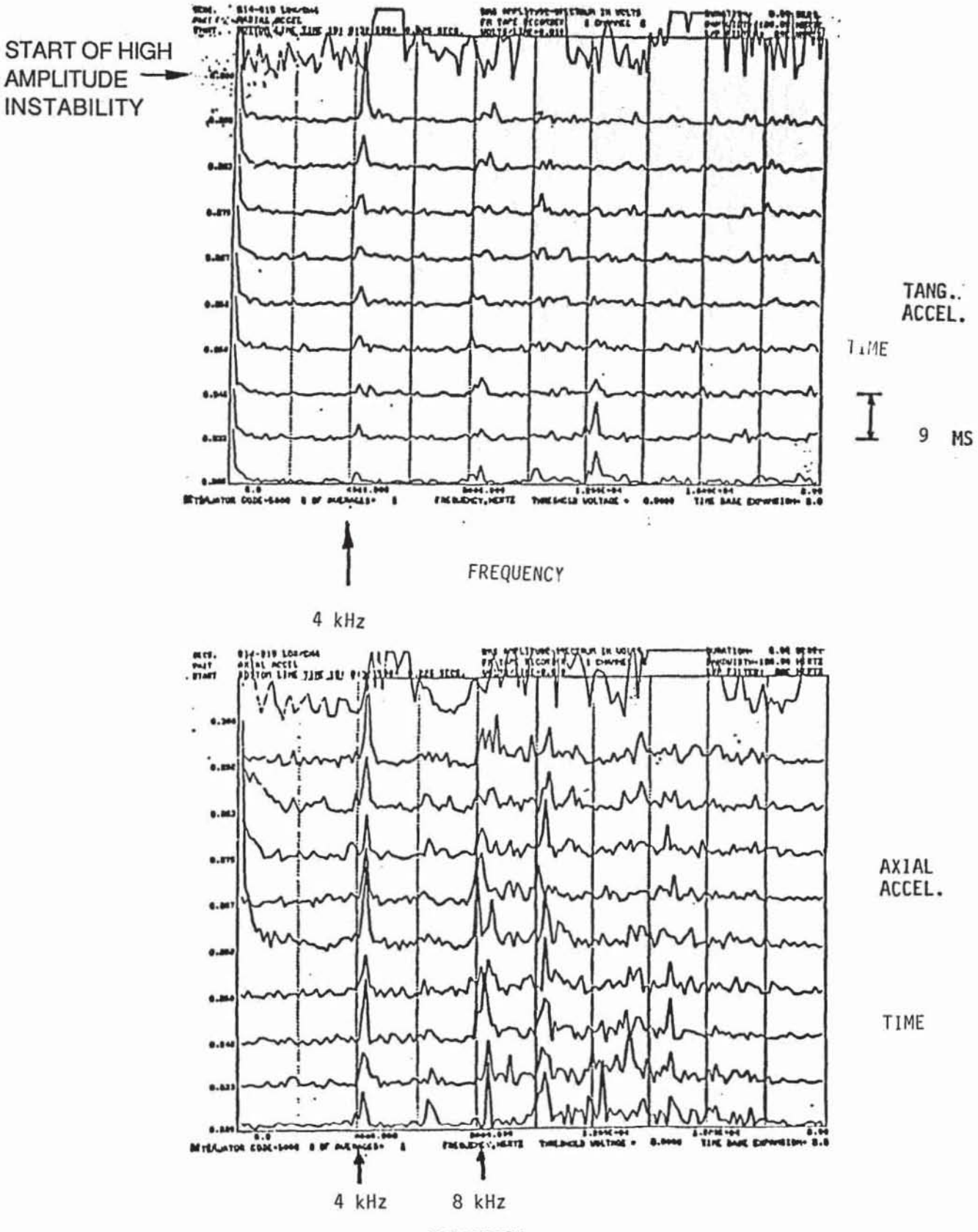

Figure C3 - Accelerometer Isoplots for Test 014-019

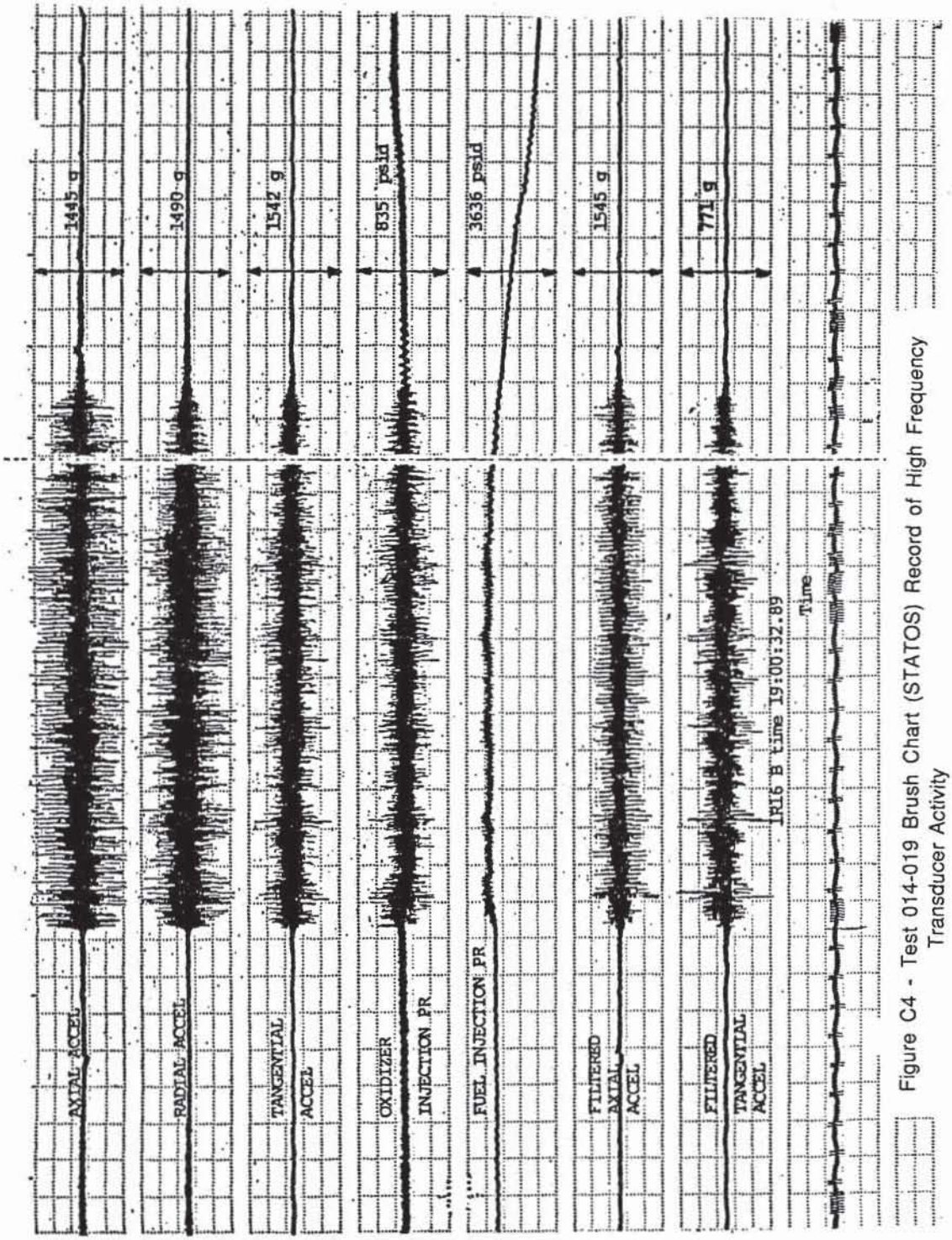

Figure C4 - Test 014-019 Brush Chart (STATOS) Record of High Frequency Transducer Activity

A compressed brush chart record for test 014-019 is shown in Figure C4, indicating the peak-to-peak amplitudes of the accelerometers and manifold pressures prior to and during the instability. Fuel and oxidizer manifold pressure peak-to-peak amplitudes prior to the instability are in the range of 70 to 80 psid. Typical peak-to-peak amplitudes on the (unfiltered) accelerometers are between 750 and 1500 g's during the instability, as seen from Figure C4. This compared with a range of from 750 to 900 g's during test 014-004. During the instability, peak-to-peak pressures of approximately 400 psid are seen in the manifolds, similar to test 014-004.

The two interfering waveforms corresponding to the two instability frequencies give rise to a beating phenomenon at 600 to 700 Hz. Considerable high frequency content at and above 10 KHz is seen in the oxidizer injection pressure and the accelerometer data. The source of this activity is not clear, and it does not appear in the high frequency fuel manifold pressure record. Power spectra from the unstable portions of tests 014-019 and 014-004 are shown in Figures C5 through C7. The distinctive dual frequency peak 1-T mode is seen on the radial accelerometer and fuel injection power spectra.

C.2 Phase B Testing Through Test 014-025

Phase B tests 014-020 through 014-025 included three tests in which a high frequency combustion instability was encountered at a repeatable temperature as the fuel temperature was ramped downward. A spontaneous instability occurred on one other test at lower than nominal mixture ratio conditions. The nature of each type of instability is discussed along with some hypotheses. Despite some similarities to LOX/hydrogen fuel temperature ramping stability rating tests conducted at NASA-LeRC and elswhere, many characteristics appear to distinguish the LOX methane test results from LOX/hydrogen.

Test 014-020 through 014-025 are summarized in Table C.II. Tests 014-020, and 014-023 through 014-025 featured a downward ramp in fuel temperature. Fuel temperature ramping (decreasing fuel injection temperature at constant mixture ratio) has been used by NASA-LeRC and others as a reliable method to rate the relative stability of LOX/hydrogen coaxial injectors. Temperature ramping tests yield a quantitative indication of the relative stability of a given LOX/hydrogen coaxial injector by determining the magnitude of the temperature reduction below the nominal operating temperature that is necessary to produce an instability. For example, stable injectors require a large reduction in fuel temperature before an instability occurs. Marginal injectors exhibit instabilities at fuel temperatures only slightly below nominal. The temperature at which an instability occurs during LOX/hydrogen tests has been shown to be repeatable on a test-by-test basis for a given injector

$\frac{PSI^2}{Hz}$

Oxid Inj Pr
Test 004

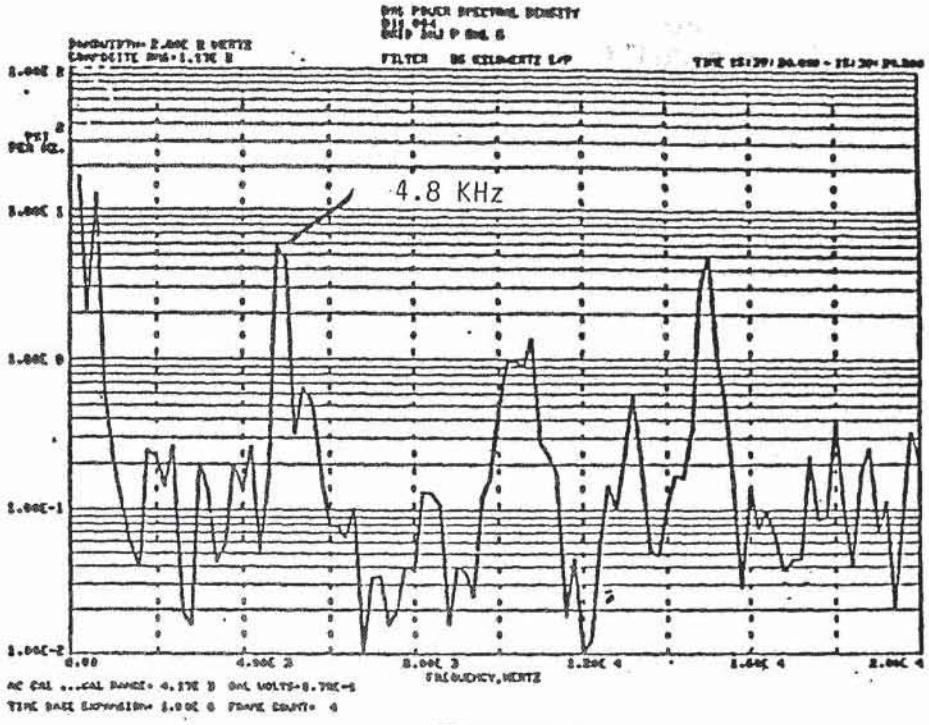

$\frac{PSI^2}{Hz}$

Oxid Inj Pr
Test 019

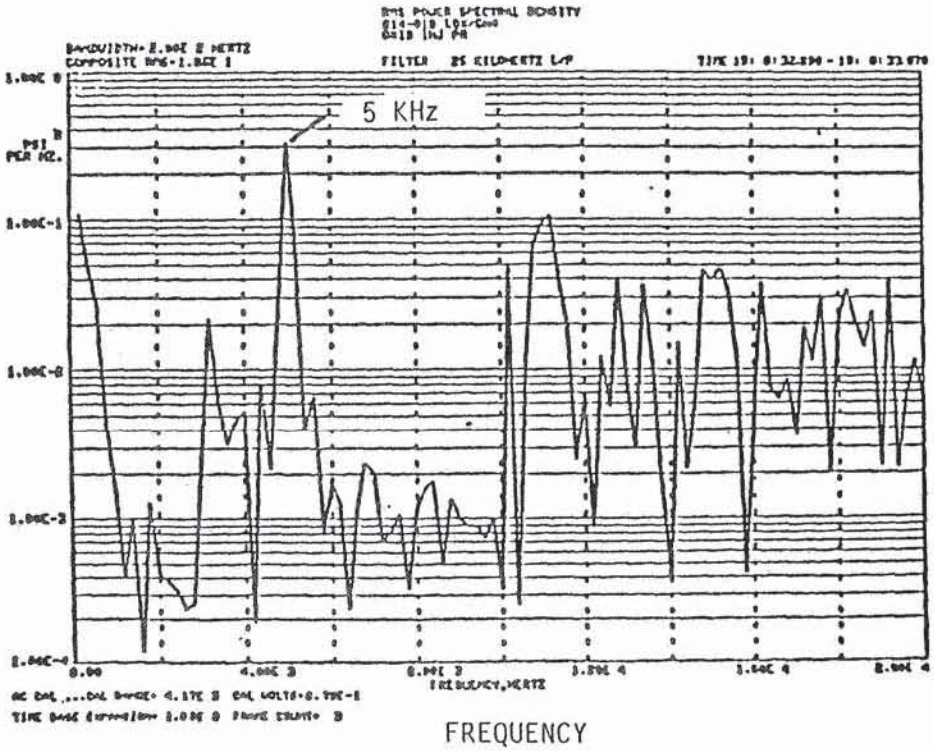

Figure C5 Oxidizer injection pressure power spectra during unstable portions of indicated tests

$\frac{PSI^2}{Hz}$

Fuel Inj Pr
Test 004

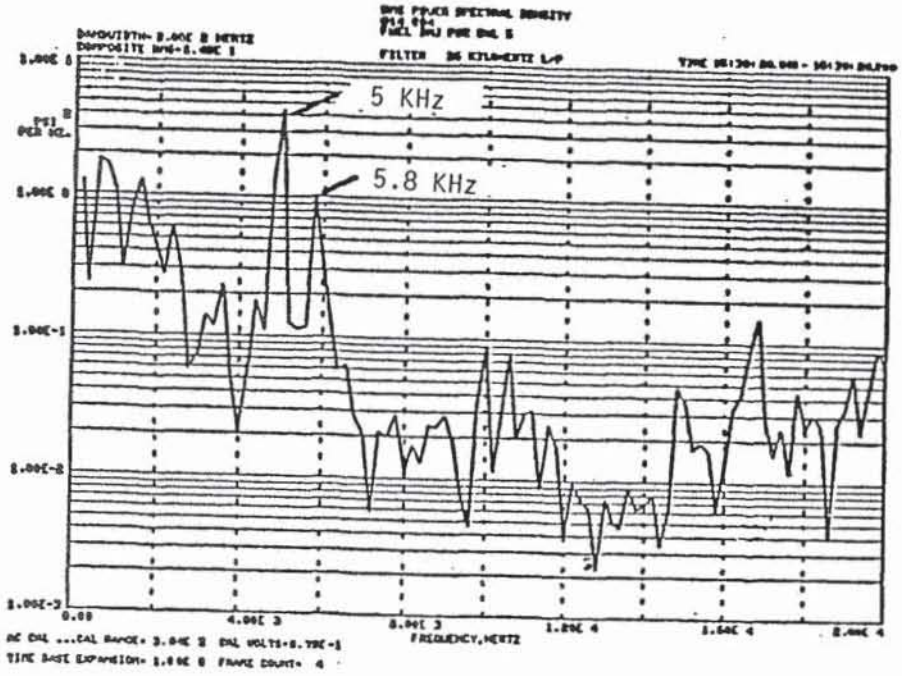

$\frac{PSI^2}{Hz}$

Fuel Inj Pr
Test 019

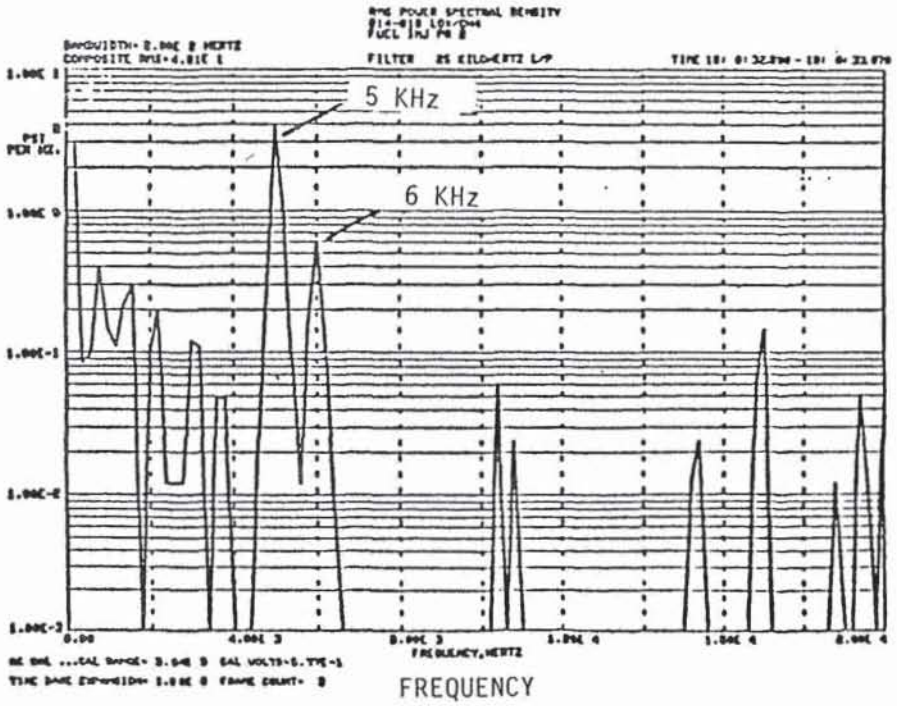

Figure C6 - Inner manifold fuel injection pressure power spectra during unstable portions of indicated tests

$\frac{(g's)^2}{Hz}$

Radial Accel
Test 004

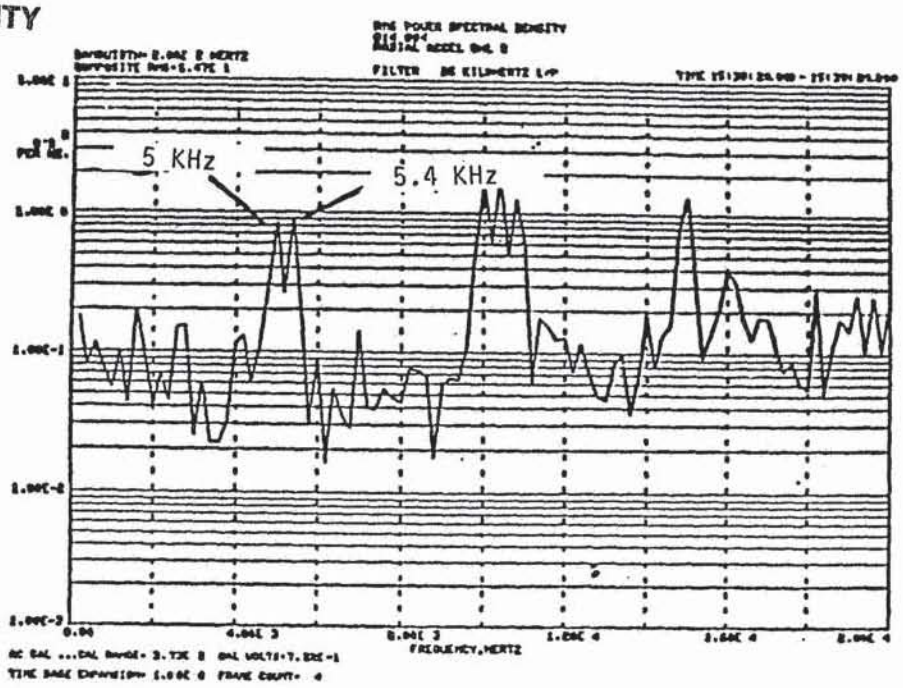

FREQUENCY

$\frac{(g's)^2}{Hz}$

Radial Accel
Test 019

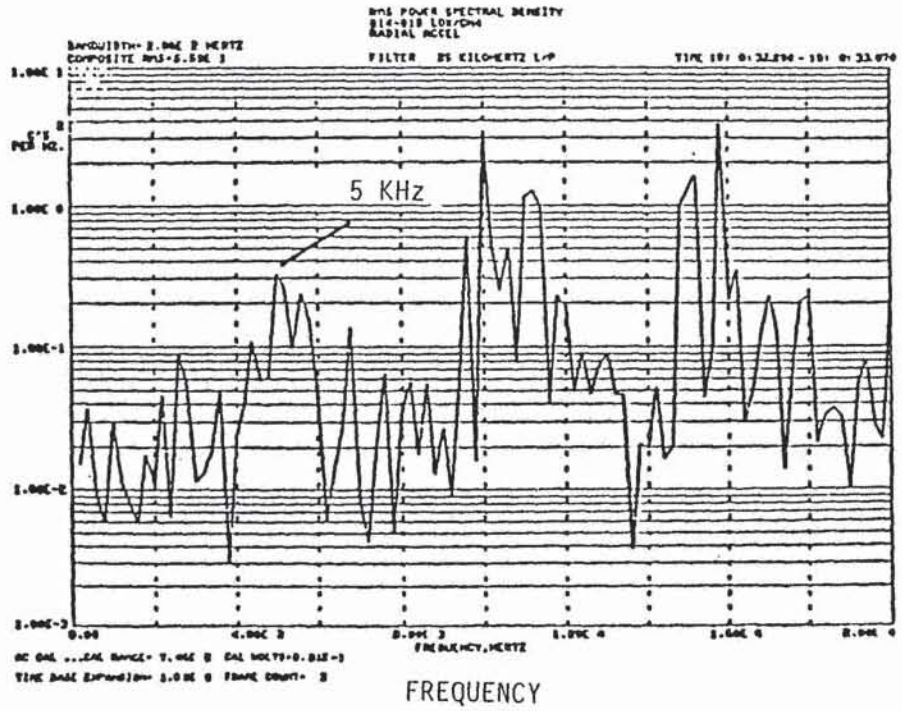

FREQUENCY

Figure C7 - Radial accelerometer power spectra during unstable portions of indicated tests

Table C.II - Test -020 through -025 Test Summary

Test	Pc (psia)	MR (O/F)	Fuel Inj. Temp. (R)	Comments
020	2070	3.22	498	Fuel temperature ramp
021	1990	3.10	494	Facility redline cut prior to mainstage
022	2030	3.01	489	Spontaneous 1T instability
023	2037	3.19	433	14 kHz instability during fuel temperature ramp
024	2020	3.06	428	14 kHz instability during fuel temperature ramp
025	2015	3.06	427	14 kHz instability during fuel temperature ramp

configuration and given flow rates.

Test 014-022, which is the only other test of significant duration in this series, encountered an instability before the temperature ramp began. The 1-T mode instability frequency was nominally at 5 KHz, with a secondary peak at approximately 5.8 KHz. This dual peak result is consistent with two other tests (014-004 and -019) in which the 1-T mode was excited. Amplitudes were in the range of 900 g's peak-to-peak. The instability was preceded by 4.4 and 8.7 KHz activity on the accelerometers. These frequencies are close to theoretically predicted LOX post modes. Additionally, the LOX manifold PCB detected 19 KHz activity at approximately 200 psid peak-to-peak at 24 msec prior to the high amplitude instability. This is seen in Figure C8. Similar to tests 014-004 and -019, propellant manifold pressures rose and the chamber pressure dropped at the onset of instability.

Tests 014-023, -024, and -025 are the most significant tests in this series. Test 014-020 was also temperature ramped, but was cut early due to fuel valve oscillations, and did not exhibit any instabilities. The general characteristics of these tests are shown in Figure C9. The test duration was approximately 6.5 seconds. After approximately 2 seconds, the fuel temperature was reduced in a continuous fashion at approximately 20 degree R per second. This fuel temperature reduction rate relative to the overall test sequence is shown in Figure C10.

As shown in Table C.III, all three tests went unstable at 14 KHz. However, 14 KHz does not correspond to any expected acoustic combustor modes. The nearest combustor modes are the 3-T/4-L,, 1-R/5-L, and 8-L at 13.8, 14.0, and 14.3 KHz, respectively. Prior to the onset of high amplitude 14 KHz activity, the high frequency records indicated low level 14 KHz and 8.6 KHz (on the accelerometer channels) activity that shifted in frequency from approximately 12 KHz to 14 KHz during the temperature ramp. Figure C11, an isoplot for the axial accelerometer, shows these phenomena. Figure C12 shows the accelerometer and manifold high frequency pressure transducer brush chart records before and during the high amplitude 14 KHz activity.

The indicated amplitudes on the accelerometers were from 200 to 900 g's. However, the accelerometers exhibit attenuation at frequencies above 10 KHz. Hence, the actual acceleration levels were likely higher. Fuel and oxidizer manifold pressure oscillations were about 100 and 500 psi peak-to-peak, respectively. As indicated in Figure C9, the fuel manifold pressure typically decreased (as the resistance decreased due to lower fuel injection temperatures) until the fuel and oxidizer manifold pressures are equal. The instability occurs at that point and both manifold pressures rise the same amount (approximately 300 psi). Simultaneously, the chamber pressure drops approximately 250 psi. Table C.IV summarizes these

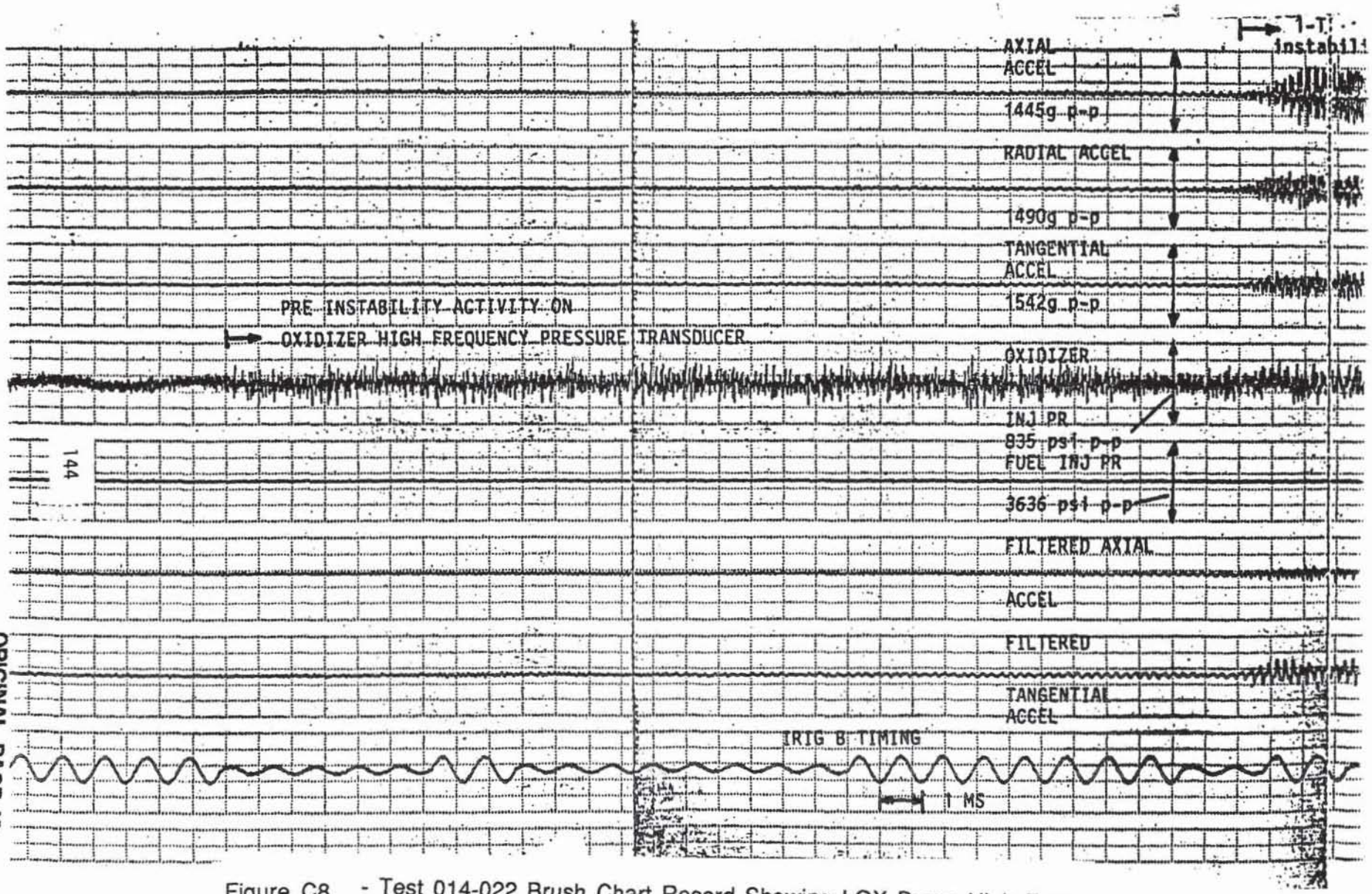

ORIGINAL PAGE IS
OF POOR QUALITY

Figure C8 - Test 014-022 Brush Chart Record Showing LOX Dome High Freq. Activity Prior to 1-T Instability

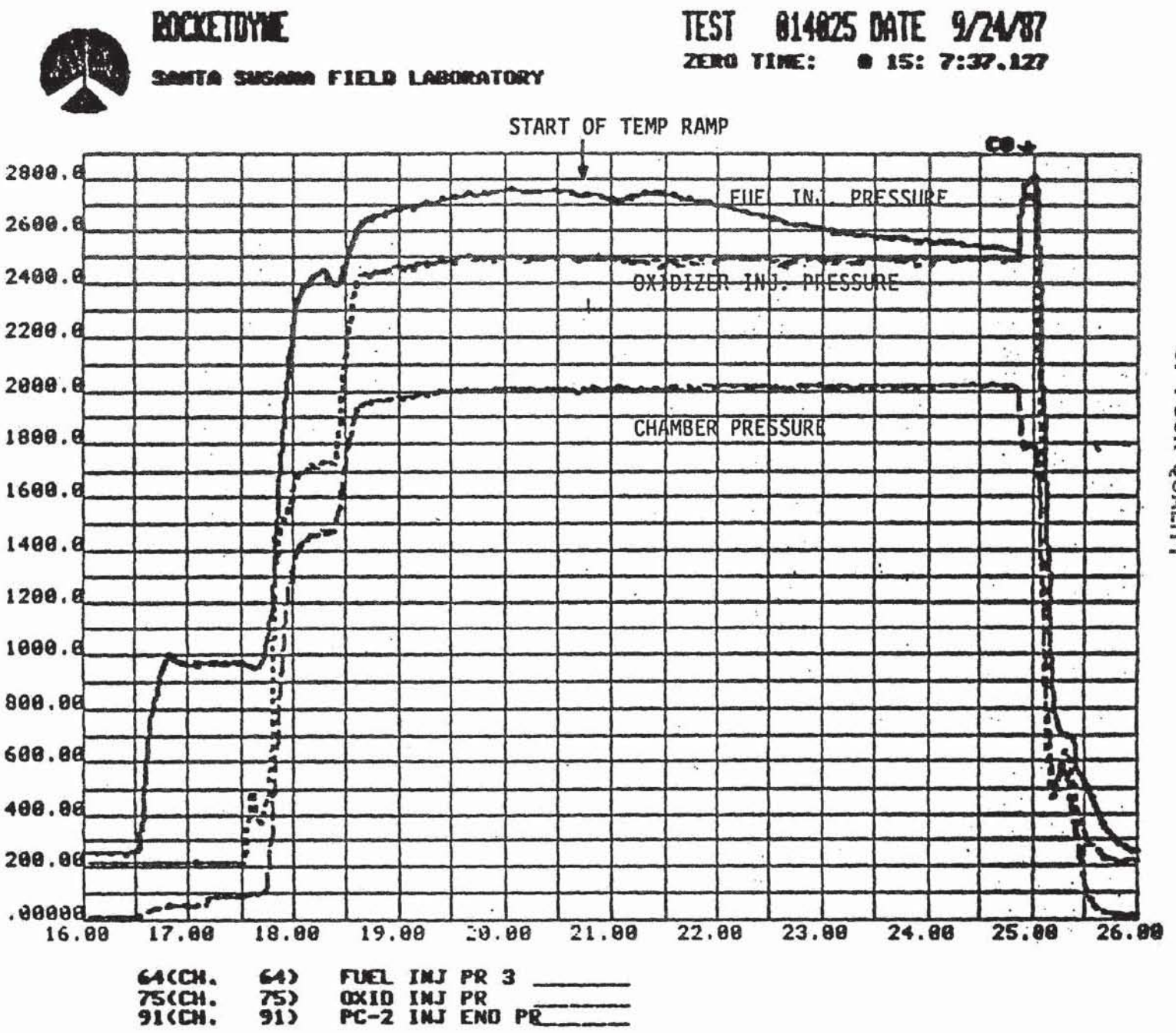

Figure C9 - MANIFOLD AND CHAMBER PRESSURES DURING TEST 014-025
A TYPICAL FUEL TEMPERATURE RAMP TEST.

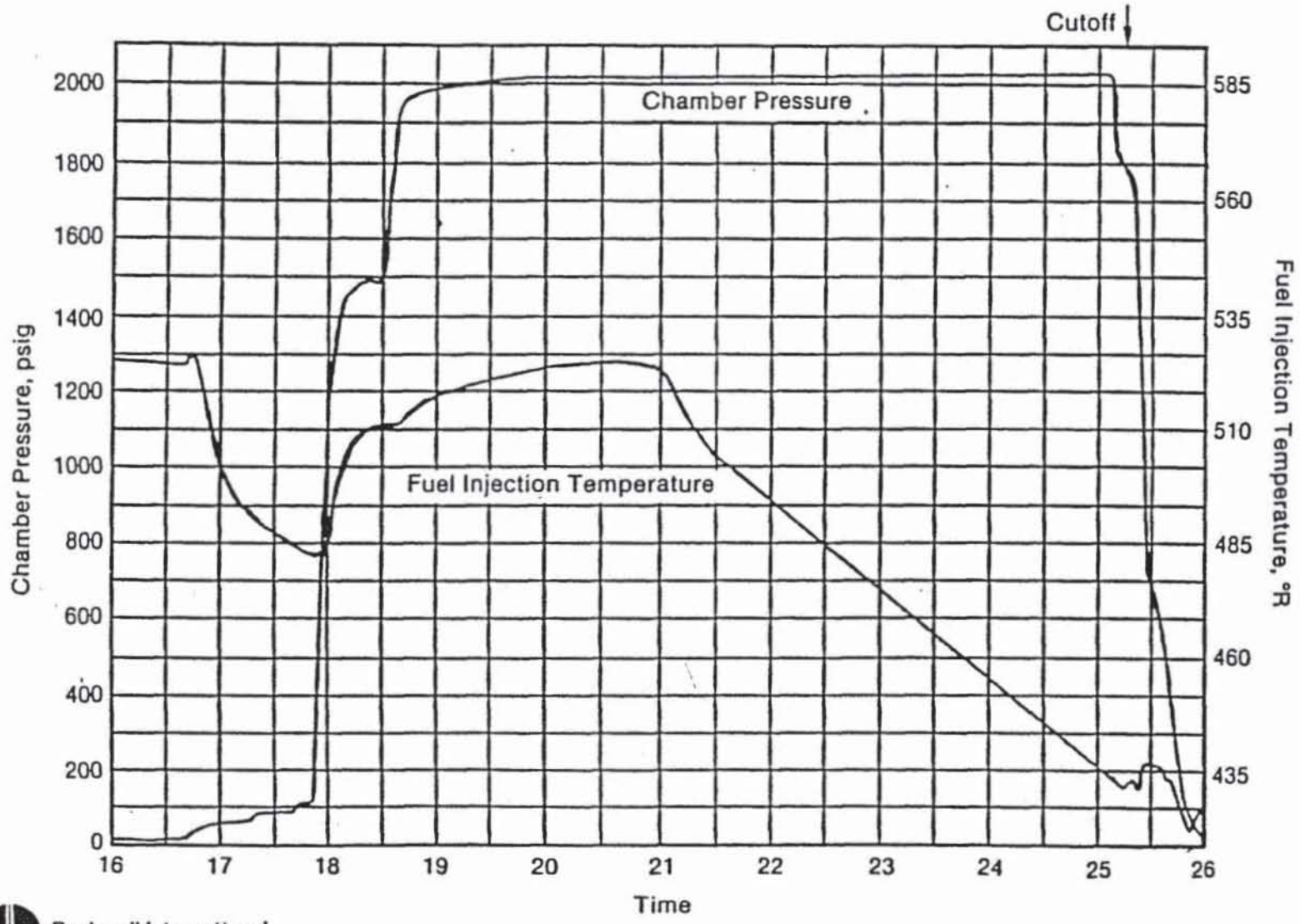

Rockwell International
Rocketdyne Division

87D-9-2690

Figure C10 - Stability Temperature Ramp Test History

TABLE C.III - Comparison of Low Mixture Ratio and Fuel Temperature Ramp Instabilities

	LOW M/R	TEMP RAMP
M/R	2.8/3.25/3.33 (15° CHAMFER)	3.35-3.5
MODE	1-T	14 KHz
PRE-INSTABILITY ACTIVITY	4.4, 8.6, 10, 12-13 KHz	8.6/12-14 KHz
MANIFOLD PRESSURES AT INSTABILITY	$P_{IF} \neq P_{IO}$	$P_{IF} = P_{IO}$
SHIFT IN PRESSURES AT INSTABILITY	P_{IF}, P_{IO} APPROX 100 PSI ↑ P_C APPROX 150 PSI ↓	P_{IF}, P_{IO} 200 TO 300 PSI ↑ P_C APPROX 250 PSI ↓
FUEL TEMP (MEASURED MANIFOLD) (CALCULATED INJECTION)	36 TO 50°F 23 TO 29°F	-18 TO -24°F APPROX. -50°F

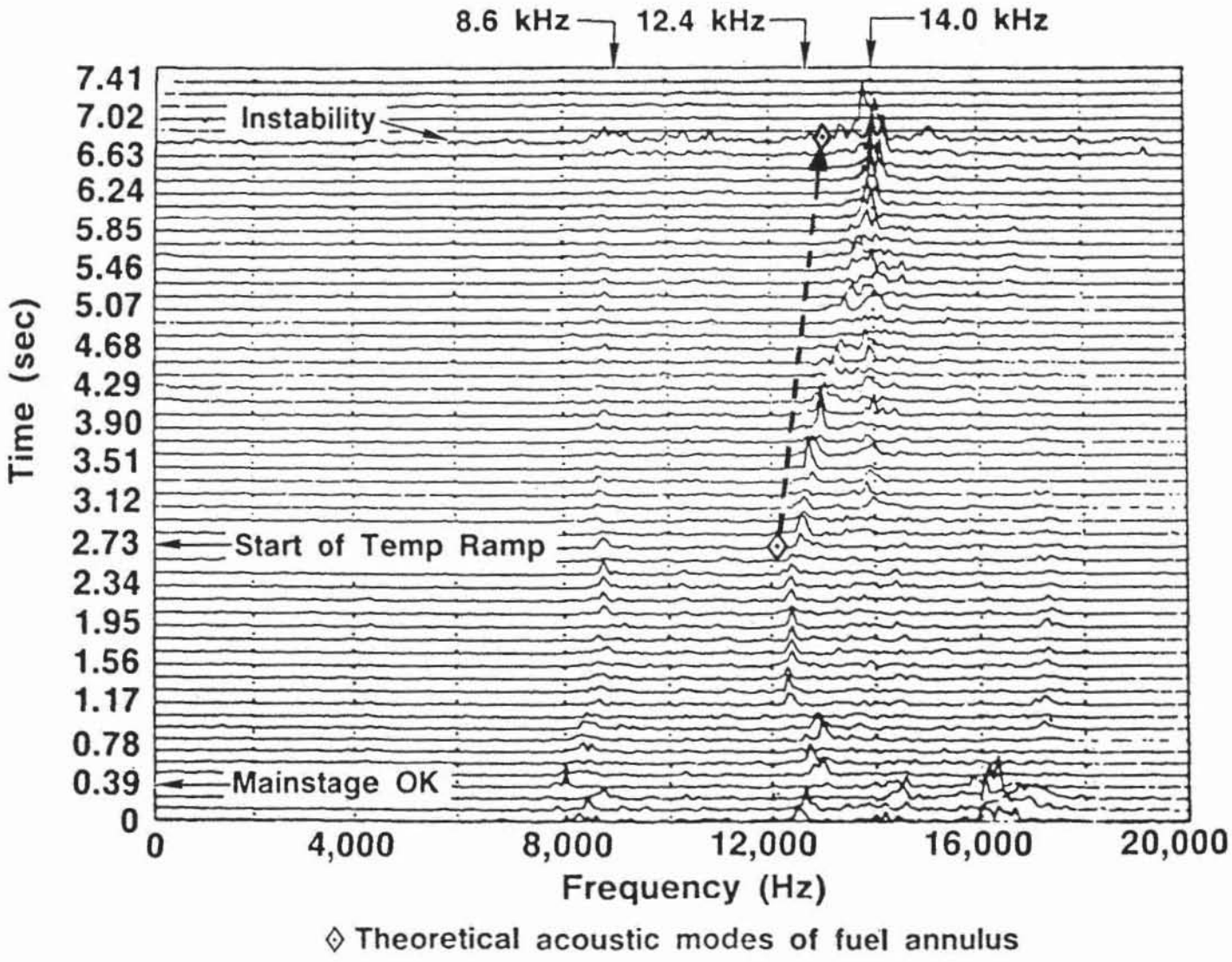

Figure C11 - Axial Accelerometer for Test 014-025
(Temperature Ramping Test)

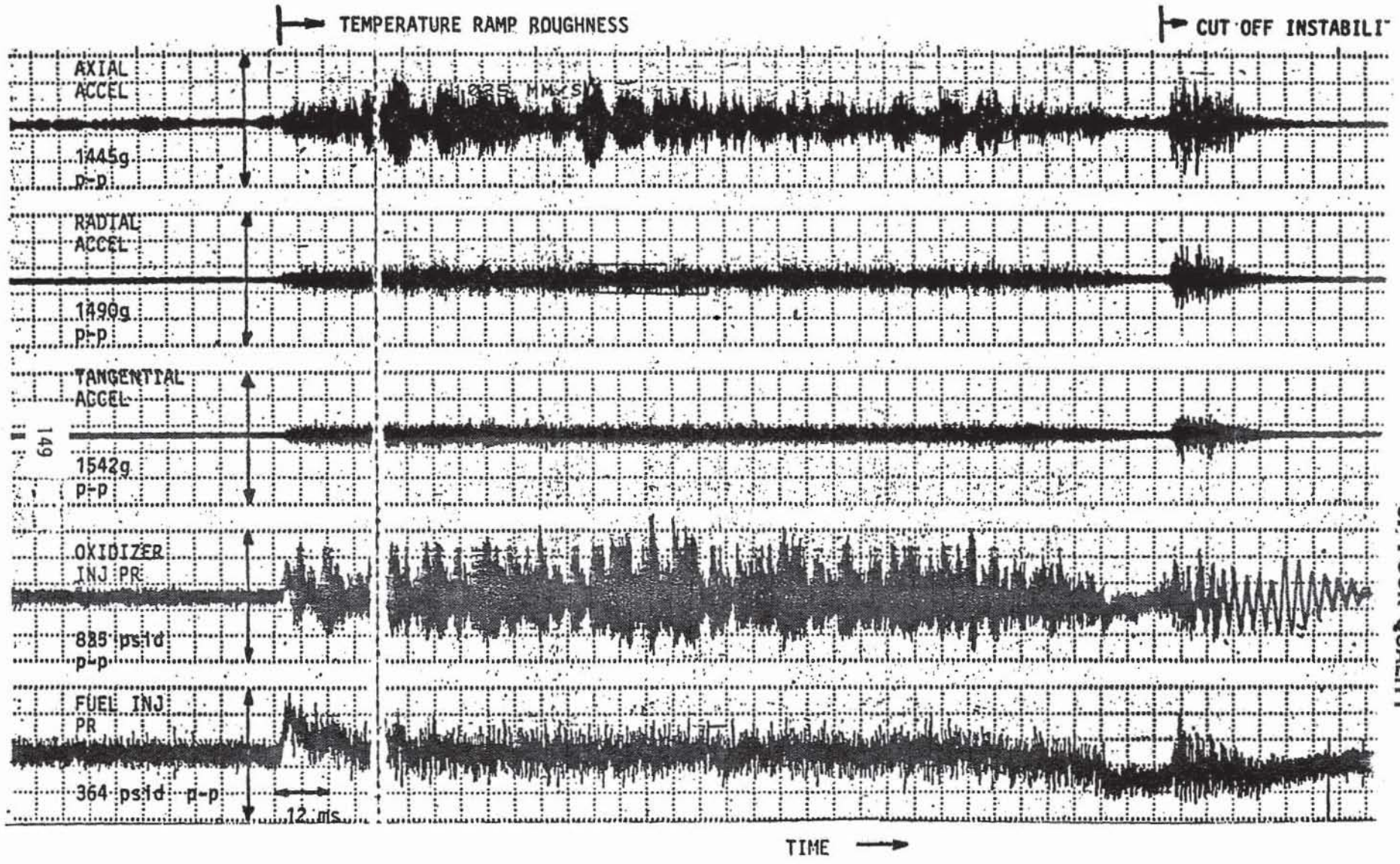

Figure C12 -BRUSH CHART RECORDS FOR TEST 014-025,
A TYPICAL FUEL TEMPERATURE RAMP TEST

TABLE C.IV COMPARISON OF LOW M/R AND FUEL TEMP RAMP INSTABILITIES

	LOW M/R	TEMP RAMP
M/R	2.8/3.25/3.33 (15° CHAMFER)	3.35-3.5
MODE	1-T	14 KHz
PRE-INSTABILITY ACTIVITY	4.4, 8.6, 10, 12-13 KHz	8.6/12-14 KHz
MANIFOLD PRESSURES AT INSTABILITY	$P_{IF} \neq P_{IO}$	$P_{IF} = P_{IO}$
SHIFT IN PRESSURES AT INSTABILITY	P_{IF}, P_{IO} APPROX 100 PSI ↑ P_C APPROX 150 PSI ↓	P_{IF}, P_{IO} 200 TO 300 PSI ↑ P_C APPROX 250 PSI ↓
FUEL TEMP (MEASURED MANIFOLD) (CALCULATED INJECTION)	36 TO 50°F 23 TO 29°F	-18 TO -24°F APPROX. -50°F

characteristics and compares them with the instability characteristics on tests which exhibited 1-T (approximately 5 KHz) instabilities. As indicated, the two types of instabilities show notable differences in manifold and chamber pressure behavior as well as in the measured frequencies. The rise in the manifold pressures and the drop in chamber pressure which occur at the onset of all the instabilities are larger for the fuel temperature ramping tests.

APPENDIX D - Phase C Test Chronology

Phase C testing involved a series of bomb tests conducted at various mixture ratios and fuel injection temperatures. Table D.I summarizes the Phase C testing results. A series of seven tests were attempted of which five tests yielded significant stability data. Of the five tests, two tests experienced spontaneous instabilities before mainstage was established whereas the remaining three tests were successfully bombed in mainstage.

Test 014-026 was the first test attempted in the Phase C effort. Test 014-026 was terminated by a tangential accelerometer redline cut immediately after opening the main LOX valve. The accelerometer redline values had been set too low to allow continuation of the sequence through the vibrational environment encountered on start-up. A peak-to-peak vibrational level of 330 g's was measured yet the redline on the tangential accelerometer had been set at 250 g's. To alleviate this problem, a redline value of 600 g's peak-to-peak was established for both the tangential and axial accelerometers on the subsequent test.

Test 014-027 was successfully bombed in mainstage and achieved a duration cut-off as planned 50 milliseconds after bomb firing. Figure D1 shows that the bomb produced a chamber pressure overshoot of approximately 1080 psi (55 % of Pc). High frequency data indicated that the 1T mode was excited after bomb firing. Heat flux data from the water-cooled nozzle revealed that the heat flux at the throat was reduced by over 60 percent relative to the phase A and B testing due to the zirconia coating (Figure D2).

Test 014-028 was the first attempt at bomb testing with sub-ambient fuel injection temperature. The test was terminated by a TASCOS accelerometer cut during transition to mainstage. A self-induced 1T instability occurred while the main oxidizer valve was opening (135 percent/sec.) to the mainstage position and while fuel injection temperature was dropping (160 degrees R/sec.) to the target value of 467 degrees R. The instability occurred in transition when the mixture ratio was approximately 2.73 and chamber pressure was 1600 psia. The isoplot of chamber pressure is shown in Figure D3. The figure illustrates 4 KHz activity leading up to the high amplitude 1-T instability.

To avoid ramping the fuel temperature and opening the main oxidizer valve simultaneously, a sequence change was made for test 014-029 in which the mixer liquid valve opening would be delayed. Test 014-029 was prematurely terminated by minimum fuel venturi pressure redline cut during transition to full fuel flow. The redline violation occurred because of higher than anticipated pressure drop across the main fuel valve. For this test the main fuel valve position had been lowered from the 55 percent open position used on previous tests to 50 percent open in an attempt

TABLE D.I - Phase C Test Summary

Test	P_c (psig)	MR (O/F)	Fuel Inj. Temp (°R)	Comments
026	1175	--	475	Accel redlines set too low - cut before mainstage
027	1950	3.38	528	Bombed unstable - 1T mode excited
028	1510	≈ 1.87	471	Spontaneous instability while in transition to mainstage
029	1480	--	496	Redline cut (low fuel venture pressure)
030	1950	3.18	482	Bombed unstable - 1T mode excited
031	1870	≈3.36	498	Spontaneous instability while in transition to mainstage
032	2119	3.69	462	Bombed stable - all parameters except the axial accelerometer recover

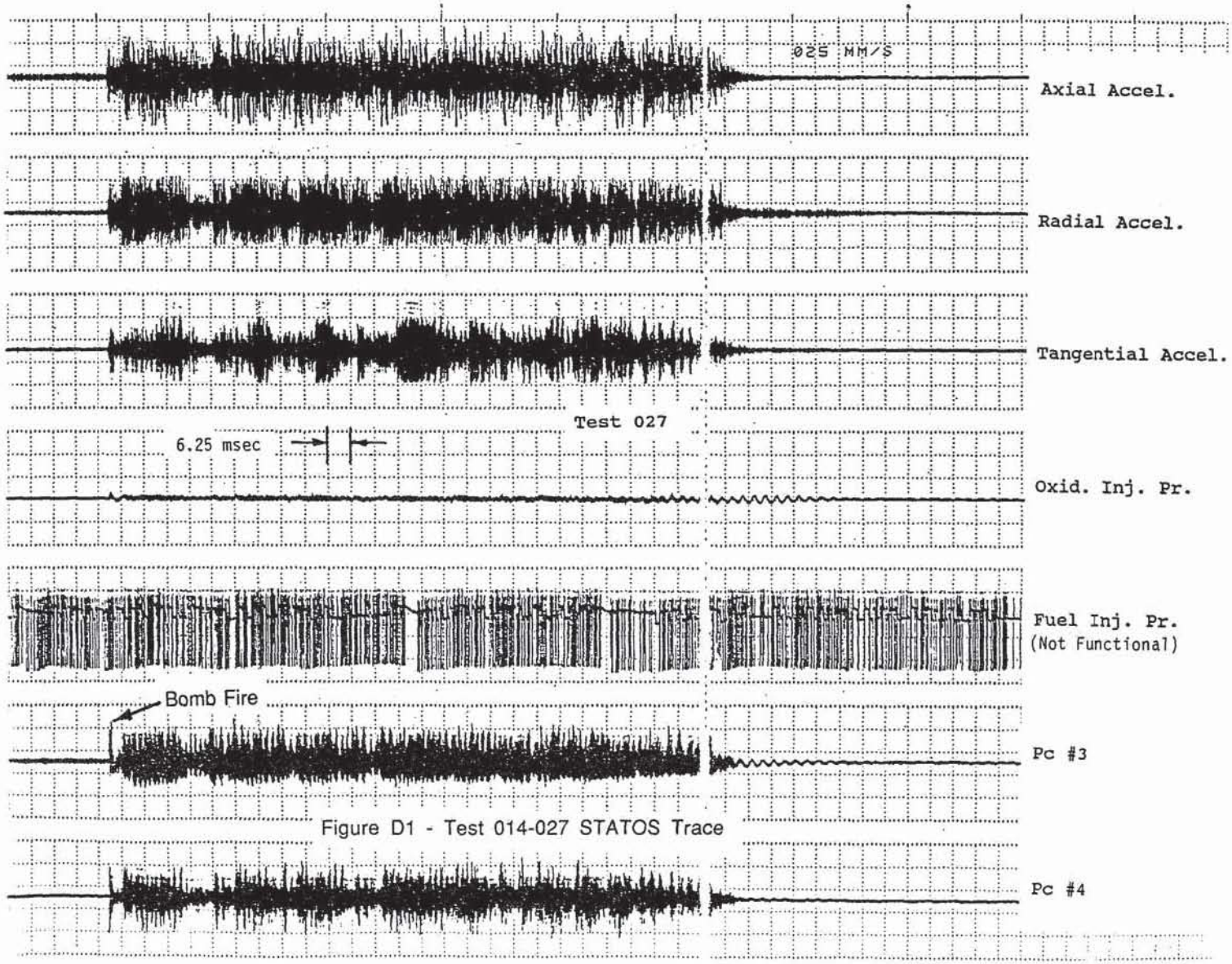

Figure D1 - Test 014-027 STATOS Trace

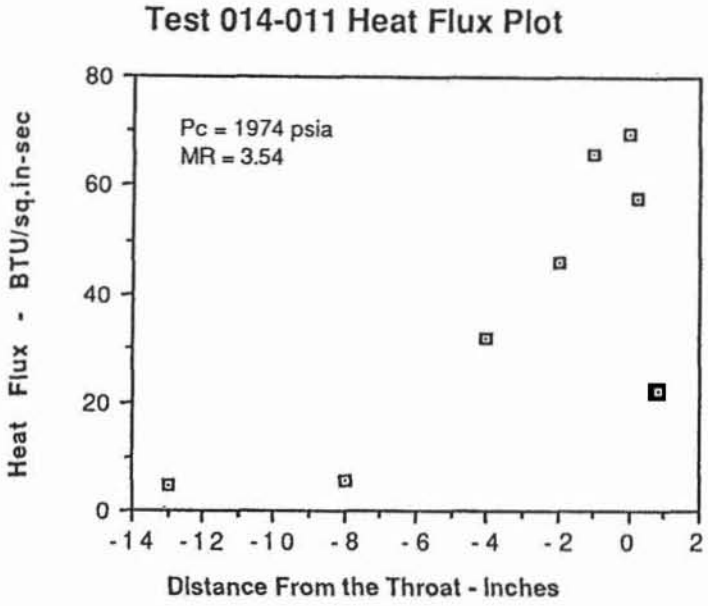

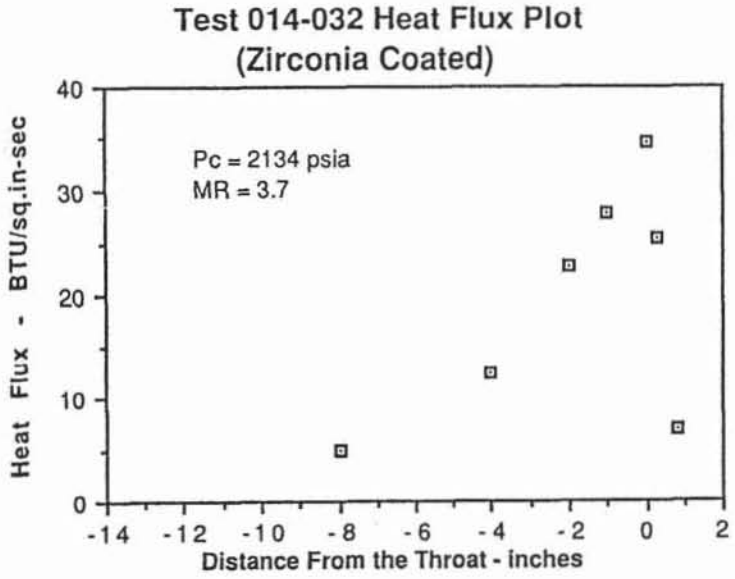

Figure D2 - Heat Flux Profile Comparison of Coated and Uncoated Chambers

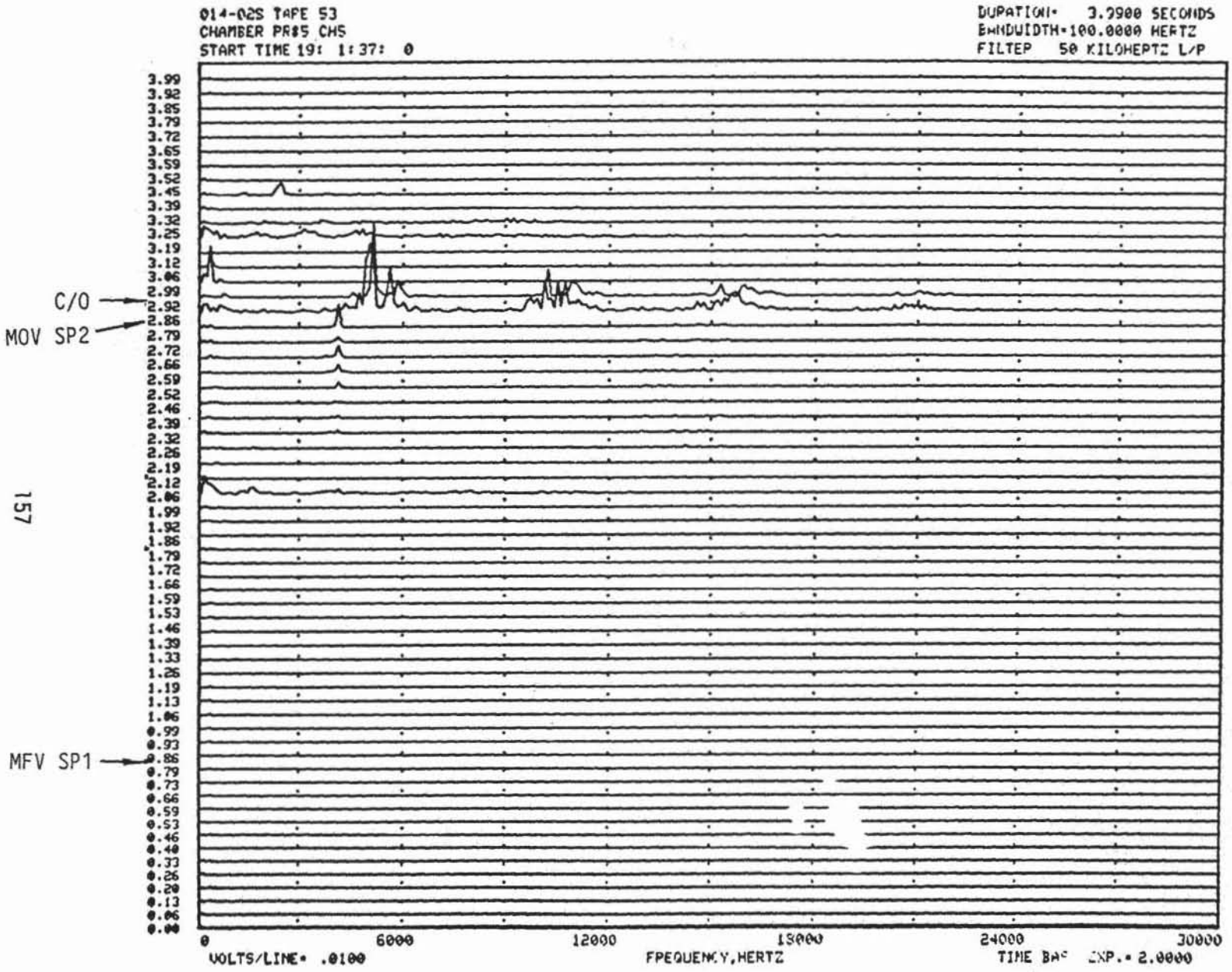

Figure D3 - Test 014-028 Chamber Pressure Isoplot

to maintain the same fuel flow rate as the previous tests while considering the increase in density of the colder fuel. An analysis of the minimum fuel venturi pressure redline value indicated that it could be safely lowered by 400 psi yet still be used to verify acceptable fuel flow in mainstage. This redline value was lowered from 2200 psig to 1800 psig on subsequent tests.

Test 014-030 was successfully bombed in mainstage. However, the target fuel injection temperature was not achieved at the time the bomb was fired. The target condition was missed due to a 600 millisecond delay between the time that the mixer liquid fuel valve opened and the time that the fuel injection temperature starts to drop. As illustrated in Figure D4, the fuel injection temperature had just started to drop when the bomb was commanded to fire. In spite of this, the fuel injection temperature was 49 degrees Rankine lower than fuel injection temperature on the previous successful bomb test (test 014-027) because of lower atmospheric temperature and overcast skies on the day of the latter test had lowered the gaseous methane tank temperature.

Following the bomb firing on test 014-030, a 1T mode combustion instability was excited. Prior to the bomb firing, a significant 4 KHz disturbance appeared in the high frequency chamber pressure data. This can be seen in Figure D5. The 4 kHz mode is believed to be a longitudinal (organ pipe) mode of the lox post. Also, it is interesting to note that after the bomb fired, there is an 11 millisecond period of relatively low amplitude activity before the onset of high amplitude 1T instability. The brush data in Figure D5 show the dynamics of the bomb fire, delay period, and high amplitude instability.

To allow sufficient time for the fuel injection temperature to reach the target value before firing the bomb, the mainstage duration was extended by 200 milliseconds for test 014-031. Also, the LOX tank pressure was increased to provide higher mixture ratio. Test 014-031 experienced a self-induced 1T instability as the main LOX valve was in transition to mainstage conditions. Mixture ratio and chamber pressure were 3.36 and 1900 psia respectively at the onset of the instability. Fuel injection temperature had not begun to drop at the onset of the instability.

In a desperate attempt to avoid a self-induced instability while in transition to mainstage, the main LOX valve setting in prestage was lowered by four percent to allow a slightly lower mixture ratio in prestage. Test 014-032 was run at the same conditions as test 014-031 except for this valve position change. Test 014-032 achieved mainstage and was successfully bombed. Target mixture ratio and fuel injection temperature were attained. After the bomb fired, all significant parameters recovered except the axial accelerometer. Figure D7 shows the high frequency traces and indicates that no high amplitude instability was excited after the bomb fired.

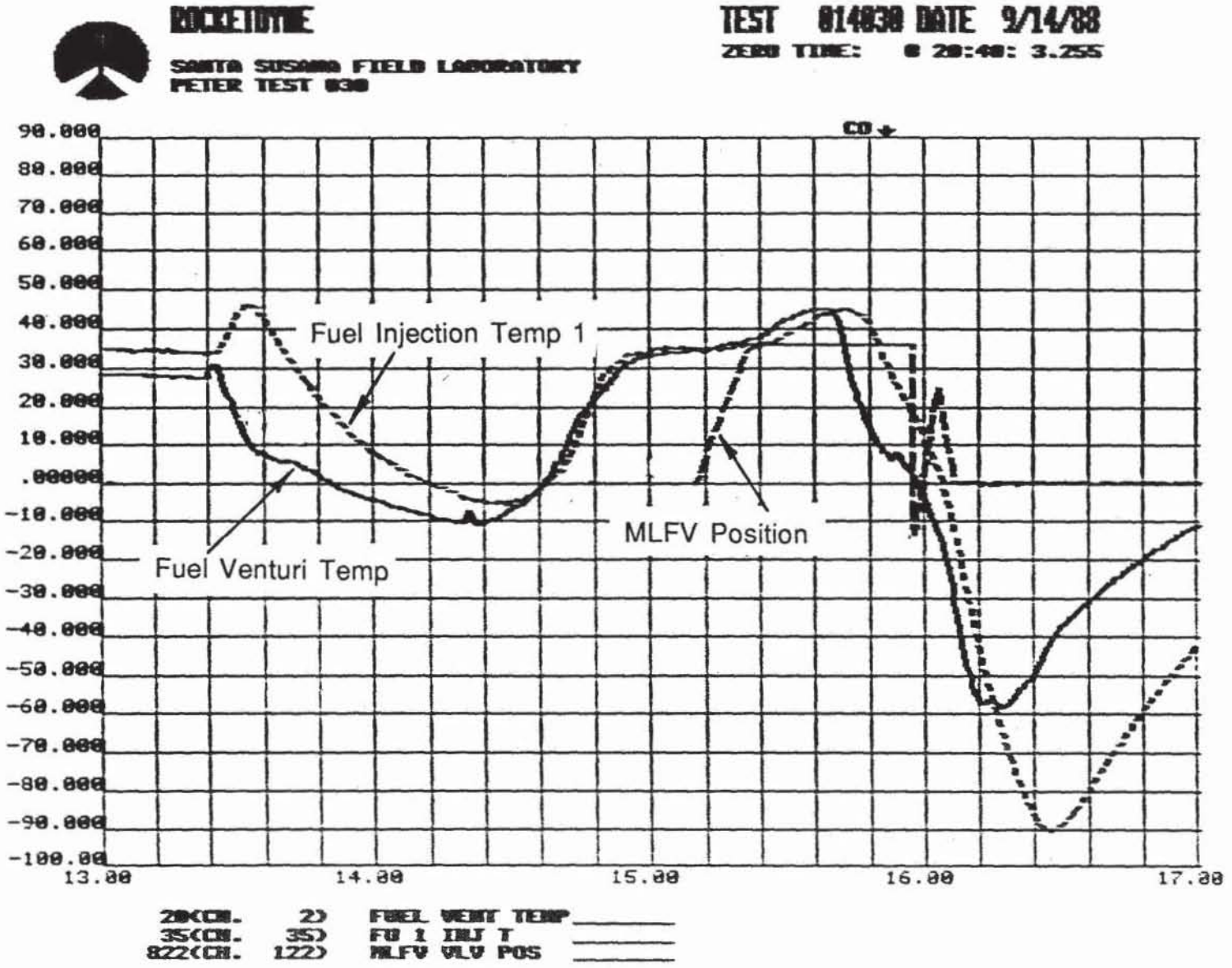

Figure D4 - Methane System Temperature History for Test 014-030

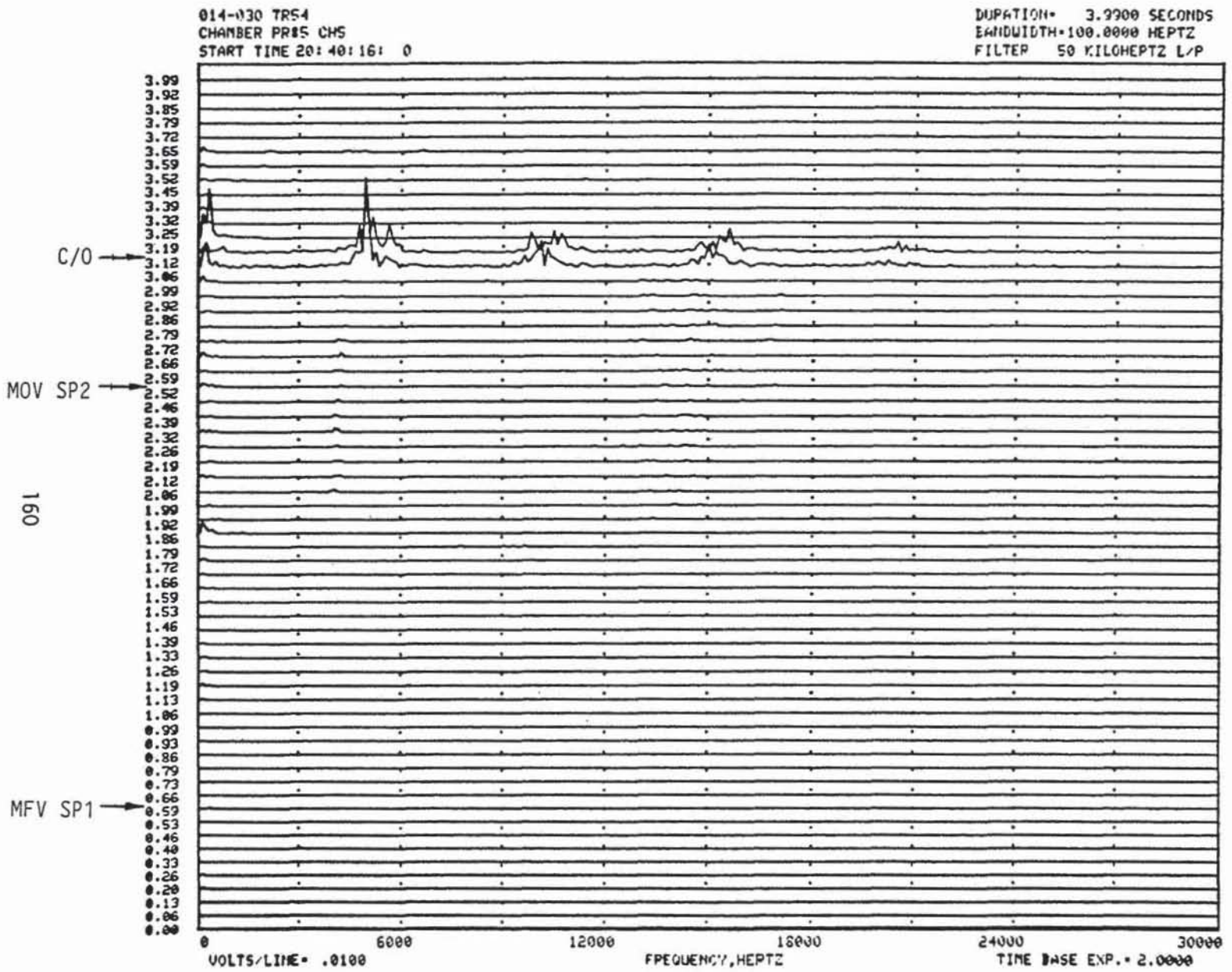

Figure D5 - Test 014-030 Chamber Pressure Isoplot

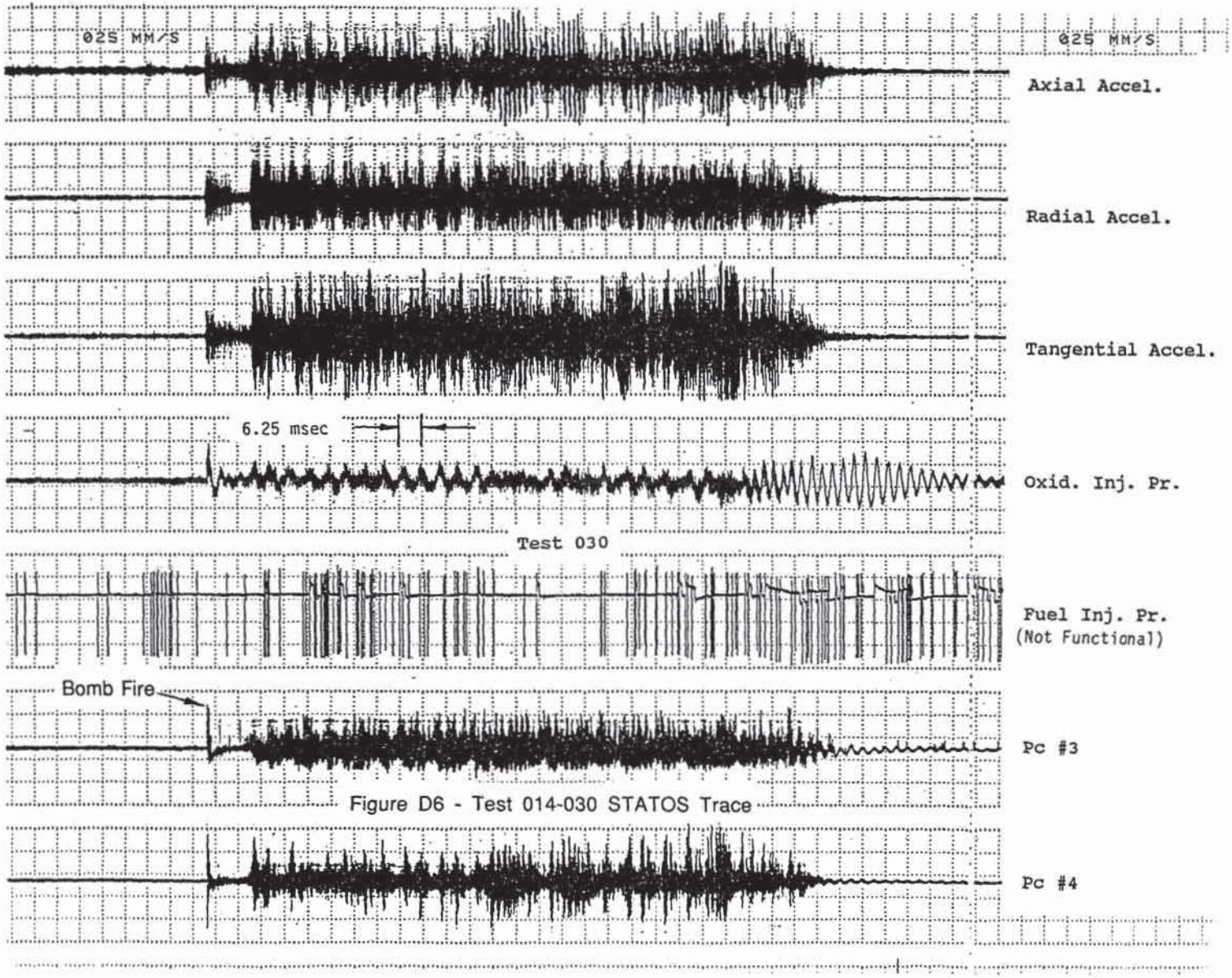

Figure D6 - Test 014-030 STATOS Trace

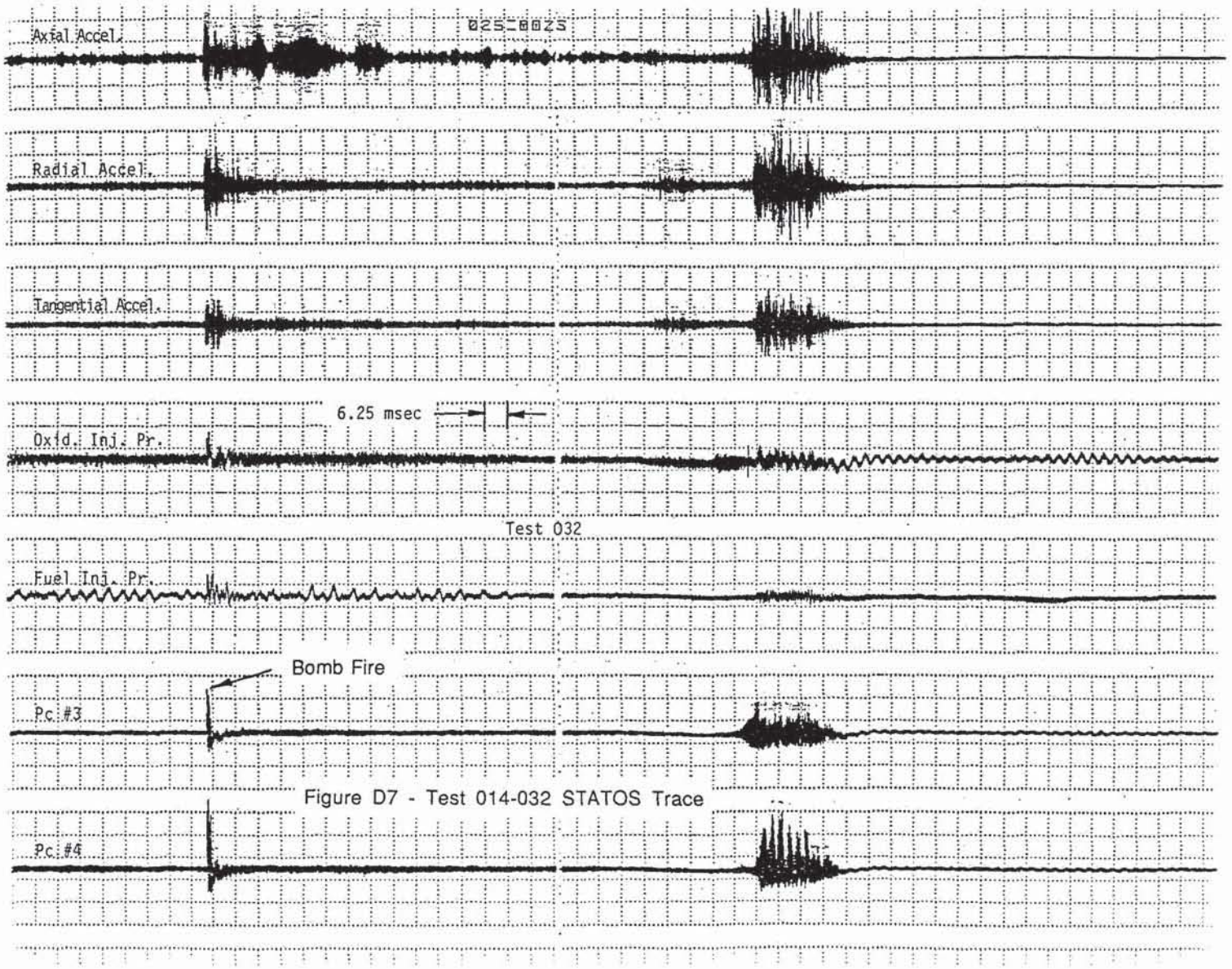

Figure D7 - Test 014-032 STATOS Trace

Appendix E - Test 014-030 Power Spectral Density and Transfer Function Data for Stable and Unstable Operation

A complete set of power spectral density (PSD) plots of the high frequency pressure transducers is presented in this appendix for both stable and unstable conditions encountered during test 014-030. Data from test 030 was chosen for presentation in this appendix in order to illustrate the frequency content of a typical 1T mode instability and the associated 4 kHz precursor activity which was often seen during the test program. Test 030 was successfully bombed in mainstage at a chamber pressure of 1964 psia and a mixture ratio of 3.18. A first tangential mode instability ensued approximately 13 milliseconds after detonation of the bomb.

Figures E1 through E5 are PSD's for stable mainstage conditions. Also shown (in Figures E6 through E17) is the transfer function data (coherence, gain, and phase) for all high frequency pressure transducers referenced to chamber pressure PCB transducer 3 for stable mainstage conditions. Transfer function data was obtained in an effort to gain insight into the cause and mode of the 4 kHz activity which preceded the 1T mode instability. Peaks in chamber pressure at approximately 4 and 8 kHz are seen during the stable (pre-bomb) period. Strong coherence is also shown between all three chamber pressure transducers near 4 and 8 kHz. Additionally, 8 kHz activity is seen in the LOX dome.

Figures E18 through E24 are PSD's for unstable (post-bomb) mainstage conditions for test 030. Other significant stable and unstable PSD's and transfer function plots for tests other than test 030 are presented in the body of the report and in Appendix B and C.

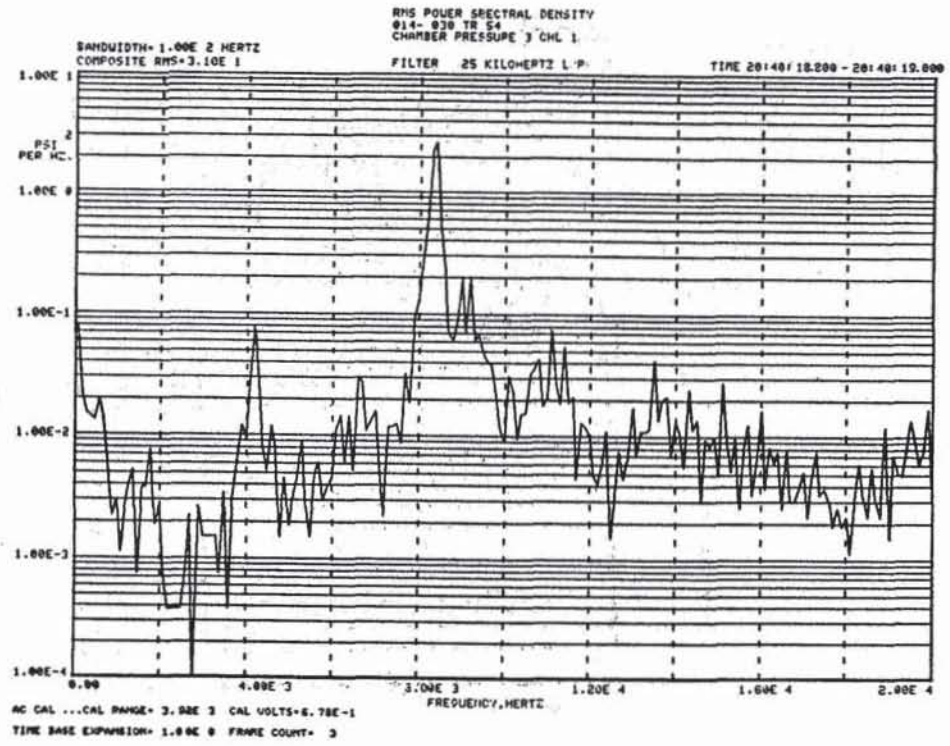

Figure E1 - Chamber Pressure 3 PSD (Test 030, stable)

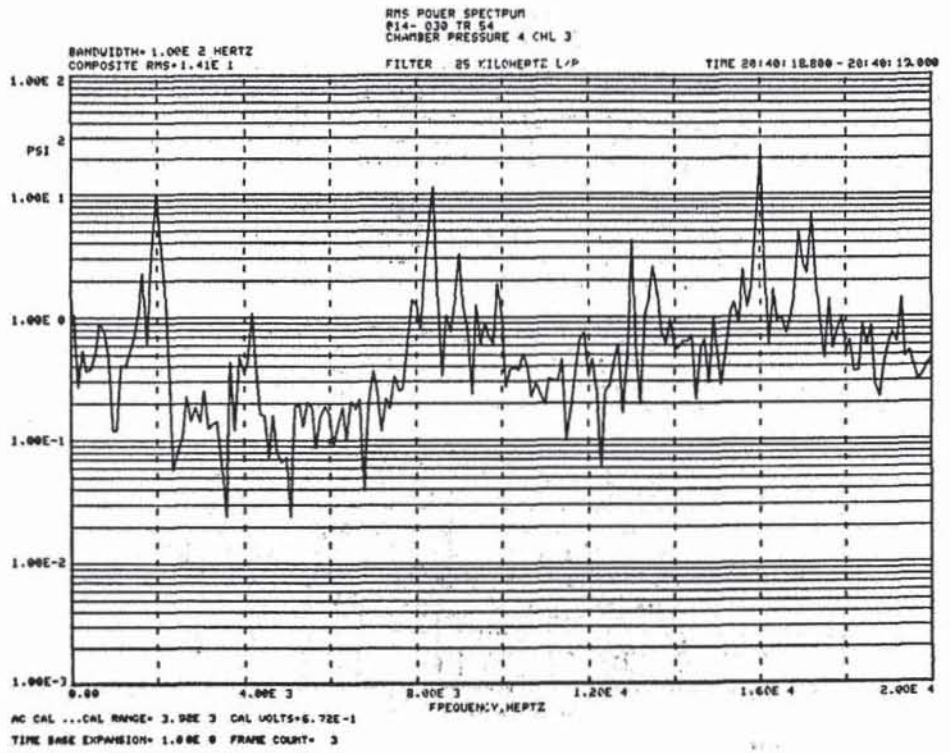

Figure E2 - Chamber Pressure 4 PSD (Test 030, stable)

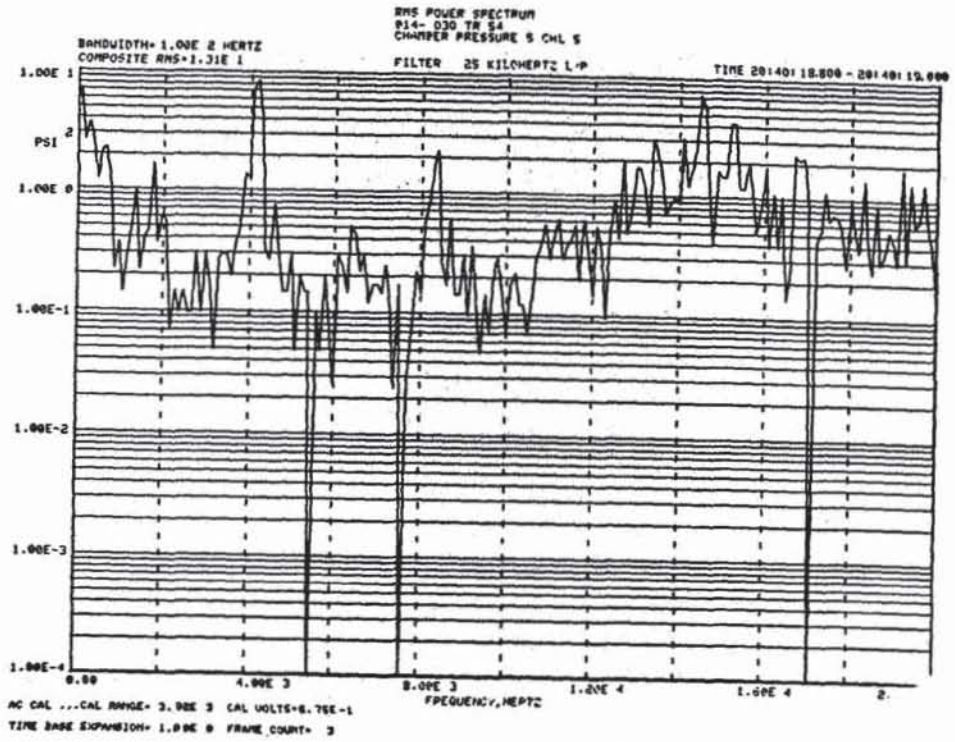

Figure E3 - Chamber Pressure 5 PSD (Test 030, stable)

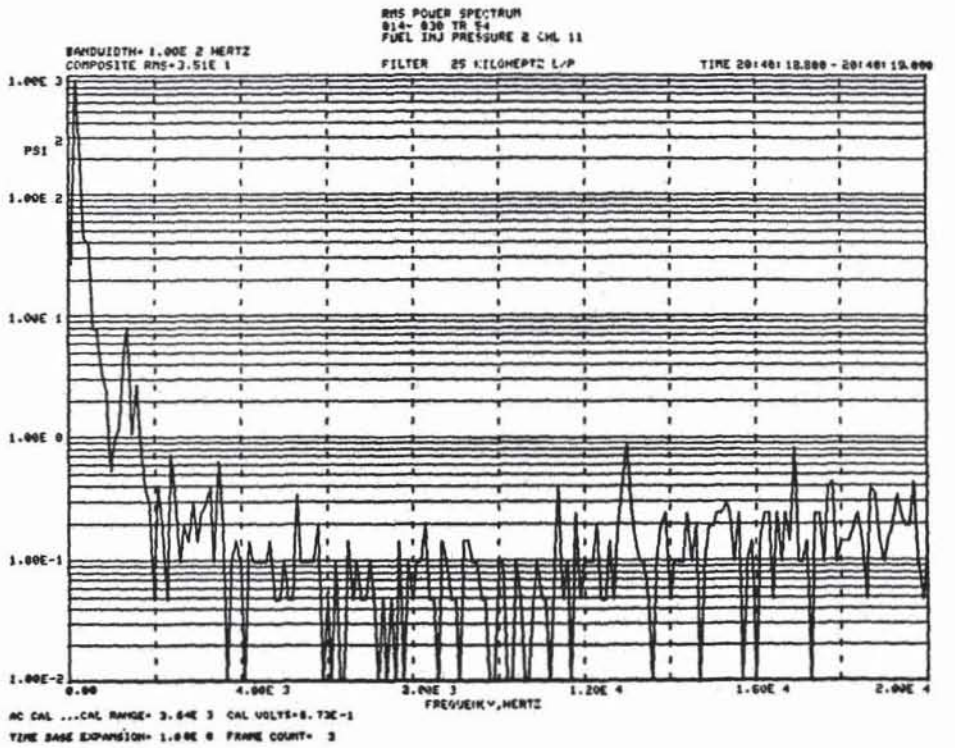

Figure E4 - Fuel Manifold Pressure 2 PSD (Test 030, stable)

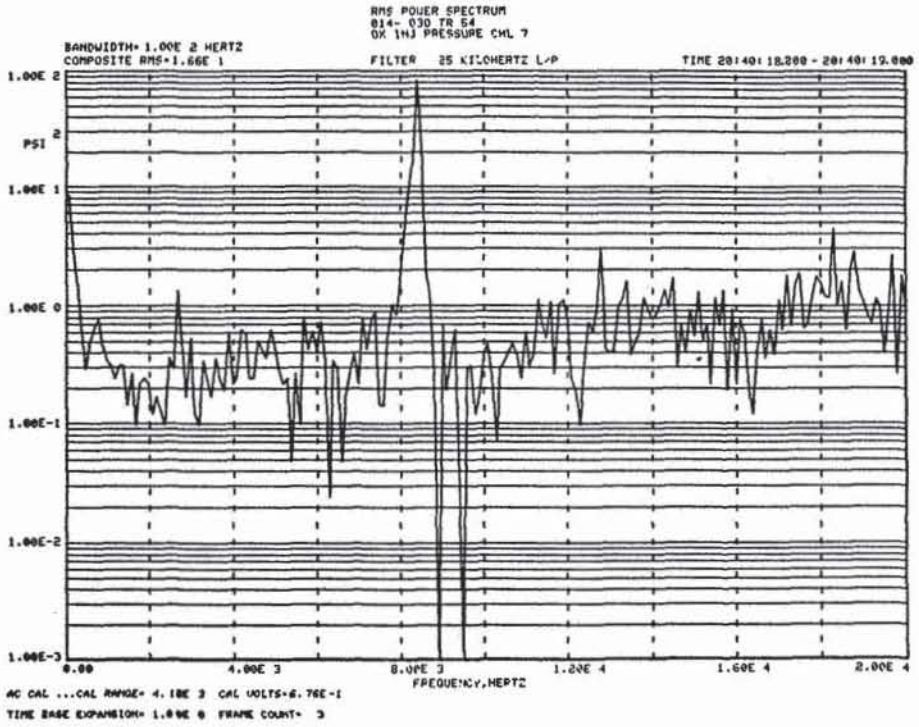

Figure E5 - Oxidizer Manifold Pressure PSD (Test 030, stable)

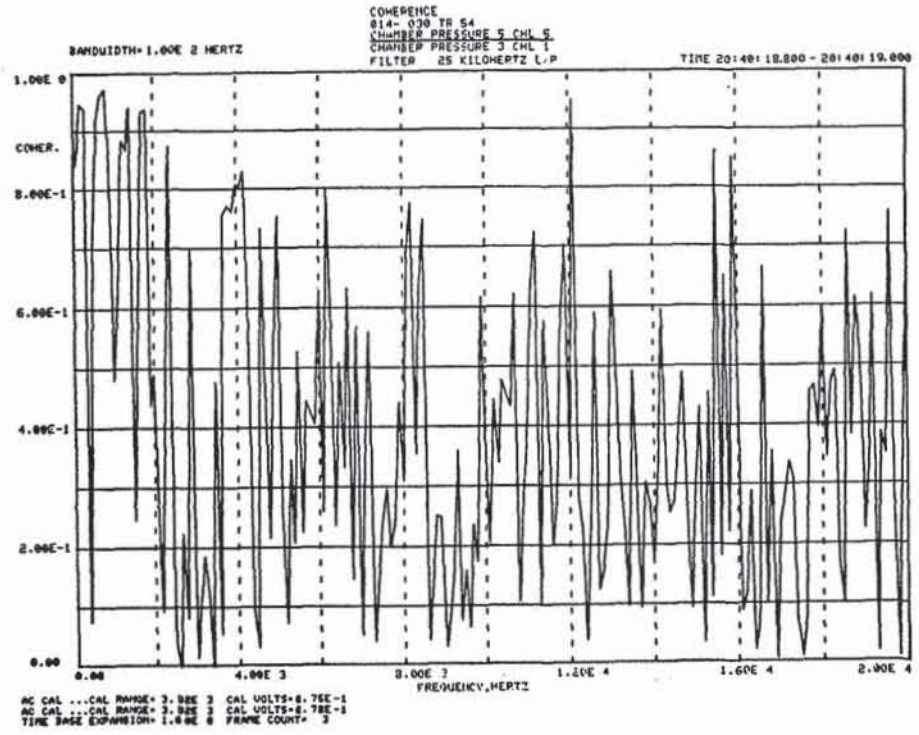

Figure E6 - Chamber Pressure 5 Coherence for Stable Conditions (Referenced to Chamber Pressure 3)

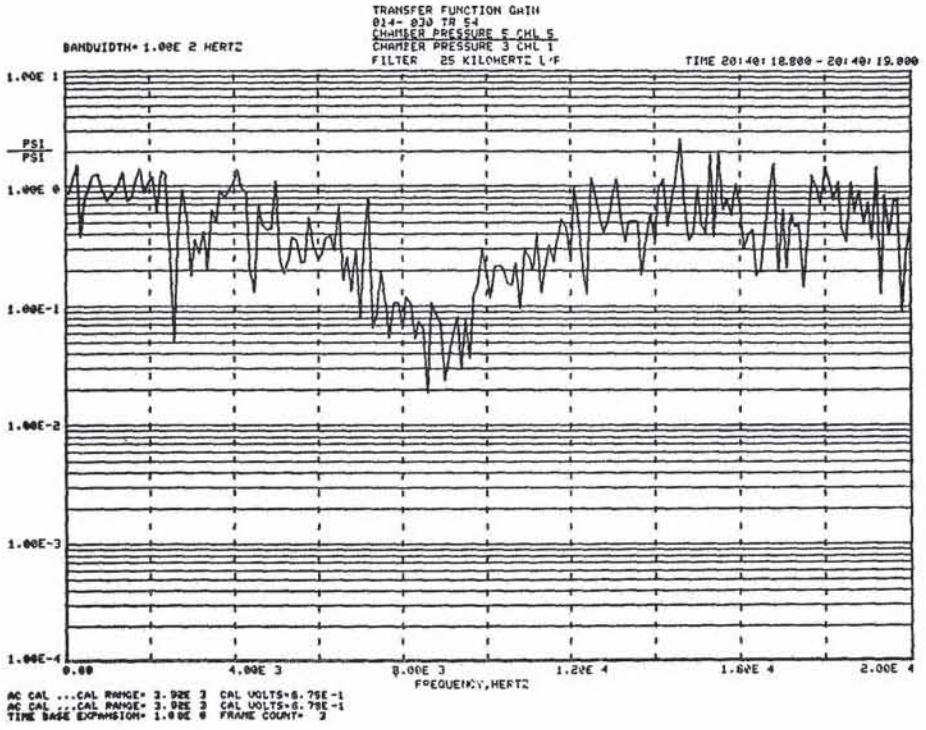

Figure E7 - Chamber Pressure 5 Gain for Stable Conditions
(Referenced to Chamber Pressure 3)

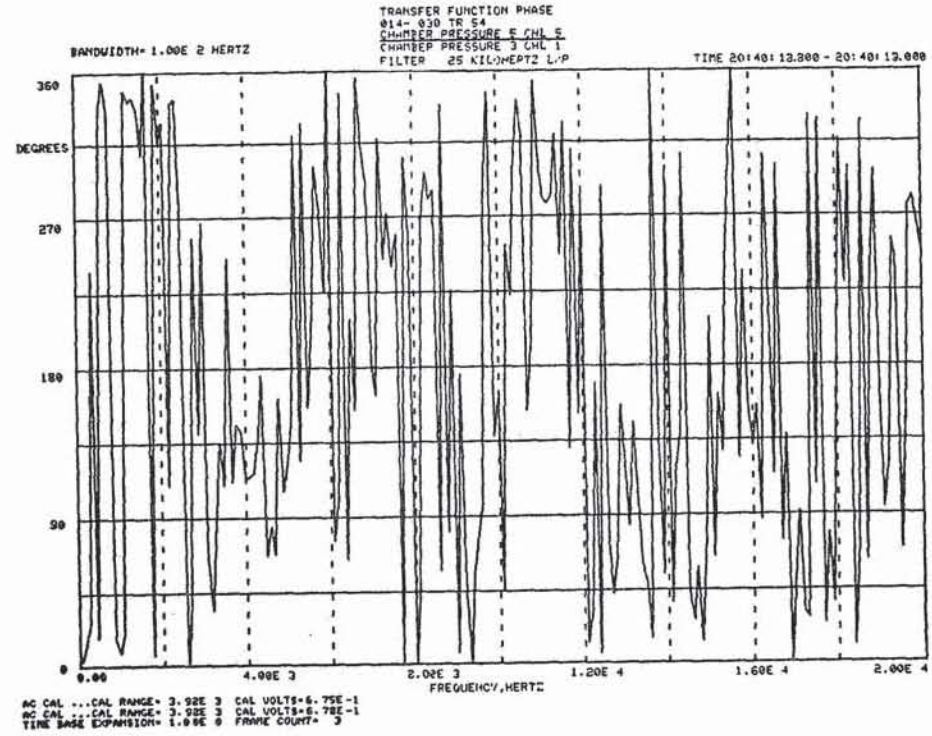

Figure E8 - Chamber Pressure 5 Phase for Stable Conditions
(Referenced to Chamber Pressure 3)

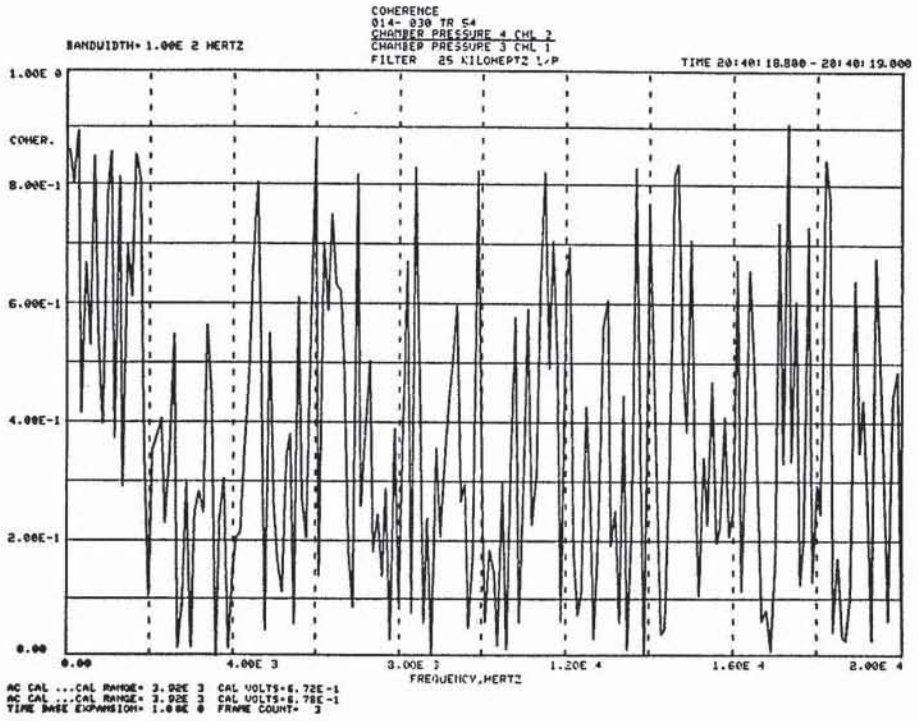

Figure E9 - Chamber Pressure 4 Coherence for Stable Conditions (Referenced to Chamber Pressure 3)

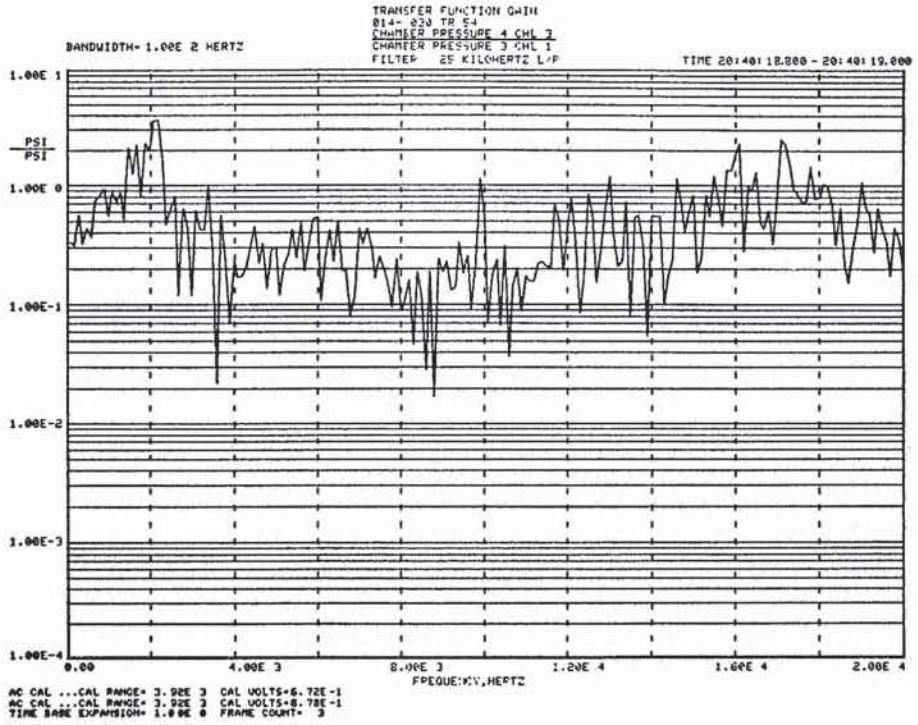

Figure E10 - Chamber Pressure 4 Gain for Stable Conditions (Referenced to Chamber Pressure 3)

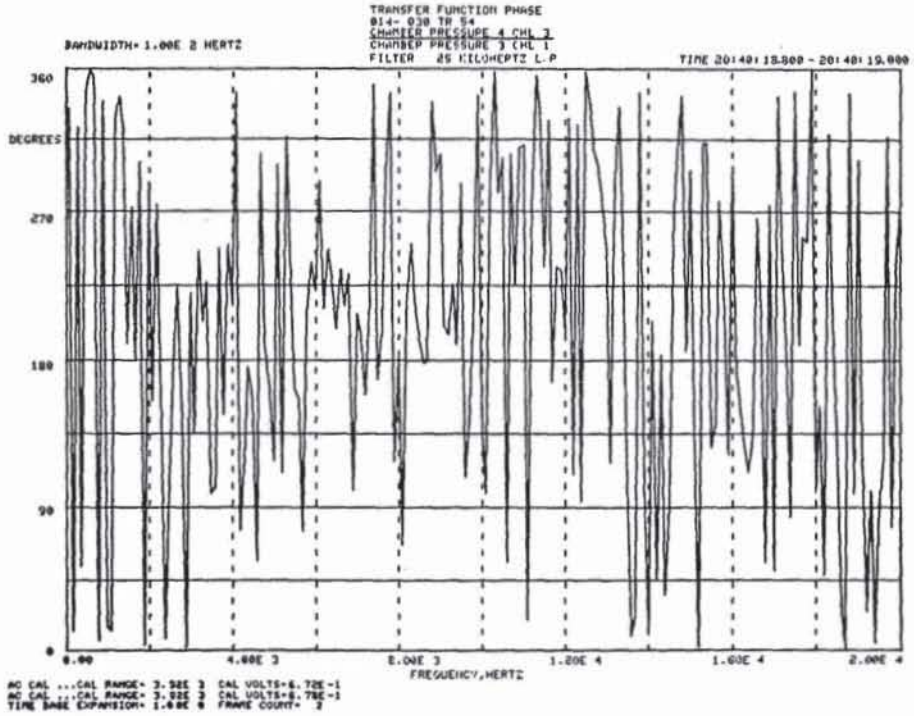

Figure E11 - Chamber Pressure 4 Phase for Stable Conditions
(Referenced to Chamber Pressure 3)

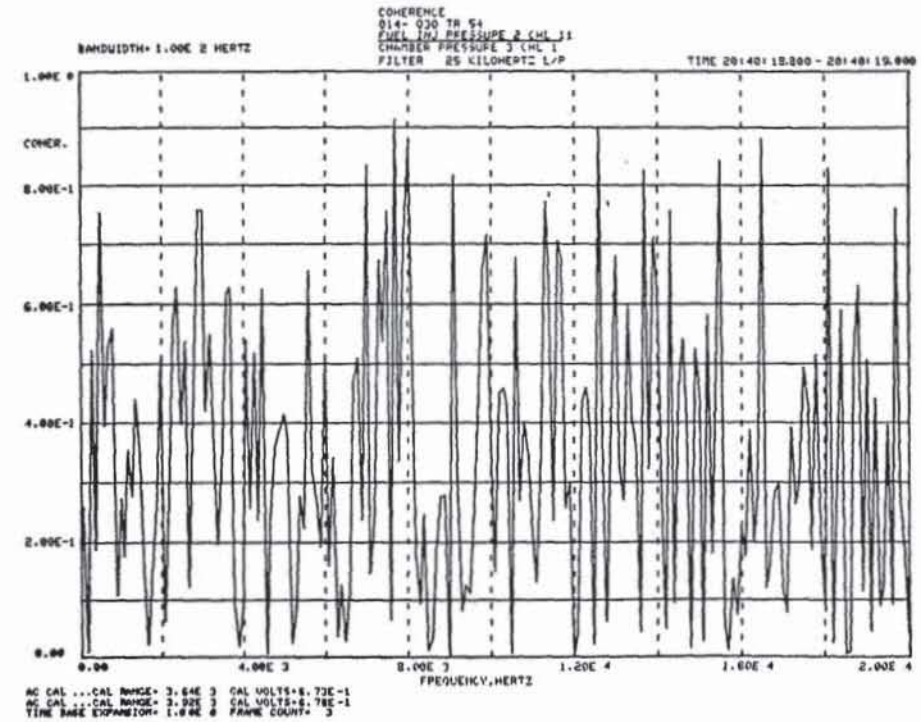

Figure E12 - Fuel Manifold Pressure 2 Coherence for Stable Conditions
(Referenced to Chamber Pressure 3)

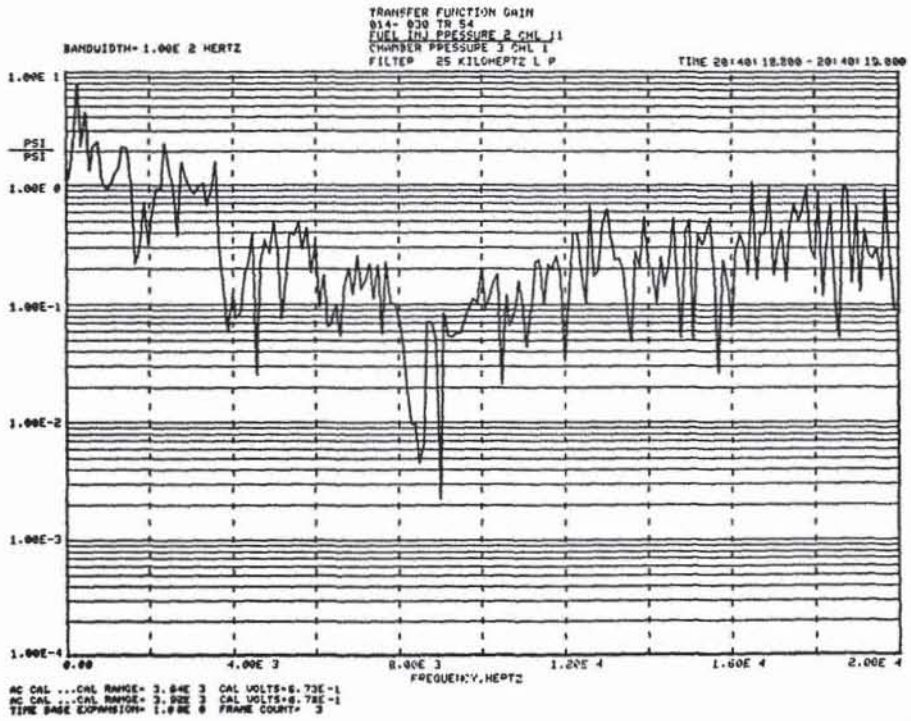

Figure E13 - Fuel Manifold Pressure 2 Gain for Stable Conditions (Referenced to Chamber Pressure 3)

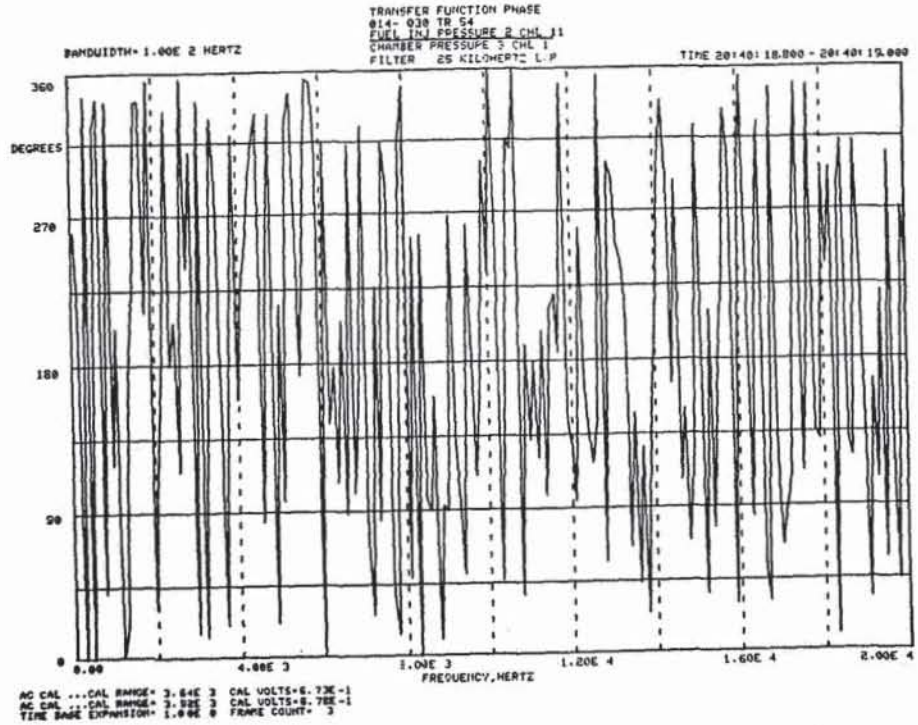

Figure E14 - Fuel Manifold Pressure 2 Phase for Stable Conditions (Referenced to Chamber Pressure 3)

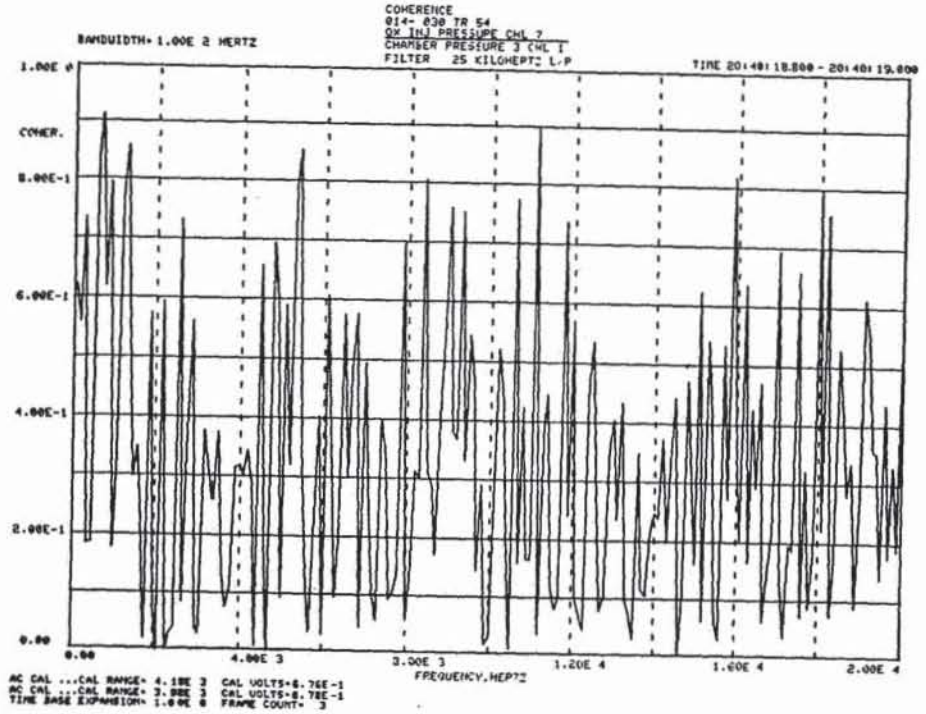

Figure E15 - Oxidizer Manifold Pressure Coherence for Stable Conditions (Referenced to Chamber Pressure 3)

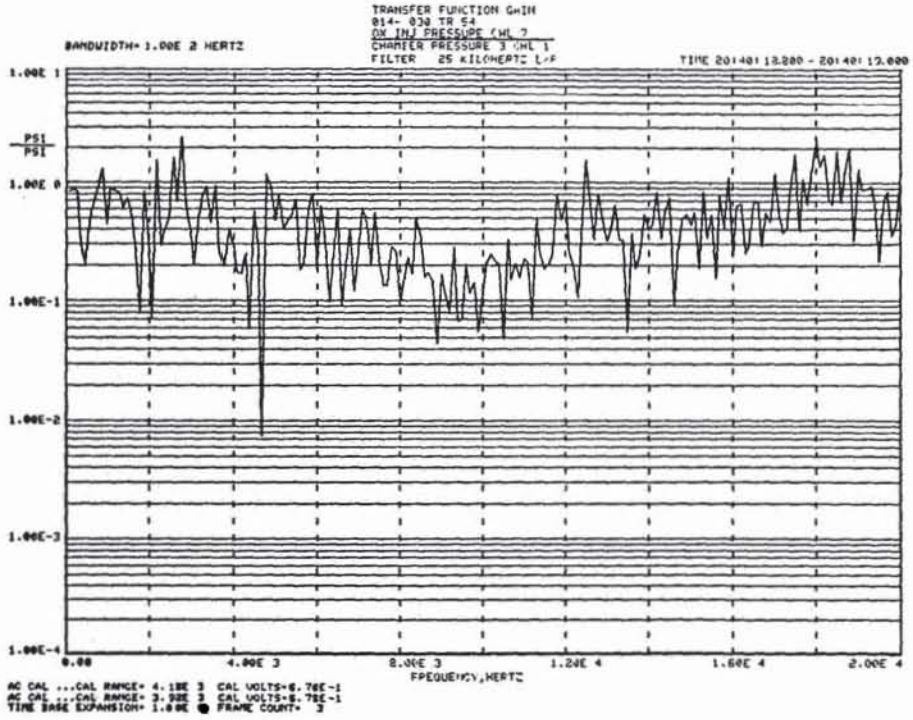

Figure E16 - Oxidizer Manifold Gain for Stable Conditions (Referenced to Chamber Pressure 3)

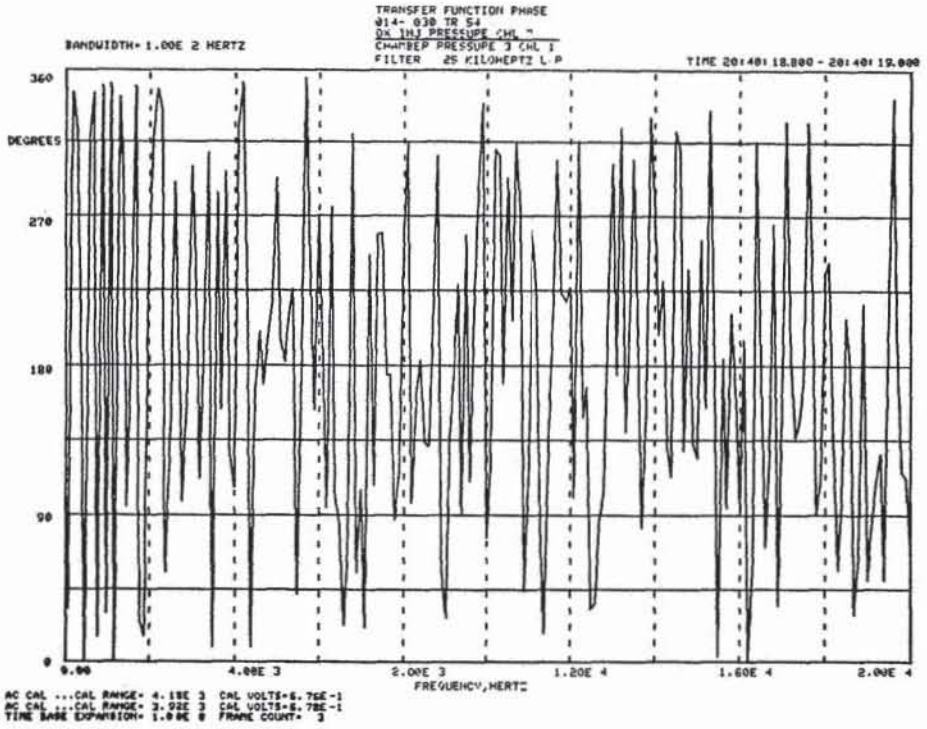

Figure E17 - Oxidizer Manifold Phase for Stable Conditions (Referenced to Chamber Pressure 3)

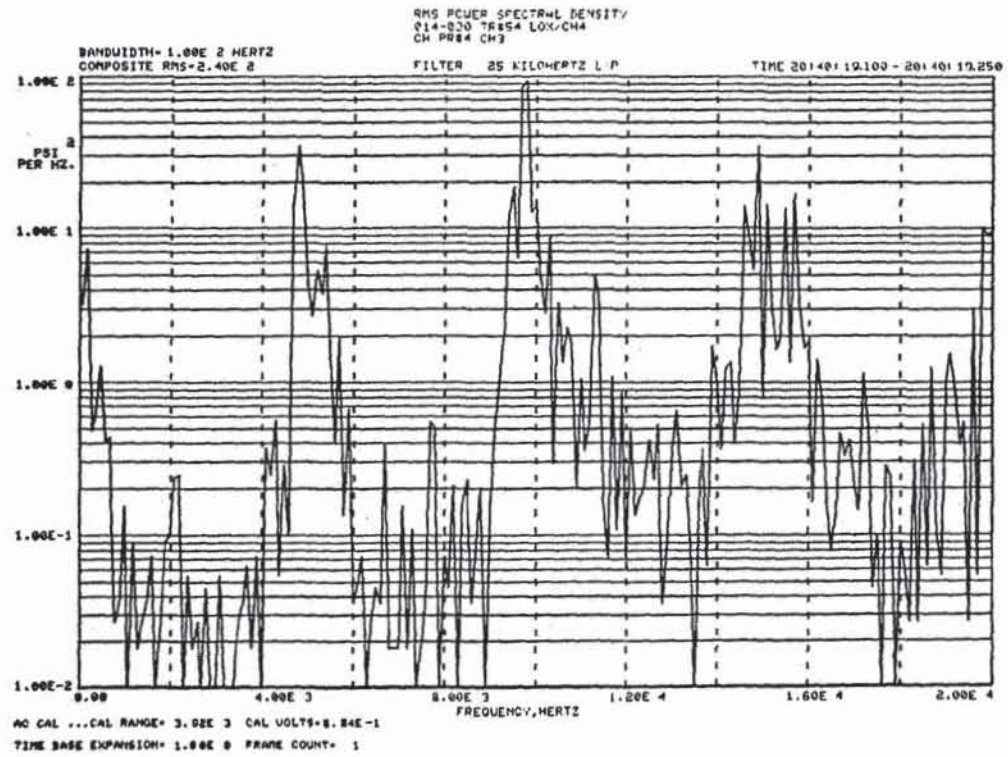

Figure E18 - Chamber Pressure 4 PSD (Test 030, unstable)

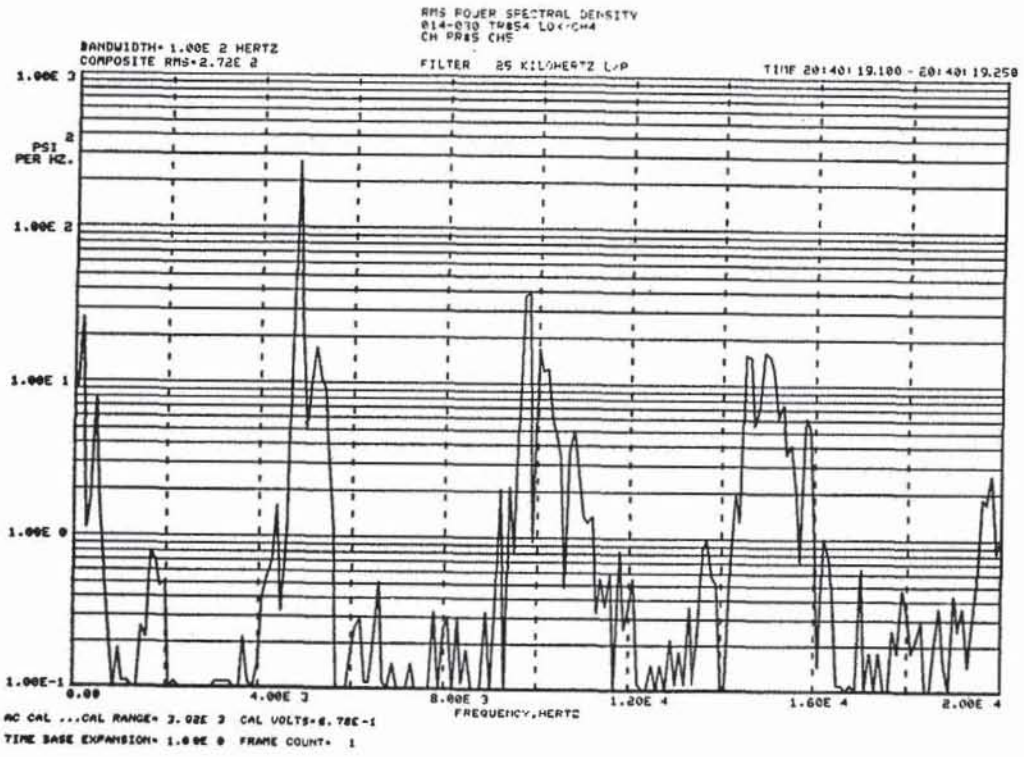

Figure E19 - Chamber Pressure 5 PSD (Test 030, unstable)

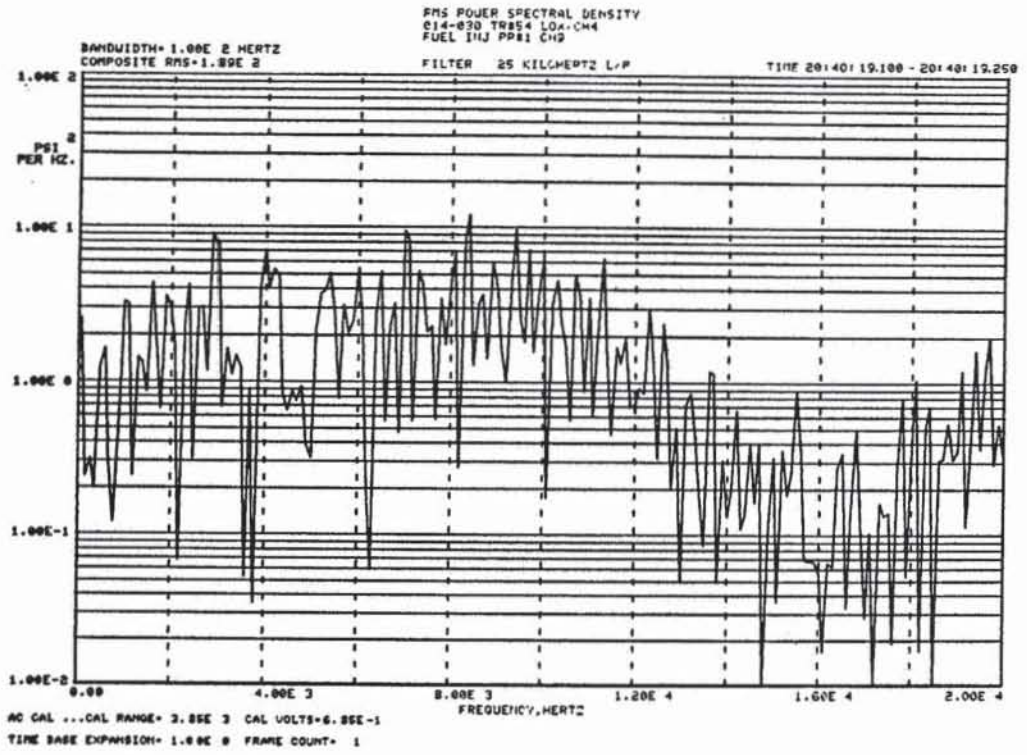

Figure E20 - Fuel Manifold Pressure 1 PSD (Test 030, unstable)

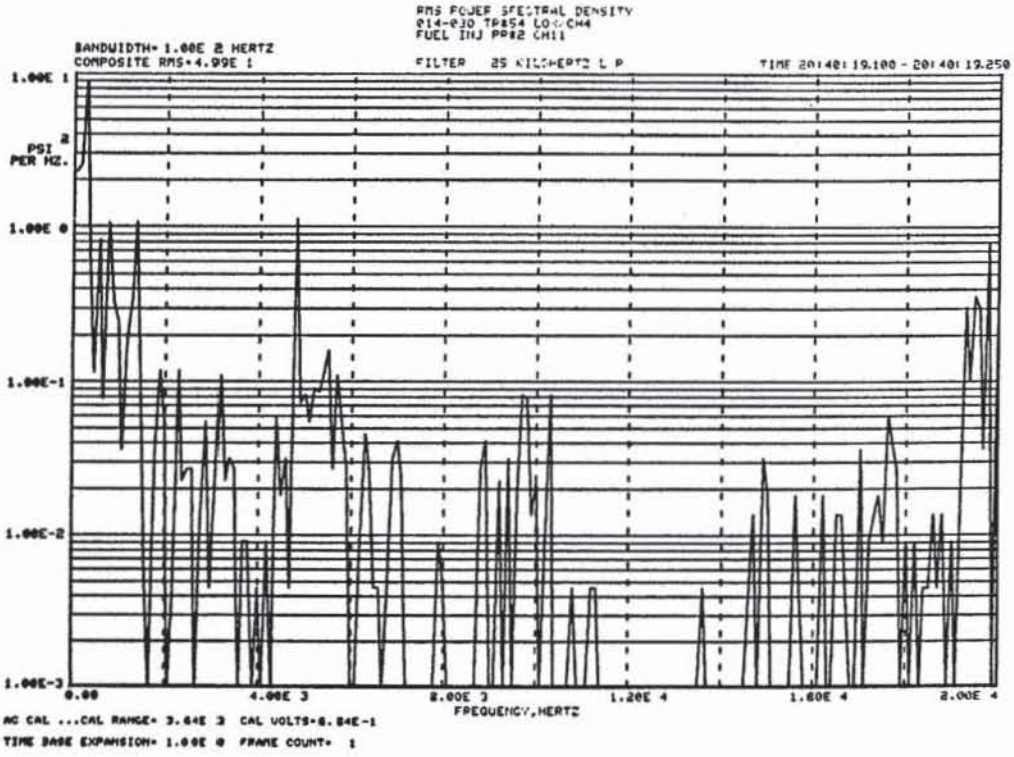

Figure E21 - Fuel Manifold Pressure 2 PSD (Test 030, unstable)

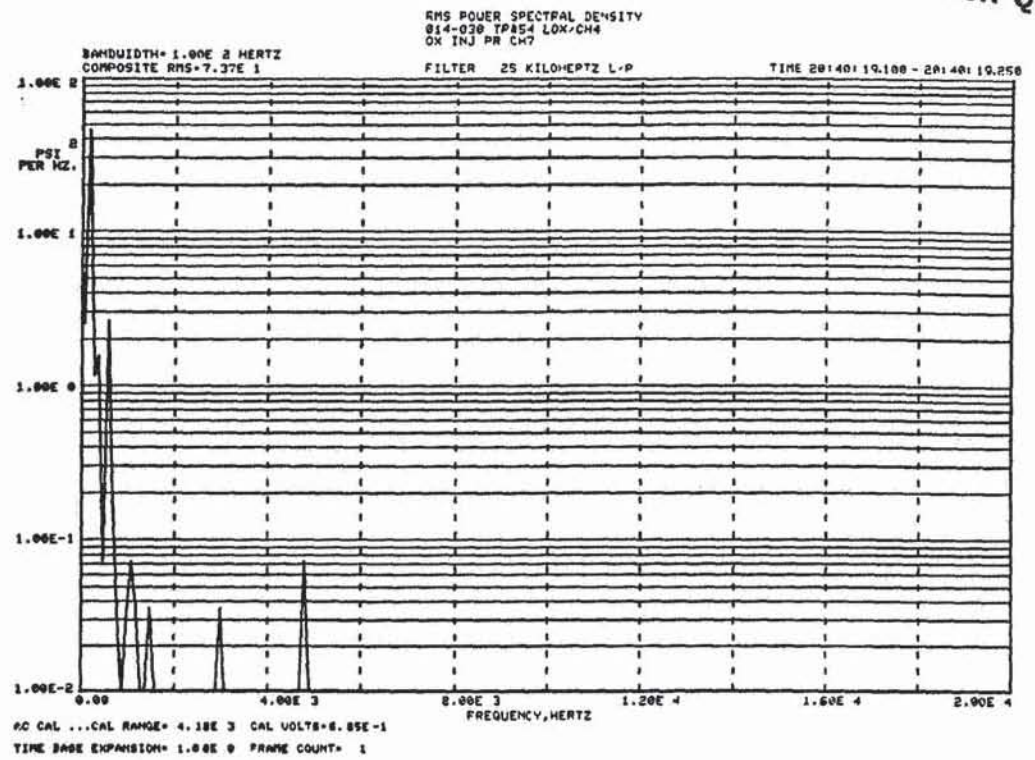

Figure E22 - Oxidizer Manifold Pressure PSD (Test 030, unstable)

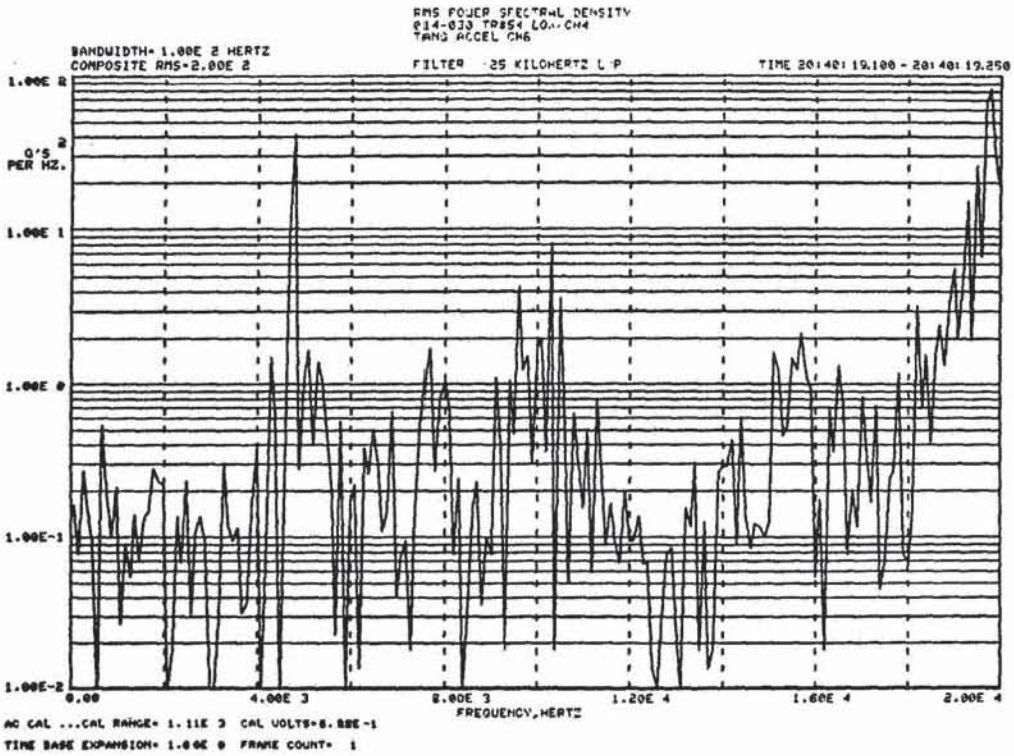

Figure E23 - Tangential Accelerometer PSD (Test 030, unstable)

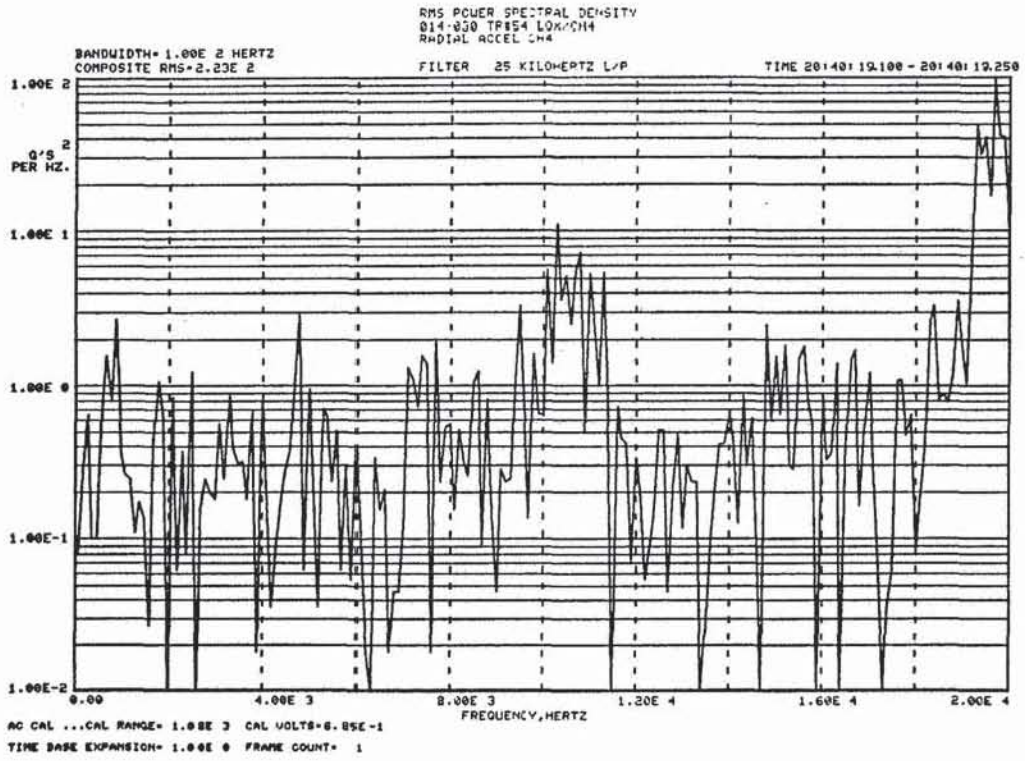

Figure E24 - Radial Accelerometer PSD (Test 030, unstable)

☆U.S. GOVERNMENT PRINTING OFFICE: 1989- 748-158/00204

NASA
National Aeronautics and Space Administration

Report Documentation Page

1. Report No.	2. Government Accession No.	3. Recipient's Catalog No.
NASA CR-182249		

4. Title and Subtitle	5. Report Date
LOX/Hydrocarbon Combustion Instability Investigation	July 1989
	6. Performing Organization Code

7. Author(s)	8. Performing Organization Report No.
R.J. Jensen, H.C. Dodson, and S.E. Claflin	RI/RD 89-179
	10. Work Unit No. 582-01-31

9. Performing Organization Name and Address	11. Contract or Grant No.
Rockwell International Rocketdyne Division 6633 Canoga Avenue Canoga Park, California 91303	NAS3-24612
	13. Type of Report and Period Covered Contractor Report Final
12. Sponsoring Agency Name and Address	14. Sponsoring Agency Code
National Aeronautics and Space Administration Lewis Research Center Cleveland, Ohio 44135-3191	

15. Supplementary Notes

Project Manager, Mark D. Klem, Space Propulsion Technology Division, NASA Lewis Research Center.

16. Abstract

The LOX/Hydrocarbon Combustion Instability Investigation Program (NAS3-24612) was structured to determine if the use of light hydrocarbon fuels (such as methane) with liquid oxygen (LOX) produces combustion performance and stability behavior similar to the LOX/hydrogen propellant combination. The hot fire program probed the combustion behavior of methane from ambient to subambient (438 deg R in the manifold) temperatures. Very interesting results were obtained from this program that have potential importance to future LOX/methane development programs. This report contains a very thorough and carefully reasoned documentation of the experimental data obtained. Subscale performance and stability rating testing was accomplished using 40,000 lb thrust class hardware. Stability rating tests used both "bombs" and fuel temperature ramping techniques. The test program was thus successful in generating data for the evaluation of the methane stability characteristics relative to hydrogen and for anchoring stability models. Data correlations, performance analysis, stability analyses, and key stability margin enhancement parameters are discussed.

17. Key Words (Suggested by Author(s))	18. Distribution Statement
Combustion stability; Combustion instability; Combustion; Injector performance; Injector; Methane; Heat flux	Unclassified – Unlimited Subject Category 20

19. Security Classif. (of this report)	20. Security Classif. (of this page)	21. No of pages	22. Price*
Unclassified	Unclassified	178	A09

NASA FORM 1626 OCT 86

*For sale by the National Technical Information Service, Springfield, Virginia 22161